Multi-Scale Modelling of Cold Regions Hydrology

A Thesis Submitted to the
College of Graduate and Postdoctoral Studies
in Partial Fulfillment of the Requirements
for the degree of Doctor of Philosophy
in the Department of Geography and Planning
(Centre for Hydrology)
University of Saskatchewan
Saskatoon

By
Christopher B. Marsh

Permission to Use

In presenting this thesis in partial fulfilment of the requirements for a Postgraduate degree from the University of Saskatchewan, I agree that the Libraries of this University may make it freely available for inspection. I further agree that permission for copying of this thesis in any manner, in whole or in part, for scholarly purposes may be granted by the professor or professors who supervised my thesis work or, in their absence, by the Head of the Department or the Dean of the College in which my thesis work was done. It is understood that any copying or publication or use of this thesis or parts thereof for financial gain shall not be allowed without my written permission. It is also understood that due recognition shall be given to me and to the University of Saskatchewan in any scholarly use which may be made of any material in my thesis.

Requests for permission to copy or to make other use of material in this thesis in whole or part should be addressed to:

Department of Geography and Planning
117 Science Place
University of Saskatchewan
Saskatoon, Saskatchewan S7N 5C8
Canada

OR

Dean
College of Graduate and Postdoctoral Studies
University of Saskatchewan
116 Thorvaldson Building, 110 Science Place
Saskatoon, Saskatchewan S7N 5C9
Canada

Abstract

Numerical computer simulations are increasingly important tools required to address both research and operational water resource issues related to the hydrological cycle. Cold region hydrological models have requirements to calculate phase change in water via consideration of the energy balance which has high spatial variability. This motivates the inclusion of explicit spatial heterogeneity and field-testable process representations in such models. However, standard techniques for spatial representation such as raster discretization can lead to prohibitively large computational costs and increased uncertainty due to increased degrees of freedom. As well, semi-distributed approaches may not sufficiently represent all the spatial variability. Further, there is uncertainty regarding which process conceptualizations are used and the degree of required complexity, motivating modelling approaches that allow testing multiple working hypotheses. This thesis considers two themes. In the first, the development of improved modelling techniques to efficiently include spatial heterogeneity, investigate warranted model complexity, and appropriate process representation in cold region models is addressed. In the second, the issues of non-linear process cascades, emergence, and compensatory behaviours in cold regions hydrological process representations is addressed. To address these themes, a new modelling framework, the Canadian Hydrological Model (CHM), is presented. Key design goals for CHM include the ability to: capture spatial heterogeneity in an efficient manner, include multiple process representations, be able to change, remove, and decouple hydrological process algorithms, work both at point and spatially distributed scales, reduce computational overhead to facilitate uncertainty analysis, scale over multiple spatial extents, and utilize a variety of boundary and initial conditions. To enable multi-scale modelling in CHM, a novel multi-objective unstructured mesh generation software *mesher* is presented. Mesher represents the landscape using a multi-scale, variable resolution surface mesh. It was found that this explicitly captured the spatial heterogeneity important for emergent behaviours and cold regions processes, and reduced the total number of computational elements by 50% to 90% from that of a uniform mesh. Four energy balance snowpack models of varying complexity and degree of coupling of the energy and mass budget were used to simulate SWE in a forest clearing in the Canadian Rocky Mountains. It was found that 1) a compensatory response was present in the fully coupled models' energy and mass balance that reduced their sensitivity to errors in meteorology and albedo and 2) the weakly coupled models produced less accurate simulations and were more sensitive to errors in forcing meteorology and albedo. The results suggest that the inclusion of a fully coupled mass and energy budget improves prediction of snow accumulation and ablation, but there was little advantage by introducing a multi-layered snowpack scheme. This helps define warranted complexity model decisions for this region. Lastly, a 3-D advection-diffusion blowing snow transport and sublimation model using a finite volume method discretization via a variable resolution unstructured mesh was developed. This found that the blowing snow calculation was able to represent the spatial redistribution of SWE over a sub-arctic mountain basin when compared to detailed snow

surveys and the use of the unstructured mesh provided a 62% reduction in computational elements. Without the inclusion of blowing snow, unrealistic homogeneous snow covers were simulated which would lead to incorrect melt rates and runoff contributions. This thesis shows that there is a need to: use fully coupled energy and mass balance models in mountains terrain, capture snow-drift resolving scales in next-generation hydrological models, employ variable resolution unstructured meshes as a way to reduce computational time, and consider cascading process interactions.

Acknowledgements

This has been a long journey and I would like to thank my friends and family who helped me along the way. My parents have been immensely supportive throughout my academic career and for their support I will be forever grateful. My wife Megan has been exceptionally tolerant and supportive, and I would not have been able to do it without her support. Thank you to my friends who were non-willing participants to long rants about school and hydrology. There are countless members of the scientific community whose feedback and discussions on my work has helped make it what it is today. Both Drs. Nic Wayand and Vincent Vionnet took a risk to work with CHM and as a result have helped me push CHM past what I expected it could be when I started; for this I am extremely grateful. My lab mates Phillip Harder, Holly Annand, Zhibang Lv, and Nico Leroux have helped maintain my sanity during this process and their support and critical feedback ensured that my work was of a higher quality. The financial support from the Governments of Saskatchewan and Canada, and the University of Saskatchewan made this research possible. Research like this thesis depends on the effort of countless field staff and students who help collect data, maintain field stations, and provide logistical support. One such member is Ric Janowicz who ensured the development and long-term success of the Wolf Creek Research Basin, and whose data was used herein. Sadly, Ric passed away before the competition of this thesis. His warmth, friendliness, and excitement for the hydrological sciences will be deeply missed. Lastly, it has been a great pleasure to work with Drs. Pomeroy and Wheater during this thesis. Their combined expertise, critical feedback, and guidance were unparalleled. Thank you both very much.

To my wife.

Contents

List of Tables

List of Figures

1 Introduction

1.1 Overview

In an era of unprecedented global change, numerical computer simulations ("models") are increasingly important tools required to address both research and operational water resource issues related to the hydrological cycle. These include improving our understanding of complex interactions affecting streamflow, helping inform water management decisions, quantifying the effects of climate- and landcover-change, determining the changing frequency of extreme events, predicting flood impacts, and designing future infrastructure (Freeze and Harlan, 1969; Mote et al., 2005; Milly et al., 2008; Nazemi et al., 2013; Debeer et al., 2015; Wheater, 2015; Musselman et al., 2017). Forecasting these changes requires successful prediction of the full sequence of hydrological processes and their cascading interactions. The research presented in thesis addresses key deficiencies in the ability to do so of cold regions modelling.

Despite the need for hydrological modelling, predictive capabilities are hampered by significant limitations in our modelling ability. For instance these limitations arise from data scarcity, substantial heterogeneity in surface and sub-surface parameters (Freeze, 1974), no single scale at which homogeneity of control volumes is achieved (Klemeš, 1983; Beven, 1989; Blöschl and Sivapalan, 1995; Shook and Gray, 1996; Clark et al., 2011b), and mis-matches between underlying theory and scales of application (Or et al., 2015). These limitations manifest as 1) uncertainties in model parameters, initial conditions, boundary conditions, and forcing data (Beven and Binley, 1992; Diaconescu et al., 2012; Raleigh et al., 2015b; Haghnegahdar et al., 2017) and; 2) incomplete process representations (e.g., sub-grid variability), selections, and linkages (Beven, 1993; Clark et al., 2008, 2011b; Hughes, 2010; Beven and Westerberg, 2011; Wagener and Montanari, 2011; Slater et al., 2013; Raleigh et al., 2015b; Fatichi et al., 2016). Including the appropriate use of physics-based equations, the number of parameters, forcing data requirements, and type of spatial discretization (Beven, 1993; Clark et al., 2008; Hughes, 2010; Hrachowitz and Clark, 2017) may help reduce the impact of these limitations.

These limitations impact predictive capacity and are exacerbated in the complex topography of high latitude and high altitude mountainous regions located throughout the world. In these 'water towers of the world' (Viviroli et al., 2007), seasonal snowpacks store a significant portion of the annual precipitation. The melting of these spatially variable snowpacks can result in the largest discharge of the year (Gray and Male, 1981;

Davies et al., 1987) and provides a critically important source of fresh water to many downstream regions (Groisman and Davies, 2001; Mote et al., 2005; Stewart et al., 2008; Woo et al., 2008), including ecosystems (Davies et al., 1987; Groisman and Davies, 2001; Boyd and Banzhaf, 2007; Stewart et al., 2008; Woo et al., 2008), and agricultural, industrial, and municipal users (Nazemi et al., 2013; Harder et al., 2019b). Data deficiencies for these mountainous regions are an ongoing issue due to, for example, instrument failures and poorly measured values due to winter-time processes such as snow-capping of instruments (Raleigh et al., 2015b), low meteorological station density (Viviroli et al., 2011; Debeer and Pomeroy, 2016), and low elevation and latitude biases in site locations (Brown and Braaten, 1998; Viviroli et al., 2011; Debeer and Pomeroy, 2016). Due to the significant role mountains play in the global water supply, the fragility of arctic and mountain ecosystems (Bring et al., 2016), and these regions' sensitivity to anthropogenic climate change (Mote et al., 2005; Duarte et al., 2012; Rasouli et al., 2015; Musselman et al., 2017), there is substantial motivation to provide timely and accurate predictions of snowpack evolution, spring ablation, and runoff in these cold-regions.

The hydrological community has focused much effort over the last 50-plus years on improving simulation capabilities. Two key activities have been a focus on improvement of the understanding of important hydrological processes and the refining of how hydrological systems are conceptualized (Klemeš, 1983; Beven, 1996, 2006b; Kirchner, 2006; Tetzlaff and McDonnell, 2008; Woo et al., 2008; Spence, 2010). Model performance in cold regions is generally improved when including physically identifiable parameters, explicit mass and energy balances, and explicit spatial heterogeneity (Bartelt and Lehning, 2002; Bowling et al., 2004; Etchevers et al., 2004; Dornes et al., 2008a; Raderschall et al., 2008; Essery et al., 2009, 2013; Fang et al., 2013; Kumar et al., 2013; Pomeroy et al., 2013; Endrizzi et al., 2014; Fiddes and Gruber, 2014; Mosier et al., 2016; Painter et al., 2016a; Harder et al., 2018). The use of physically measurable parameters may help reduce model uncertainty (Pomeroy et al., 2007; Hrachowitz and Clark, 2017), although these *a priori* estimated parameters often require calibration to be adequately constrained (Paniconi and Putti, 2015). Without care, addition of model complexity can result in overly parameterized models (Perrin et al., 2001) that are highly uncertain, difficult to verify (Beven, 1993; Hughes, 2010), and, importantly, have limited realism (they should be 'right for the right reasons'). However, the continued reliance on highly calibrated models using historical data is increasingly uncertain (Vaze et al., 2010; Brigode et al., 2013) due to a loss of stationarity in meteorological and streamflow data due to anthropogenic influences such as climate and landcover change (Mote et al., 2005; Milly et al., 2008). This motivates the careful use and development of physically realistic, physics-based models derived from field observations.

Complex systems, such as hydrological systems, may give rise to emergent phenomena. These are macroscale behaviours that arise out of the interactions of the underlying processes within a system (Darley, 1994; Goldstein, 1999; Golden et al., 2012). These behaviours can be understood from the nature and behaviour of the parts (i.e., system processes), plus the knowledge of how the parts interact (Crick, 1994). It is

likely that the hysteresis, damping behaviours (insensitivity), feedbacks, threshold behaviours, and temporal pattern dynamics observed in hydrological systems are emergent behaviours. If so, correctly simulating such behaviours may give insight into model design and aid in quantifying model simulation success. The hydrological literature contains many examples of behaviours that fit the above definition of emergence, e.g., Eder et al. (2003 temporal dynamics and scaling); Lehmann et al. (2007 dynamic connectivity); McDonnell et al. (2007 thresholds, hysteresis, scaling); Tetzlaff and McDonnell (2008 thresholds, hysteresis, scaling); Spence (2010 thresholds, scaling); Musselman et al. (2015a accumulation of processes). However, few of these studies explicitly identify these examples as emergent phenomena or consider the full sequence of linked processes that produce such emergent phenomena. There is uncertainty in the optimum level of model realism (e.g., right for the right reasons), complexity (e.g., data requirements, numerical formulations), and process representation linkages (e.g., how sub-system components are linked in model) required in cold region hydrological models to produce these behaviours (Avanzi et al., 2016; Clark et al., 2017), and this complicates simulation of these behaviours. There is likely a minimum threshold of model complexity required to produce these behaviours (Darley, 1994; Goldstein, 1999; Aziz-Alaoui, 2006; Bliudze and Krob, 2009; Golden et al., 2012). It is likely that consideration of such emergent features may represent a path towards gauging the correctness of a model by comparing not only integrated outputs (e.g., streamflow), but also individual process representations and their impact on coupled processes.

Correctly representing the distribution of landscape heterogeneity and small spatial scales to account for the high spatial variability in vegetation, soil properties, snow, and energy fluxes is thought to be a key aspect of simulating many hydrological processes, especially those in cold regions (Marks et al., 1992; Grayson and Blöschl, 2000; Pomeroy et al., 2003; Dornes et al., 2008b; DeBeer and Pomeroy, 2009, 2010). Topographic relief is a large source of this surface spatial variability, with slope and aspect the dominant contributors, resulting in immediate impacts to the hydrological system, including runoff generation in many environments (Dozier et al., 1981; Ryerson, 1984; Carey and Woo, 1998, 2001; Pomeroy et al., 2003; Woo and Young, 2004; Hiller et al., 2008; Michlmayr et al., 2008; Marsh et al., 2012; Fiddes and Gruber, 2014). Therefore, terrain representation in models is a core aspect of a model and how the physical system is conceptualized. There are a variety of approaches for terrain representation including raster grids, Hydrological Response Units (HRUs) (Flügel, 1995) or Grouped Response Units (GRUs). The desire to capture the small spatial scale heterogeneity and lateral mass and energy exchanges motivates using high-resolution spatial discretization such as raster grids versus spatially averaged approaches such as the HRU. However, as finer spatial discretizations are used, the computation costs may increase so as to render the simulation time prohibitively long. In addition, as hydrological processes have different characteristics at different spatial and temporal scales (Klemeš, 1986; Seyfried and Wilcox, 1995), refinement of grids past what may be supported by process understanding or parameter availability increases the model uncertainty and limits predictive capacity and verification (Beven, 1993). A discretization approach that is not commonly used in hydrology is unstructured triangular meshes, typically referred to as Triangulated Irregular Networks (TINs) in GIS literature. A few examples exist of

their use in hydrological models, e.g., Slingsby (2002); Qu (2004); Ivanov et al. (2004b). Due to their variable resolution, unstructured meshes likely offer a solution to the problems of a fixed spatial resolution intrinsic to structured meshes and issues of oversimplification of the landscape intrinsic to lumped approaches. Without care, unstructured meshes can be a poor approximation of the surface. Therefore, additional research is required to better understand the advantages of this approach to terrain discretization.

As models represent increased spatial heterogeneity and larger spatial extents in order to address current hydrological challenges regarding future scenarios, uncertainties in model boundary conditions, initial conditions, and model parameters increase, and these uncertainties are likely to impact model outcomes (Diaconescu et al., 2012). Over the last forty years, improvements to remote sensing platforms, such as satellites, have resulted in an increased availability of high quality and high spatial- and temporal-resolution data for a variety of Earth-systems sciences (Hoffmann, 2005). Observations of the Earth's surface have benefitted the most with the advent of Light Detection and Ranging (LiDAR) producing sub-meter digital elevation models (DEMs), e.g., Wulder et al. (2007a); Hopkinson and Chasmer (2009); Westoby et al. (2012), improved high-resolution satellite imagery, e.g., Roy et al. (2014), the introduction of unmanned aerial vehicles ("drones") (Harder et al., 2016), and improved atmospheric observations (Stephens and Kummerow, 2007). These data have, in conjunction with advances in Numerical Weather Prediction (NWP) models, resulted in high-quality datasets that are available to parametrize and initialize the surface characteristics of a model. However, sub-surface observations have not benefited to the same degree; soil moisture measurements from satellites remain restricted to the top 5 cm of the soil (Entekhabi et al., 2010), and soil properties, such as permeability, storage capacities, and hydraulic conductivity, are unmeasurable from remote sensing platforms. Sub-surface groundwater measurements, such as The Gravity Recovery and Climate Experiment (GRACE) (Tapley and Bettadpur, 2004), are at too coarse ($\approx$ 100,000 km^2 resolution (Vishwakarma et al., 2018)) a spatial resolution to be used in many hydrological models for anything other than large scale validation. However, it is likely that these observational data will become increasingly accurate, of sufficient resolution, and readily available as technology improves. As there is an increased reliance upon new and improved data sources, such as remote sensing data and atmospheric model data, next-generation models should be designed to be sufficiently flexible to utilize these data when available.

In summary, there is an ever-increasing need for using hydrological models in all aspects of scientific hydrology and water resource management. Although there have been significant advances in process understanding and model conceptualization, the above discussion has outlined a few areas where it is believed that considerable advances in hydrological modelling can be made. Specifically, the need for multi-scale (Samaniego et al., 2017), hyper-resolution (sub-1 km) (Wood et al., 2011), and snow-drift resolving (Pomeroy and Bernhardt, 2017) scales (~1 m to 100 m) in cold regions hydrological models is becoming clear. However, contemporary cold-regions models suffer from shortcomings when run over large extents at these high spatial resolutions. In addition, these models may have limited structural flexibility for incorporating multiple modelling philoso-

phies (e.g., Dornes et al. (2008b), Clark et al. (2011a)) and examining the implications of emergent and compensatory behaviours. Lastly, limitations in incorporating next-generation data products may further limit large extent application. In order to address the scientific and societal demands placed on hydrologic models, there is a need for a new generation of hydrological models.

As noted above, snow-covered mountain terrain provides large sources of freshwater and also presents one of the greatest challenges for hydrological processes. As a result, and in order to consider the main themes of this thesis, emergent and compensatory behaviours, warranted and appropriate model complexity, and high-performance computing, this thesis will concentrate on snow-covered mountain landscapes. All of the model techniques developed in this thesis will of course be applicable to snow free mountains as well.

This thesis will: 1) result in recommendations for future advances in hydrological modelling; a preliminary hydrological model required to test the above-noted emergent behaviours; and a model framework that will lead to an improved robust, multi-scale hydrological model for cold regions mountains that will assist in identifying the impacts of changing climate and vegetation cover on floods, droughts, and water supply that derive from mountainous regions. Future use of such a model will not be limited to the study area, but is expected to be applicable to many environments across Canada and elsewhere; and 2) contribute to the hydrological sciences by examining a number of issues, noted above, related to emergent phenomena and compensatory behaviours, warranted model complexity, realism, and the impact of uncertainty when considering emergence and warranted model complexity and realism in cold region mountain hydrology. This thesis will further contribute through the use of modern coding techniques and usage of computational methods that remain novel in the hydrological community.

1.2 Research Questions

Cold region hydrological models have unique requirements that motivate the inclusion of explicit spatial heterogeneity via semi- and fully distributed discretizations and field-testable process representations. This is especially true for improved understanding and simulation of process interactions and cascades, and ultimately emergent behaviours. Numerical models often require a trade-off between computational complexity (e.g., algorithms, landscape representation, initial conditions, parameters, and terrain discretization), model realism (e.g., right for the right reasons, i.e., based on field-observable data and theories), and model performance (e.g., modelled versus observed). The appropriate inclusion of explicit spatial heterogeneity and physics-based models generally improves simulation capacity and allows for capturing the spatial heterogeneity that is observed in snow-covered basins. However, using standard techniques such as raster discretization leads to prohibitively large computational costs and increased uncertainty due to increased degrees of freedom, especially at large spatial extents. Thus, there is a tendency towards lumped models or arbitrary model

reductions in order to limit these demands. Nonetheless, if emergent behaviours do play an important role in the hydrological cycle, it is likely that current hydrological models may not appropriately consider such behaviours. For example, simulating these behaviours with rigid model structures (i.e., an inability to compare process representation approaches) and neglecting spatial heterogeneity is problematic. The inability of a model to capture these phenomena is likely responsible for degraded hydrological simulations in some conditions.

This thesis will focus on a suite of tightly integrated issues that have largely been ignored by the hydrological community. It is believed that advances in these issues will produce guidelines that will influence hydrological model design and will prove important to developing the improved hydrological models needed for research and water resources management. The integrated package of issues that this thesis will address is two-fold. First, development of improved modelling techniques to efficiently include spatial heterogeneity and to allow testing of the above behaviours including: 1) warranted model complexity and appropriate process representation, and 2) the use of novel spatial discretization methods. Second, using a combination of modelling and field data, this thesis will consider the issues of process cascades, emergence, and compensatory behaviours in cold regions hydrological systems in the context of process couplings, non-linear feedbacks, and the extreme spatial variability of mass and energy.

The following research questions arise and will be addressed in this thesis:

1. What are the technical and software design decisions for a hydrological model that can enable the investigation of the impact of model structure, process representation and coupling, and spatial discretization on process cascades and emergence?
2. Can variable resolution, unstructured triangular meshes represent surface heterogeneity, including topography and vegetation, for use in a distributed model?
3. How does the coupling of mass and energy balance in snowpack models impact: a) model sensitivity to uncertainty in parameters and forcing data?; and b) possible compensatory behaviours, and might these behaviours be important?
4. Can blowing snow redistribution equations be up-scaled to variable resolution unstructured meshes to capture the spatial heterogeneity of snow covers at multiple scales?

The overall approach to addressing the above-described research questions is first to develop a model framework specifically designed to more readily represent process interactions and to test model structure decision impacts on these interactions. To do so requires a multi-scale approach to the landscape so as to be computationally tractable, but that also preserves the important landscape heterogeneities. With such a framework in place, attention must return to the smaller extents to quantify the process response of snowpack models to investigate the sensitivity and compensatory response of a key process — snowpack process representations. By doing so, investigating compensation can lead to warranted model complexity decisions based on a

response of a complex-system. Lastly, a key process that shapes the winter snowcover landscape is blowing snow. This process is known to dramatically impact spring snowcover ablation rates by creating large drifts, as well as impacting spring streamflow generation. The formation of these hydrologically important drifts arises from the feedbacks present in the system where large areas of a basin act as sources that transport snow towards drift areas. These source areas have complex, non-linear feedbacks and threshold behaviours due to topographic impacts on wind, vegetation, and snow accumulation. A new multi-resolution blowing snow model is presented, and this set of process cascades is investigated as a case study of emergence.

This approach is detailed over the following five chapters. The literature review in Chapter 2 provides the scientific context and establishes the scientific gap for new modelling approaches in cold regions hydrology. Detailed outlines of the subsequent chapters that address the research questions is given below:

To simulate the complex inter-process interactions that lead to important cold regions hydrological features, a variety of features must exist within a distributed, process-based modelling framework. Such a framework is a critical tool required in order to further investigate these processes. Chapter 3 addresses research question one. This chapter outlines the philosophy, design goals, and details of a new hydrological model, the Canadian Hydrological Model (CHM). The development of this modelling framework addresses the above outlined limitations of many existing hydrological models and contributions to cold regions modelling. This objective focuses on the overall model philosophy and design and provides a small number of cold-regions specific features and examples to pursue research questions via a distributed modelling framework.

A principal goal of CHM is to provide reduced computational and data availability costs in the surface representation, while maintaining the important heterogeneity in the landscape. To do so, a novel surface representation is introduced in Chapter 4, addressing research question two. This presents novel multi-objective unstructured mesh generation software that allows mesh generation to be constrained to an arbitrary number of important features while maintaining a variable spatial resolution. Including these additional constraints results in a better representation of spatial heterogeneity than from classic topography-only constraints. This objective provides the model framework with a surface representations that allows for capturing important surface heteroniety, a key feature of emergent, cascading processes likely of importance in hydrology.

Investigations into transferability of model structure and parameter sets has led to studies of model robustness, e.g., Bárdossy and Singh (2008); Guerrero et al. (2013). Substantial effort has been made to investigate differences in model behaviour due to process representation (Essery et al., 2009, 2013; Clark et al., 2011a; Lafaysse et al., 2017) and input forcing uncertainty (Slater et al., 2013; Raleigh et al., 2015a). This objective, outlined in Chapter 5 and addressing research question three, extends these studies by using a set of point-scale energy balance snowmelt models of varying physical and numerical complexity and realism to investigate the response of simulated snowcover and surface energy balance components to various parameter and input

perturbations. This provides a case-study of an important complex-systems feature in cold regions and allows for model complexity decisions via diagnosing the ability to capture such a behaviour.

Blowing snow redistribution is ubiquitous in cold, windswept environments such as mountainous terrain, grasslands, and arctic tundra and results in spatial patterns of snowpack ablation or deposition, leaving highly heterogeneous snowcovers (Pomeroy et al., 1997; Marsh, 1999; Sturm et al., 2001; Fang and Pomeroy, 2009; MacDonald et al., 2010; Mott et al., 2010; Winstral et al., 2013; Freudiger et al., 2017; Wayand et al., 2018). The omission of blowing snow processes is a fundamental misrepresentation of alpine snow hydrology and increases model uncertainty. However, the inclusion in distributed models increases computational costs and uncertainty. Consideration of a new model technique for efficiently representing this process is described in Chapter 6, addressing research question four. The non-linear feedbacks that result in drift and scour formations may be considered an emergent property that requires careful use of field-testable process representations.

In summary, this thesis presents a new, multi-scale cold regions model that captures landscape heterogeneity and reduces computational and data requirements via a novel landscape representation. An important cold regions process, the snowcover representation, is investigated for compensatory behaviours that can be used to make warranted model complexity decisions. Lastly, this model framework is used to efficiently model blowing snow, and the thresholds, feedback, and process cascades therein are investigated as a case study of emergence.

2 Literature review

2.1 Overview

As described in the introduction, the complex behaviours observed in hydrological systems may examples of emergent behaviours. Simulation of some, if not all, of these emergent behaviours demonstrates insight into the underlying sub-system processes and importantly, process interactions. It is likely that consideration of such emergent features may represent a path towards gauging the correctness of a model by comparing not only integrated outputs (e.g., streamflow), but also individual process representations and their impact on coupled processes, such as compensation. It may also provide better predictive capacity considering significant anthropogenic changes where traditional calibration approaches may struggle. There is substantial evidence that using spatially explicit hyper-resolution and snow-drift resolving scales and physics-based models likely provides a way towards improved predictive capacity. In addition, it likely this represents an avenue for examining emergent behaviours. However, to include these advances requires new modelling approaches and techniques. The following literature review provides the scientific context and establishes the scientific gap for investigating new modelling approaches in cold region hydrological models.

In Chapter 2.2, complex systems are defined, and the term reviewed for its applicability to hydrological systems. Specifically, this forms the foundation on which to understand the hydrological systems of interest and develop appropriate modelling systems. This links to the current understanding of emergent behaviours in hydrology, reviewed in Chapter 2.3. Key points from this section include: limited use of the term emergent behaviours in the hydrological literature despite many observations that support the existence of them; an opportunity to employ a hydrology-first working definition of emergence; and limited modelling capacity for such behaviours. In Chapter 2.4, examples of emergent processes from the hydrological literature are reviewed and the types of behaviours that numerical models should represent, but often have limited capacity to do so, are established. These examples represent a key literature gap, and it is argued here that simulation of such processes should be a priority for hydrological models. In Chapter 2.5, a review of current state-of-the-art model characterizations is done. In conjunction with Chapter 2.6, a literature gap is identified such that commonly used model technqiues may preclude the simulation of emergent behaviours, especially in a cold-regions context. This provides guidance for future model framework development. Specifically, it is found that there is a strong motivation for using physics-based, distributed models in cold regions hydrology.

However, such models often have significant burdens (e.g., computational cost, data requirements) that limit wide-spread application. New modelling approaches that attempt to solve this problem must still contend with the significant limitations and availability of meteorological data, parameters, initial conditions, and boundary conditions for many regions, including the critically important mountain headwater basins. These data constraints are described in Chapter 2.7 and although this thesis will not address the multitude of data-acquisition research topics, it will rely heavily upon currently available remote-sensed and *in situ* data. Critically, next-generation models must be poised to utilize next-generation data products, and these future products should inform model development. Lastly, state-of-the-art cold-regions process representations are reviewed (Chapter 2.8 and Chapter 2.9) to provide the context for how these processes will inform model development and data requirements, as well as how they will be integrated into a model framework with the ultimate goal of successfully simulating process interactions to produce macro-scale cold regions emergent behaviours.

2.2 Complex systems

The conceptualization of physical systems, such as hydrological systems as complex systems is the foundation upon which hydrological models conceptualize the physical system for successful simulation (Bliudze and Krob, 2009). A complex system exhibits system-wide behaviours that are due to the interaction of numerous sub-system processes (Darley, 1994; Goldstein, 1999; Golden et al., 2012). In a hydrological system, these are the numerous sub-basin and inter-computational element interactions that lead to the hydrological features of interest for numerical modelling and prediction. Such a conceptualization also provides a metric upon which successful model simulation can be judged, such that both the system and sub-system interactions are sufficiently simulated (Grayson et al., 1992; Wagener, 2003). This section provides the context for complex systems in hydrology and how this idea provides the background for model development.

A useful definition of a complex system is twofold: first, that a 'system' is a set of interconnected parts and second, that 'complex' denotes that the system has properties as a result of the interactions of these interconnected parts (Aziz-Alaoui, 2006; Golden et al., 2012). Hydrological models that aim to capture these complex systems must consider static complexity and dynamic complexity. Static complexity addresses how the system is conceptualized and assembled (as shown in a static flow chart for example) whereas dynamic complexity addresses how much temporal variability and how many process interactions are present (Aziz-Alaoui, 2006). Static complexity relates to the model structure decisions in developing a hydrological model and which process representations are included. The incorporation of increasingly complex dynamics in a model tends to result in shorter time steps, increasing spatial representation, physics-based representations, and more coupled process representations. A numerical simulation that conceptualizes a dynamic system has a step-by-step transition from one state to another (Golden et al., 2012). The dynamic progression forward in

time results in behaviour functions (process representations) transforming input data (e.g., forcing data) and thus modifying the internal system state. In short, these are system descriptions, e.g., hydrological process representations, that require simulation to understand their progression through time.

2.3 Emergence

Some complex systems may give rise to macro-scale behaviours, termed *emergent phenomena*. Described in detail below, these behaviours can be understood from the nature and behaviour of the sub-system components, plus the knowledge of how they interact (Crick, 1994). Therefore, correctly simulating such behaviours in a hydrological model provides evidence that aspects of the underlying process interactions are being sufficiently simulated. The applicability of using emergent behaviours to describe hydrological processes and quantify model behaviours is described below.

General defining characteristics of emergent phenomena include that they: exhibit radical novelty, where behaviours at larger scales are observed; demonstrate coherence or correlation and maintain some sense of identity over space or time; are system level, such that the emergent has a property of 'wholeness'; are dynamical and a product of the temporal evolution of a system; and are ostensive (perceived, apparent, and evident) (Goldstein, 1999). That is, they are a descriptive term that conceptualizes the patterns, structures, or properties exhibited on the macro-scale (Goldstein, 1999).

A description of emergence may be further refined by distinguishing between emergent behaviours as being either weakly emergent or strongly emergent. The weakly emergent view asserts that an improved understanding of a behaviour could be further understood by an improved understanding of the interacting, smaller-scale processes (Darley, 1994). That is, it allows for reducibility of the emergent behaviour to its individual processes in principle (Bedau, 2011). In contrast, the strongly emergent view asserts that a behaviour could *not* be further understood by an improved understanding of the interacting, smaller-scale processes (Darley, 1994). That is, the behaviour is irreducible and greater than the sum of its parts (Crick, 1994; Bedau, 2011). Simulating emergent behaviours is likely best done through a reductionist lens, where improved understanding and simulation of interacting sub-processes can lead to simulations of emergent behaviours (Darley, 1994). This simulation requires a 'minimum' amount of complexity to predict (Darley, 1994; Lissack, 1999; Bedau, 2011). The successful simulation of these interacting processes thus motivates continued process understanding.

The hydrological literature contains many examples of behaviours that fit the definition of emergence, such as the variability of basin properties (e.g., connectivity, mass, and energy) across varying timescales (annual, monthly, daily) (Eder et al., 2003), hillslope outflow thresholds as a result of flow pathway connectivity (Lehmann et al., 2007), hysteresis, feedbacks, threshold and scaling behaviours, and temporal pattern dynam-

ics (McDonnell et al., 2007), catchment similarity (Wagener et al., 2007) and form (Tetzlaff and McDonnell, 2008), and temporal storage dynamics (Spence, 2010). However, not all explicitly identify these behaviours as emergent phenomena or consider the full sequence of linked dynamic processes that produce such emergent phenomena. One of the few definitions of emergent behaviours was provided by Eder et al. (2003) who identifies emergent properties as related to scaling issues. Unfortunately, this only covers a narrow range of emergent phenomena. In order to overcome this deficiency in the literature, the following definition is proposed in order to cover a range of hydrological conditions: *Emergence is the arising of large-scale behaviours in a complex system as the result of the temporal and dynamic interaction of small-scale processes. Specifically, these behaviours are the result of the accumulation of non-linear interactions within the system.* In summary, many hydrological systems likely exhibit emergent phenomena due to multi-scale, non-linear processes behaviours such as thresholds, hysteresis, and dynamic connectivity.

It is proposed that in order to model and conceptualize emergence in hydrological systems, the small-scale processes and their cascading interactions must be considered, and only investigating aggregate responses, e.g., streamflow, may not provide insight into the emergent processes. Although it is an open research question as to what level of model complexity and realism is sufficient for modelling emergence in a catchment, beginning with top-down, empirical conceptualizations will likely not provide insight into the behaviours as these conceptualizations aim to simulate the aggregate response (i.e., consider the behaviour as strongly emergent). The value in considering emergent behaviours as weakly emergent is it provides motivation to understand, conceptualize, and predict the process cascades' impact across the simulation domain. That is, it aims to understand how the behaviours arise, and it may provide increased predictive capacity if these process interactions change in the future. Although considering these behaviours to be strongly emergent may be applicable to some aspects of hydrology, it is suggested here that there is likely sufficient evidence to support investigation of emergent processes in hydrology through a weakly emergent lens. Therefore, weak emergence will be considered exclusively in this thesis.

McDonnell et al. (2007) specifically cite hysteresis, feedbacks, threshold behaviours, and temporal pattern dynamics as all being emergent. It is argued that if the prediction of such complexities is to ever be possible, weak emergence must be embraced. If it is not, it is unlikely that improved predicting of extreme events or of simulating the integrated effects of climate and vegetation changes on, for example, soil moisture, evapotranspiration and streamflow can be done. Non-linearities within these processes may not be adequately conceptualized via a top-down approach. Generalization to large, lumped scales will only provide aggregate averages (Klemeš, 1983) that are unlikely to provide adequate insight into extreme events or spatially covariant processes in a basin due to a loss of the high-frequency components of the smaller-scale processes (Kavvas, 1999). Successfully simulating emergent phenomena indicates insight into the underlying process interactions. The development of such models should therefore be a long-term goal of hydrology.

2.4 Examples of emergence in hydrology

Examples of emergent phenomena are seen throughout the hydrological literature, despite not always being explicitly labeled as such. A non-exhaustive list of examples of these spatial interactions follows in order to demonstrate the importance of considering these cascading effects and how intrinsically emergence is tied to heterogeneity.

Emergent behaviours are strongly linked to the interactions of non-linear processes in a heterogeneous landscape and are likely of substantial important for many hydrological systems. Heterogeneity will be taken in this thesis to describe the spatial variability in hydrological parameters (e.g., hydraulic conductivity, porosity, slope, aspect, and roughness), boundary conditions (e.g., precipitation and wind fields), and hydrological fluxes (e.g., flow discharge, infiltration rate, and evapotranspiration rate) (Kavvas, 1999).

1) In cold regions, spatially and temporally variable winds speed due to complex topographic and vegetation interactions are key drivers of blowing snow redistribution. Wind accelerates over hills and ridge crests (Jackson and Hunt, 1975; Mason and Sykes, 1979; Walmsley et al., 1984; Wood, 2000) resulting in enhanced snowpack erosion (Essery et al., 1999). Subsequent deceleration over lee slopes, in topographic depressions, and behind tall vegetation or snow fences (Tabler et al., 1990; Pomeroy et al., 1995; Gerber et al., 2017) can result in large snowdrift deposits (Mott et al., 2008, 2018). Snowpack metamorphism and stratification can result in the formation of avalanches that can have basin-wide impacts (Zalikhanov, 1971; Elder et al., 1991). These avalanches transfer large amounts of snow from the ridge tops high above the valleys to the valley bottoms below. The massive amounts of snow accumulation in the valley bottoms, when combined with low solar radiation and low melt rates in the narrow valley bottoms, may result in the formation of glaciers that may otherwise not exist (as they exist below the snow line) (Tushinsky, 1975; Schaerer, 1988) such as the Turkestan, Lawinen, and Mustagh type glaciers of Central Asia (Hewitt, 2011).

2) Spatially variable snowpacks can, during the Spring, provide the dominant control on melt patterns such that deep snowpacks melt last, regardless of the spatial variability in fluxes (Anderton et al., 2004). At small scales, pre-melt frequency distributions are due to snow redistribution via blowing snow or canopy interception, whereas at larger scales differences in snowfall may influence the spatial variability (Pomeroy et al., 2004). Non-linear feedbacks between low-albedo areas and local lateral advection produces patchy snow covers (Shook and Gray, 1997; Harder et al., 2019a). Buried shrubs may spontaneous spring up, immediately altering the surface albedo and energetics (Sturm et al., 2001; Ménard et al., 2014a). These patchy snowcovers may profoundly affect spring melt patterns and may contribute to increased spatial variability of energy fluxes, e.g., Hood (2013); Harder et al. (2019a).

3) Sidle et al. (2001) found that observed hillslope outflow was the emergence of transient patterns of

saturation due to lateral macro-pore flow. Saturation patterns may be further variable due to energy fluxes and sub-surface ice interactions (Carey and Woo, 2001). Because of a spatial and temporal variability in soil moisture patterns, vegetation regimes could be dramatically altered. These vegetation patterns may shift from shrub-cover to forest-cover, or from tundra to shrub, thereby altering the winter-time snow accumulation, causing a feedback in soil moisture and snow regimes (Sturm et al., 2001; Ménard et al., 2014a).

4) McDonnell et al. (2007) suggests that hysteresis, feedbacks, threshold behaviours, and temporal pattern dynamics are examples of emergence. As an example they suggest is that landscape connectivity over various scales is as a result of spatial heterogeneity; as described above in point three. They further suggest that how the connectivity pathways change with time due to interactions with climate and landscape elements is an emergent property.

From the above examples, two observations can be made: first, the spatial heterogeneity of the terrain and fluxes creates many small-scale process that are heterogeneous throughout the basin, as suggested by Eder et al. (2003); second, these interactions lead to process covariances, novel cascading interactions, and feedbacks that change with time all of which ultimately produce emergent phenomena within a basin. This is likely a fundamental control of the hydrological response. Models that do not consider these interactions at a small scale, that are calibrated against the emergent processes, and have insufficient temporal and spatial heterogeneity will be fundamentally unable to predict many of the key hydrological conditions that are of concern to society under uncertain natural and anthropogenic changes and influences.

2.5 Model characterization

A hydrological model is a hypothesis of how a hydrological system functions (Savenije, 2009). Models should help improve the hypothesis; model performance should be quantified by 'appropriate' model structure, 'good' performance, and 'small' parameter uncertainty (Savenije, 2009). This depends on how the hydrological system is conceptualizatized, i.e., the scientific reasoning required to mimic observed hydrological phenomena (Young, 2013). The way in which this conceptualization is done can dramatically impact the kinds of simulated behaviours possible. This section provides context for the current state-of-the-art model characterization and how these characterizations may shape the ability to reproduce observed complex-system and emergent behaviours.

Classification schemes describe how the model represents aspects of the physical world. For example: how spatial heterogeneity is characterized, the degree to which effective parameters exist and are calibrated, and the number of parameters and boundary conditions required that are physically measurable. Wheater et al. (1993) suggest models should be classified as one of physics-based, conceptual (a priori model structure

and calibration from observations), or metric (relationships derived primarily from observations). Model conceptualization falls broadly into two groups: top-down and bottom-up.

Top-down approaches (conceptual/metric) examine the system to determine the dominant processes and the system is modeled from this viewpoint (Savenije, 2009). With limited process representation, complexity and realism is added until the model performs 'adequately'. The parameter sets may not be physically measurable or the parameters may be the result of lumping multiple physical processes into a single term. For example, they may be conceptual representations of spatially and temporally heterogeneous aspects of the hydrological system (Vrugt et al., 2008). Calibration is used to obtain optimal values for these parameters, often using *a priori* knowledge of the basin to guide the selection (Beven, 1993). However, calibration is susceptible to situations where a good fit is obtained at the expense of unrealistic values for some parameters due to compensating for conceptual errors in the model structure and parametrization (Klemeš, 1983). Noisy input data can also result in poor calibration results for metric approaches (Schoups et al., 2008). Different model structures and parameter sets may equally result in 'good' performance due to equifinality (Beven, 1993) — correct results do not imply correct model conceptualization (Savenije, 2009). The ability to represent small-scale process interactions is generally non-existent. However, these types of models allow for an initial conceptualization of a system and may help inform the structure of bottom-up models. Although top-down approaches are simpler to parametrize due to the limited number of variables required, due to the spatial and temporal averaging this approach may not allow for the development of emergent phenomena, and hence be unable to simulate important hydrological phenomena.

In contrast, a bottom-up approach follows a reductionist viewpoint whereby increasing model complexity, realism, and spatial and temporal resolutions are thought to provide improved predictive capabilities. These approaches tend to be physics-based models that use a limited amount of calibration, and utilize equations derived from first principles (Wheater et al., 1993). Many process representations are included and a first-principles mass-energy balance conservation approach is used for each spatial model unit, e.g., raster grid cell or HRU. In cold-regions this approach tends to improve simulations (Bartelt and Lehning, 2002; Bowling et al., 2004; Etchevers et al., 2004; Dornes et al., 2008a; Raderschall et al., 2008; Essery et al., 2009, 2013; Fang et al., 2013; Kumar et al., 2013; Pomeroy et al., 2013; Endrizzi et al., 2014; Fiddes and Gruber, 2014; Mosier et al., 2016; Painter et al., 2016a; Harder et al., 2018). Such approaches encourage using physically measurable parameters where possible and landscape discretizations that exclicitly represents observed landscape hetereogenity (Dornes et al., 2006; Pomeroy et al., 2007; Hrachowitz and Clark, 2017). However, care must be taken to avoid over-parameterized models (Perrin et al., 2001) that are highly uncertain and difficult to verify (Beven, 1993, 2006a; Perrin et al., 2001; Das et al., 2008). Using increasingly complex conceptualizations of a system does not always correlate with improvements in the results (Grayson et al., 1992). *A priori* estimated parameters may still require calibration to adequately constrain them (Paniconi and Putti, 2015) as in principle these may be physically measurable parameters but not in practice (Beven, 1993;

Savenije, 2009; Beven and Young, 2013). Mismatches in scales between model elements and observed scales can limit validation (Beven, 1989). The use of models with limited calibration is increasingly important for simulating future conditions as climate non-stationarity increases the uncertainty of highly-calibrated models (Vaze et al., 2010; Brigode et al., 2013). Distributed, physics-based models are thus often the most appropriate type of hydrological model for simulating distributed cold-region state variables (Dornes et al., 2008a; Fatichi et al., 2016), simulating areas of extreme heterogeneity (Kumar et al., 2013), or when simulating process interactions (Horne and Kavvas, 1997; Dornes et al., 2008a; Maxwell and Kollet, 2008). These improvements motivate the continued development of spatially discrete, physics-based models despite the difficulties associated with careful use.

To summarize, the hydrological literature has considered the problem of appropriate model complexity from two distinct points of view: first, increasing the complexity and realism of conceptual and calibrated models (top-down), and second decreasing the complexity of physics-based models (bottom-up) in an attempt to find the middle ground. There remains considerable debate in the hydrological community as to which approach will lead to the needed improvements in hydrological models. It is clear that there is a need to utilize hydrological models that are realistic enough to sufficiently (as defined by the end-user) simulate the important hydrological processes, whilst remaining correct for the right reasons. However, it is often difficult to determine the best of these approaches as diagnosing model performance is often done solely by comparing a single integrating output, such as streamflows. Whilst it is extremely important to properly simulate streamflow, using only streamflows to test model predictive ability does not allow for the determination of the ability to predict the internal states, especially in cold regions. An alternative approach is to diagnose model performance by considering and quantifying modelled system behaviours, including feedbacks, process interactions, and compensating behaviours.

2.6 Spatial representation

Complex-system behaviours are strongly linked to the dynamic interactions of non-linear processes in a heterogeneous landscape. Therefore, how a model represents this landscape is a key component of model characterization. This is especially true with respect to the possible prediction of complex sub-basin processes and cascading process interactions. This section reviews how current state-of-the-art models represent the landscape and provides context for spatial representation choices for next-generation models that aim to simulate emergent behaviours.

Scale corresponds to the level of aggregation at which a process is considered (Klemeš, 1983, 1986; Kavvas, 1999). It may mean the temporal resolution (e.g., hourly, daily, or monthly) or spatial resolution (e.g., 1 m, 1 km, or 30 km). Parameterizations of processes may be only appropriate at a given scale and are often not

immediately applicable to higher or lower scales (Klemeš, 1983). This is because parameterizations developed for use at a larger scale are often averages of the processes dominant at a lower scale level; one element at a given scale arises from an interaction of a vast number of elements at a lower scale (Klemeš, 1983). Hydrological processes have different characteristics at different spatial and temporal scales with varying degrees of sensitivity to the landscape heterogeneity (Klemeš, 1986; McDonnell et al., 2007). Because of this, hydrological models may operate at a variety of scales simultaneously or extrapolate information between various scales. This transfer of information is termed scaling, and the various problems associated with this are scale issues (Blöschl and Sivapalan, 1995).

Although not clearly articulated in the literature, scaling within hydrology is intrinsically linked to emergent phenomena, e.g., Eder et al. (2003); McDonnell et al. (2007), and the spatial and temporal scales of process interactions are an important aspect of emergence in catchments. There is a tendency towards higher spatial and temporal resolution (Melsen et al., 2016). Because many hydrological models operate at a fixed resolution, the algorithms selected represent the dominant processes at that scale of representation (Seyfried and Wilcox, 1995), and thus non-linear process interactions are included within this integrated result.

The spatial variability of terrain is a key component to any hydrological model. Regardless of how sophisticated, physics-based, and spatially explicit a hydrological model may be, at some level the hydrological system is conceptualized and aggregated into a control volume (Vrugt et al., 2008). These control volumes vary from lumped aggregations at the basin scale to fine-scale model elements metres in size.

A structured mesh, also known as a raster or grid in the GIS nomenclature, is a landscape representation where the landscape is discretized by uniformly sized cells. A raster based DEM is an example of a structured mesh, where each cell has an elevation value. Raster-based hydrological models are common because their computer representation is trivial to implement using two-dimensional arrays, a feature intrinsic to modern programming languages (Tucker, 2001). Widespread use of rasters, such as in remote-sensed data, makes using rasters a natural choice in hydrological models. Despite their widespread use, rasters have a number of significant limitations for usage in hydrological modelling, the most significant being the need to use a fixed spatial resolution of the raster over the entire basin (Tucker, 2001). For regions with great variations in topography, e.g., steep slopes and large flat valleys, this results in significant computational inefficiencies. They may also increase uncertainty due to increased degrees of freedom resulting from the fixed resolution, especially at a high-resolution. This may be due to the landscape being broken up in a manner that does match either the process representation, the parameters, effective or otherwise, or the process understanding (Beven, 1993).

Unstructured triangular meshes, typically referred to as Triangulated Irregular Networks (TINs) in GIS literature, represent the topography via a set of variably sized, non-overlapping connected triangles, where each triangle face is of a constant gradient (Shewchuk, 1996; Chang, 2008). Unstructured meshes offer a

solution to the problem of a fixed spatial resolution intrinsic to structured meshes. Areas of large topographic variability can have a higher density of small triangles in order to capture the spatial variability and areas of relatively homogeneous topography have fewer large triangles. This reduction in computational elements can be up to 90% (Ivanov et al., 2004a). Despite these advantages, a practical downside is that due to widespread availability of raster data, many GIS tools do not support unstructured meshes. As well, almost all remote-sensed data are in a raster format, making a conversion to an unstructured mesh required. This may introduce further uncertainty, and this must be kept in mind when working with this representation.

The computation of lateral mass and energy fluxes must account for the irregular geometry of the triangle mesh elements. For neighbour-to-neighbour transfers, the methods used in raster models can be used. However if PDEs are discretized on the mesh, the numerical formulations require use of more sophisticated numerical methods. For example, the finite element or finite volume approaches must be used to estimate spatial gradients. However, use of these techniques on triangular meshes is common when estimating shallow water flows (Hagen et al., 2002), and has been used with success in hydrological models (Qu and Duffy, 2007; Kumar et al., 2009b).

The Hydrological Response Unit (HRU) is a semi-distributed approach that assumes that a basin can be sub-divided into uniform elements (response units) that are delineated based on a combination of one or more of elevation, land cover, slope, aspect, soil type, and precipitation (Flügel, 1995; Grayson and Blöschl, 2000). It is assumed that each response unit responds uniformly to a hydrological event, and the variability in internal dynamics of the HRU is limited compared to neighbouring HRUs (Flügel, 1995). For example, a HRU may be the portion of the basin that is 'forested, north-facing, and $< 20^{\circ}$ slope. HRUs can be at any scale, from small scale such as a hillslope, to large scale, such as a sub-basin (Pomeroy et al., 2007). Due to the HRU approach treating the landscape in a lumped manner, without care this approach suffers from a tendency towards a mean characteristic. Therefore, a 'sufficient' number of HRUs must be created to avoid this. However, this may be counterproductive by resulting in creating a distributed lumped model.

The various spatial representations outlined above represent the common range of methods used by hydrological models and demonstrates the typical trade-offs between input data requirements, computational time, and ability to explicitly represent surface heterogeneity (Clark et al., 2011b). Many studies have demonstrated that some degree of spatial heterogeneity must be considered for hydrological processes to be represented, especially in cold regions. By lumping together similar areas of the basin, the HRU approach allows for reduced computational and data demands. However, by assuming such a control volume in terrain with large changes in slope and aspect over small distances, even small basins may end up requiring a large number of HRUs to capture at least some of the important heterogeneity present. At the other extreme is the raster representation of a basin where the surface heterogeneity is represented at some fixed spatial resolution, greatly increasing the computational and data requirements. The advantage, however, is that process interactions across elements are possible and thus more explicitly represent process heterogeneity. Unstructured meshes

have the advantages of rasters, but due to the variable spatial resolution, allow for fewer computational elements, thus decreasing computational time and potentially data requirements and uncertainty versus a raster. Given the limited attention that unstructured mesh based hydrological models have been given, there is a great need for continued research to consider the potential advantages.

2.7 Data constraints

Observational data deficiencies, especially in mountainous regions, are an ongoing issue due to the extreme winter conditions (Raleigh et al., 2015b), low meteorological station density (Viviroli et al., 2011; Debeer and Pomeroy, 2016), and low elevation and latitude biases in observation site locations (Brown and Braaten, 1998; Viviroli et al., 2011; Debeer and Pomeroy, 2016). Technological improvements and miniaturization, along with decreasing costs have resulted in increasingly accessible remote sensing platforms and data sets available for hydrological modelling. However, there remain significant data limitations that impact a model's ability to simulate complex behaviours. As next-generation models are defined and built, they should be sufficiently flexible to take advantage of a multitude of existing datasets as well as be able to easily integrate future datasets. This section outlines what some of the challenges are and how they may be addressed in the future. This is to provide context for model design decisions that would provide the best possibility of successfully simulating complex behaviours.

Surface datasets have benefited the most from these technological improvements. High spatial resolution DEMs and land-cover from improved remote sensing techniques such as Light Detection and Ranging (LiDAR), high-resolution satellite images (Chen and Cihlar, 1996; Kite and Pietroniro, 1996; Corripio, 2004; Wulder et al., 2007a; Hopkinson and Chasmer, 2009; Westoby et al., 2012; Roy et al., 2014), and unmanned aerial vehicles ("drones") (Harder et al., 2016) have become common place.

Despite the abundance of these surface datasets, sub-surface heterogeneity remains difficult to measure at large spatial extents and at the resolutions required for small-scale hydrological modelling (Beven and Germann, 2013; Mohanty, 2013). Adaptation of various geophysical techniques to observe groundwater conditions, e.g., McClymont et al. (2011), have had some success however these approaches remain difficult to conduct at large spatial extents. Remote sensing platforms that directly measure sub-surface water, including soil moisture and groundwater, are now possible. The Gravity Recovery and Climate Experiment (GRACE) program (Tapley and Bettadpur, 2004) measures groundwater via gravity anomalies and has had reasonable success in estimating seasonal water cycles, e.g., Yeh et al. (2006; Tiwari et al., 2009). However, due to the large spatial scale of hundreds of kilometres, this data source remains non-ideal for small-scale hydrology. Other remote sensing platforms can provide soil moisture estimates in the top ≈ 5 cm of the soil (Mohanty, 2013), such as the SMOS platform (scales of tens-of-kilometres via microwave imaging), synthetic aperture

radar (SAR) (Hoffmann, 2005), and the soil moisture active passive (SMAP) mission (Entekhabi et al., 2010). However, direct measurements of key vadose zone soil properties, such as unsaturated hydraulic conductivity, are not possible. Approximations are generally obtained via inverse modelling or proxies such as soil moisture, land surface temperature, and/or evapotranspiration measurements (Mohanty, 2013).

Surface meteorological forcing data are sparse. Data from numerical weather prediction (NWP) models and atmospheric reanalysis products, e.g., Mesinger et al. (2006); Mahfouf et al. (2007); Dee et al. (2011);Fortin et al. (2015), are readily available for use in hydrological models. Although biases in these data are present, they have been used with success in data-sparse regions and are a way towards distributed modelling in these regions (Krogh et al., 2015; Wagner et al., 2016; Krogh and Pomeroy, 2018b).

However, few hydrological models currently take full advantage of such high resolution data sets due to problems with model structure, the potentially large increase in model run time, and even hydrologists' unfamiliarity with such data sets and the different data structures these data often are provided in. Although these remote sensing platforms do not provide an immediate solution to sub-surface heterogeneity due to their large-scale resolution, remote-sensed data are a promising future source of data. It is likely that the use of these remote sensed data (surface and, to a certain extent, sub-surface) and NWP data will allow for insight into complex system interactions that cannot be studied through point-scale observations alone, or through traditional lumped and heavily calibrated hydrological models. Further, these data will help inform decisions of model complexity, model realism, and appropriate model use. Additional challenges are associated with the computational methods used with such large datasets, and a failure to properly utilize and understand modern computational and numerical methods can impair scientific advancement. In summary, increased model resolution is likely to be supported by current and future high-resolution data products, as well as efficient use of computational resources. This inclusion may allow for improved simulation of spatial process interactions.

2.8 Snow processes

As noted earlier, there are many examples of possible emergent phenomena in cold regions. However, one that is of special importance is the integrated sequence of processes from snow accumulation, to melt, to soil moisture, to hillslope runoff, that finally leads to streamflow. It is this sequence of processes that this thesis will consider. The following will give a brief outline of these processes. A full discussion of the detailed modelling approaches required to incorporate these into a new, unstructured mesh-based model is beyond the scope of this review, but will be detailed in subsequent chapters.

In windswept environments such as mountainous terrain, grasslands, and arctic tundra blowing snow redistribution is ubiquitous. The horizontal mass transport results in highly heterogeneous snowcovers (Pomeroy

et al., 1997; Marsh, 1999; Sturm et al., 2001; Fang and Pomeroy, 2009; MacDonald et al., 2010; Mott et al., 2010; Winstral et al., 2013; Freudiger et al., 2017; Wayand et al., 2018). Wind accelerates over hills and ridge crests (Jackson and Hunt, 1975; Mason and Sykes, 1979; Walmsley et al., 1984; Wood, 2000) resulting in enhanced snowpack erosion (Essery et al., 1999). Deceleration over lee slopes, topographic depressions, and behind tall vegetation or snow fences (Tabler et al., 1990; Pomeroy et al., 1995) can result in large snowdrift deposits. Many wind models exist for gently rolling terrain, e.g., Walmsley et al. (1984); Walmsley et al. (1989); Wensong et al. (2000); Liston and Elder (2006). Although these models may produce reasonable point wind speeds, they may be unsuitable for blowing snow simulations (Musselman et al., 2015a). This is likely a further example of an emergent process where the macro-scale output (wind field) may seem correct however dependent processes are insufficiently represented. As a result of high rates of ventilation of blowing snow particles, substantial mass loss occurs due to sublimation in undersaturated atmospheres (Dyunin, 1954; Schmidt, 1972, 1982; Pomeroy et al., 1993; Bowling et al., 2004; Vionnet et al., 2014). The resulting heterogeneity in pre-melt snowcovers is an important factor for the timing and magnitude of spring runoff (Marsh and Pomeroy, 1996; Pomeroy et al., 1997; Luce et al., 1998; Woo and Thorne, 2006; Dornes et al., 2008b; Fang et al., 2013) and thus inclusion of blowing snow is critical for capturing the spatial variability of snow accumulation.

Determining the precipitation phase is critically important in mountain catchments; proper prediction is required for correcting wind effects, understanding the hydrological response to a precipitation event, and for modelling rain on snow (Marks et al., 2013). Because precipitation phase is governed by atmospheric conditions such as temperature and humidity (Stewart, 1985), estimating phase from ground based measurements is difficult at best. Various attempts to include additional atmospheric parameters include including the dew point, seasonal corrections, diurnal temperature ranges, and near-surface boundary layer structure; see Harder and Pomeroy (2013) for a detailed review. Another approach is to incorporate model output from atmospheric models that includes the required atmospheric structure and precipitation phase at each elevation of interest. In mountainous headwaters where coniferous canopies dominate, these canopies may intercept up to 60% of incoming snowfall (Hedstrom and Pomeroy, 1998; Pomeroy et al., 1998b; Roesch et al., 2001). Thus correct phase-determination is critically important for all subsequent process representations.

The underlying physics of the snowpack energy balance are governed by the available energy that is input to the snowpack. This relies on accounting for available energy instead of using empirical relations (such as degree-day, e.g., Hock (2003)) for calculating melt. For a snow pack with an upper snow-air boundary and a lower snow-ground boundary, the bulk snowpack energy balance is given by Gray and Male (1981). Once melt occurs, melt water infiltrates through the snowpack and can pond at stratigraphic horizons, e.g., created by snow metamorphism or freezing rain when this layer was at the surface of the snow pack. When water penetrates these horizons, flow fingers may form, where meltwater is conducted through narrow zones of the snowpack. As these percolate to the cold lower layers of the snowpack they can re-freeze, resulting in a major

source of latent heat to the snowpack (Marsh and Woo, 1984). As the snow pack ablates, melt water may runoff or infiltrate into the soil. The total melt energy may then be used to determine a total melt volume via the latent heat of fusion and the density of water.

Many models solve this surface energy balance equation using one, e.g., UEB (Tarboton et al., 1996), a few, e.g., SNOBAL (Marks et al., 1999), or many, e.g., SNTHERM (Jordan, 1991), snowpack layers. Although the most common approach is via a single layer, it is not ideal for deep snow packs. There are several processes that need to be solved in order to calculate the surface energy. Often the turbulent fluxes are typically estimated via Monin-Obukov similarity theory (Monin and Obukhov, 1954). Solar radiation is generally corrected for terrain slope following Garnier and Ohmura (1968), although shadowing from surrounding terrain is often ignored. If included explicitly, it is generally a variant of Dozier and Frew (1990) although the method of Montero et al. (2009) is more efficient for unstructured meshes, e.g., Marsh et al. (2011). Longwave radiation is corrected for sky view, and a variety of methods to estimate emissivity are present. The method of Sicart et al. (2006) has been well tested in the Rocky Mountains. This thesis will use the algorithms mentioned above and implemented in current-generation cold regions models of GeoTop (Endrizzi et al., 2011, 2013), SNTHERM (Jordan, 1991), Alpine3D (Lehning et al., 2006), CRHM (Pomeroy et al., 2007), and SNOWPACK (Lehning et al., 2002).

As described above, there has been substantial research in improving key components of the cold-regions surface processes representations. Capturing the spatial heterogeneity of snow mass and energy fluxes along with the cascading process interactions is a key aspect of this thesis. However, there are limitations to these approaches for use in next-generation models that aim to simulate these process cascades at large extents. For example, despite the critical importance of blowing snow in developing the spatial heterogeneity of snow mass, it is often neglected due to computational constraints. Existing algorithms have been designed for use on fixed resolution grids, increasing the computational burden. As outlined previously, there are multi-resolution approaches via unstructured meshes that may aid in reducing this computational burden. An open research question is then how to apply and adapt these existing process representations for multi-scale simulations across complex landscapes.

2.9 Runoff processes

Once water from a melting snowpack reaches the base of the snowpack it either infiltrates the soil, or runs off laterally as overland flow. It is the complex interactions of infiltration, lateral subsurface flow, and overland flow (runoff processes) that determines the timing and volume of streamflow. A brief review of these near surface processes is outlined below as they are likely strongly linked to the process interactions described in the preceding sections and likely lead to emergent behaviours.

Runoff processes in cold regions mountains are generally dominated by water inputs from spring snowmelt resulting in the largest stream discharge of the year (Gray and Male, 1981; Davies et al., 1987; Gray et al., 2001) and the seasonal melt of mountain snow covers provide water for streamflow that can affect ecosystems far downstream from the source snowpack (Groisman and Davies, 2001). Mountainous basins are characterized by spatially and temporally variable frozen thin and rocky soils (Lehning et al., 2006; McClymont et al., 2011) overlying relatively impermeable materials, such as bedrock or ice (Carey and Woo, 2001). Frozen soils have distinct thermal and hydraulic properties versus unfrozen soils (McCauley et al., 2002). Gray et al. (2001) suggest grouping frozen soils into three categories dependent upon their ability to infiltrate water. As soils thaw due to input energy, the soils become increasingly less restricted. Therefore including a coupling with the above-surface conditions is needed to correctly predict sub-surface thaw and freeze. Zhang et al. (2008) provides a detailed review of the many empirical and physics-based methods for ground thaw and freeze. Richards' equation can be modified to account for above- and below-freezing temperatures (Hansson et al., 2004; Dall'Amico et al., 2011) and may be extended to include macro-pores (Beven and Germann, 2013).

An input of water to these mountain soils leads to temporary thinly saturated zones that can be a significant contributor to event responses (Dingman, 2002), and interflow is generally the dominant runoff component (Lehning et al., 2006). Perched, locally saturated areas have been identified as a primary mechanism in a variety of steep catchments (Sloan and Moore, 1984; Tani, 1997; Rice and Hornberger, 1998; Evans et al., 1999; Carey and Woo, 2001). Pipe-flow along chains of connected macro-pores allows for a preferential runoff mechanism (Uchida et al., 1999; Carey and Woo, 2000) and can result in velocities greater than Darcian flows (Tanaka et al., 1988); see Beven and Germann (2013) for a detailed review. Although the classical Hortonian infiltration-excess overland-flow model is generally inadequate for explaining the hydrological response of many catchments (Freeze, 1974; Beven and Wood, 1983), in cold-regions where snowmelt may occur rapidly, melt rates may be larger than the frozen soil infiltration, generating high runoff rates (McCartney et al., 2006). Generally though, due to the above mentioned sub-surface heterogeneity and perched areas of saturation, certain areas of a basin may contribute more than others (Freeze, 1974) and within a given watershed, the spatial extent of the saturated areas is widely variable with time (Dingman, 2002). This is termed the variable contributing area concept, introduced by Hewlett (1961) and Dunne and Black (1970) and describes the expansion and contraction of the saturated zone intersecting with the surface. This saturation zone increases towards the surface as a result of increased water inputs. These contributing areas produce runoff in slope concavities where water arrives faster than it can be transmitted downlsope as subsurface flow, in concave slope breaks, and where the hydraulic conductivity decreases abruptly, forming perched saturated zones above low-conductivity layers (Dingman, 2002).

Due to the heterogenity of sub-surface characteristics, cold-regions runoff is spatial variable and tightly linked with areas of snow accumulation. Various models have attempted to characterize the behaviours of

cold regions runoff and a few of the well-used models are reviewed below. In GeoTop (Endrizzi et al., 2013), subsurface flow is calculated via a three-dimension solution to the Richards equation, runoff is routed according to the kinematic scheme accounting for rill formations and spatial heterogeneity of the roughness parameters, and channel flow is described with the convolution of the incoming discharge with the solution to the Saint-Venant equations. In the Penn State Integrated Hydrologic Model (PIHM) (Qu, 2004), overlandflow is solved using the Saint-Venant equation simplified to a diffusion wave equation via a non-linear effective hydraulic conductivity, sub-surface flow is solved via the Richards' equation, infiltration is caused by precipitation, Hortonian, or Dunne overlandflow. Richards' equation has been applied in cold regions with reasonable success, e.g., (Hansson et al., 2004; Rigon et al., 2006). Despite being used in cold regions, e.g., Kumar et al. (2013), frozen soils with permafrost and coupling with the surface snowcovers has not been done. In the Simultaneous Heat And Water (SHAW) model (Flerchinger and Saxton, 1989b, 1989a), a one-dimensional coupling of a multi-layer snowpack and soils are linked through a coupled heat and mass transfer and is well suited for frozen soils. The Cold Regions Hydrological Model (CRHM) (Pomeroy et al., 2007) contains various algorithms for overland flow and frozen soils and has been successfully applied in cold regions.

Like the snow processes described in the previous section, there is a clear need to capture spatial heterogeneity in runoff processes in cold regions due to the substantial control of surface snow accumulation. Significant work has been done showing success at both the HRU and fixed-raster scales in doing so. However, run-off processes are an even greater challenge than the surface snow processes due to increased uncertainty due to dramatic heterogenity in sub-surface processes, including the difficulty in observations of measurable and effective parameters, initial conditions, and boundary conditions. Using a fixed resolution representation across the landscape can increase uncertainty by over-representing areas and needlessly increasing the degrees of freedom. However, HRU-scale models may miss important spatial and temporal heterogeneity and thus miss the cascading process interactions of interest. Multi-scale models may provide a best-of-both-worlds approach that ensures the landscape is not over represented but provides sufficient heterogeneity and representation. How to integrate these processes into an unstructured mesh alongside cold-regions processes remains an open research question.

3 The Canadian Hydrological Model (CHM) A multi-scale, multi-extent, variable-complexity hydrological model – Design and overview

3.1 Manuscript status

A version of this chapter has been submitted as a manuscript to Geoscientific Model Development as is currently in review.

Marsh, C. B., Pomeroy, J. W., and Wheater, H. S., (2019), The Canadian Hydrological Model (CHM): A multi-scale, multi-extent, variable-complexity hydrological model – Design and overview, Geoscientific Model Development, www.geosci-model-dev-discuss.net/gmd-2019-109/

Author contributions are as follows:

C. Marsh: Initial idea, coding, analysis, manuscript preparation

J. Pomeroy: Idea refinement, analysis refinement, manuscript revision

H. Wheater: Idea refinement, manuscript revision

3.2 Abstract

Despite debate in the rainfall-runoff hydrology literature about the merits of physics-based and spatially distributed models, substantial work in cold regions hydrology has shown improved predictive capacity by including physics-based process representations, relatively high-resolution semi- and fully-distributed discretizations, and use of physically identifiable parameters with limited calibration. While there is increasing motivation for modelling at hyper-resolution ($<$ 1 km) and snow-drift resolving scales (~1 m to 100 m), the capabilities of existing cold-region hydrological models are computationally limited at these scales.

Here, a new distributed model, the Canadian Hydrological Model (CHM), is presented. Although designed

to be applied generally, it has a focus for application where cold-region processes play a role in hydrology. Key features include the ability to capture spatial heterogeneity in the surface discretization in an efficient manner; to include multiple process representations; to be able to change, remove, and decouple hydrological process algorithms; to work both at a point and spatially distributed; the ability to scale to multiple spatial extents and scale; and to utilize a variety of forcing fields (boundary and initial conditions). This manuscript focuses on the overall model philosophy and design, and provides a number of cold-region-specific features and examples.

3.3 Introduction

Hydrological models are important tools for understanding past and predicting future hydrological events, informing infrastructure design, and evaluating anthropogenic impacts on natural systems (Freeze and Harlan, 1969). They are used for both research and operational water resource issues under contemporary and future climates (Mote et al., 2005; Milly et al., 2008; Nazemi et al., 2013; Debeer et al., 2015; Wheater, 2015). Despite the need for hydrological modelling, predictive capabilities are hampered by significant limitations in our modelling ability due to, for instance, substantial heterogeneity in surface and subsurface parameters (Freeze, 1974), the fact that there is no single scale at which homogeneity of control volumes is achieved (Klemeš, 1983; Beven, 1989; Blöschl and Sivapalan, 1995; Shook and Gray, 1996), and mismatches between underlying theory and applied scales (Or et al., 2015). These limitations manifest as 1) uncertainties in model parameters, initial conditions, boundary conditions, forcing data; 2) incomplete process representations, selections, and linkages (Beven, 1993; Clark et al., 2008; Beven and Westerberg, 2011; Wagener and Montanari, 2011; Slater et al., 2013; Raleigh et al., 2015b; Fatichi et al., 2016); and 3) issues of complexity including the degree of physics-based equations, the number of parameters, forcing data requirements, and spatial discretization requirements (Beven, 1993; Clark et al., 2008; Hrachowitz and Clark, 2017). Without care, physically based, mechanistic approaches can result in over parameterized models (Perrin et al., 2001) that are highly uncertain and difficult to verify (Beven, 1993). Difficulty in validating a model stems from a mismatch in model element and observed scales and limited high-resolution spatially distributed data (Beven, 1989). Physically based models should be used critically, with proper appreciation of the strengths and the limitations, and dependent on the purpose of the modelling (Beven, 1993, 2006a; Perrin et al., 2001; Das et al., 2008).

Due to the significant role mountains play in global water supply as 'water towers' (Viviroli et al., 2007), the fragility of arctic and mountain ecosystems (Bring et al., 2016), and these regions' sensitivity to anthropogenic climate change (Mote et al., 2005; Duarte et al., 2012; Rasouli et al., 2015; Musselman et al., 2017), there is substantial motivation to provide timely and accurate predictions in these cold regions. However, hydrological modelling in cold regions has unique challenges compared to temperate regions. Although there is uncertainty

in the optimum levels of complexity required in cold region hydrological models (Avanzi et al., 2016; Clark et al., 2017), such models have unique requirements and considerations; a brief summary follows. The largest discharge event of the year often results from the melt of the seasonal snowpack (Gray and Male, 1981; Davies et al., 1987) and therefore substantial effort has been invested in snow model development, e.g., Jordan (1991), Marks et al. (1998), Bartelt and Lehning (2002), Vionnet et al. (2012), Leroux and Pomeroy (2017), and flexible snowcover modelling systems, e.g., the Factorial Snow Model (FSM) (Essery, 2015) and ES-CROC (Ensemble System Crocus) (Lafaysse et al., 2017). Streamflow discharge is impacted by snowmelt spatial heterogeneity that is due to: variability in surface energetics (Munro and Young, 1982; Olyphant, 1986a; Dozier and Frew, 1990; Marks et al., 1992; Carey and Woo, 1998; Pomeroy et al., 2003; Mott et al., 2013; Schlögl et al., 2018; Harder et al., 2019a), precipitation spatial variability (Lehning et al., 2008; Harder and Pomeroy, 2013; Marks et al., 2013), vegetation interception (Hedstrom and Pomeroy, 1998; Kuchment and Gelfan, 2004), and mass redistribution via wind processes (Pomeroy et al., 1993; Essery et al., 1999; Winstral et al., 2002; MacDonald et al., 2009; Mott et al., 2010). Snowmelt runoff is further complicated due to frozen soils that limit infiltration rates (Zhao and Gray, 1999; McCauley et al., 2002) such that standard infiltration representations are insufficient (Lundberg et al., 2016). Active layer depth above permafrost dramatically impacts surface characteristics (e.g., topography, vegetation, soils), streamflow seasonality, and water partitioning (Walvoord and Kurylyk, 2016). In cold regions, the numerous lakes and wetlands impact the local climate during ice-free periods (Rouse et al., 2005; Latifovic and Pouliot, 2007; Shook et al., 2015).

Numerous studies suggest that model performance is greatly improved in cold regions when including explicit spatial heterogeneity, identifiable parameter spaces, and a full range of cold regions hydrological processes, e.g., Bartelt and Lehning (2002), Bowling et al. (2004), Etchevers et al. (2004), Raderschall et al. (2008), Dornes et al. (2008b), Essery et al. (2013), Essery et al. (2009), Pomeroy et al. (2013), Fang et al. (2013), Fiddes and Gruber (2014), Kumar et al. (2013), Endrizzi et al. (2014), Mosier et al. (2016), and Painter et al. (2016a). Better understanding of the physical system instead of soley focusing on parameter optimization (Bahremand, 2015) and ensuring that models are not needlessly constrained by rigidity of model structure, choice of parametrization, and representation of spatial variably and hydrological connectivity (Mendoza et al., 2015) are expected to further predictive capacity. Physics-based models may also limit the reliance upon calibrated effective values and decrease uncertainty due to requiring physically-identifiable parameters (Pomeroy et al., 2013; Fatichi et al., 2016). The use of lightly- or uncalibrated models is increasingly important for simulating future conditions as climate non-stationarity increases the uncertainty of calibrated models (Vaze et al., 2010; Brigode et al., 2013). Distributed, physics-based models are thus often the most appropriate type of hydrological model for simulating distributed state variables (Dornes et al., 2008a; Fatichi et al., 2016), simulating catchments with extreme heterogeneity (Kumar et al., 2013), or when simulating process interactions (Horne and Kavvas, 1997; Dornes et al., 2008a; Maxwell and Kollet, 2008). These improvements motivate the continued development of spatially discrete, physics-based models.

Although the need for multi-scale (Samaniego et al., 2017), hyper-resolution (sub-1 km) (Wood et al., 2011), and snow-drift resolving scales (~1 m to 100 m) (Pomeroy and Bernhardt, 2017), is becoming clear, contemporary cold-region models suffer from shortcomings when run over large extents and high spatial resolutions and may be limited to what spatial scale they operate at. In addition, these models may have limited structural flexibility for incorporating multiple modelling philosophies (e.g., Dornes et al. (2008b), Clark et al. (2011a)), or have limitations in incorporating next-generation data products. In order to address the scientific and societal demands placed on hydrologic models, there is a need for a new generation of hydrological models that allow:

1. *Multi-scale, spatially distributed process representation*

   Although semi-distributed schemes such as the Group Response Unit (GRU) or Hydrological Response Unit (HRU) approach have had substantial success in cold regions, e.g., Pietroniro et al. (2007), Pomeroy et al. (2007), and Clark et al. (2015), complex spatial behaviours cannot be modelled unless the HRUs are constructed *a priori* to produce the behaviours. This limits simulating cascading processes and emergent behaviours, e.g., accumulation of non-linear process interactions leading to basin-wide behaviours. Representing mass and energy heterogeneities and interactions, at multiple spatial scales (Hrachowitz and Clark, 2017; Samaniego et al., 2017), and moving towards regional predictions (Sivapalan, 2017) has been suggested as a path to improving predictive capacity. Fully distributed, raster-based models are inefficient with the need for many raster cells, greatly limiting the applicability for both high resolution, and over large extents. The deficiencies in HRU, GRU, and raster-based models points towards a need for an improved terrain representation that allows both high resolution as needed and applicability for modelling over large extents.

2. *Flexible model structure*

   Many models use a rigid model structure that does not allow for easily changing model algorithms nor easily testing different algorithms or hypotheses. An improved approach is to allow process modularity for easily modifying aspects of a model's structure and complexity. Such model flexibility has been present in many rainfall-runoff models, e.g., MMS (Leavesley et al., 2002), FUSE (Clark et al., 2008), SUPERFLEX (Fenicia et al., 2011), but to the authors' knowledge, such modularity in cold-region models has been limited to the Cold Regions Hydrological Model (CRHM) (Pomeroy et al., 2007) and SUMMA (Clark et al., 2015). These are both modular, physics-based, semi-distributed hydrological response unit (HRU) cold region models. A flexible model structure should allow for easily scaling between temporal scales (i.e., time-stepping), spatial extents, spatial resolutions, and process representations as required. Assumptions on explicit coupling between processes leads to difficulty in testing different process representations and limits inclusion of existing code. Despite the rich set of cold regions snow and hydrological models, e.g., Alpine3D (Lehning et al., 2006), iSnobal (Marks et al.,

1998), GeoTOP (Endrizzi et al., 2014), MESH (Pietroniro et al., 2007), CRHM (Pomeroy et al., 2007), SUMMA (Clark et al., 2015), SRGM (Gelfan et al., 2004; Kuchment and Gelfan, 2004), ESCROC (Lafaysse et al., 2017), and VIC (Cherkauer et al., 2003), there are no explicitly distributed, modular cold regions models.

3. *Ease of changing model parameters, initial/boundary conditions*

   Model parameters, initial conditions, and boundary conditions are uncertain in hydrological systems and are a significant constraint on model complexity and validity. Hard-coded parameters can be a significant source of uncertainty as they are effectively treated as physical constants (Mendoza et al., 2015). Modern models must be developed so that changing initial conditions, parameters, and all aspects of the model configuration are trivial and easily done within the context of an uncertainty framework. Due to the long temporal durations for which climate change scenarios are done, flexibility in changing surface parameters with time, e.g., vegetation cover, needs to also be possible.

4. *Efficient use of computational resources*

   Unlike GRU or HRU based models, distributed models are generally discretized using a raster approach with a fixed spatial resolution. This can lead to either increased computational requirements or non-optimum use of computer resources due to the over representation of the surface (e.g., homogenous locations), while choosing a coarser sized mesh may result in failure to capture quickly varying, and extremely important heterogeneity. Because of the general over representation of topography via a fixed-resolution raster, these distributed models become difficult to parametrize, and computationally expensive to run, limiting their applicability to large spatial extents. Using more efficient terrain representations as well as modern high-performance computing paradigms can reduce this wasted computational effort.

5. *Allow appropriate model complexity*

   Raster-based models with high resolution grid cells, and wasted computational effort as noted above, often led to arbitrary complexity reduction and process removal due to computational constraints. Reducing the model runtime is often a justification for simpler conceptual models, for simpler landscape representations, and for fewer computational elements. Hydrological model complexity should be warranted based upon the simulation results and needs and not for simplicities sake.

Although there are substantial advantages to the benefits of using physics-based, fully distributed models, data (forcing and validation) and computational limitations that have slowed their development and adoption. However, recent technological progress has been progressively removing some of these limitations. For example, unmanned aerial vehicle (UAV) imagery is providing sub-metre digital surface and elevation maps (Bühler et al., 2016; Harder et al., 2016), vegetation classification (Spence and Mengistu, 2016), hydrologi-

cal features (Spence and Mengistu, 2016), as well as initial conditions, e.g., snowcover (Bühler et al., 2016; Harder et al., 2016). Surface geophysical methods are improving characterization of large-scale subsurface properties (Hubbard et al., 2013). Remote sensing products of soil properties are of increasingly higher quality (Mohanty, 2013), and high resolution satellite imagery can be used to diagnose spatial patterns of snowcover (Wayand et al., 2018). Wide-spread access to High Performance Computing (HPC) resources, e.g., Compute Canada [Canada], Extreme Science and Engineering Discovery Environment (XSEDE) [United States], National Computational Infrastructure (NCI) [Australia], Horizon2020 initiative [European Union], can help offset the increased computational cost of the simulations and of the uncertainty analysis needed to constrain *a priori* estimated physically-based parameters (Paniconi and Putti, 2015). Lastly, efficient uncertainty analysis frameworks such as VARS (Razavi and Gupta, 2016), can also decrease the total number of required simulations to estimate uncertainty, further reducing the computational burden. However, estimates of critical subsurface properties such as hydraulic conductivity cannot be represented a priori with sufficient confidence, nor at the correct scale, viz. effective model element parameters (Binley et al., 1989), to avoid calibration (Freeze, 1974).

In summary, models will always require a trade-off between computational complexity (e.g., algorithms, landscape representation, initial conditions, parameters, and terrain discretization) and model performance (e.g., modelled versus observed). Cold region hydrological models have unique requirements that motivate the inclusion of explicit spatial heterogeneity via semi and fully distributed discretizations. To simulate the complex inter-process interactions that lead to important hydrological features, a variety of features must exist within a distributed, process-based modelling framework.

This manuscript outlines the philosophy and details of a new hydrological model, the Canadian Hydrological Model (CHM), and how the development of this modelling framework addresses the above outlined limitations of many existing hydrological models and contributes to cold regions modelling. This manuscript focuses on the overall model philosophy and design and provides a small number of cold-region specific features and examples.

3.4 Design and Overview

3.4.1 Overview

The Canadian Hydrological Model (CHM) is a spatially distributed, modular modelling framework. Although not restricted to cold regions, it is designed with cold region processes in mind and has various capabilities that facilitate the modelling of these domains. The design goal of CHM is to use existing high quality open source libraries and modern high-performance computing (HPC) paradigms. By providing a framework that allows

for as loose or tight a coupling between processes as required, CHM allows integration of current state-of-the-art process representations and makes no assumptions about the complexity of these process representations. For example it allows testing of the representations in a consistent manner, diagnosing model behaviour due to parameter changes, process representation changes, and basin discretization. Spatially, it allows for domains at point (10^{-6} km^2), hillslope (1 km^2 to 10 km^2), basin (100 km^2), regional (8000 km^2), and provincial/state ($>$ 1 000 000 km^2) scales. The following sections outline the framework features, including terrain representation, surface parameterization, process representation, meteorological inputs, parallelism, uncertainty analysis, visualization and analysis, and adaptation of raster algorithms. Although the CHM will eventually include the entirety of the hydrological cycle, snow accumulation and surface meteorology processes are currently implemented. Additional model components are being developed, and will be available in future versions of CHM.

3.4.2 Terrain representation

The spatial variability of terrain is a key component to any model and is an important component of model complexity. Regardless of how sophisticated, physics-based, and spatially explicit a hydrological model may be, at some level the hydrological system is conceptualized and aggregated into a control volume (Vrugt et al., 2008). Structured meshes, also known as rasters and grids, are a landscape discretization where the landscape is discretized by uniform sized cells. Raster-based hydrological models are common (Tucker, 2001) because their computer representation is trivial, and widespread use of rasters, such as in remote-sensed data, makes using them a natural choice in hydrological models. However, rasters have a number of significant limitations, the most limiting being a fixed spatial resolution over the entire basin (Tucker, 2001). This results in potentially large computational inefficiencies due to over-representation of topography. This arises as a result of requiring small raster cells (elements) to capture the spatial variability in areas of high topographic variability or (sub-) surface variability (e.g., vegetation, soils), which results in over-representation of areas that have limited spatial variability. Coarse resolution rasters also have discontinuities in the elevation data, where adjacent cells may have large elevation differences.

Unstructured triangular meshes, sometimes referred to as Triangulated Irregular Networks (TINs), represent the topography via a set of irregularly sized, non-overlapping connected triangles, where each triangle face is of a constant slope (Chang, 2008). Areas of large topographic variability can have a higher density of small triangles in order to capture the spatial variability and areas of relatively homogeneous topography have fewer large triangles. This a more efficient terrain representation than rasters (Shewchuk, 1996), and may have up to a 90% reduction in computation elements (Ivanov et al., 2004a; Marsh et al., 2018). Despite these computational advantages, a practical downside is that due to the widespread availability of raster data, conversion to an unstructured mesh is required. This results in increased uncertainty due to aggregation of the

landscape into control volumes. The CHM uses a novel multi-objective approach for unstructured triangular mesh generation, *Mesher*, detailed in Marsh et al. (2018). A brief summary follows: quality Delaunay meshes are generated ensuring a smooth graduation between small and large triangles; triangles are bounded with minimum and maximum triangle areas to ensure process representations match the physical scale; triangles are generated to fulfil tolerances (e.g., RMSE) to the underlying topographic raster and other important landscape features such as vegetation and soils. This mesh generation attempts to limit the amount of error introduced by the approximating surface given by the unstructured mesh and provide mechanisms to ensure spatial heterogeneity in the landscape is correctly preserved.

Using this mesh generation, simulation domains can be constructed at a variety of spatial extents, and importantly, spatial scales. An example of this variable resolution triangulation mesh for a region west of Calgary, Alberta, Canada in the Canadian Rockies is shown in Figure 3.1. The triangular edges are shown in grey lines. The variable resolution produces larger triangles in the valley bottoms, where topographic variability is limited, and small triangles in the mountains, where the heterogeneity is greater. This allows for matching the process representation to the correct model length scale. Further constraints could ensure streams are accurately defined.

3.4.3 Triangle parameterization

Setting values of parameters for the triangles, such as assigning vegetation or soil type to the triangle, is done during the mesh generation phase. The parameter values are stored in a file separate from the underlying mesh, and thus can be easily changed at run time. This allows for easily investigating the impact of parameter values on outputs. The parameterization of the triangles is done by a) determining the valid raster cells under each triangle and b) calculating an error metric for these cells and assigning this value to the triangle. Maximum and mean are the two most commonly used methods, but it can be any user-defined function. For classified data, the mode is used. This would allow, for example, selection of the most dominant landcover class. In addition, a user-specified classifier function can be given to easily classify continuous input parameters; e.g., classifying vegetation-heights into vegetation classes. Lastly, CHM provides mechanisms to write model output to a format that can be used as input; that is, CHM can use its output to set triangle values for future simulations.

3.4.4 Modular process representation structure

A hydrological model is a hypothesis based on assumptions of how a hydrological system works (Savenije, 2009). Modular model structures allow for rigorously testing process representations and have been used with success in cold regions hydrology, e.g., Cold Regions Hydrological Model (CRHM) (Pomeroy et al., 2007),

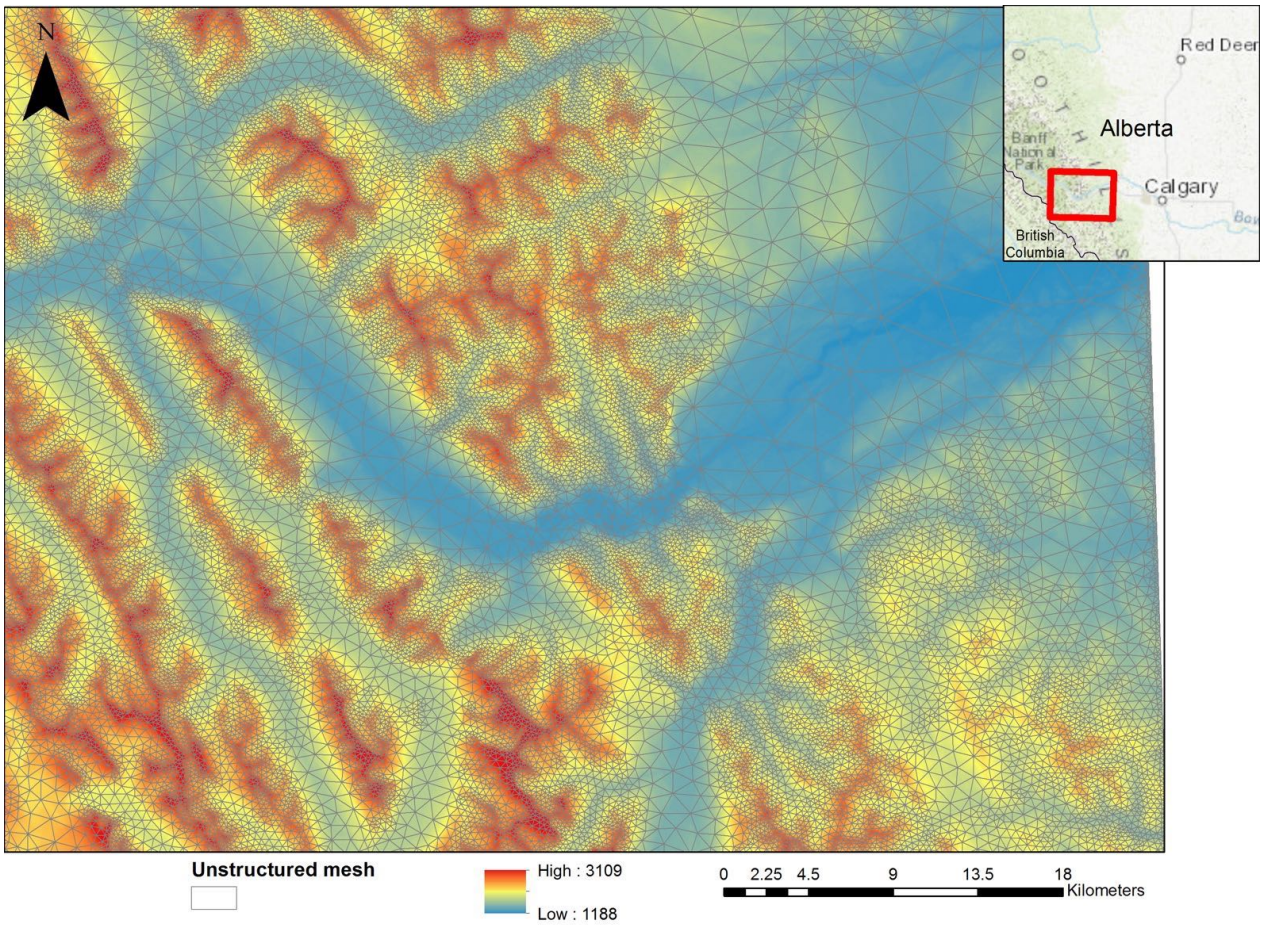

Figure 3.1: Example of variable resolution triangulation mesh as produced by Mesher for a region west of Calgary in the Canadian Rocky Mountains. The triangular edges are shown as grey lines overlain on the original DEM.

and Structure for Unifying Multiple Modeling Alternatives (SUMMA) (Clark et al., 2015). A key feature of CHM is that it provides a modular process representation that is suitable for distributed modelling, while maintaining high computational performance and flexibility.

In CHM, process representations are conceptualized into *modules*. A principal design goal of the module system is that a module has an enforced set of pre- and post-conditions. Pre-conditions represent the variables that must be computed prior to a given module running, and post-conditions encapsulate variables that must be computed by the currently running module so-as to be available as input for other modules. At run time, the user-selected set of modules are linked together into a directed acyclic graph based on these variable dependencies, and module execution order is determined via a topological sort of this graph. This sort ensures that modules are run in an order so-as to fulfill the pre-condition (i.e., the variable dependencies). Linkages between modules showing these dependencies are shown in Figure 3.2. The lines with arrows show how variable dependencies are resolved between modules. The lines going from a module are the post-conditions that satisfy the pre-conditions of the next-to-be-run module. In this example, a snowcover model, Snobal, is being driven by meteorology with the output of Snobal being used as input to a frozen soil infiltration model (Gray_inf).

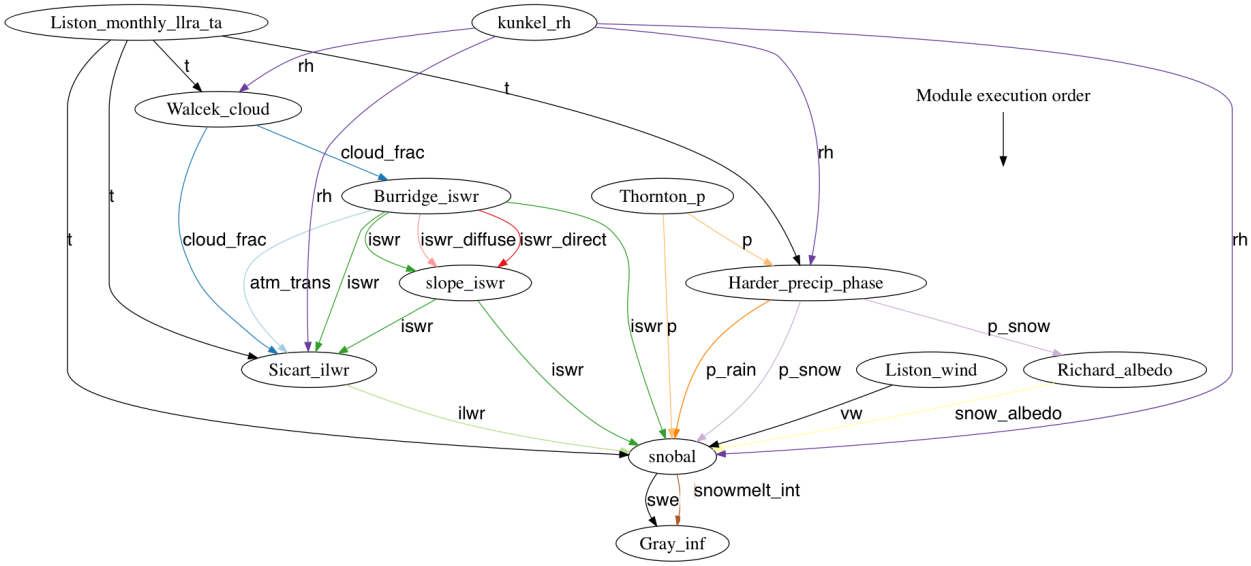

Figure 3.2: Directed acyclic graph showing module dependencies. Lines point to the module that requires the listed dependency. In this example, a snowcover model, Snobal, is being driven by meteorology in order to drive a frozen soil infiltration model (Gray_inf)

The hydrological literature has a diverse set of process representations that are either one-dimensional with no lateral exchange between elements (point-scale) or are explicitly coupled with surrounding elements (Todini, 1988). CHM makes no assumption about either, and modules may either operate on a single triangle, or on the entire domain. If only point-scale modules are selected, then CHM may be optionally run at a point-scale, effectively disabling the rest of the distributed framework. As there are substantial merits to mixing

top-down and bottom-up process representations (Hrachowitz and Clark, 2017), CHM makes no assumptions on the complexity or type of process representation in a module – modules may be a mix of complex physics based representations and conceptual representations. This also applies to process coupling. For example, a module could be a single process (e.g., a snow model), a coupled set of processes (e.g., coupled heat and energy snowmodel + frozen soil routine), or an entire existing model.

Due to the strict pre- and post-conditions required for module dependency resolution and the abstraction used in CHM, existing libraries and code can be used in a model. There is no need to rewrite the code. Therefore, any code that may be called via a C interface (e.g., Fortran, R, Python, Matlab) is suitable to be used (with a few considerations) as a CHM module. Shown in Table 3.1 are a list of the processes currently available in CHM.

Table 3.1: Cold regions surface process representations currently available in CHM

Process	**Type/name**
Canopy	Open/forest (exp/log) (Pomeroy et al., 1998b; Ellis et al., 2010)
Snowpack	2-layer Snobal (Marks et al., 1999); Multi-layer Snowpack (Bartelt and Lehning, 2002); Various albedo e.g., CLASS (Verseghy, 1991)
Soil	Frozen soil infiltration (Gray et al., 2001)
Snow mass redistribution	PBSM3D (Marsh et al. (2019), in review); Snowslide (Bernhardt and Schulz, 2010)

3.4.5 Input meteorology

Input meteorology is prescribed as a point source (herein, 'virtual station') defined by latitude, longitude, and elevation. However, a virtual station may have an arbitrary location and elevation and need not be within the simulation domain, nor correspond to a real meteorological station. This allows a virtual station to be located at, for example, the centre of a numerical weather prediction output grid centre. Because all input meteorology is given as a point source, various spatial interpolants are present in CHM to provide a distributed field across all triangles.

Spatial interpolates are present as inverse distance weighting (IDW) and thin plate spine with tension. In some cases, no interpolation is desired, and therefore a third option called 'nearest' is available – this uses the nearest virtual station without any spatial interpolation. Over large domains, such as when using numerical weather prediction output, every virtual station in the simulation domain should not be used in the interpolation to every triangle. Therefore, interpolates may query a list of either: a) virtual stations within some distance of the triangle or b) the closest n virtual stations. This ensures that only nearby virtual stations are used

to form the interpolant. Vertical elevation correction is provided by a set of specialty modules. All virtual stations are corrected to a common reference level using these modules prior to spatial interpolation. A list of these algorithms is given in Table 3.2.

Table 3.2: List of available meteorology interpolants.

Variable	Type
Air temperature	Linear lapse rates (measured, seasonal, constant, neutral stability) (Kunkel, 1989; Dodson and Marks, 1997; Cullen and Marshall, 2011)
Relative humidity	Linear lapse rates (measured, seasonal, constant)(Kunkel, 1989)
Horizontal wind	Topographic curvature (Liston and Elder, 2006); Mason-Sykes (Mason and Sykes, 1979); Uniform wind
Precipitation	Elevation based lapse (Thornton et al., 1997)
Precipitation Phase	Linear; Psychometric (Harder and Pomeroy, 2013); Threshold
Solar radiation	Terrain shadows (Dozier and Frew, 1990; Marsh et al., 2012); Clear sky transmittance (Burridge and Gadd, 1975); Transmittance from observations; Cloud fraction estimates (Walcek, 1994); Direct/diffuse splitting (Iqbal, 1980)
Longwave	T, RH based (Sicart et al., 2006); Constant (Marty et al., 2002)

Input meteorology may be given as either text files or as NetCDF files (Rew and Davis, 1990). When NetCDF files are used, the timesteps' data are lazy-loaded such that only the current timestep is read. This decreases the up-front load time as well as decreases total memory usage. An example of NetCDF usage is shown in Figure 3.3 for a domain west of Calgary, Alberta, Canada over the Bow River Valley (red = high elevation, blue = low). Virtual stations are shown in black and these correspond to the cell centres from the 2.5 km Global Environmental Multiscale (GEM) model (Côté et al., 1998) 2-day forecast.

3.4.6 Input filters

Input filters provide a mechanism to modify input meteorology during runtime. This is similar to the filter feature in MeteoIO (Bavay and Egger, 2014). Filters are assigned to each virtual station, and each virtual station may have an arbitrary number of filters. The purpose of filters is to allow, for example, values outside of a certain range to be filtered, or to perform a correction such as taking an observed windspeed at 2 m and changing it to 10 m for use later in a process module. Filters operate per-timestep and therefore can consider the previous model timestep for use in the correction; e.g., including snowdepth to perform vertical windspeed height correction.

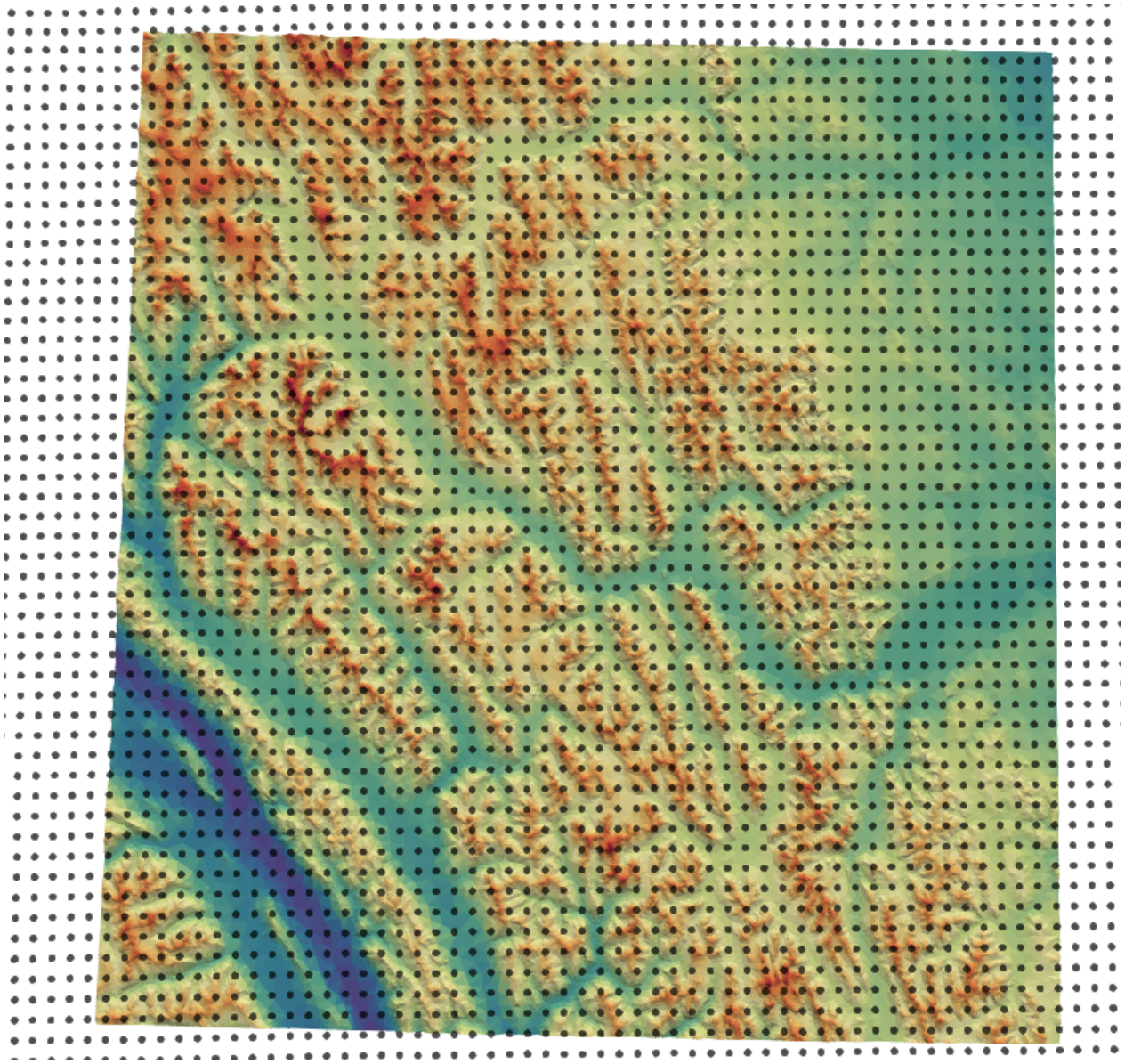

Figure 3.3: A domain west of Calgary, Alberta, Canada over the Bow River Valley is shown (red = high elevation, blue = low), with virtual stations, shown in black, that correspond to the cell centres from the 2.5 km GEM 2-day forecast.

3.4.7 Point mode

Due to the difficulty in validating spatial models due to limited spatial observations, evaluation is generally performed using point observations. CHM may be run in point-mode that allows for simulating a single triangle without lateral interactions, using a specialized input module to pass a hydrometerological station's observation data directly to the underlying process models. This is intended to simulate a point collocated with an input observation meteorology dataset and allows for traditional point simulations.

3.4.8 High Performance Computing

In CHM, parallelism is currently implemented via the shared memory OpenMP library. Coding a process representation into a module will generally result in either a point-scale module (e.g., point-scale snowcover model) or it will be a spatially coupled model (coupled advection-diffusion equation). The first type, owing to the fact it does not require knowledge of its neighbours to compute a value, corresponds to an embarrassingly parallel problem. Herein, these are referred to as data parallel. Spatially coupled models require the solution at their neighbour triangles in order to compute a solution. These neighbours, in turn, require solutions at *their* neighbours, and so on. Therefore, this is a much more challenging type of problem to introduce parallelism to. Herein, these are referred to as domain parallel. Data parallel modules automatically have the parallelism implemented and require no special consideration from the developer. Domain parallel modules, however, require the module developer to implement parallelism as appropriate for the module.

Mixing these two types of parallelism complicates the implementation of parallel code. To provide as much seamless parallelism as possible, each module declares the type of algorithm it is: data parallel or domain parallel. After the topological sort is performed to determine module execution order, the modules are scheduled together into groups that share a parallelism type. For example, consider the following sorted list of modules, with their parallelism type in brackets:

mod_A (parallel::data)

mod_B (parallel::data)

mod_C (parallel::data)

mod_D (parallel::domain)

mod_E (parallel::data)

These would then be scheduled together into 3 groups:

Group 1

mod_A (parallel::data)

mod_B (parallel::data)

mod_C (parallel::data)

Group 2

mod_D (parallel::domain)

Group 3

mod_E (parallel::data)

The modules in group 1 are run in parallel together. Because they are data parallel, only one iteration over the mesh is required. Then, groups 2 and 3 are run. This scheduling mechanism reduces the overhead of a modular approach by limiting total iterations over the mesh and minimizing thread creation. Further, as most hydrological process representations are point-scale, it allows for abstracting parallelism, resulting in "free" parallelism for the developer.

3.4.9 Uncertainty analysis

CHM provides a mechanism to easily allow modules to obtain parameter values from configuration files (JSON format), overriding the default hard-coded value. Changes to the model structure (i.e., choosing modules), initial conditions, and parameter files (e.g., landcover) are also done via this mechanism. Users may, via the command line, change any configuration value – thus simplifying uncertainty testing. This mechanism reduces situations were changes require re-compilation.

The Python code snippet shown in Listing 3.1 demonstrates changing values on the command line (via Python). This code is setting the name of three output files and adding a new module to be run.

Listing 3.1 Example to setting output file names and adding a new module.

```
1  import subprocess
2  import shutil
3
4  prj_path = "CHM.config"
5
6  cf1 = "-c output.VistaView.file:vv_dodson.txt"
7  cf2 = "-c output.UpperClearing.file:uc_dodson.txt"
8  cf3 = "-c output.FiserraRidge.file:fr_dodson.txt"
9  cf4 = "--add-module Dodson_NSA_ta"
10
11 subprocess.check_call(['./CHM %s %s %s %s %s' % (prj_path, cf1, cf2, cf3,cf4)], shell=True
```

3.4.10 Visualization and analysis

The output format used is the ParaView (Ahrens et al., 2005) unstructured mesh format. This allows for visualization of the simulation results in full 3D, with timeseries analysis in ParaView, as shown in Figure 3.4. The addition of a ParavVew plugin for CHM allows for displaying the date and time of the output. The animation view allows for exploring the spatio-temporal results in the results. It also allows for immediate diagnosis of modelling errors. There are many post-processing filters and tools available in ParaView, such as plotting an individual triangle's values over time. Because ParaView uses the Visualization Toolkit (VTK) library (Schroeder et al., 2006), the ParaView files can easily be loaded and post-processed using the Python VTK library in conjunction with traditional Python libraries such as NumPy (E, 2006) and SciPy (Jones et al., 2018).

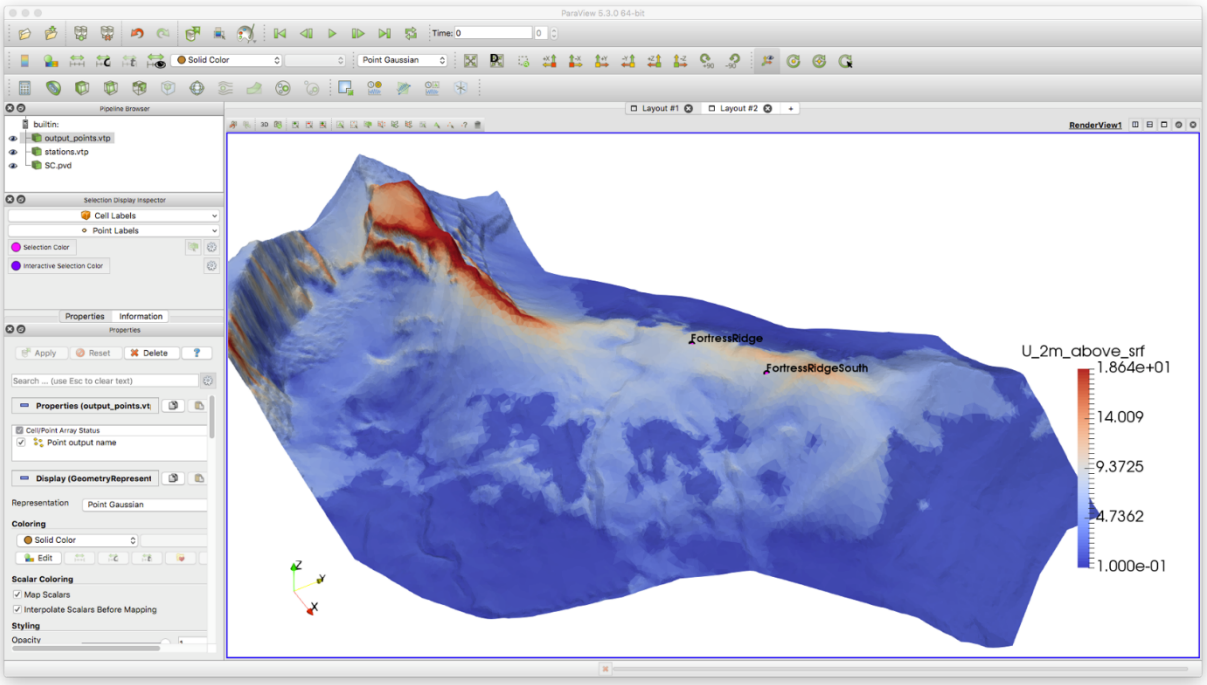

Figure 3.4: Output from CHM is in the ParaView format, allowing for timeseries analysis and full 3D visualization in ParaView.

In addition to the ParaView output, CHM provides a set of post-processing scripts that allows for converting the Paraview file to a rasterized GeoTiff or NetCDF file. This allows for using the output in post-processing algorithms that require arrays, or in GIS.

3.4.11 Adaptation of raster-based algorithms

Adaptation of raster-based algorithms is an important aspect of CHM as many existing algorithms are raster-based. Frequently, raster-based algorithms employ logic that performs queries such "look X length units in direction Y". This is easily done on a structured mesh, however on an unstructured grid, this process is non-obvious. Iterating over each triangles' neighbours results in a random walk across the domain, and brute-force iteration search methods are needlessly slow. CHM uses the k-d spatial search tree available within the dD Spatial Searching (Tangelder and Fabri, 2018) package in the Computational Geometry Algorithms Library (CGAL) to optimize spatial queries. Briefly, a k-d tree is a generalization of a binary search tree in high dimensions that decomposes the search domain into a set of small sub-domains (Bentley, 1975). This tree structure can then be reclusively searched resulting for efficient spatial look-ups. The k-d tree implementation is how nearby stations are determined. This technique for spatial searching can also be used to calculate terrain parameters, such as the terrain curvature.

3.5 Model application

3.5.1 Overview

The following section describes the methodology for evaluating various features of CHM as well as providing examples of usage. Although the CHM will eventually include the entirety of the hydrological cycle, snow accumulation and surface meteorology processes are currently implemented. Marmot Creek Research Basin (MCRB) in the Canadian Rockies in Alberta, Canada is used as a location to test the two snow modules and various models to provide the driving meterological forcing for these models that are currently implemented in CHM. The meteorological interpolants are tested in a leave-one-out validation across the MCRB. In addition, an adaptation of a raster-based terrain-shadowing for shortwave irradiance calculation is presented, demonstrating the conversion of an algorithm from a raster to unstructured mesh. Finally, the parallel computation aspect of CHM is tested by performing a scaling analysis using different number of CPUs.

3.5.2 Study Site

3.5.2.1 Marmot Creek

Marmot Creek Research Basin (MCRB) (Golding, 1970) is located in the Kananaskis River Valley of the Canadian Rockies, as shown in Figure 3.5. It is a 9.4 km^2 basin covered predominately by needle-leaf forest (Fang et al., 2013). The climate is dominated by continental air masses with long and cold winters; however

these are interrupted by frequent chinooks (Foehns) in mid-winter (DeBeer and Pomeroy, 2009). It spans an elevation range from 1700 m to 2886 m (Rothwell et al., 2016) and snow covers the upper elevations of the basin from October to June. The average seasonal precipitation is approximately 600 mm at low elevations increasing to over 1140 mm at the tree line (Rothwell et al., 2016).

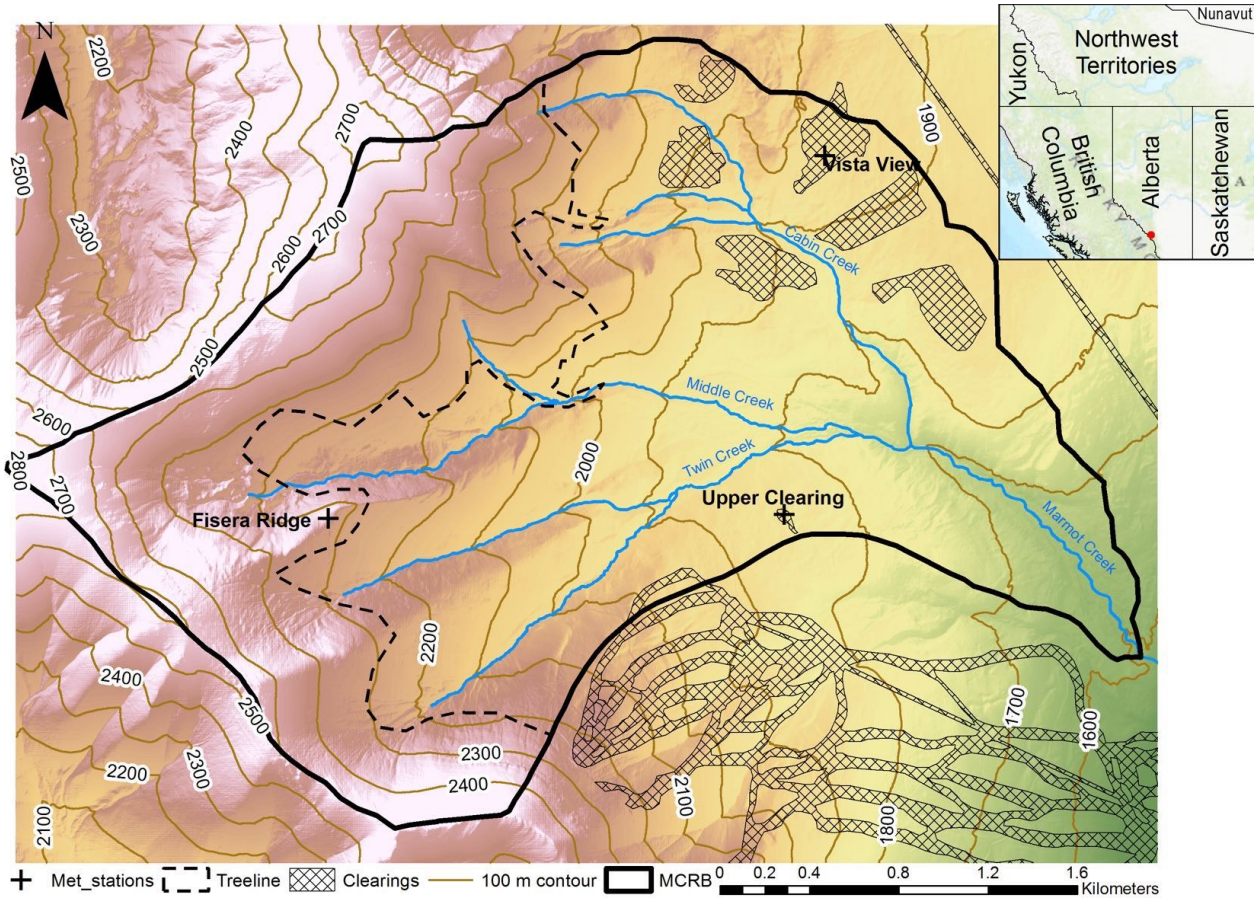

Figure 3.5: Marmot Creek Research Basin, Kananaskis Valley, Alberta in the Canadian Rocky Mountains. The basin outline is given as solid black, 100 m contour lines shown in brown, stream channels shown in blue, and man-made clearings shown as hatched areas. The meteorological stations used for this study are shown as crosses. The southern-most set of clearings is the Nakiska Ski Resort.)

3.5.2.2 Meterological observations

Meteorological observations for air temperature, relative humidity, wind speed, precipitation, soil temperature, and incoming shortwave radiation for the Upper Clearing site (1860 m), Vista View (1956 m), and Fisera Ridge (2325 m) sites, shown as crosses in Figure 3.5, were used. Gap filled, quality corrected 15 min data for the water years 2007 to 2016 (inclusive) were used. Please see Fang et al. (2019) for further details. Precipitation was measured with Alter-shielded Geonor weighing precipitation gauges and corrected for wind-induced under-catch (Smith, 2009). Precipitation phase was determined via the psychrometric energy balance method of Harder and Pomeroy (2013). Longwave irradiance was calculated following Sicart et al.

(2006). This was developed for mountainous terrain and was shown to have an error of less than 10% over the snowmelt season. This method has been used with success at the MCRB.

Periodic snow surveys of depth and SWE on long transects at Upper Clearing were conducted by various members of the Centre for Hydrology and used to quantify snowpack density. For each transect, there were at least 25 snow depth measurements and at least 6 gravimetric snow density measurements using an ESC-30 snow tube (Fang et al., 2019).

3.5.3 Models

3.5.3.1 Snow models

Point-scale evaluation of the two snow models in CHM, Snobal and Snowpack, was done at the Upper Clearing site.

Snobal (Marks et al., 1999) is a physics-based, two layer snowpack model designed specifically for deep mountain snowpacks and approximates the snowpack by two-layers where the surface fixed-thickness active layer (taken here as 0.1 m) is used to estimate surface temperature for outgoing longwave radiation and atmosphere-snow exchange of sensible and latent heat via turbulent transfer. Snobal features a coupled energy and mass balance, internal energy, and liquid water storage calculations. Turbulent fluxes are explicitly calculated via Marks et al. (1992), a bulk transfer approach that includes a Monin-Obukhov stability correction. The ground heat flux is calculated from conduction with a single soil layer of known temperature.

Snowpack (Bartelt and Lehning, 2002; Lehning et al., 2002) is a multi-layer finite element model of mountain snowpacks, with application for avalanche hazard forecasting. It describes the microphysical properties of a snowpack and includes the dynamic addition/removal of snow layers using a system of PDEs. These are discretized vertically into an arbitrary number of snow layers in a Lagrangian coordinate system. It has a coupled energy and mass balance, internal energy, and liquid water storage calculations with a bulk-transfer turbulent flux scheme with Monin-Obukhov stability correction (Michlmayr et al., 2008).

Both Snowpack and Snobal were configured to use the albedo routine of Verseghy et al. (1993). The snow models are driven with observed precipitation, shortwave irradiance, wind speed, air temperature, relative humidity, and soil temperature at a 15-minute time interval. Because of the sheltered nature of the the Upper Clearing, no blowing snow was simulated (Musselman et al., 2015b). Snowmodel parameters, such as roughness length, were set following Pomeroy et al. (2012).

3.5.3.2 Mesh generation

The unstructured mesh was created using the *Mesher* software. A 1 m x 1 m input elevation LiDAR DEM (Hopkinson et al., 2011a) was used. The resulting mesh was generated to have a minimum triangle area equivalent to a 25 m x 25 m raster and represented the topography to within 25 m RMSE. This resulted in approximately $\approx 100,000$ triangles.

3.5.3.3 Raster algorithm adaptation (shadowing)

An example of the adaptation of a raster algorithm to the unstructured mesh is shown for a terrain shadowing algorithm that calculates the shadows cast from surrounding terrain. The "look X length units in Y direction" query is required for finding obstructing terrain (e.g., a tall mountain) by searching along the azimuthal direction towards the sun. As a demonstration of the k-d tree usage in CHM, the shadowing algorithm of Dozier and Frew (1990) (herein DF90) was implemented for unstructured triangular meshes. In brief, the DF90 algorithm searches along an azimuthal direction within some horizontal distance and attempts to find terrain that is above the solar elevation. This is illustrated in Figure 3.6. For an observer A, a search along the azimuth that corresponds to the solar vector S is performed. For each terrain element found, a new vector (H) is calculated. If the slope of H is greater than that of S, A is in shadow. Terrain is searched from the observer towards some maximum search radius, in steps of size dx. Specifically, this adaptation of DF90 required using the k-d tree to find the triangle at a distance X m from the source triangle (A) along an azimuth that corresponded to the solar vector, S.

The DF90 shadowing algorithm was run for all of Marmot Creek, using the mesh described in Section 3.2. A maximum search radius of 1000 m was used, discretized into 10 steps. The DF90 implementation was compared to: observed shadowed area (see below), the Marsh et al. (2012) shadowing model, and the Solar Analyst (Fu and Rich, 1999) shadow model. Solar Analyst is an extension in the ArcGIS software by Environmental Systems Research Institute (ESRI). The observed shadowed area are from time-series images from the field campaign detailed in Marsh et al. (2012) and were orthorectified using the software of Corripio (2004). Shadow location for February 1, 2011 at 17h00 was used in this comparison. The output from CHM was rasterized from the unstructured mesh at a 1 m x 1 m spatial resolution.

3.5.4 Leave one out comparison

To test the efficacy of the meteorological interpolates, a leave-one-out comparison was conducted for the Upper Clearing, Vista View, and Fisera Ridge stations. This entailed using two of the three meterological stations as input for CHM, in order to predict the third. For example: Upper Clearing and Vista View were

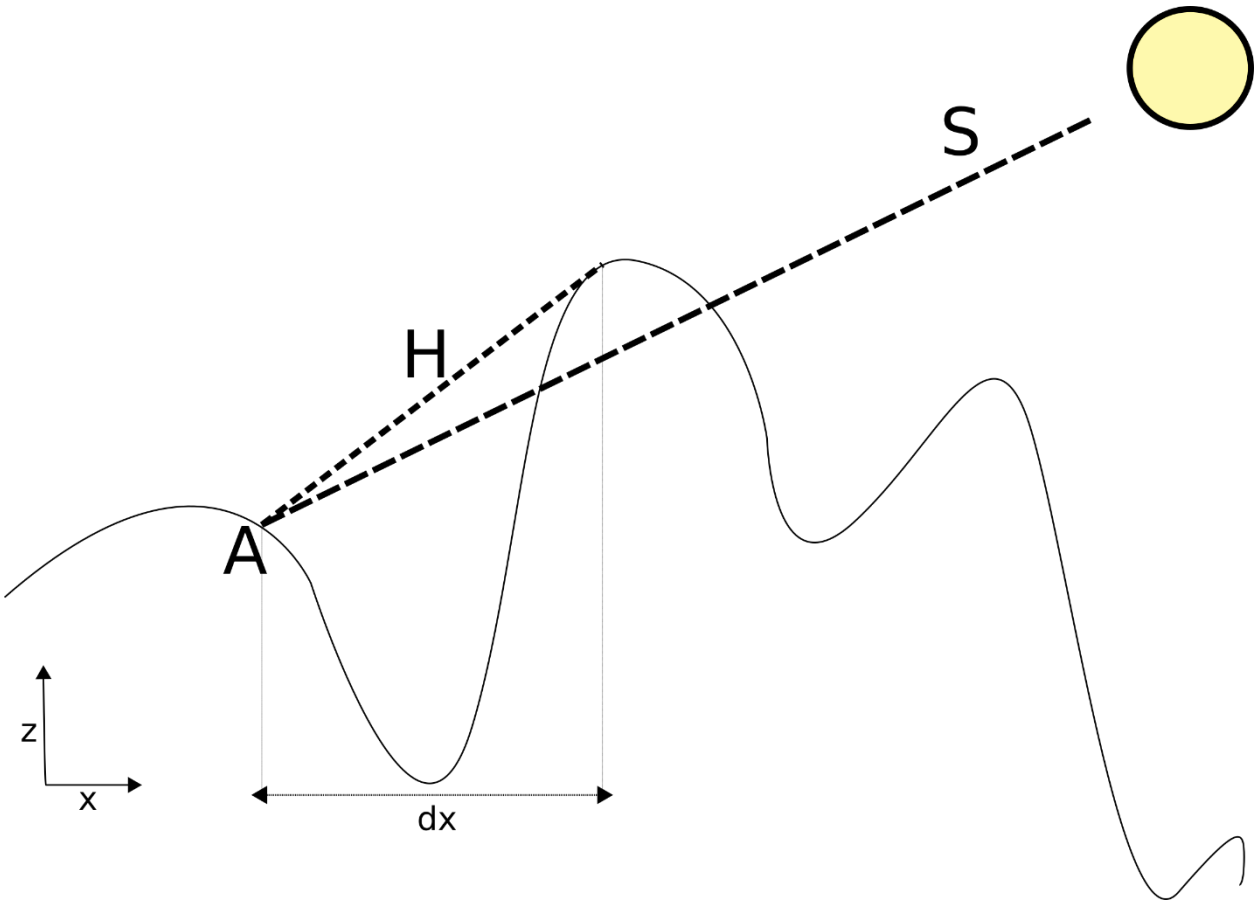

Figure 3.6: Dozier and Frew (1990) horizon shadowing algorithm. For observer A, a search along the azimuth that corresponds to the solar vector S is performed such that if the slope of H is greater than that of S, A is in shadow.

used to predict meteorological conditions at Fisera Ridge; Vista View and Fisera Ridge were used to predict Upper Clearing; et cetera.

Ten water years using 15-minute data were simulated. The following meteorological interpolants were used: terrain shadowing (Dozier and Frew, 1990), cloud fraction (Walcek, 1994), air temperature (Cullen and Marshall, 2011), relative humidity (Kunkel, 1989), precipitation phase (Harder and Pomeroy, 2013), precipitation (Thornton et al., 1997), and solar radiation transmittance estimated from observed incoming shortwave values.

3.5.5 Parallel scaling

The heterogenous Westgrid cluster Graham was used to investigate the scaling performance of the CHM code with various numbers of CPUs. The base nodes were used. These have two Intel E5-2683 v4 Broadwell CPUs at 2.1Ghz for a total of 32 cores and 128GB of RAM. The modules run include the data parallel Snobal snowpack module, as well as a domain parallel advection-diffusion blowing snow module (Marsh et al., 2019 in review).

Simulations were run for a mesh with $\approx 100,000$ triangles. The model was run with 1, 2, 4, 6, 8, 16, and 32 cores, and for each core-count scenario, the fastest of 5 runs was taken. File output was disabled for these runs. The speedup for the n core run (core_n) was computed relative to the 1-core run (core_1):

$$\text{speedup} = \frac{\text{core}_1}{\text{core}_n}. \tag{3.1}$$

3.6 Results

3.6.1 Point scale snowmodel

Shown in Figure 3.7 is the simulated snow water equivalent (SWE [mm]) for Snowpack (blue) and Snobal (red). The water year is denoted above each plot. Snow course observations are shown as black dots. The RMSE and MB values for both models, for each water year, are shown in Table 3.3 and averaged over all years in Table 3.4.

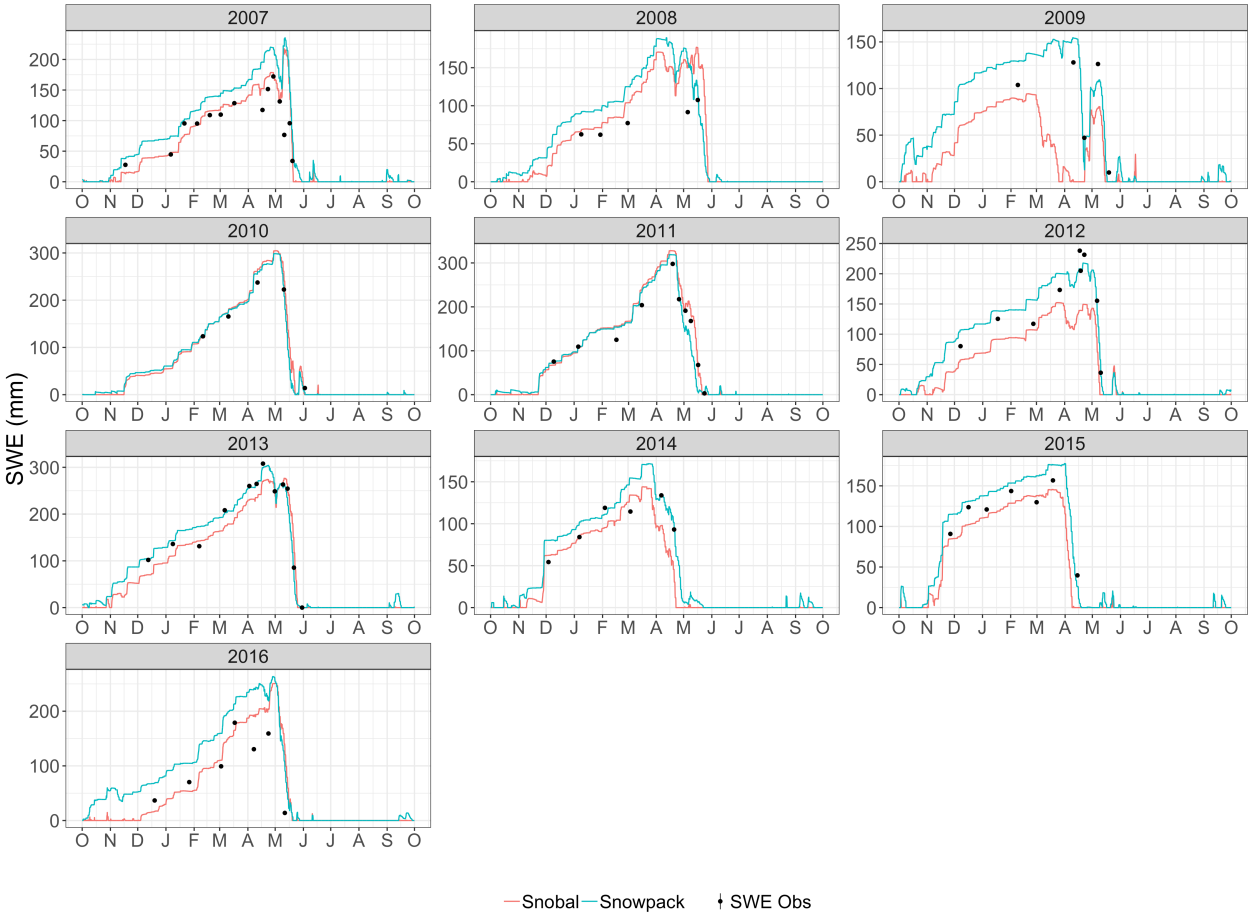

Figure 3.7: Comparison of Snobal (red) and Snowpack (blue) run as a point simulation within CHM for the Upper Clearing site at Marmot Creek Research Basin for 10 hydrological years. Manual snowcourse observations are shown as black dots with 10% uncertainty (vertical line within dot).

Table 3.3: Root mean squared error (RMSE [mm]) and Mean bias (MB [mm]) for the Snowpack and Snobal models at the Upper Clearing site, for each water year.

Year	Snobal RMSE (mm)	Snowpack RMSE (mm)	Snobal MB (mm)	Snowpack MB (mm)
2007	40.7	56.73	18.24	45.56
2008	42.47	42.42	33.65	38.15
2009	65.07	23.22	-49.54	-1.5
2010	20.55	11.24	10.81	3.94
2011	24.18	32.43	15.07	-7.578
2012	57.12	22.26	-49.05	6.92
2013	27.21	15.51	-9.591	-0.05
2014	28.81	21.12	-13.6	13.69
2015	19.19	19.41	-13.54	13.84
2016	55.55	66.87	27.08	60.7

Table 3.4: Root mean squared error (RMSE [mm]) and mean bias (MB [mm]) errors averaged over all years.

Model	RMSE (mm)	MB(mm)
Snobal	38	-3
Snowpack	31	17

In 2007, Snowpack over estimates peak SWE more than Snobal, although ablation timing between the two is identical. In 2007, early season SWE is over estimated by Snowpack although late season SWE is better estimated by Snowpack. Water year 2009 is poorly simulated in general, especially by Snobal. It is not clear what causes this poor performance. During the cold winters of 2010 and 2011, both models perform well. In 2012, Snobal underestimates peak SWE versus Snowpack. For years 2013 to 2015 Snowpack better captures peak snow and the ablation period than Snobal. In 2016 Snobal better estimates SWE as Snowpack overestimates during accumulation and for peak SWE. Snowpack tends to be more consistent in its prediction capacity, although it tends to over estimate, whereas Snobal tends to underestimate total SWE. Overall Snowpack tends to perform better than Snobal, although there are individual years where Snobal edges out Snowpack.

3.6.2 Adaptation of raster-based algorithm

Shortwave irradiance corrected for slope and aspect, with horizon (cast) shadows via an adaptation of the Dozier and Frew (1990) shadowing algorithm for unstructured meshes for the Marmot Creek Research Basin is shown in Figure 3.8. Simulation is for 2011-02-01 17:00 local time. High irradiance is shown in red, and shadows shown in dark blue; and these areas are receiving only diffuse radiation. The region north of Fisera Ridge is shown in detail in Figure 3.9. This figure shows an orthorectified terrestrial photo of a shadow passing over Mt. Collembola from Fisera Ridge. The location of the shadowed region for 2011-02-01 17:00 local time is shown for the DF90 algorithm described herein (green), the observed shadow (red), the ArcGIS Solar Analyst shadow (black), the Marsh 2012 algorithm (blue), and the white region is the region not covered by the photograph. The DF90 implementation agrees quite well with observed shadow locations and a sensitivity test (not shown) shows improved agreement with increasingly small triangles. The triangular shaped bumps along the shadow line are from the unstructured triangular mesh elements.

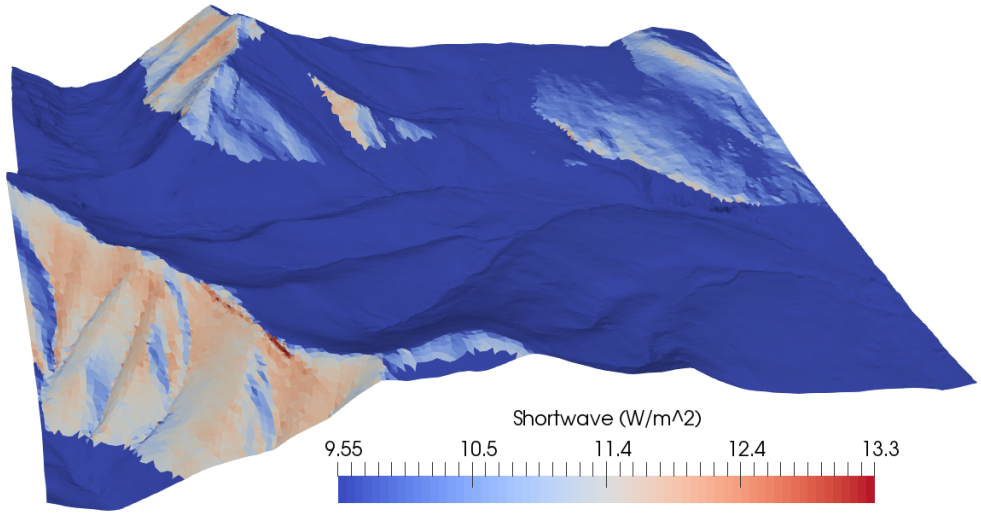

Figure 3.8: Incoming shortwave radiation for the Marmot Creek Research Basin for 2011-02-01 17:00 local time. The shadowing algorithm of Dozier and Frew (1990) (DF90) has been implemented on the unstructured mesh. Uniform dark blue are shadowed areas.

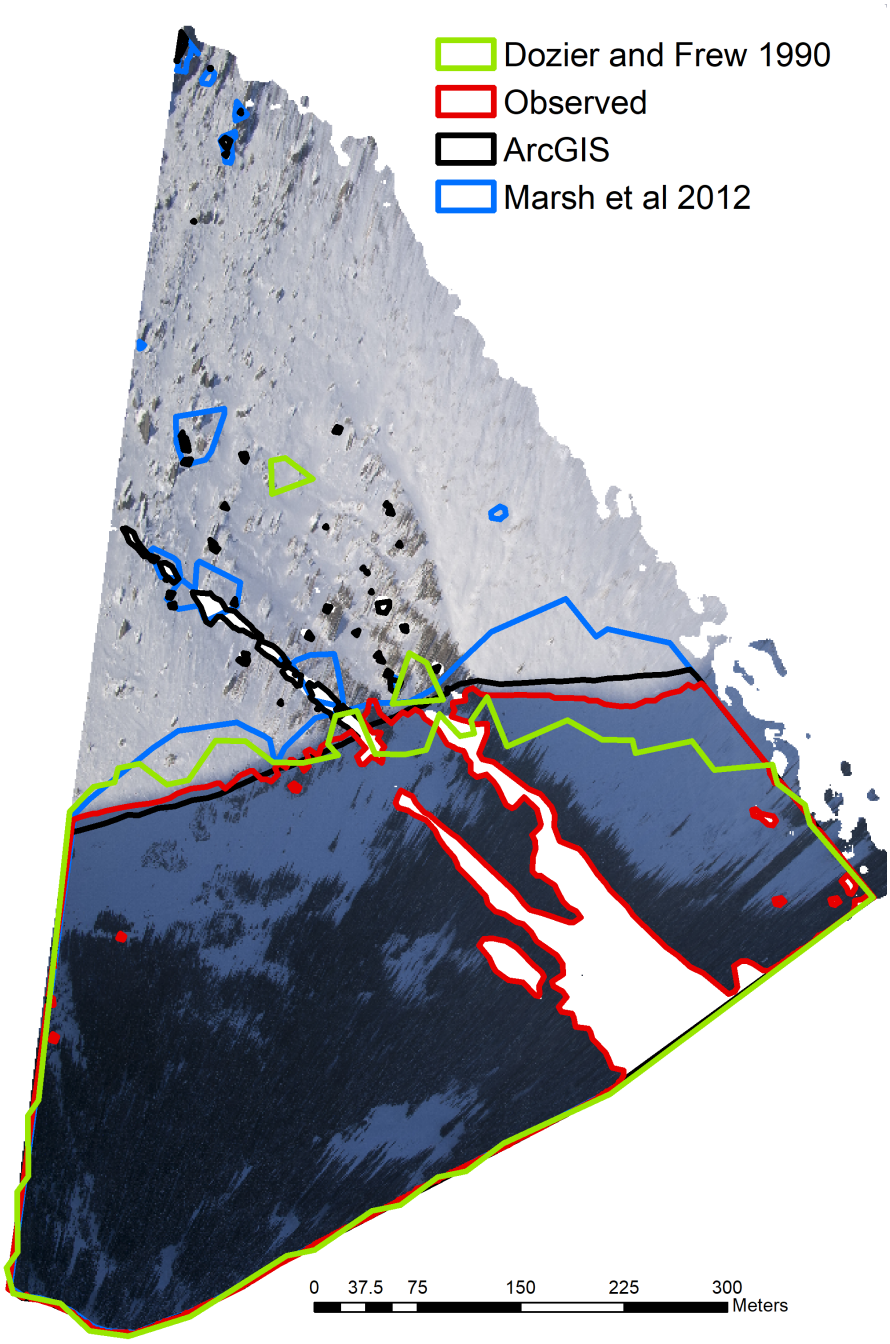

Figure 3.9: This shows an orthorectified terrestrial photo of a shadow passing over Mt. Collembola from Fisera Ridge – details are found in Marsh et al. (2012). The location of the shadowed region for 2011-02-01 17:00 local time is shown for the DF90 algorithm described herein (green), the observed shadow (red), the ArcGIS implementation for a 1m x 1m LiDAR raster (black), and for the Marsh et al. (2012) algorithm (blue).

3.6.3 Leave one out validation

The leave one out validation is shown in Figure 3.10 for Vista View (top row), Upper Clearing (middle row), and Fisera Ridge (bottom row). The dashed line is the 1:1 line, and the solid black line is a linear regression line of best fit. The r^2 value for this fit is shown in the bottom right corner. Due to significant over-plotting of the data points, the values have been binned into 100 hex-bins and coloured using the log of the normalized per-bin count. Hex-bins divide the x-y plane into 6-sided bins and counts values in these bins. The hexes avoid the visual artefacts that can occur with square bins. Grey values are bins that have a normalized count of less than 0.01. Because of the significant number of low and zero values in the shortwave and precipitation timeseries, this resulted in the per-bin colouring being difficult to read. Values of ISWR < 50 W m^{-2} and p < 1 mm were removed for the colouring. Please note that these data *were not removed* for the linear fit, r^2, MBE, or RMSE metrics.

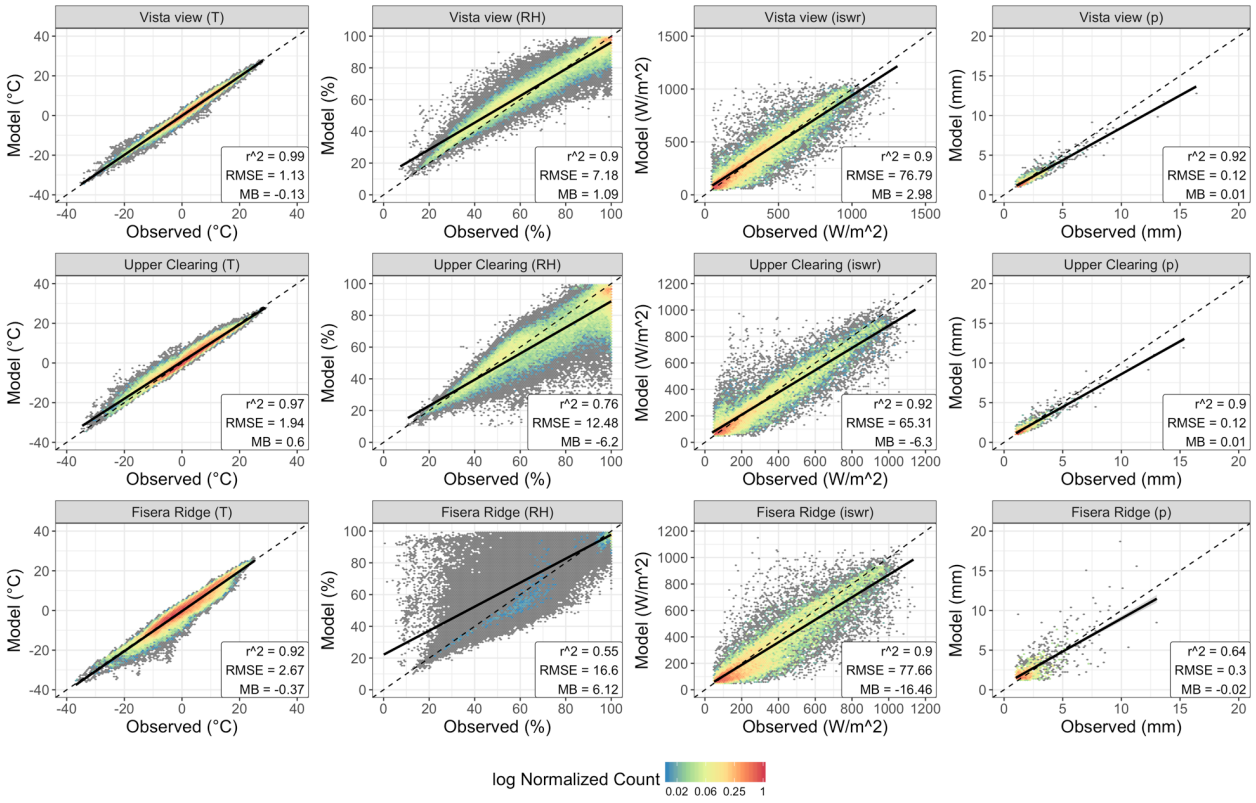

Figure 3.10: Leave one out analysis for Vista View (top row), Upper Clearing (middle), and Fisera Ridge (bottom). The values have been binned into 100 hex-bins and coloured using the log of the normalized per-bin count. Grey values are bins that have a normalized count of less than 0.01.

Temperature was well predicted at all sites with r^2 values of 0.99, 0.97, and 0.92 for Vista View, Upper Clearing, and Fisera Ridge respectively. Both mid-elevation sites were better predicted than the high elevation (Fisera Ridge) site. The majority of the data lies close to the 1:1 line. Upper Clearing had a warm bias

(MB=1.11 °C), whereas Fisera Ridge had a cold bias (MB=-0.37 °C). Less spread was observed in the summer months (not shown), matching the results of Cullen and Marshall (2011). Relative humidity was the most poorly predicted variable. Vista View was the most accurately predicted (r^2=0.9) with a slight (1.09%) positive bias. Upper Clearing had more spread with a distinct negative bias (-6.2%) and decreased r^2 (0.76). Fisera Ridge was exceptionally poorly predicted (r^2=0.55, MB=6.12%). A separate analysis that grouped the data into winter and summer periods (not shown) showed improved results and less spread during the summer months, especially for Fisera Ridge; this summer period had: r^2=0.7, MB=7.84%, RMSE=15.32%. Due to the proximity to vegetation, summer evapotranspiration may result in less temporal variability, dampening the responses. The interpolation methods assume a free-atmosphere, and thus do not capture these canopy impacts. During the winter months, the observed RH is predominately dominated by synoptic scale forcing (Cullen and Marshall, 2011) and may be influenced by the sublimation of intercepted snow in the canopy (Pomeroy et al., 2012) which are not captured by this interpolation. The Fisera Ridge data has had substantial infilling for the RH variable (Fang et al., 2019), and the poor fit of CHM to these infilled data may be as a result of the infilled data using a higher elevation, exposed ridge, that may not be representative of Fisera Ridge. Shortwave irradiance is generally well captured, although Fisera Ridge has a larger negative bias (-15.79 W m^{-2}) than the other two sites. Precipitation at Vista View and Upper Clearing was well predicted, and Fisera Ridge is again the least well predicted. The underestimation of precipitation is likely due to the lapse rates being too low for this region.

3.6.4 Parallel scaling

Shown in Figure 3.11 are the scaling results for 1, 2, 4, 6, 8, 16, and 32 cores. Good scaling is observed with a 1.97x speedup with 2 cores, 7.23x speedup with 8 cores, a 12.3x speedup with 16 cores, and a 20.5x speedup with 32 cores. A sub-linear scaling is expected due to the mixing of domain and data parallel modules. As most compute nodes are approximately 32 cores, this shows good per-node scaling and thus demonstrates motivation for moving towards a distributed memory model, such as MPI.

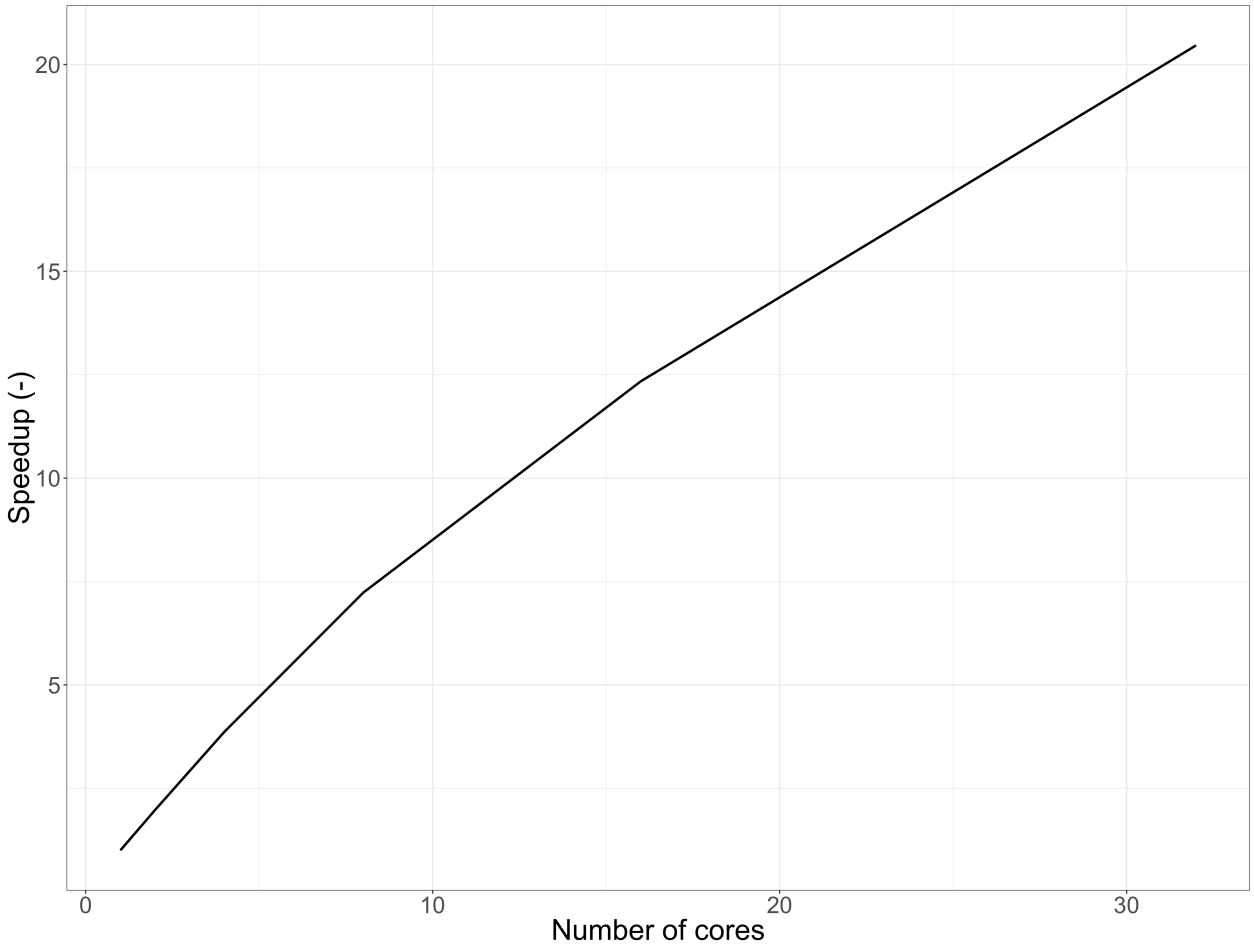

Figure 3.11: Speedup for a $\approx 100,000$ triangle mesh using 1, 2, 4, 6, 8, 16, and 32 cores.

3.7 Conclusion

Simulations of hydrological phenomena are increasingly important for management and prediction of the hydrological cycle under anthropogenic climate change impacts. Cold regions are some of the most sensitive regions to these impacts. However, they have unique modelling challenges. Increasing importance is being given to rigorous uncertainty analysis, process representation testing, and multiple hypothesis testing. Spatially distributed models are generally thought to produce improved predictions in cold regions when spatially explicit prognostic variables are required, however substantial challenges including initial conditions, boundary conditions, parameterizations, and computational costs all conspire to limit their applicability. Despite this, hyper-resolution models are increasingly being applied for water management and design decisions.

There is a significant opportunity for next-generation models to address challenges in existing models and adapt the large successes from hydrological modelling. These challenges include seamless prediction at various spatial and temporal scales, utilization of hyper-resolution data obtained by new remote sensing platforms, quantify of structural uncertainty in distributed models, and utilization of modern high-performance computing infrastructure.

In this paper, a new modelling framework, the Canadian Hydrological Model (CHM), was presented as a first step towards these goals in cold regions. A new unstructured mesh implementation of the well-known Dozier and Frew (1990) shadowing algorithm was derived to demonstrate adaptation of raster-based algorithms. Key features of CHM include the ability to capture spatial heterogeneity in an efficient manner; to include multiple process representations; to be able to change, remove, and decouple hydrological process algorithms; to work both at a point and spatially distributed; the ability to scale to multiple spatial extents and scale; and to utilize a variety of forcing fields (boundary and initial conditions).

4 Multi-objective unstructured triangular mesh generation for use in hydrological and land surface models

4.1 Manuscript status

A version of this chapter has been published as a manuscript in the journal Computers and Geoscience.

Marsh, C. B., R. J. Spiteri, J. W. Pomeroy, and H. S. Wheater (2018), Multi-objective unstructured triangular mesh generation for use in hydrological and land surface models, Computers & Geosciences, 119, 49 67, doi:10.1016/j.cageo.2018.06.009.

Author contributions are as follows:

C. Marsh: Initial idea, coding, analysis, manuscript preparation.

R. Spiteri: Idea refinement, manuscript revision.

J. Pomeroy: Idea refinement, analysis refinement, manuscript revision.

H. Wheater: Idea refinement, manuscript revision.″

4.2 Abstract

Unstructured triangular meshes are an efficient and effective landscape representation that are suitable for use in distributed hydrological and land surface models. Their variable spatial resolution provides similar spatial performance to high-resolution structured grids while using only a fraction of the number of elements. Many existing triangulation methods either sacrifice triangle quality to introduce variable resolution or maintain well-formed uniform meshes at the expense of variable triangle resolution. They are also generally constructed to only fullfil topographic constraints. However, distributed hydrological and land surface models require triangles of varying resolution to provide landscape representations that accurately represent

the spatial heterogeneity of driving meteorology, physical parameters and process operation in the simulation domain. As such, mesh generators need to constrain the unstructured mesh to not only topography but to other important surface and sub-surface features. This work presents novel multi-objective unstructured mesh generation software that allows mesh generation to be constrained to an arbitrary number of important features while maintaining a variable spatial resolution. Triangle quality is supported as well as a smooth gradation from small to large triangles. Including these additional constraints results in a better representation of spatial heterogeneity than from classic topography-only constraints. Keywords hydrology; mesh generation; modelling; unstructured grid; multi-objective refinement

4.3 Introduction

Distributed hydrological and land surface models aggregate the surface and sub-surface into internally homogenous control volumes (Vrugt et al., 2008). These control volumes are used to discretize the mass and energy conservation equations or to apply point-scale models. Correct selection of these control volumes has profound implications for the numerical stability of the discretized equations (Berger and Colella, 1989; Hagen et al., 2000; Parrish and Hagen, 2007; Caviedes-Voullième et al., 2012). Cold regions are characterized by seasonal snowcover and snowfall; here, snow-landscape interactions and energy flux considerations further complicate the selection of control volumes. In these regions, landscape heterogeneity such as vegetation, slope, aspect, and elevation are often critical controls on important processes such as blowing snow (Pomeroy et al., 1997; Essery et al., 1999; Mott et al., 2008), vegetation interactions (Pomeroy et al., 1998b; Gelfan et al., 2004; Ménard et al., 2014a), snowmelt (Anon, 2004; Dornes et al., 2008a; Grünewald et al., 2010; Marsh et al., 2012; DeBeer and Pomeroy, 2017), and runoff dynamics (Carey and Woo, 2001). Surface heterogeneity is also critical for land-atmosphere interactions(Foken, 2008; Husain et al., 2016). The commonly used fixed-resolution control volume, e.g., raster approach, often has substantial computation burdens (Vivoni et al., 2004; Caviedes-Voullième et al., 2012), as well as high uncertainty when applied to areas of interest for water resources such as mountain watersheds. There is a motivation for a discretization that balances surface heterogeneity, numerical requirements, and a reduction in computational elements for use with hydrological and land-surface models.

Triangular meshes represent the topography via a set of irregularly sized, non-overlapping connected triangles (Chang, 2008). Meshes with variable sized and shaped elements are unstructured. Areas of high spatial variability can have a greater density of small triangles than areas that are more homogeneous, providing a more efficient terrain representation than the raster format (Shewchuk, 1996) by reducing computational elements in models by up to 90% (Ivanov et al., 2004a). Efficiency increases of this magnitude make distributed modelling approaches more feasible and less uncertain due to reduced parameter sets, initial conditions, and wall-clock time (e.g., Ivanov et al. (2004a); Kumar et al. (2009b); Kumar et al. (2009a)). Due to the

widespread availability of raster data, unstructured meshes for hydrology are typically derived from raster digital elevation models (DEMs). Because these meshes act as an approximation to landscape variability, care must be taken during creation, and constraints on triangle shape, size, and error to the underlying raster(s) should be included to ensure suitability for hydrological modelling (Caviedes-Voullième et al., 2012; Bilskie and Hagen, 2013).

Two common methods for mesh creation exist: point selection and domain constraints. There are five popular selection algorithms: Heuristic, Hierarchy, Skeleton, Filter (also known as Very Important Points VIP)(Lee, 1991; El-Shimy et al., 2005; Chang, 2008), and ArcGIS tools. These share the trait that possible stopping criteria be either a pre-set number of points to be selected or pre-set differences in elevation between the selected point and neighbouring raster cells (Lee, 1991). Importantly, these methods make no guarantees concerning triangle quality. Therefore, long skinny triangles can be created with poor gradations from small to large triangles. These triangles are generally unsuitable for use as a discretization mesh in numerical applications. An example of poor point selection is shown in Figure 4.1, where the selected points (green dots) duplicate the structured mesh corners, doubling the number of elements (black lines are triangle edges). In areas of generally flat topography, such as plains or broad valley bottoms, constraining meshes only to topography fails to capture the spatial heterogeneity of hydrologically important characteristics. Alternatively, inner and outer domain boundaries such as basin delineation, streams, and lakes are defined and triangles are inserted to cover the area defined by these boundaries. Triangular mesh generation using this technique is generally done via constrained Delaunay triangulation (Ruppert, 1995; Shewchuk, 2002). Strong guarantees on triangle shape and inner angles ensures suitability for use as a discretization mesh for numerical applications.

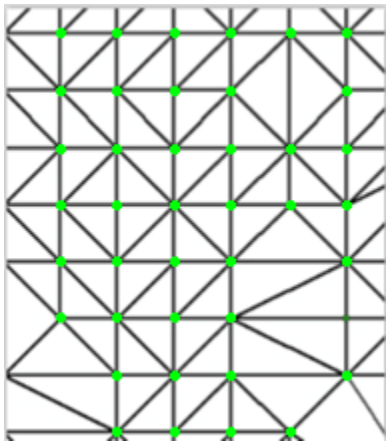

Figure 4.1: Example of poor mesh generation from a raster. Raster cells have been cut in half, doubling the number of computational elements in places. Triangle edges are in black.

In this paper, a multi-objective meshing tool, Mesher, is presented. Based on an existing, high-quality implementation of constrained Delaunay triangulation, its novel contribution is in how triangles are chosen for refining. Mesher uses various objective functions to measure triangle error with the underlying primary raster as well as constraining to non-topographic discrete and classified data (e.g., land cover, soils). This

permits variably sized triangles throughout the domain, allows for guarantees about triangle quality and shape, and ensures that spatial heterogeneity in secondary features is represented. Specifically, this meshing software is optimized for use in hydrological and land surface models that mix many point-scale and non-PDE (partial differential equation) distributed algorithms along with PDE discretizations. Due to this mixing of methods, meshes are generated considering only the landscape, e.g., elevation, vegetation, and soil, and not the discretization of physical processes such as Hagen et al. (2002) or Parrish and Hagen (2007) who consider numerical error in the mesh generation. This meshing tool is quantitatively tested against an existing mesh generation method, and a surface heterogeneity measure is used to quantify whether important landscape characteristics are well approximated.

4.4 Meshing algorithm

4.4.1 Overview

The core meshing algorithm is built upon the constrained Delaunay meshing algorithm of Shewchuk (2002), as implemented in the Computational Geometry Algorithms Library (CGAL; Rineau (2016)). In brief, Delaunay meshes constrain triangle inner angles, edge lengths, number of total triangles, and the gradation from small to large triangles in the domain (Shewchuk, 2002). This gradation is important to avoid sharp gradients. Delaunay meshes have been used with success for a coupled representation of surface-sub-surface processes (Qu and Duffy, 2007) and for shallow water flow equations (Hagen et al., 2001, 2002; Kumar et al., 2009b). Due to the importance of including sub-mesh scale vertical features (Bilskie et al., 2015) as well representing rivers and streams, these constraint features may be included. Boundary and inner feature constraints are defined via planar straight-line graphs (PSLGs). The pre- and post-processing steps, as well as the multi-objective refinement algorithm, are detailed below.

4.4.2 Details

Outlined in Figure 4.2, the meshing algorithm uses the extent of the DEM to bound the meshing area. All optional secondary input parameters (e.g., vegetation and soils) are converted to the DEM's coordinate system and are clipped to the DEM's spatial extent, allowing mismatched raster resolutions and extents in these data. The data/no-data region of the DEM is used to generate an (optionally simplified) outer PSLG. The z-value of the triangle vertices (v_z) are assigned a value from the DEM. However if the PSLG is simplified it may result in a vertex laying outside the original raster extent. These invalid vertices have their z-value interpolated from neighbour vertices. More novel DEM to mesh interpolation techniques such as Bilskie and Hagen (2013) could be included if required. These pre-processing steps are done in Python. The core meshing

algorithm is written in C++11. All geospatial manipulation is done via the Geospatial Data Abstraction Library(GDAL; Team, 2016).

```
   input  : A digital elevation map DEM
   input  : An optional set of secondary constraints parameters P
 1 Extent ← Extent(DEM)
 2 nodata ← NoDataValue(DEM)
 3 Projection ← GetProjection(DEM)
 4 foreach  p in P do
 5 |  ClipExtent(p, Extent)
 6 |  NoDataValue(p)← nodata
 7 |  Project(p, Projection)
 8 end
 9 PSLG ← Polygonize(DEM)
10 mesh ← Mesher(PSLG, DEM, P)
11 foreach v in Mesh verticies do
12 |  if v outside Extent then
13 |  |  Interpolate v_z from connected verticies
14 |  end
15 end
```

Figure 4.2: High-level outline of the pre- and post-processing steps.

The Delaunay algorithm inserts triangles that fill the PSLG region. Each candidate triangle that is generated may either be accepted or rejected for further refinement; this is outlined at a high-level in the IsBad function in Figure 4.3. Further refinement of a triangle may be required if the triangle's total area is above a threshold, if it poorly represents the underlying raster, or if it has inner angles that are below a threshold (skinny triangles). This refinement strategy enforces a rigorous application of supplied tolerances. A minimum area constraint is used to stop the meshing algorithm from over-refining a triangle. If triangles are to be produced at a similar resolution as the input DEM, an iterative smoothing can be applied to the input DEM to reduce stair stepping in the output mesh.

An example of a candidate triangle is shown in Figure 4.4. Overlain on the elevation raster (coloured; red = high, blue = low) is the in-construction unstructured mesh (black lines). The triangle has been rasterized and the bounding box to this triangle is shown by the extent of the black area. Cells touched by the triangle within this bounding box are shown in grey and those untouched are shown in black. The cells in this mask exactly correspond to cells in the underlying raster. Using a plane interpolant defined by this triangle, in combination with the rasterized binary triangle mask, an error metric between the underlying raster and the triangle can be computed. Multiple error metrics were used: Root Mean Square Error (RMSE), maximum

```
   input    : A set of rasters R, at least 1 topographic raster
   input    : A candidate triangle produced by the CGAL meshing
              algorithm tri
   input    : Maximum allowed error between triangle and raster tol
   optional: An optional set of categorical constraints C
   optional: Maximum category mode constraint cat_tol
   optional: Maximum area maxarea
   optional: Minimum area minarea
 1 Function IsBad (tri)
 2     if inner angle < 22.5 then return true ;
 3     if tri area > maxarea then return true ;
 4     if tri area <= minarea then return false ;
 5     foreach r in R do
 6         if ErrorMetric(tri) > t then return true;
 7     end
 8     foreach c in C do
 9         if Mode(tri) < ct then return true;
10     end
11     return false
12 Function ErrorMetric (tri)
13     v0, v1, v2 ← triangle vertexes
14     bbox ← bounding box of v0, v1, v2
15     if bbox extent > DEM extent then
16         bbox ← Clipbbox
17     end
18     rtri ← GDALRasterizeGeometries(tri, bbox)
19     foreach Cell in rtri do
20         if Cell in triangle then
21             Pred ← Predicted value from plane equation
22             Error ← Accumulate difference Cell − Pred as required
23         end
24     end
25     return Error
```

Figure 4.3: High-level description of the rejection/acceptance algorithm.

difference, and difference in mean value. All error metrics (E) are compared to some threshold (ε; $E < \varepsilon$). RMSE is given as

$$RMSE = \sqrt{\frac{\sum_{i=1}^{n} \left(z_o(x_i, y_i) - f(x_i, y_i)\right)^2}{n}} \tag{4.1}$$

and is computed between the plane interpolant $f(x, y)$ and the raster cell value $z_o(x, y)$ for n non-masked cells, i.e., the grey cells in Figure 4.4, given by normalized coordinates (x, y). Maximum difference (herein tolerance *Tol*) is given as the maximum of the set of differences between the plane interpolant ($f(x, y)$) and raster ($z_o(x, y)$) values for non-masked cells. Numerically, this is given as

$$Tol = \left(\{|z_o(x_i, y_i) - f(x_i, y_i)|\}\right) \tag{4.2}$$

Mean difference (MD) is given as:

$$MD = \left| \frac{\sum_{i=1}^{n} z_o(x_i, y_i)}{n} - \frac{z_0 + z_1 + z_2}{3} \right|, \tag{4.3}$$

where z_0, z_1, z_2 are the three z-coordinates of the triangle vertices and $z_o(x, y)$ are the n non-masked raster cells. Effectively, this computes the difference of the mean of each triangle vertex and the mean of all the non-masked raster cells.

A triangle may be further constrained to any arbitrary set of continuous or classified data. (e.g., vegetation, soils). For classified data, the dominant feature class in this triangle is checked for exceeding a coverage threshold; e.g., 70% of a cell is covered by a single vegetation class. For discrete constraints, the above-described error metrics may be used.

Alternatively, a more generic weighted approach is also possible. Each input raster constraint is assigned a weight w_r such that $\sum_{r=1}^{R} w_r = 1$, and a total weight tolerance to exceed is specified. This is a not a completely rigorous approach; however, it allows for prioritizing various constraints over others. This algorithm is detailed in Algorithm 4.5. In contrast to the rigorous tolerance checking detailed above, where failing to meet any raster constraint results in refinement, the weighting approach checks each raster tolerance before determining acceptance of the triangle. The total triangle weighted quality threshold W is given as

$$W = \sum_{r=1}^{R} \alpha_r w_r, \tag{4.4}$$

where w_r is the raster weight for each raster of the total set of raster constraints . The term α_r is set as follows: $\alpha_r = 1$ when the triangle meets that raster constraints tolerance, and $\alpha_r = 0$ when it does not. This requires a certain number of constraints are met before accepting the triangle. Small-angled triangles and

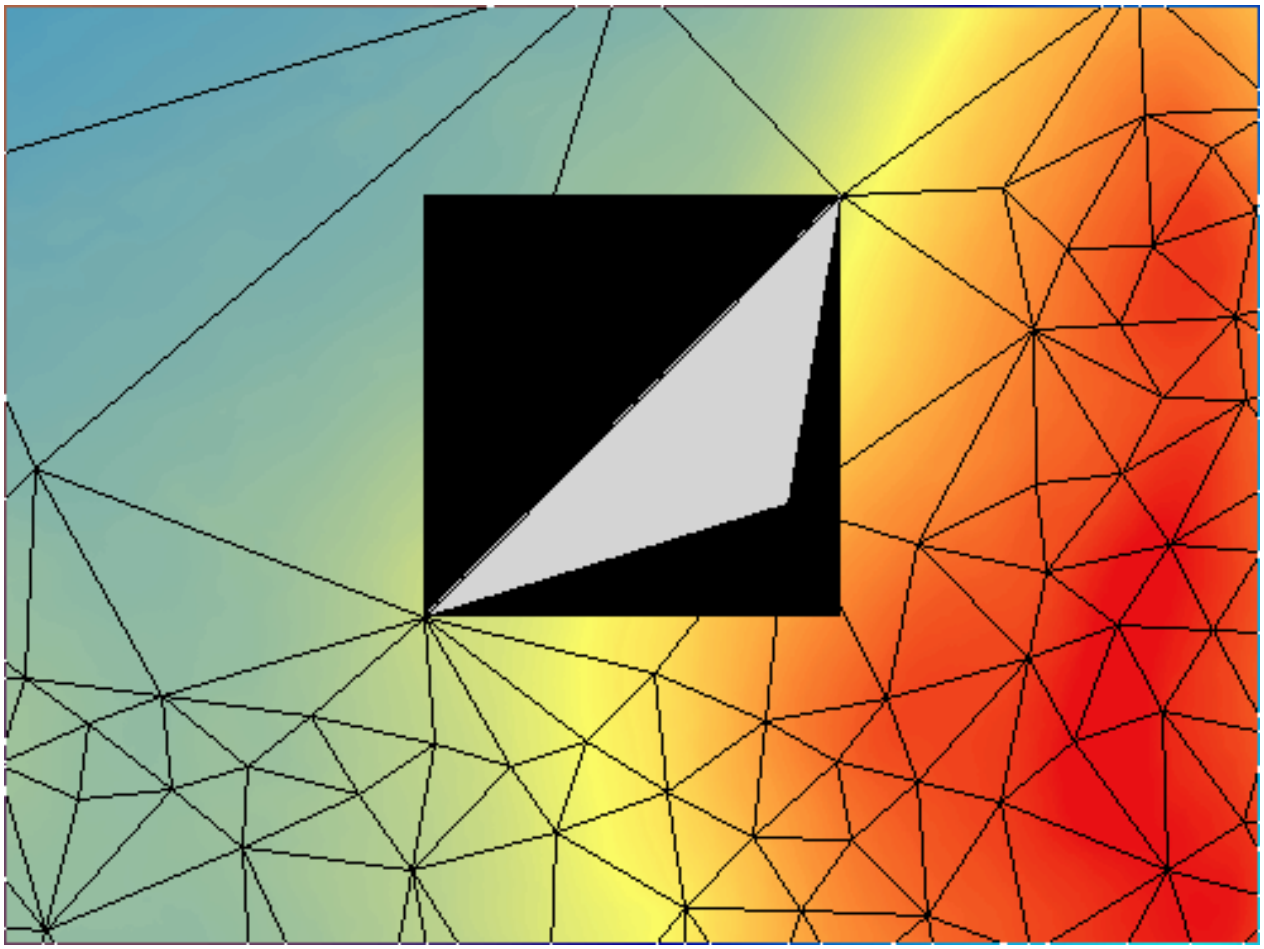

Figure 4.4: Elevation raster (colour; red = high, blue = low) overlain by in-construction unstructured mesh (black lines). Candidate rasterized triangle shown centre. Black shows raster cells not touched by the triangle, grey for those that are. This is used in determining error between triangle and underlying raster.

triangles larger than the specific maximum area are unconditionally rejected and triangles at or below the specified minimum area are unconditionally accepted as they cannot be refined further.

The mesh generation outlined herein has been designed to address a gap in mesh generation for hydrological and land-surface numerical models that combine various types of process representation, such as point scale, distributed, and PDE discretized equations. These models are commonly applied to large spatial extents and to cold regions where dominant processes change during the year. It is therefore difficult to optimize the mesh using either error truncation analysis or *a posteriori* metrics for a single process. However, *a posteriori* refinement such as John (2000) and Verfürth (2005) could be integrated into the triangle selection/rejection routine. Inclusion of truncation error in the mesh generation has been shown to improve results and decrease computational burden (Parrish and Hagen, 2007).

Two examples of this algorithm (rigorous variant) in progress are shown in Figure 4.6; Figure 4.7. In Figure 4.6, an idealized Gaussian hill has been meshed. Each panel shows an iteration of the meshing algorithm, and the triangles are coloured with the RMSE of the triangles. For the first iteration, PLGS filling triangles are inserted. However, the error of each triangle is large, and so the triangles are rejected and further refined. Due to the conic shape of the hill, that lies on a flat plane, the outer triangles converge quickly. As the meshing continues, increasingly small triangles are inserted near the peak of the hill to capture the sharp curvature. At the final iteration, the triangle tolerance has been met and the algorithm terminates. In Figure 4.7, a domain meshed using an elevation and vegetation constraint (expanded in detail in Chapter 4.5; shown in Figure 4.11) is shown at various stages of completion. The triangle faces are coloured based upon one of: triangle is ok, has failed elevation tolerance, has failed vegetation tolerance, or has failed both. Due to the large sizes of the initial two triangles, a single vegetation class is sufficiently dominating to pass the vegetation tolerance. However, elevation fails. As the mesh is refined, triangles begin to pass the elevation tolerance but now fail the vegetation tolerance. By iteration 869, there are triangles on the right-hand side of the domain located in an area of patchy vegetation that still require refinement. Because these triangles have been refined to the minimum triangle size, they are unconditionally accepted. Although many iterations are required, fewer and fewer triangles are refined in each iteration, resulting in fast convergence.

After generation of the mesh, a post-processing Lloyd optimization (Tournois et al., 2010) step can be performed that relaxes the mesh further to improve gradation from small to large triangles. This step does negate the guarantees of the rigorous tolerance checking because triangle geometry is changed. Once the final mesh has been generated, it is saved as: a shapefile for use in a GIS, an unstructured mesh file (vtu) for visualization in ParaView, and a JSON-based text format for use in a model.

```
input    : A set of rasters R, at least 1 topographic raster
input    : A candidate triangle produced by the CGAL meshing
           algorithm tri
input    : Maximum allowed error between triangle and raster tol
input    : Weight tolerance to exceed to accept tolweight
optional: An optional set of categorical constraints C
optional: Maximum category mode constraint cat_tol
optional: Maximum area maxarea
optional: Minimum area minarea
optional: Weights for each raster weights
optional: Total weight for this triangle totalweight
optional: Weight given to a raster w
Function IsBad_weighted (tri)
    totalweight =0
    if inner angle < 22.5 then return true ;
    if tri area > maxarea then return true ;
    if tri area <= minarea then return false ;
    foreach r in R do
        if ErrorMetric(tri) > t then totalweight += w;
    end
    foreach c in C do
        if Mode(tri) < ct then totalweight += w;
    end
    if totalweight > tolweight then return false ;
    return true
Function ErrorMetric (tri)
    v0, v1, v2 ← triangle vertexes
    bbox ← bounding box of v0, v1, v2
    if bbox extent > DEM extent then
        bbox ← Clipbbox
    end
    rtri ← GDALRasterizeGeometries(tri, bbox)
    foreach Cell in rtri do
        if Cell in triangle then
            Pred ← Predicted value from plane equation
            Error ← Accumulate difference Cell − Pred as required
        end
    end
    return Error
```

Figure 4.5: Instead of rigorously ensuring each tolerance is met, a weighted approach is possible. This allows giving priority to various input constraints. For this approach, a weight (w_r) is specified for each constraint raster, where $\sum_{r=1}^{R} \alpha_r w_r = 1$. Each raster is evaluated for fulfilling the corresponding tolerance, and success or failure is weighted by the raster weight. A final weighted quality threshold must be exceeded to accept the triangle.

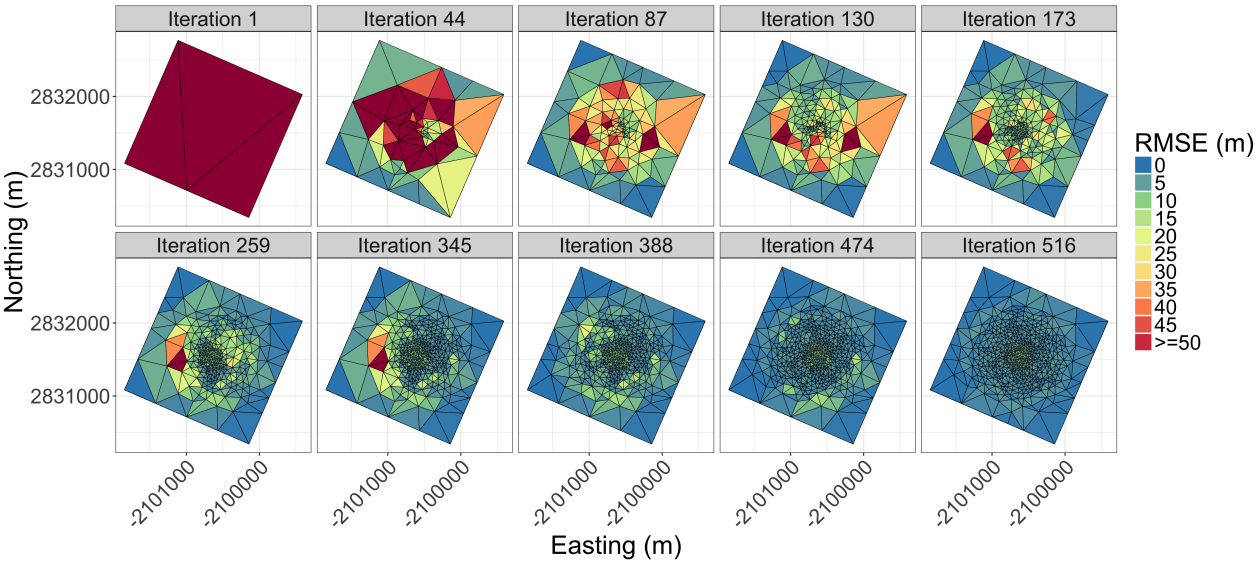

Figure 4.6: Output from the meshing algorithm at various stages of refinement for an idealized Gaussian Hill that lies on a flat plane. The triangulation is optimizing only on elevation RMSE. Initially three PLSG filling triangles are inserted into the domain. Due to the high RMSE, these are rejected, and small triangles are inserted into the domain. As the meshing continues, increasingly small triangles are inserted near the peak of the hill to capture the sharp gradients. At the end, the triangle tolerance has been met and the algorithm terminates.

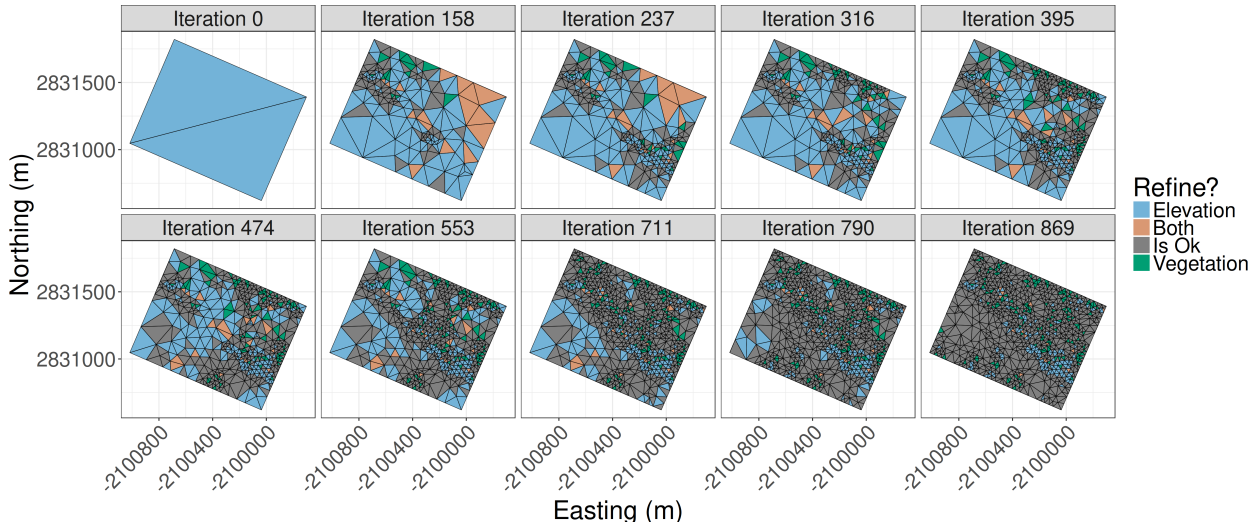

Figure 4.7: Output from the meshing algorithm at various stages of refinement for a vegetated hillslope (detailed in Chapter 4.5; shown in Figure 4.11). The triangulation is optimizing for elevation and vegetation cover. Initially two PLSG filling triangles are inserted into the domain. Due to the high RMSE with elevation, these are rejected, and small triangles are inserted into the domain. As the meshing continues, increasingly small triangles are inserted along the ridge-valley interface (middle of domain). The upper plateau (left hand side) is relatively flat with homogenous vegetation and therefore converges early. At the end, the triangles on the right-hand side plateau (location of patchy vegetation) require further refinement. However, these triangles have been refined to the minimum triangle size – they are therefore unconditionally accepted.

4.4.3 Hydrology considerations

Shape files that describe important features, e.g. rivers and roads, can be used to constrain the triangulation. An example is shown in Figure 4.8 where a flat plane has been constrained to an *a priori* determined stream network. Figure 4.9 demonstrates using flow accumulation (D8; O'Callaghan and Mark, 1984), calculated using the RichDEM (Barnes, 2017) tool, to constrain input. Triangles are coloured using the log10 of the flow accumulation where high flow accumulations such as streams occur, and low flow accumulations are shown in blue. The main stream network is visible. Smaller triangles are present along these flow paths with a gradation towards larger triangles on the uplands.

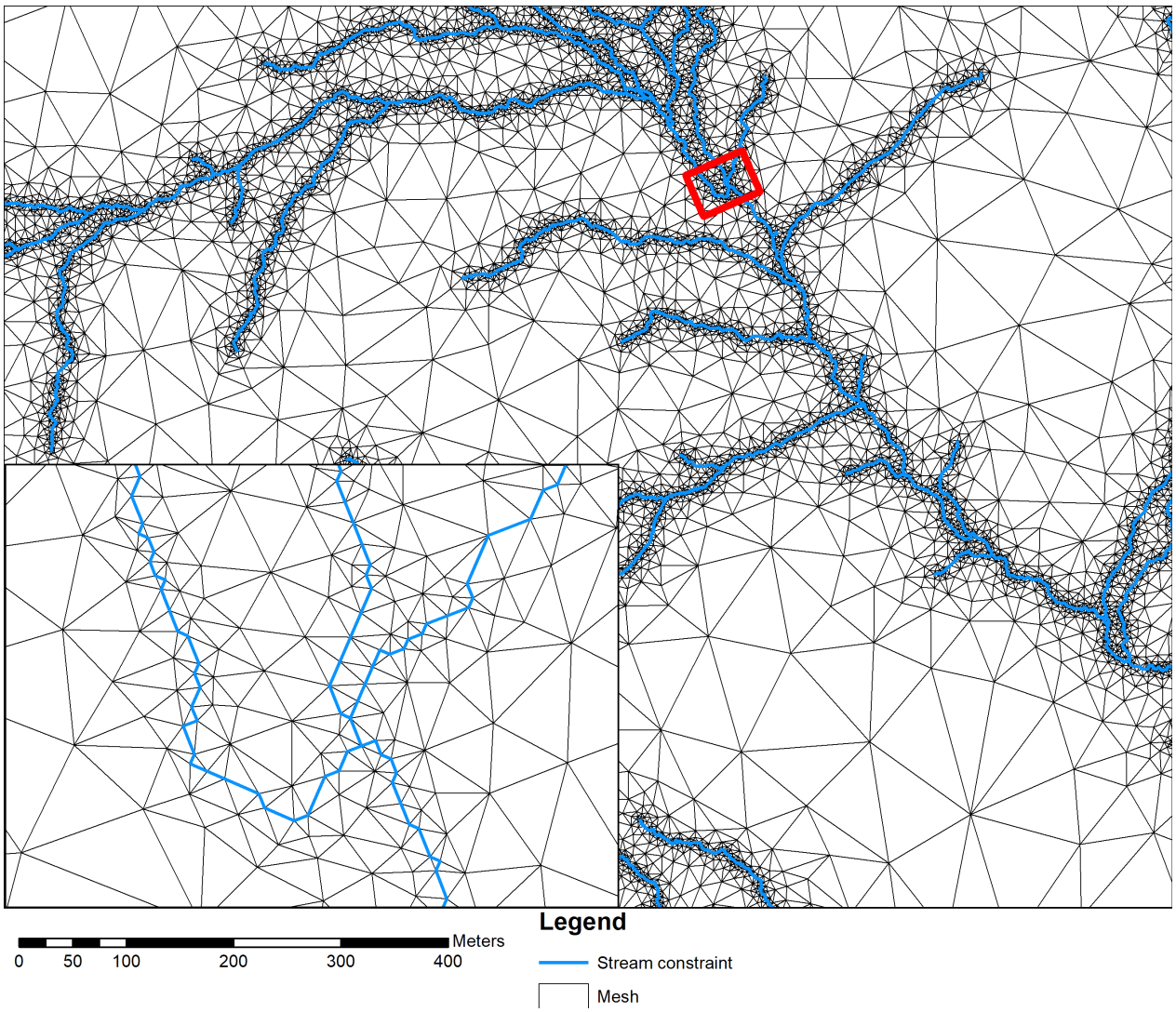

Figure 4.8: A flat plane corresponding to the Granger creek sub-basin was constrained with an a priori stream network. A small inset shows the constraint in blue along with the mesh in black.

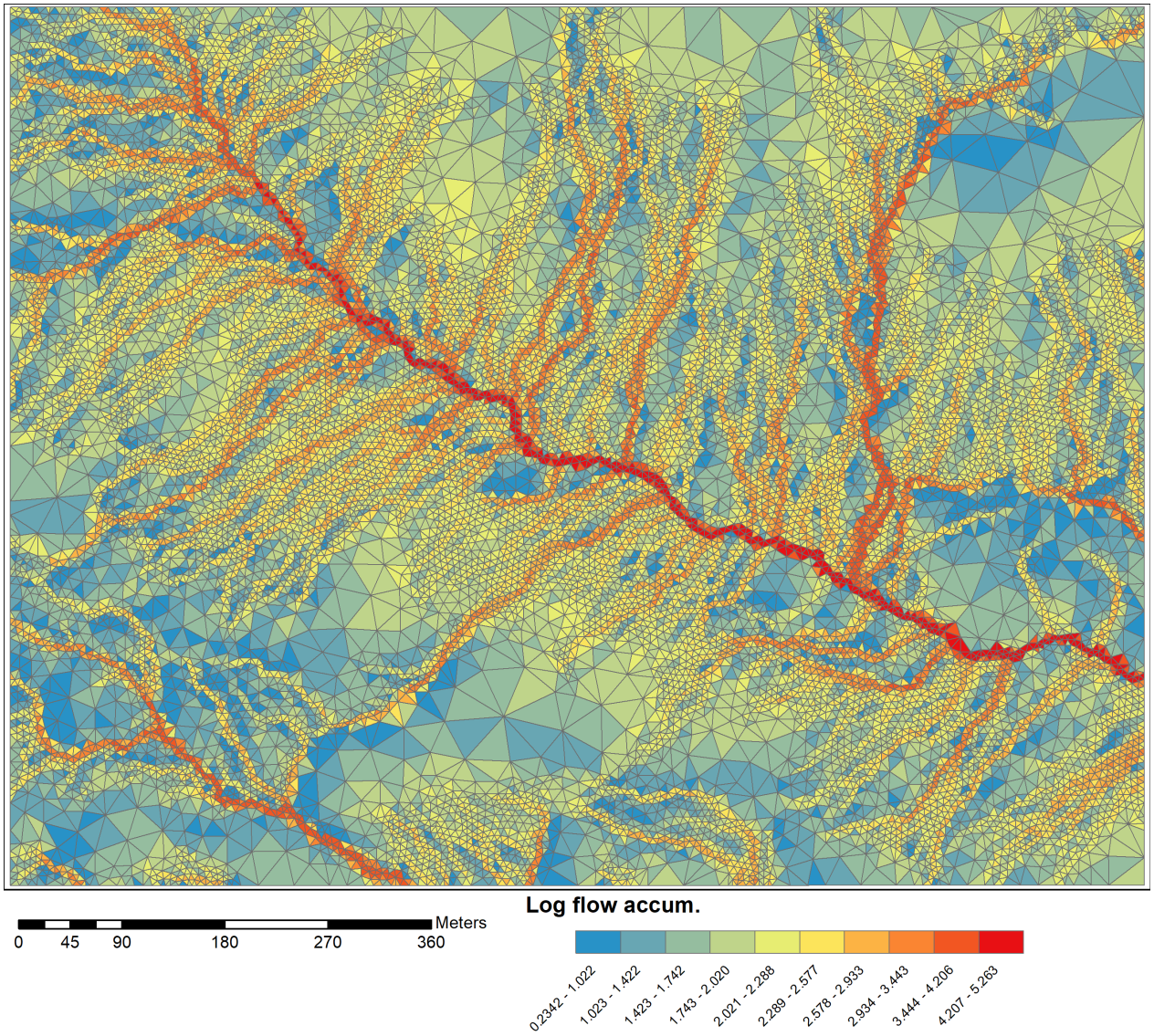

Figure 4.9: A flow accumulation raster was used to conform the triangulation, in addition to elevation. Shown is the log10 of the calculated flow accumulation where high flow accumulation (e.g., stream) is shown in red, and low flow accumulation (e.g., source area) is shown in blue. Small triangles are present along the high flow paths, and larger triangles in the low flow accumulation areas on the uplands.

4.5 Methodology

4.5.1 Spatial domain

4.5.1.1 Wolf Creek

The 179 km^2 Wolf Creek Research Basin, located in the Coast Mountains near Whitehorse, Yukon Territory, Canada, was used to test the meshing algorithm. It consists of three main vegetation covers: boreal forest, shrub-tundra, and sparse tundra (Pomeroy et al., 2006). Elevation ranges from 654 m to 2080 m. A 1 m x 1 m resolution LiDAR derived DEM is available for this basin, with 3.6×10^8 data cells. This is shown in Figure 4.10. Vegetation classes (17 in total) are available via the Landsat-7 derived Earth Observation for Sustainable Development of Forests (EOSD) (Wulder and Nelson, 2003; Wulder et al., 2007b) 25 m x 25 m vegetation classification, shown in Table 4.1.

Table 4.1: Vegetation classes as derived from EOSD (25 m x 25 m) data for the Wolf Creek Research Basin.

Class number	Type	% Area
212	Coniferous-open	12
33	Exposed / Barren land	3.0
213	Coniferous-sparse	6.7
52	Shrub low (< 2 m)	50
51	Shrub tall	5.5
100	Herb (vascular, non-woody)	16
211	Coniferous-dense	2.6
221	Broadleaf-Dense	0.30
232	Mixedwood-open	0.050
32	Rock/rubble	1.5
31	Snow/ice	0.030
83	Wetland-herb	0.13
222	Broadleaf-open	0.90
20	Water	1.1
82	Wetland-shrub	0.17
81	Wetland-tree	0.030
12	Shadow	0.060

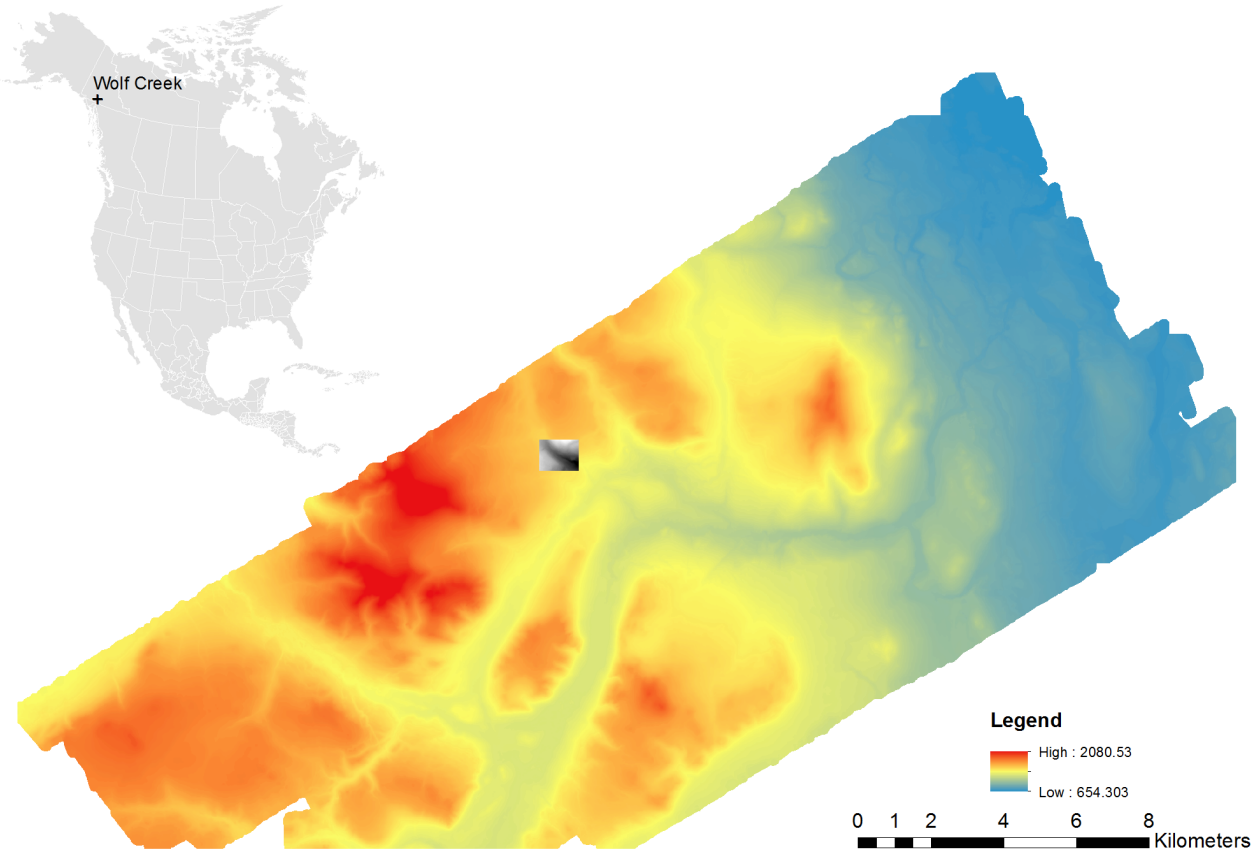

Figure 4.10: Wolf Creek Research Basin LiDAR derived $1m^2$ DEM. The sub-area of the Granger-Creek sub-basin location is shown in black and white.

4.5.1.2 Granger Creek

A tributary stream feeding Wolf Creek is the 8 km^2 Granger Creek sub-basin (McCartney et al., 2006). A sub-area of Granger Creek, shown as a black and white extent in Figure 4.10 and expanded in Figure 4.11. This domain is 1089 m x 867 m (1 m x 1m resolution; LiDAR derived; #cells = 944,163). Topographically, this area has two upper plateaux divided by moderately steep slopes (approx. 50 degrees) and a lower valley bottom filled with tall shrubs (McCartney et al., 2006; Dornes et al., 2008b).

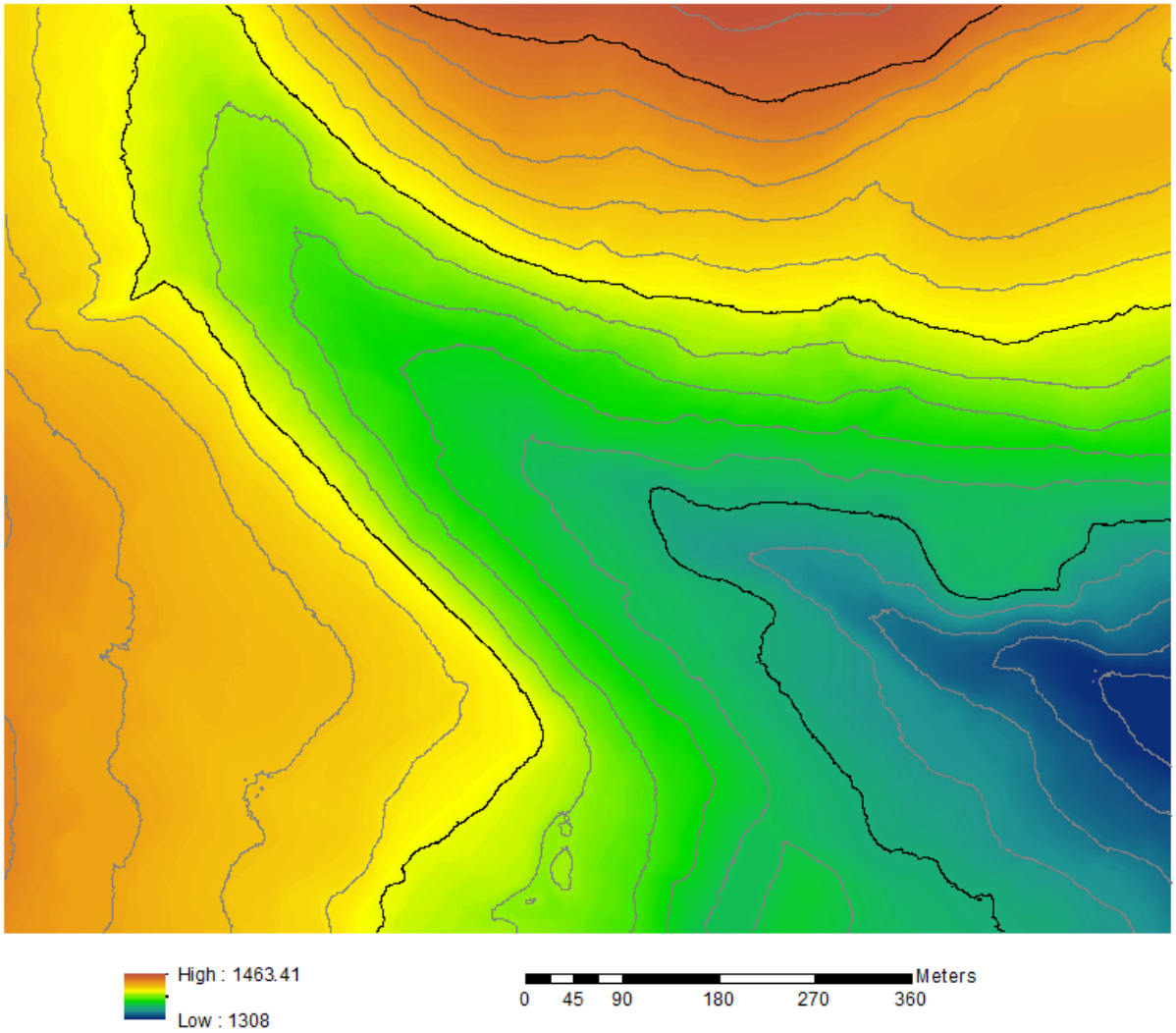

Figure 4.11: Small valley sub-area of the Granger Creek valley. LiDAR DEM at 1m x 1m resolution. Contours are every 10 m (grey) and 50 m (black). The domain is approximately 1000 m by 900 m.

4.5.2 Mesh quality comparison

Three meshes were generated for the sub-area of Granger Creek sub-basin: one by ArcGIS tools and two by Mesher. The ArcGIS TIN is constrained to tolerance=1 m, and the Mesher algorithm mesh is constrained to tolerance = 1 m and to an RMSE = 1m.

To diagnose mesh generation for a larger extent, all of the Wolf Creek Research Basin was used. Various combinations of tolerance and minimum triangle area were used to determine the impact on generated meshes. These tests used a single-objective constraint to the topography. RMSE values were: 1 m, 2 m, 5 m, 10 m, 25 m, 50 m, and 100 m. Minimum triangle areas were: 2 m^2, 4 m^2, 100 m^2, 900 m^2, 10,000 m^2, 90,000 m^2, and 100,000 m^2.

4.5.3 Spatial heterogeneity

Because vegetation is a patchy and spatially heterogeneous component of the surface, it provides a useful test-case for the capability of the multi-objective constraint. The use of vegetation is only meant to illustrate and test the meshing algorithm; in principle, any other surface or subsurface feature can be used.

Three approximating meshes were generated: one that did not constrain to the vegetation and two that did. The two constrained meshes required >50% and >75% of a triangle to be covered by a single vegetation class. Minimum triangle size was set to 625 m2 (25 m x 25 m equivalent) and RMSE = 1 m for all meshes.

To identify disjoint patches of vegetation, a connected components labelling algorithm was used to identify groups of pixels (Chang and Chen, 2003). The fractal dimension was calculated for each of these patches that quantifies the complexity of planar shapes using perimeter-area scaling relationships (McGarigal and Marks, 1994). Values vary between 1 (simple Euclidean shapes) and 2 (more complex, non-Euclidean). For instance, snow patches on the ground (Shook et al., 1993a, 1993b) and in forest canopies (Pomeroy and Schmidt, 1993) around the world have $D \approx 1.3$. For a patch with perimeter P and area A, the fractal dimension D relates the two as

$$P = kA^{D/2} \tag{4.5}$$

where k is a scale coefficient related to the resolution of measurement. To calculate the fractal dimensions of the meshes, the three triangular meshes were rasterized to a 25 m x 25 m raster, corresponding to the original EOSD data set. Both the connected components labelling algorithm and the fractal dimension calculation were computed via the R package SDMTools (VanDerWal, 2016).

The distribution of fractal dimensions and thus the patch complexity between the original and unstructured mesh should be similar. Quantile-quantile (Q-Q) plots allow for visually diagnosing differences between distributions. The two-sample Kolmogorov-Smirnov (K-S) (Conover, 1971) test was used to statistically

compare the distributions. This is a non-parametric test that determines if two probability distributions originate in the same distribution. The null hypothesis is that the two test distributions originate in the same distribution. Significance was determined for $p < 0.01$.

In addition to the patch geometry, patch area should also be preserved. This is visually tested via Korcak's law, an empirical size-distribution for geographical objects (Imre and Novotný, 2016). These results are shown via Korcak plots where the (normalized) number of areas that are in exceedance excess $F(a)$ of a threshold area A are plotted versus the area. The patch area distributions were statistically compared using the K-S test. Significance was determined for $p < 0.01$.

In summary, the per-patch complexity metric distribution and per-patch area distribution for three unstructured meshes, each with an increasingly strict vegetation criterion, were compared against the distributions derived from the original vegetation raster dataset. If the distributions are significantly different, then it can be surmised that the unstructured mesh is not correctly capturing the heterogeneity.

4.5.4 Weighting

The sub-basin domain was meshed using the weighting algorithm for two test cases. In all cases, the elevation tolerance was given as 5 m, with a minimum triangle area of 5 m x 5 m. For the high weight case, vegetation was given a weight of 0.8. For the low weight case, vegetation was given a weight of 0.2. A cut-off weight threshold of 0.8 was used.

4.5.5 Performance tests

Performance tests were done on a workstation with an Intel Dual Intel Xeon E5–2630 (six core HT, 2.6GHz) CPU, 128GB DDR3 ECC RAM, and 7200rpm mechanical harddrive, running Ubuntu 14.10. The domain used was the Wolf Creek domain. Tolerances used were 1 m, 2 m, 5 m, 10 m, 25 m, 50 m, and 100 m. Minimum triangle areas were 2 m^2, 4 m^2, 100 m^2, 900 m^2, 10,000 m^2, 90,000 m^2, and 100,000 m^2. Each tolerance-area combination was run five times, taking the minimum wall-clock time. Wall-clock times include the entirety of the pre- and post-processing steps. Therefore, some disk I/O performance is implicitly measured.

4.6 Results

4.6.1 Mesh quality comparison

An unstructured mesh generated with ArcGIS (tolerance = 1 m) is shown in Figure 4.12 (top). Behind the mesh (black lines), the slope is shown in colour, with high slope in red (50 degrees) and low slope in blue (0 degrees). The mesh generation has produced fewer, larger triangles on the upper plateaus and more, smaller triangles along the hill slopes. This mesh demonstrates the generation of poorly shaped (i.e., long and skinny) triangles due to no constraint on minimum inner angles. There are 8,346 triangles in this domain, compared to 944,163 raster cells (0.88% of the raster cells). The unstructured mesh generated with Mesher (tolerance = 1m) is shown in Figure 4.12 (middle). Like the ArcGIS output, the plateaus have larger triangles and the steep slopes have smaller triangles. Due to the inner-angle constraint, there are no long skinny triangles, and there is a smooth gradation between large and small triangles. This is especially evident along the steep slopes. Fewer triangles were generated than ArcGIS; 6,107 (0.65% of the raster cells). The mesh generated with a 1m RMSE threshold using Mesher is shown in Figure 4.12 (bottom). There are 1,424 triangles in this domain (0.15% of raster cells). Fewer small triangles have been generated for the high slope areas versus the tolerance methods.

The distributions (normalized density) of the attributes of each mesh are shown in Figure 4.13, with the top showing the RMSE (m), the middle showing the internal triangle angles (degrees), and the bottom showing triangle area (m2). For both tolerance methods, Mesher and ArcGIS produce almost identical RMSE distributions. Although both the ArcGIS and Mesher meshes were constrained to a 1m maximum tolerance, an over-representation of the terrain has occurred, as shown by the low RMSE values. The tolerance of 1 m resulted in a maximum RMSE of approximately 0.5 m to 0.6 m. The ArcGIS mesh has many small-angled, skinny triangles, making for sharp transitions between areas. This is undesirable for numerical usage and leads to a 36% increase in total number of triangles versus Mesher's tolerance mesh. The 1 m RMSE mesh resulted in an almost identical distribution of inner angles as that of the Mesher tolerance mesh and a more uniform RMSE distribution is found.

4.6.2 Tolerance – minimum area relationship

The number of triangles produced for various combinations of error (RMSE) and minimum triangle areas (m^2) for the entire Wolf Creek domain are shown in Figure 4.14 (note log axes). The x-axis shows the minimum triangle area. Various approximations to the elevation (RMSE [m]) are shown in coloured lines. Vegetation constraints are shown in the facets for 0%, 50% (0.5), and 75% (0.75) area constraint. The highest-accuracy mesh is the 1 m RMSE mesh and shows a rapid reduction in total elements as the minimum area increases.

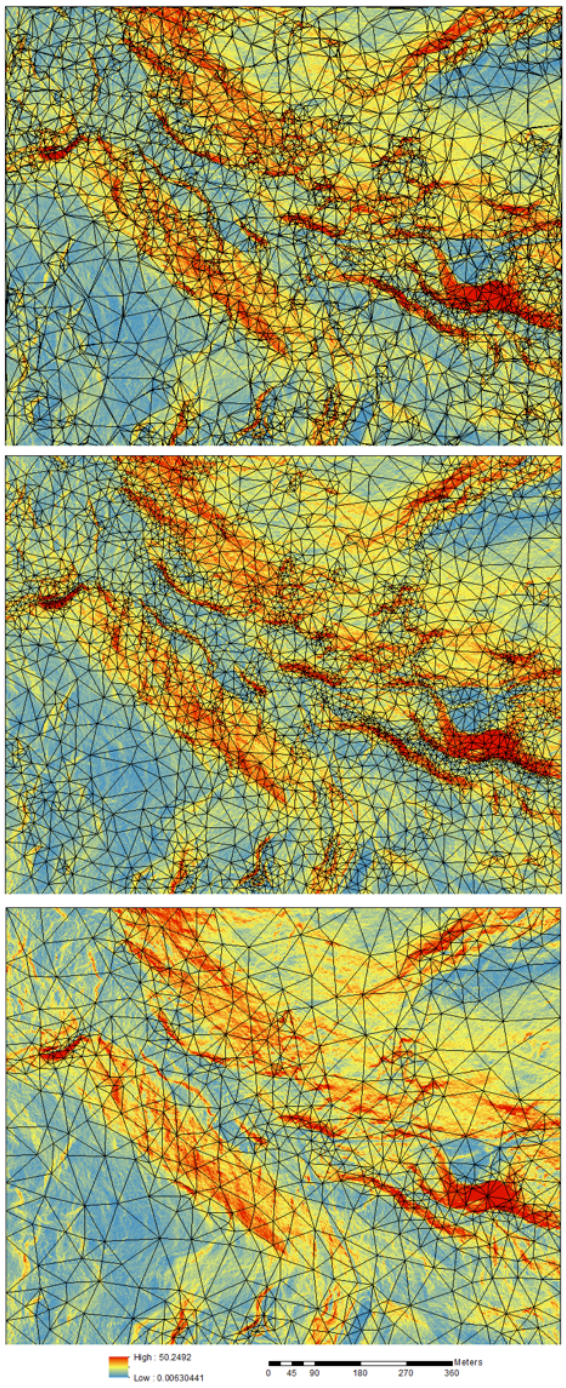

Figure 4.12: Triangulations generated from a LiDAR DEM (1 m x 1 m resolution) for the Granger Creek sub-area. Colours represent slope where red = 50 degrees and blue = 0 degrees. Top) ArcGIS TIN generation tools using a 1m tolerance. Number of triangles = 8,346. Middle) Mesher mesh using a 1 m tolerance. Number of triangles = 6,107. Bottom) Mesher mesh using a 1 m RMSE threshold. Number of triangles = 1,424.

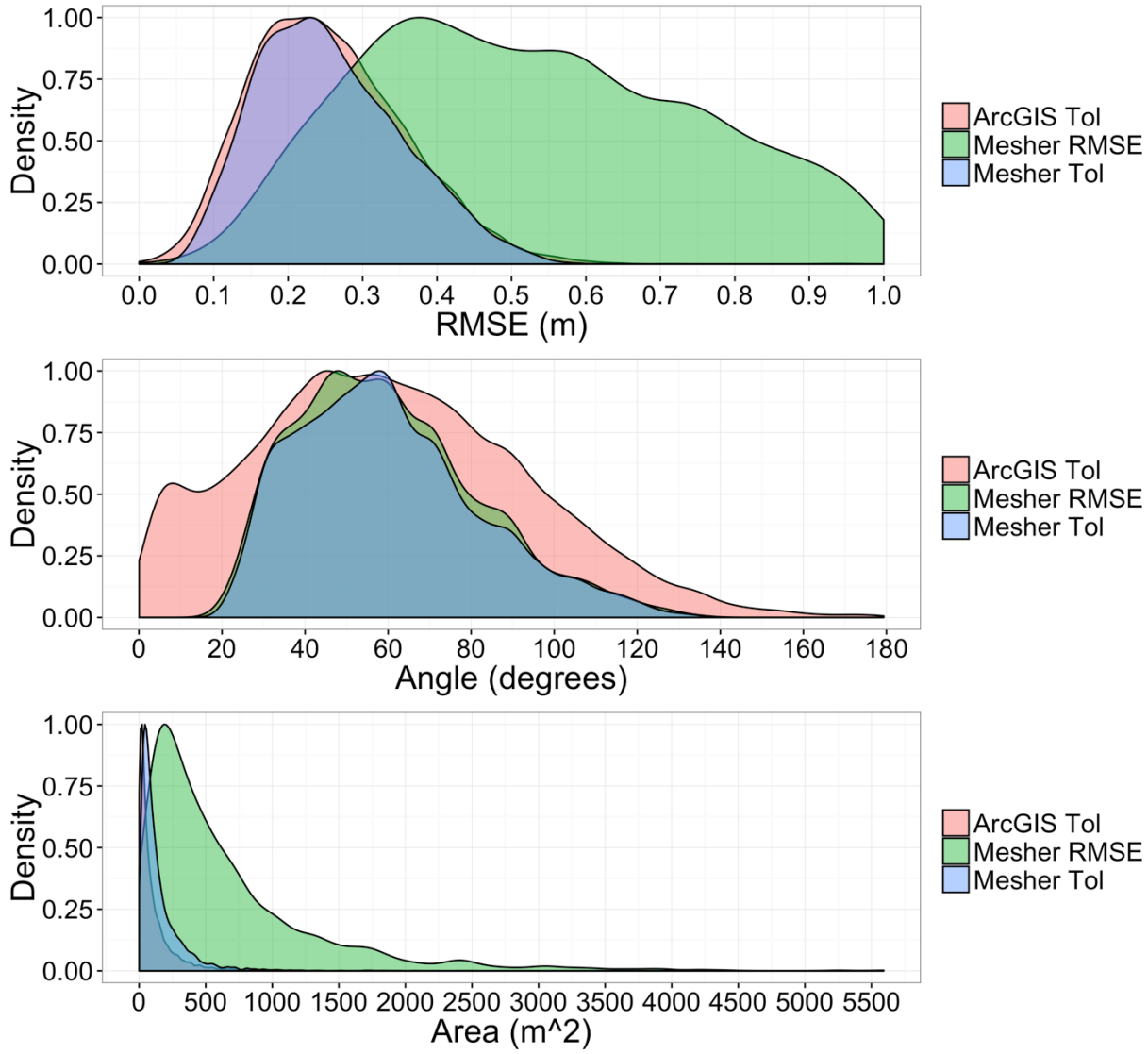

Figure 4.13: Root Mean Square Error (RMSE (m)), inner triangle area (degrees), and triangle area (m^2) for the meshes shown in Figure 4.12.

As the tolerances increase, there is a move towards a log-linear relationship between the number of triangles and minimum area. Because a triangle's minimum area overrides the tolerance calculation, the large area and high RMSEs combinations produce few triangles regardless of the tolerances provided. The finest mesh with 1 m RMSE and 2 m^2 minimum triangle area has approximately 454,000 triangles. This corresponds to a reduction of 50% in total number of elements versus the raster. A large spread in total number of triangles is found in the 0% vegetation case between all RMSE values. However, as the 50% and 75% constraints are added, all but the 1 m RMSE have almost identical numbers of total triangles produced.

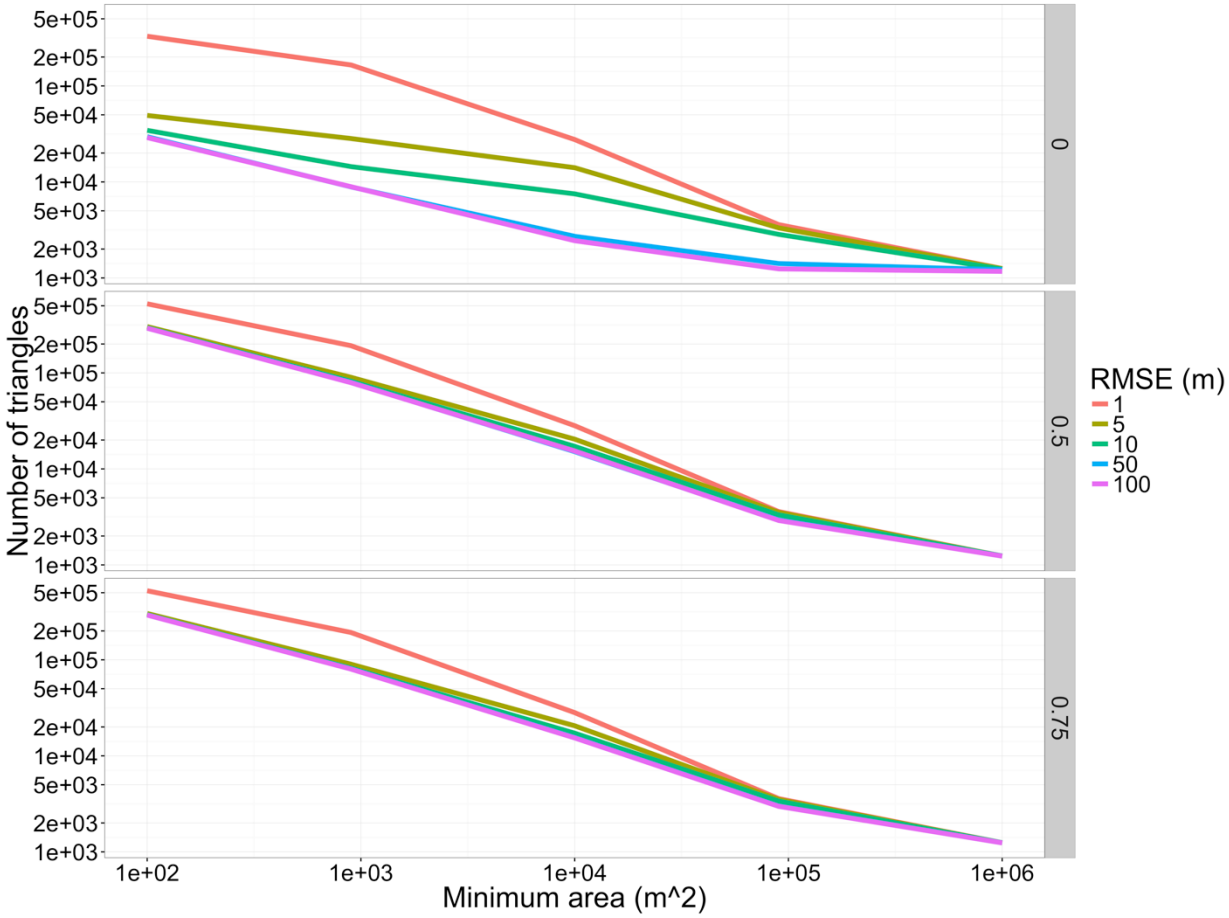

Figure 4.14: Number of triangles as a function of minimum triangle area (x-axis) and RMSE tolerance. Note log axes. The facets corresponds to a vegetation fraction constraint of 0 (top), 0.5 (middle), and 0.75 (bottom).

Shown in Figure 4.15 are three mesh outputs for RMSE tolerances 2 m, 5 m, and 10 m in combination with a maximum triangle area of 90,000 m2 (300 m x 300 m raster equivalent). In all cases, a higher density of triangles is produced along the basin boundary. This is due to the triangulation algorithm exactly representing this boundary. In practice, this is easily mitigated by simplifying the basin boundaries. The lower tolerances (5 m and 10 m) produce fewer triangles on the upper slopes (e.g., southern portion of basin). In all cases, the more complex ridges are generally represented.

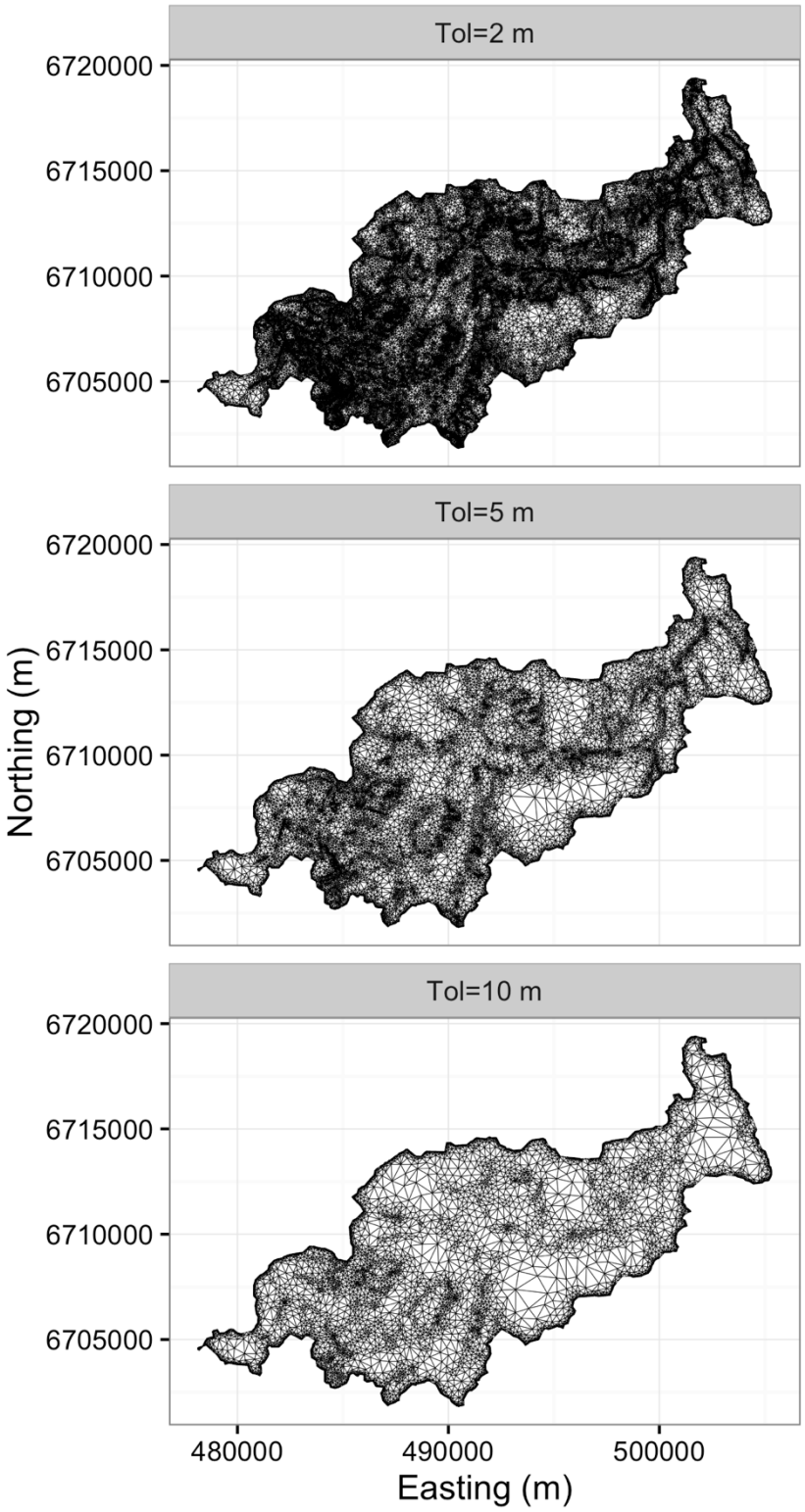

Figure 4.15: Comparison of three meshes showing impact of tolerance: 2 m (top), 5 m (middle), 10 m (bottom) and a minimum area of 90,000 m2 (300 m x 300 m raster equivalent).

4.6.3 Multi-objective constraints

A mesh for the valley location in Wolf Creek is shown in Figure 4.16 and was constrained to topography (RMSE = 1m, maximum triangle area = 225 m^2 [25 m x 25 m]) and vegetation (primary vegetation class> 50%). The vegetation is shown by the 25 m x 25 m raster, with coloured cells corresponding to different vegetation (hollow cells are low shrub). It is evident that the larger vegetation locations on the north plateau (top of domain) have had a few smaller triangles inserted to capture the bounds even though larger triangles could have been used due to small topographic variability. Individual cells in the southern-western portion (bottom left) are missed owing to the 50% constraint – increasing this allows for capturing these individual raster cells at the cost of more triangles. In the east herb area (light blue), large triangles fill the middle of this landcover but are sized to capture the bounds of the patch.

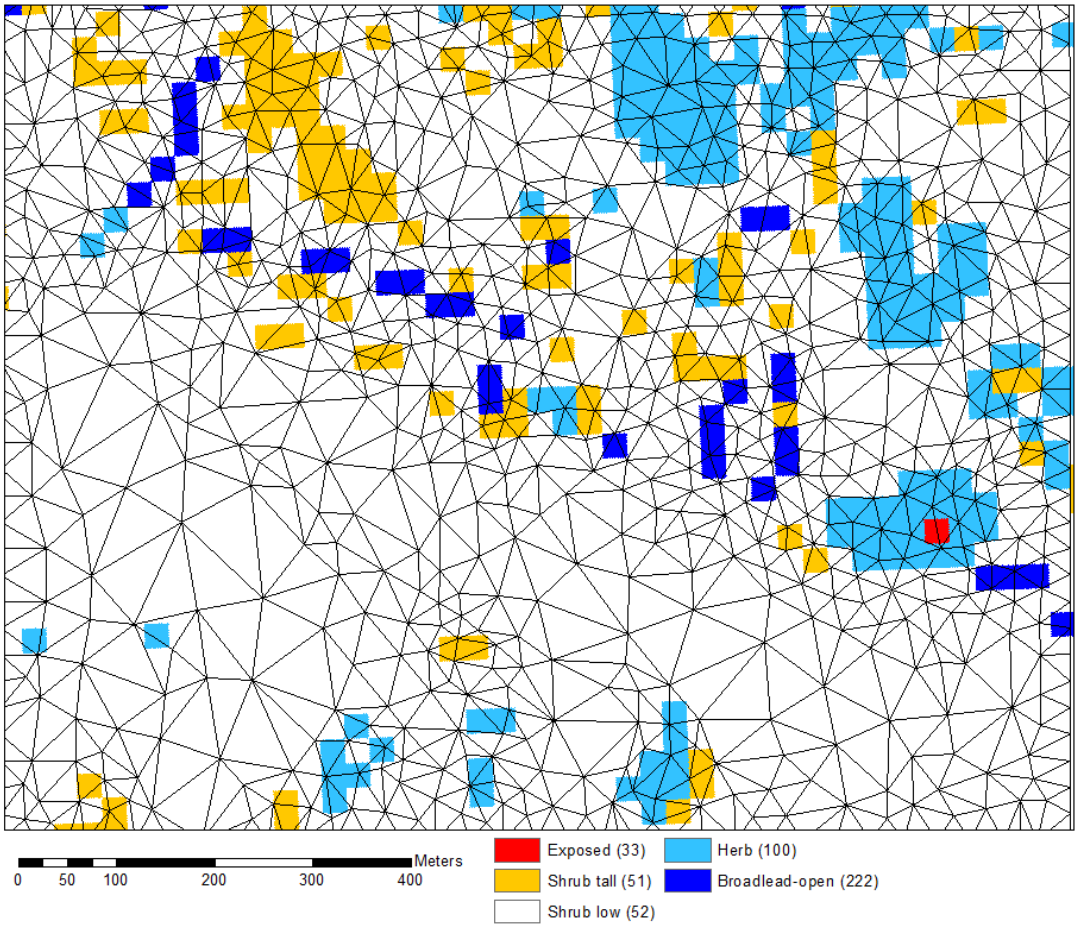

Figure 4.16: Sub-area of the Grange Creek sub-basin, constrained to topography (RMSE = 1 m, maximum triangle area = 225 m2 [25 m x 25 m]) and to vegetation (dominant class > 50%). Vegetation from the EOSD raster is shown in colour.

Shown in Figure 4.17 are the Q-Q plots of the fractal dimensions for each of the 17 vegetation classifications,

across the entirety of Wolf Creek. The fractal dimensions are shown for three cases versus the original dataset: an unstructured mesh constrained to vegetation and topography for 50% constraint (red) and 75% constraint (green) and an unstructured mesh constrained to only topography (blue). Between the 50% and 75% constrained meshes, the largest impacts are in the tails of the distribution. The mesh constrained to only topography shows a substantial simplification of the vegetation patches. Table 4.2 shows the results from comparing the distributions of fractal dimensions of each unstructured mesh approximation to the original raster dataset via the K-S test. Table entries of $p < 0.01$ show distributions that were significantly different. Non-significant p values are not shown. This table shows that 11of 17 land classes did not accurately have their heterogeneity preserved for the topography-only mesh. There is a significant improvement in preserving heterogeneity when using the 75% versus 50% meshes. In all cases, land classes 51 and 213 appear to be the most difficult to represent. Land class 51 is short shrub and represents the largest vegetation area. In many cases, it is the 'background' vegetation class in which other patches are found. Therefore, all the small errors in the approximating mesh are likely compounded for this vegetation class, leading to the observed simplification (i.e., lower fractal dimension). Land class 213, coniferous-sparse, is highly patchy with many small discontinuous locations, likely resulting in these patches being missed. For both the 50% and 75% constraints, the small patches are well represented (e.g., class 222) versus the topography-only constraint. The unstructured mesh constrained to just topography produced 95,154 triangles, the 50% vegetation constraint produced 276,026 triangles, and the 75% vegetation constraint produced 300,308 triangles. Therefore, the increased vegetation constraint between 50% and 75% does not come at a substantial increase of triangles. However, adding the vegetation constraint roughly triples the total number of triangles versus the topography-only constraint.

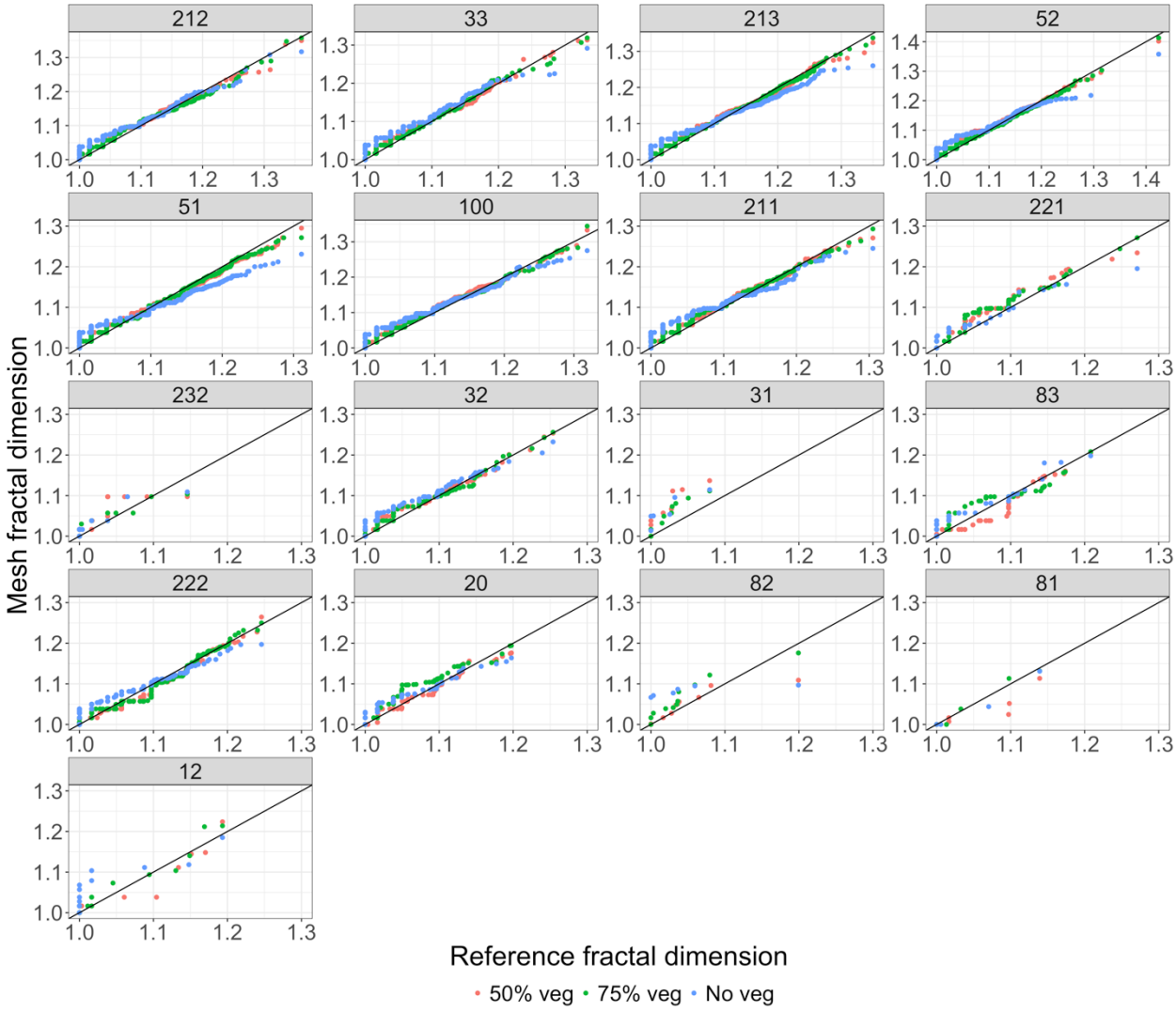

Figure 4.17: Q-Q plots of fractal dimensions for each landcover for both unstructured mesh approximations (constrained to vegetation (50%), red; constrained to vegetation (75%), green; only topographic constraint, blue), versus the original raster dataset.

Table 4.2: Kolmogorov-Smirnov tests of fractal index distributions for: non-vegetation constraint, 50%, and 75% vegetation area constraint versus original vegetation raster. Significance was determined for $p < 0.01$ and denotes the distributions are significantly different. Only significantly different distributions are listed. Distribution differences implies the approximating mesh did not capture the heterogeneity and patch complexity of the vegetation patches.

Class number	Type	Veg constraint 50%	Veg constraint 75%	No veg constraint
212	Coniferous-open			$p < 0.01$
33	Exposed / Barren land			$p < 0.01$
213	Coniferous-sparse	$p < 0.01$	$p < 0.01$	$p < 0.01$
52	Shrub low (< 2 m)	$p < 0.01$		$p < 0.01$
51	Shrub tall	$p < 0.01$	$p < 0.01$	$p < 0.01$
100	Herb (vascular, non-woody)	$p < 0.01$		$p < 0.01$
211	Coniferous-dense	$p < 0.01$		$p < 0.01$
221	Broadleaf-Dense			
232	Mixedwood-open			
32	Rock/rubble			$p < 0.01$
31	Snow/ice			
83	Wetland-herb			
222	Broadleaf-open			$p < 0.01$
20	Water			
82	Wetland-shrub			$p < 0.01$
81	Wetland-tree			
12	Shadow			$p < 0.01$

The Korcak fractional exceedance of patch areas $F(a)$ versus vegetation patch areas are shown in Figure 4.18 for each land cover type for each of the unstructured mesh constraints: 50%, 75%, and no constraint. By visual inspection, each of the tighter constraints produces an F(a)-area relationship that more closely matches the baseline dataset. Numerically, this is validated in Table 4.3. Table entries of $p < 0.01$ show distributions that were significantly different. Non-significant p values are not shown. This table shows that 11 of 17 vegetation classes did not accurately have their heterogeneity preserved for the topography-only mesh. In all cases, this analysis supports the results shown in Table 4.2.

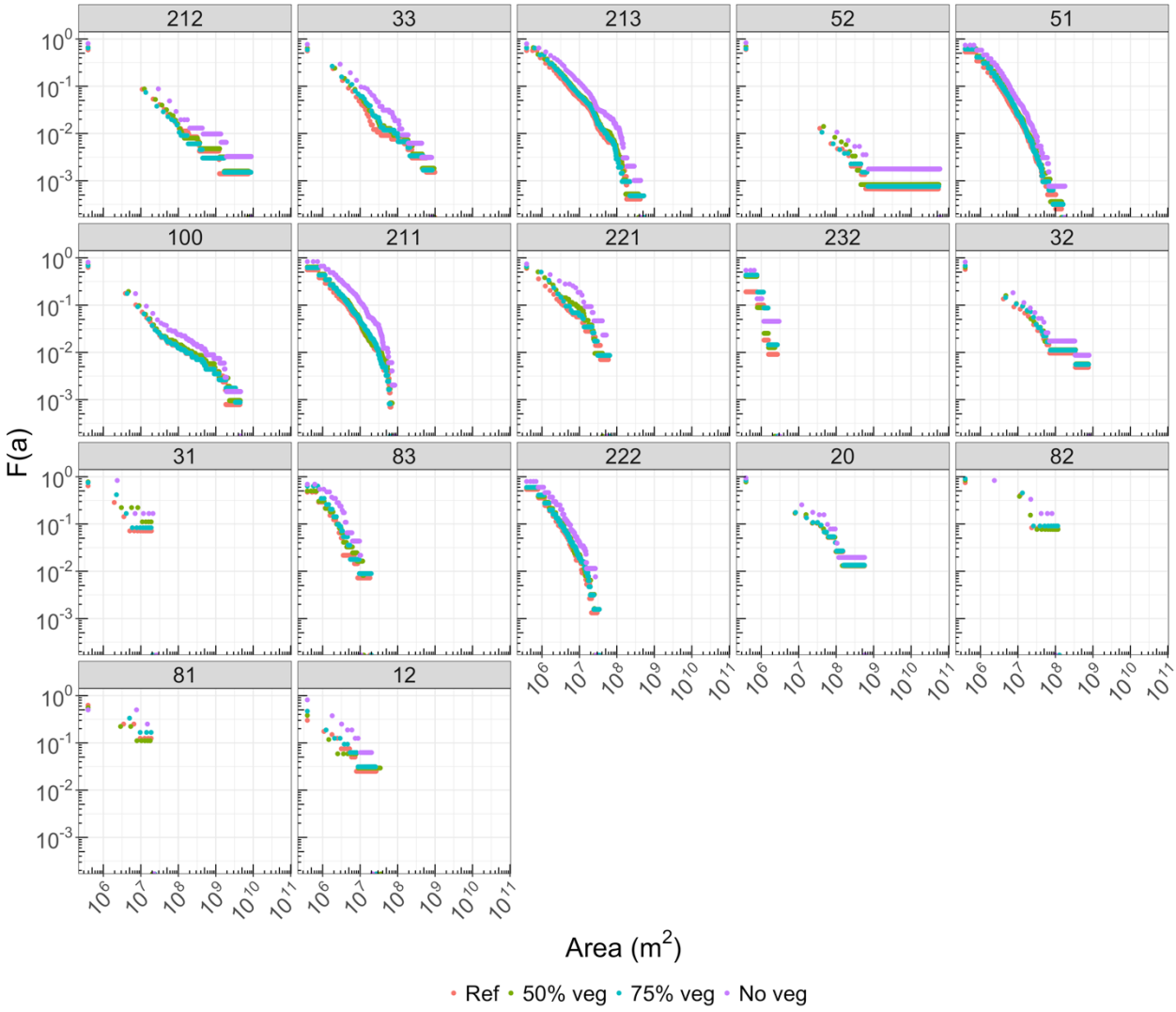

Figure 4.18: Korcak fractional exceedance area F(a) versus area for each landcover for both unstructured mesh approximations (constrained to vegetation (50%), green; constrained to vegetation (75%), blue; only topographic constraint, purple), versus the original raster dataset (red).

Table 4.3: Kolmogorov-Smirnov tests of patch area distributions for: non-vegetation constraint, 50%, and 75% vegetation area constraint versus original vegetation raster. Significance was determined for $p < 0.01$, and denotes the distributions are significantly different.

Class number	Type	Veg constraint 50%	Veg constraint 75%	No veg constraint
212	Coniferous-open			$p < 0.01$
33	Exposed / Barren land			$p < 0.01$
213	Coniferous-sparse	$p < 0.01$	$p < 0.01$	$p < 0.01$
52	Shrub low (< 2 m)	$p < 0.01$		$p < 0.01$
51	Shrub tall	$p < 0.01$	$p < 0.01$	$p < 0.01$
100	Herb (vascular, non-woody)	$p < 0.01$		$p < 0.01$
211	Coniferous-dense	$p < 0.01$		$p < 0.01$
221	Broadleaf-Dense			
232	Mixedwood-open			
32	Rock/rubble			$p < 0.01$
31	Snow/ice			
83	Wetland-herb			
222	Broadleaf-open			$p < 0.01$
20	Water			
82	Wetland-shrub			$p < 0.01$
81	Wetland-tree			
12	Shadow			$p < 0.01$

4.6.4 Weighted constraints

A comparison between weighted constraints for vegetation are shown in Figure 4.19. Due to the coarse topographic tolerance and the low vegetation weight, ensures that the meshing algorithm almost entirely ignores the vegetation. This is compared to the high vegetation weight, where, despite fulfilling the coarse elevation tolerance, triangles are refined further to capture the vegetation patches.

4.6.5 Wall-clock performance

Wall-clock times(s) to generate the mesh for the Wolf Creek basin are shown in Figure 4.20 for each combination of RMSE values delineated by marker symbol, minimum areas delineated by colour, and three vegetation constraints delineated by line type. These wall-clock times are shown as a function of total number of trian-

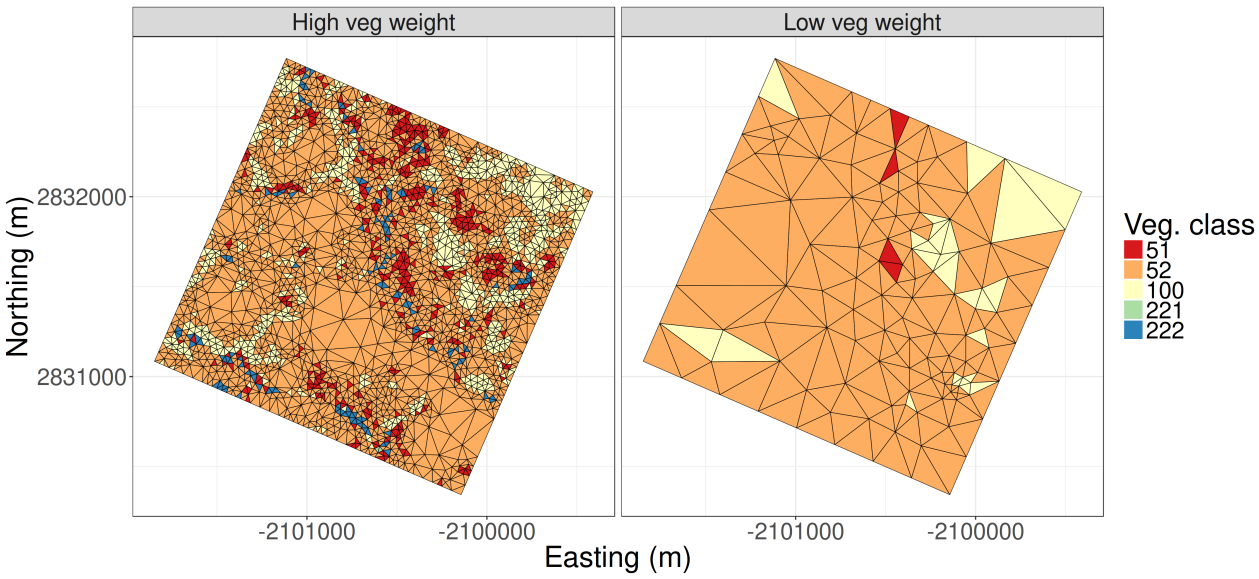

Figure 4.19: Comparison of high vegetation weight (left) and low vegetation weight (right). A coarse elevation tolerance was used. Therefore, for the low vegetation weight, the meshing algorithm almost entirely ignores the vegetation patches. For the high vegetation weight, despite fulfilling the elevation tolerances, the mesh is subsequently refined further to capture the vegetation boundaries.

gles in the final mesh. The increase in wall-clock time is approximately linear. The inclusion of the vegetation constraint did not require substantially more wall-clock time. The wall-clock time for generating the finest mesh with RMSE = 1 m was minimally different than the 50% and 75% vegetation constraint wall-clock times. The average wall-clock time of the two vegetation constraints shows that for the worst case there is a 40% increase in computational time. This increase only appears to be present in the highest resolution meshes. As the minimum area decreases, the algorithm is less able to avoid calls to the tolerance calculation as well as the secondary constraints.

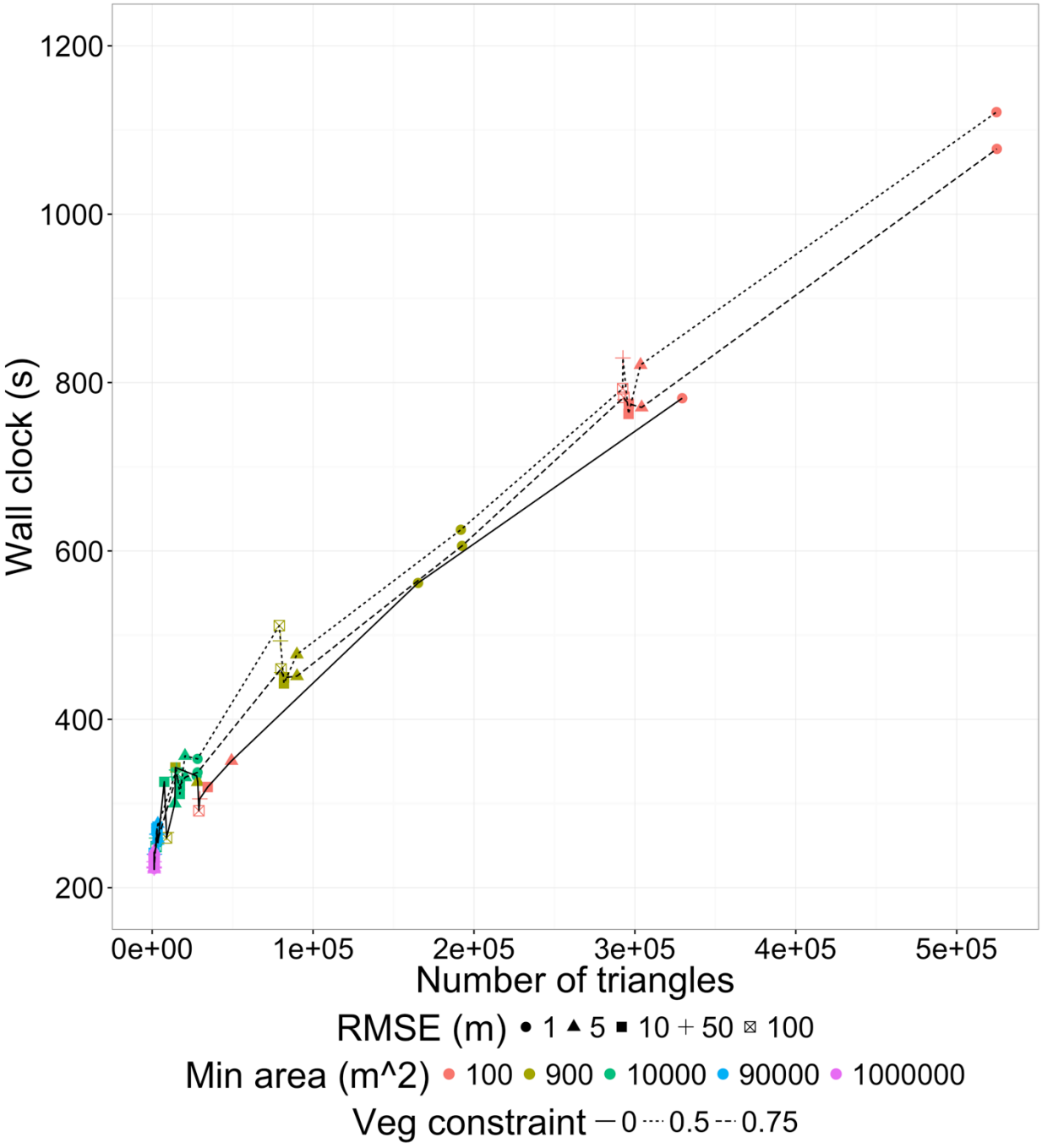

Figure 4.20: Wall-clock times as a function of total number of triangles. The marker symbols demote the tolerances (RMSE threshold), the colours denote the minimum areas (m2), and the line types show these for each vegetation constraint (fractional percent).

4.7 Conclusion

The use of a variable-resolution unstructured mesh allows for fine resolution in areas of high spatial variability and coarse resolution in areas of low spatial variability. Many of the existing triangulation methods either sacrifice triangle quality (e.g., VIP, Heuristic, skeleton) to introduce this resolution variability or guarantees well-formed uniform meshes (e.g., constrained Delaunay triangulation) at the expense of variable triangle resolution.

This work introduced a triangle selection method that coupled per-triangle error metrics, such as RMSE, with a constrained Delaunay triangulation. It was shown that such a method produces well-graded, well-formed triangles that allow for a variable spatial resolution. Using an RMSE error metric provides a better distribution of triangle sizes and errors compared to the maximum difference metric used in existing tools. Compared to the widely used mesh generation in ArcGIS, the Mesher software produced higher-quality triangles, as diagnosed by the distribution of triangle shape and size, and did not lead to an over-representation of the terrain due to its more robust error metric. A single-objective method was extended to allow for constraining to an arbitrary set of rasters. This multi-objective approach allowed for using other hydrologically important data, such as vegetation and soil data, to ensure the spatial heterogeneity of these data is preserved, even when the topography is homogenous and warrants few triangles. The fractal dimension of vegetation patch perimeter-area relationships was used as a measure of spatial heterogeneity in a secondary hydrological variable. By considering a secondary objective raster, the spatial heterogeneity was better preserved than by only constraining to the topography. Compared to a LiDAR raster, 50% to 99.9% of the total number of elements can be removed while preserving the spatial heterogeneity of topography as well as secondary landscape features due to the multi-objective refinement approach.

5 Sensitivity of snowpack energy balance models to input and parameter uncertainty in a mountain basin

5.1 Manuscript status

A version of this chapter has been submitted as a manuscript to the journal Water Resources Research.

Marsh, C. B., Pomeroy, J. W., and Wheater, H. S. (2019), Sensitivity of snowpack energy balance models to input and parameter uncertainty in a mountain basin, Water Resources Research

Author contributions are as follows:

C. Marsh: Initial idea, coding, analysis, manuscript preparation.

J. Pomeroy: Idea refinement, analysis refinement, manuscript revision.

H. Wheater: Idea refinement, manuscript revision.

5.2 Abstract

The seasonal melt of mountain snowpacks is an important contribution to streamflow and thus its accurate simulation in hydrological models is crucial. However, the representation of physical processes in snow models varies considerably, and although physically detailed models have fewer empirical relationships, simpler models have fewer parameters. Previous model comparisons have not shown physically detailed models to have a clear advantage – possibly due to parameter or forcing data uncertainty. In this work, four uncalibrated snowpack models ranging from parsimonious empirical parameterizations to a finite-element multi-layer energy balance formulation were investigated for their performance in snow water equivalent (SWE) simulation, and their sensitivity to errors in meteorological forcings and albedo. The inclusion of fully coupled energy and mass budgets improved SWE simulations, but this was not related to the number of model layers. A compensatory response was found in the fully coupled models' energy and mass balance that reduced their sensitivity to errors in shortwave irradiance. Errors that caused processes to change heat flow into the snowpack were

compensated for by changes in processes governing heat flow out of the snowpack and this compensation was not related to the number of model layers. In contrast, the parsimonious models produced less accurate simulations and were more sensitive to errors in air temperature forcing meteorology. The results suggest that the inclusion of a fully coupled mass and energy budget improves prediction of snow accumulation and ablation, but there was little advantage by introducing a finite-element multi-layered snowpack scheme.

5.3 Introduction

The melt of the seasonal snowpack in cold regions often results in the largest stream discharge of the year (Gray and Male, 1981; Davies et al., 1987). This discharge can affect ecosystems far downstream from the source of snowmelt (Groisman and Davies, 2001) and provides an important source of water for downstream agricultural, industrial, and municipal users (Nazemi et al., 2013). Snowmelt discharge contributions are, in part, controlled by the heterogeneity of snowpacks and variability in surface energetics (Munro and Young, 1982; Olyphant, 1986a; Dozier and Frew, 1990; Marks et al., 1992; Plüss and Ohmura, 1997; Carey and Woo, 1998). Properly simulating a snowpack's response to energetics is crucial for accurate estimation of snowcover ablation and subsequent stream discharge contribution in hydrological models.

Despite considerable progress in model inter-comparisons (Etchevers et al., 2004; Armstrong and Brun, 2008; Essery et al., 2009) and multi-physics frameworks (Pomeroy et al., 2007; Essery et al., 2013; Clark et al., 2015; Essery, 2015; Lafaysse et al., 2017), there remains substantial uncertainty regarding the optimal physics, process couplings, and process representations required to accurately simulate snowcovers and snowmelt in cold-region environments (Clark et al., 2011a; Essery et al., 2013; Pomeroy et al., 2016a; Lafaysse et al., 2017). Model performance in cold regions is felt by many to be improved when including physically identifiable parameters, coupled mass and energy balances, snow redistribution, increased model realism, and explicit representation of spatial heterogeneity (Bartelt and Lehning, 2002; Bowling et al., 2004; Etchevers et al., 2004; Dornes et al., 2008a; Raderschall et al., 2008; Essery et al., 2009, 2013; Fang et al., 2013; Kumar et al., 2013; Pomeroy et al., 2013; Endrizzi et al., 2014; Fiddes and Gruber, 2014; Mosier et al., 2016; Painter et al., 2016a; Harder et al., 2018). Simple models that rely on empirical calibrations, such as the widely used degree-day approach, are uncertain when simulating future conditions because of the impact of the loss of stationary due to anthropogenic climate change on future validity of past calibration periods (Vaze et al., 2010; Brigode et al., 2013). However, the use of more detailed, physics-based models can be hampered due to sparse meteorological observations, often of poor or uncertain data quality. This may result in input forcing uncertainties that can significantly impact model performance (Raleigh et al., 2015a). The use of physically measurable parameters may help reduce model uncertainty (Pomeroy et al., 2007; Hrachowitz and Clark, 2017), although these *a priori* estimated parameters often require calibration to adjust them to local conditions (Paniconi and Putti, 2015). When applied with care, the potential insights and potentially

improved predictions offered by physics-based models motivates their continued use and improvement.

There is some evidence that aspects of cold-regions hydrological systems maintain a narrow range of characteristics and persistence of features when subjected to perturbations such as climate and land cover changes (Carey et al., 2010; Harder et al., 2015, 2018; Shi et al., 2015) making the system "robust" (Carlson and Doyle, 2002; Jen, 2003; Mens et al., 2011). A numerical representation of a snowpack that includes *sufficient* process representation and coupling of mass and energy exchanges may also be robust. Model complexity is used here to describe variations in model structure (process representation, selections, and linkages), the coupling between mass and energy balances, the number of parameters and values, forcing data requirements, the numerical techniques, and spatial discretization requirements. Understanding the interplay between model dynamics, model structure, and model assumptions that leads to the dampening or compensating behaviour may aid in decisions about warranted model complexity, may allow for model simplifying decisions, and aid in quantifying sensitivity and uncertainty propagation. Although robustness, stability, resilience, and insensitivity are similar concepts, model robustness is used herein to discuss a model that is, to borrow the phrase from Kirchner (2006), insensitive for the right reasons due to process representation and process interactions, and not necessarily as a result of tuned parameter sets.

Broadly, energy balance snowpack models fall into three categories: single layer, fixed multi-layer with intermediate complexity, and detailed multi-layer (Etchevers et al., 2004; Vionnet et al., 2012). Single layer models are numerically simple and discretize the snowpack with a single lumped layer; e.g., Utah Energy Balance (UEB) (Douville et al., 1995), SVS (Husain et al., 2016), ISBA (Douville et al., 1995), Energy Budget Snow Model (EBSM) (Gray and Landine, 1988), Stubble–Snow–Atmosphere Model (SSAM) (Harder et al., 2018), and CLASS (Verseghy et al., 1993). This simplicity motivates inclusion in land-surface schemes (Armstrong et al., 2008). These may be simplified further, e.g., for use in GCMs, as an ephemeral soil layer with fixed properties to mimic snow covers (Vionnet et al., 2012). Fixed layer, intermediate complexity models vertically discretize the snowpack into 2 or more internal layers, a maximum of which is prescribed *a priori*. These models often are sufficient for moderate to deep snowcovers, such that large internal gradients are minimized. Examples include the Community Land Model (CLM) (Lawrence et al., 2011), SNOBAL (Marks et al., 1999), ISBA-ES (Decharme et al., 2016), GeoTOP (Endrizzi et al., 2014), Factorial Snow Model (FSM) (Essery, 2015), and the snow scheme in SUMMA (Clark et al., 2015). Detailed multi-layer models use a dynamic number of layers for numerical stability and to capture detailed micro-physics; e.g., SNOWPACK (Bartelt and Lehning, 2002), CROCUS (Vionnet et al., 2012), and SNTHERM (Jordan, 1991). These models generally include parameterizations for grain metamorphism and snowpack layer structure. This in turn allows for application in avalanche hazard forecasting (Bartelt and Lehning, 2002).

Investigations into transferability of model structure and parameter sets has led to studies of model robustness such as from Bárdossy and Singh (2008) and Guerrero et al. (2013). Substantial effort has been made to investigate differences in model behaviour due to process representation (Essery et al., 2009, 2013; Clark et

al., 2011a; Lafaysse et al., 2017) and input forcing uncertainty (Slater et al., 2013; Raleigh et al., 2015a). This work extends these studies by using a set of point-scale energy balance snowpack models of varying physical and numerical complexity to investigate the response of simulated snowpack energy and mass exchange components to various parameter and input perturbations. Specifically, the manuscript addresses three questions:

1. How does model performance versus observations, sensitivity to meteorological forcing, and parameter perturbations vary with model complexity?
2. How does model complexity impact the sensitivity of the surface energy balance components?
3. Are compensatory responses present in a snowpack's coupled energy and mass balance?

5.4 Methodology

5.4.1 Study Site and Observations

The study basin is the Marmot Creek Research Basin (MCRB) (Golding, 1970) located in the Kananaskis River Valley of the Canadian Rocky Mountains (see Figure 5.1). The MCRB ranges in elevation from approximately 1700 m to 2886 m (Rothwell et al., 2016). The climate is dominated by continental air masses where winters are long and cold. Winters are interrupted by frequent chinooks (foehns) (DeBeer and Pomeroy, 2009). Mid-elevation air temperatures average -6 ^{o}C between October and March (Harder et al., 2015). Snow covers upper elevations of the basin from October to June (Rothwell et al., 2016), and the melt period is April to July (DeBeer and Pomeroy, 2009).

This study uses observations from the Upper Clearing site (1860 m) for the water years 2007 to 2016 (inclusive); this site is shown in Figure 5.1 as a cross. A summary of winter (November to March) air temperatures and total precipitation for the study period is shown in Table 5.1. The Upper Clearing site is located in the middle of a mostly circular level clearing in a forest of spruce and fir. The clearing is approximately 56 m in diameter, with an average surrounding tree height of 13 m (Musselman et al., 2015b). It was instrumented with: a HMP35C relative humidity/temperature probe (2.15 m above ground surface [a.g.s]), a NRG 3-cup anemometer (2.97 m.a.g.s; before October 19, 2012), RM Young (2.85 m.a.g.s; after October 19, 2012), a Geonor weighing T200B accumulating precipitation gauge with Alter-shield, and a CM 21 shortwave radiometer (20 m.a.g.s) for the period of this study. Observations were averaged and stored every 15 min. The input meteorological data had been previously quality checked with gaps in-filled from surrounding stations and regressions, and precipitation was not corrected for under-catch due to the sheltered site (Fang et al., 2013). Precipitation phase was determined for all models via the psychometric method of Harder and Pomeroy (2013). Blowing snow and canopy effects were not considered given the sheltered clearing and

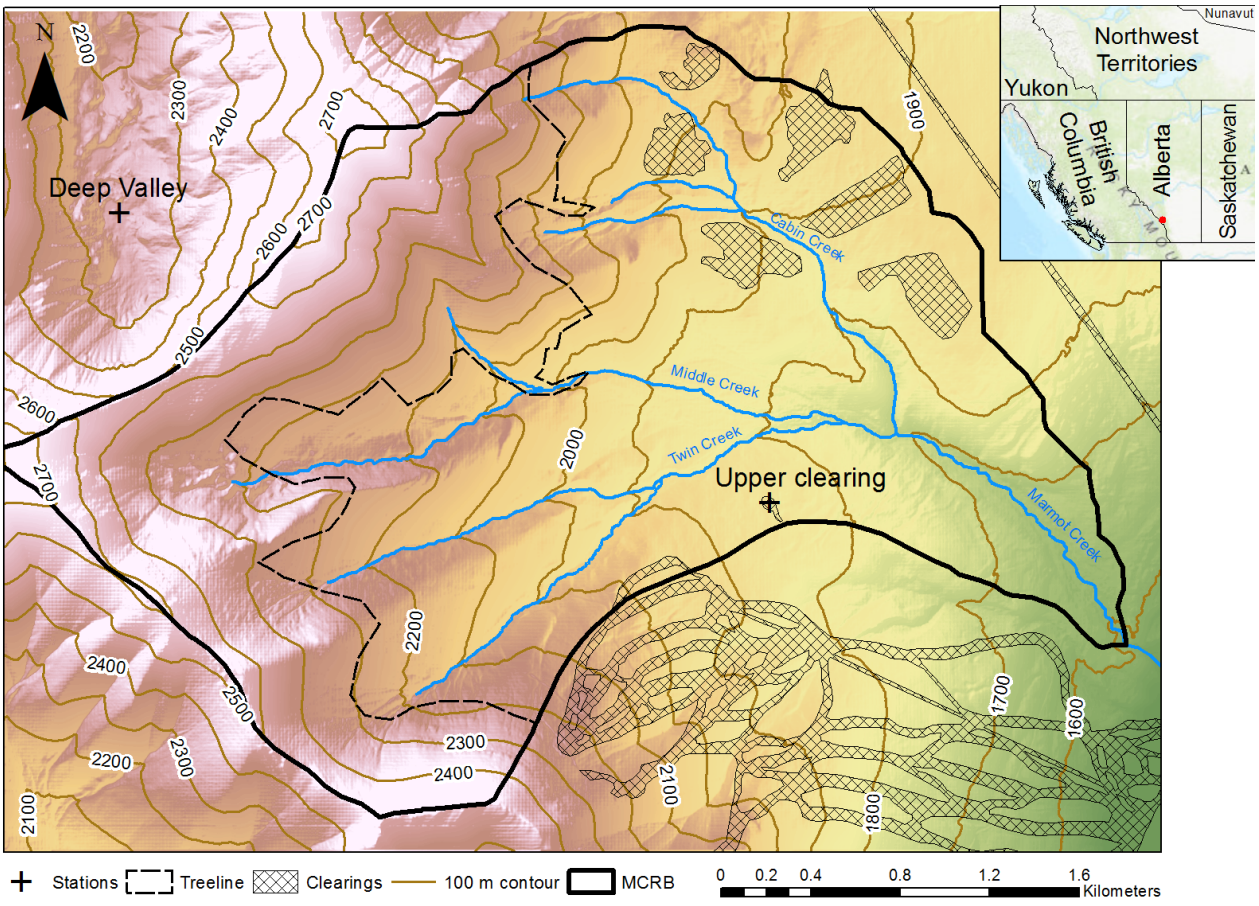

Figure 5.1: Marmot Creek Research Basin, Kananaskis Valley, Alberta in the Canadian Rocky Mountains. The two locations used in this study are show as filled circles. The basin outline is given as solid black, 100 m contour lines shown in brown, stream channels shown in blue, and man-made clearings shown as hatched areas. The Upper Clearing station was used for this study. The southernmost set of clearings is the Nakiska Ski Resort.

sufficient distance of the instrumented clearing centre from canopy-edge effects (Musselman et al., 2015b). Incoming longwave radiation was computed using the method of Sicart et al. (2006) following Fang et al. (2013). This method has been used with success at the MCRB previously, such as Fang et al. (2013), and generally has an error of less than 10% over the snowmelt season (Sicart et al., 2006). Periodic snow surveys of depth and SWE on long transects were conducted by various members of the Centre for Hydrology and used to quantify snow density. For this analysis, a hydrological year is from October 1 to September 31 of the following year and the year of October is taken as the hydrological year. For example, the period of October 2010 to September 2011 would be hydrological year 2010.

Table 5.1: Mean air temperature (°C) and precipitation (mm) for November to March at MCRB.

Year	Mean air temperature (°C)	Sum precip (mm)
2007	-7.24	171.6
2008	-7.43	191.1
2009	-5.72	152.1
2010	-8.66	208.7
2011	-6.4	285.8
2012	-6.19	184.3
2013	-8.42	233.9
2014	-4.89	201.8
2015	-4.63	182
2016	-7.56	213.1

5.4.2 Snowmodels

5.4.2.1 Overview

Four energy balance snowpack models were selected to cover a range of model complexity, including single layer, fixed multi-layer with intermediate complexity, and detailed multi-layer snowpack models. These include: [single layer] the Energy Budget Snowmelt Model (EBSM) model (Gray and Landine, 1988), [single layer] EBSM variant 1 (EBSM1 herein), [intermediate multi-layer] Snobal (Marks et al., 1999), and [detailed multi-layer] Snowpack (Bartelt and Lehning, 2002). The EBSM based models are energy balance calculations using empirical process algorithms, whilst Snobal and Snowpack employ fully coupled energy and mass balances to determine snow ablation and internal energy state. The models are briefly described below.

5.4.2.2 EBSM

The Energy-Budget Snowmelt Model (EBSM) (Gray and Landine, 1988) is a one-layer, process based, semi-empirical daily energy budget snowpack model. EBSM is driven at a daily timestep using observed snowfall, rainfall, incoming solar radiation, wind speed, air temperature, and relative humidity. Energy and mass flux terms are calculated using semi-empirical algorithms that were based on detailed field and modelling studies in the Canadian Prairies and coupled using the energy equation. EBSM sums energy terms on a daily basis for melt calculations. Internal energy is calculated using the previous day's low air temperature and snow mass, ensuring numerical stability in shallow snow covers. Ground heat flux is assumed equal to zero. Albedo changes are calculated from a classification of the melt period into "premelt", "melt" and "postmelt" and areal albedo decay accounts for the effects of snowcovered area depletion on the energy balance. The semi-empirical turbulent flux, albedo, and longwave radiation flux estimation algorithms do not require a snowpack internal or surface temperature as a state variable. Further, the energy and mass balances are uncoupled; for example, a positive/negative latent heat computation does not add/remove mass. As a result, perturbations to boundary conditions affect only one flux term and do not cascade to other energy flux terms.

5.4.2.3 EBSM1

EBSM variant 1 (EBSM1) is derived from EBSM, but with increased physical realism in net radiation fluxes by including the snow surface temperature for outgoing longwave radiation estimation (Ellis et al., 2010; Pomeroy et al., 2016a). EBSM1 has also been modified to account for mass loss/gain via sublimation and condensation and so has a greater degree of coupling of the mass and energy balances than does EBSM. EBSM1 is driven by the same observed daily meterology as EBSM, plus daily incoming longwave radiation. Despite being designed for shallow prairie snowpacks, it has been applied with reasonable success to other regions, e.g., in the Snow Model Inter-comparison Project II (Essery et al., 2009).

5.4.2.4 Snobal

Snobal (Marks et al., 1999) is a physics-based, two layer snowpack model designed for deep mountain snowpacks and initially developed in the Sierra Nevada of California. It approximates the snowpack with two-layers. The upper fixed-thickness active layer is used to estimate outgoing longwave radiation and atmosphere-snow temperature gradients for the turbulent heat flux. Snobal features a coupled energy and mass balance, internal energy storage, internal heat conduction, and liquid water storage calculations. Turbulent fluxes are explicitly calculated via Marks et al. (1992), a bulk transfer approach that includes a Monin-Obukhov stability correction based on Brutsaert (1982; Marks et al., 1992, 2008). The ground heat flux assumes a known temperature in a single soil layer. Snobal is driven using observed precipitation, incoming solar radiation,

incoming longwave radiation, wind speed, air temperature, ground temperature, and relative humidity at an hourly time interval. It has had success in model applications in the Western US, Western Canada, the Arctic and other regions (Marks et al., 2008; Pomeroy et al., 2008; López-Moreno et al., 2016, 2017).

5.4.2.5 Snowpack

Snowpack (Bartelt and Lehning, 2002; Lehning et al., 2002) is a multi-layer finite element snow model initially developed in the Swiss Alps and designed for avalanche hazard forecasting. It describes the micro-physical properties of a snowpack and includes the dynamic addition/removal of snow layers. The mass and heat fluxes are solved using a system of partial differential equations (PDEs). The snowpack is discretized vertically into many snow layers using a Lagrangian coordinate system. It has a coupled energy and mass balance, internal energy, and liquid water storage calculations. Turbulent fluxes are calculated via a bulk-transfer scheme with Monin-Obukhov (MO)stability correction (Michlmayr et al., 2008). It is driven with observed snowfall, rainfall, incoming solar radiation, incoming longwave radiation, wind speed, air temperature, ground temperature, and relative humidity at an hourly time interval. Snowpack has been applied with success to other regions in the Snow Model Inter-comparison Project II (Essery et al., 2009).

5.4.2.6 Modelling framework

EBSM and EBSM1 are available for use within the flexible and modular Cold Regions Hydrological Modelling (CRHM) Platform (Pomeroy et al., 2007) and were run in this model framework with the Gray and Landine (1987) albedo decay routine. This routine is based on point and aerial observations in Saskatchewan, Canada. It uses three periods: premelt, melt, and postmelt to calculate daily irradiance. Snobal and Snowpack were run inside the modular modelling framework CHM (described in Chapter 3). In order to keep the model structure as consistent as possible, both Snowpack and Snobal were configured to use the albedo scheme outlined in Verseghy (1991), detailed in Essery and Etchevers (2004). This albedo method has had good success at this study site when coupled to Snobal in CRHM (Fang et al., 2013). It should be noted that Snowpack can estimate an albedo from prognostic microphysics variables (Michlmayr et al., 2008). However, this albedo routine has not been previously tested at this study site.

The Verseghy (1991) albedo routine is as follows. An exponential decay with an asymptotic minimum of 0.5 is applied for melting snow. For this condition, the melting snow albedo (α) at time t is given as

$$\alpha_t = (\alpha_{t-1} - \alpha_{min}) \exp(-\delta t / a_2) + \alpha_{min} \tag{5.1}$$

where δt is the time step length (s), a_2 is the melting snow albedo decay parameter (s), and α_{min} is the

minimum snow albedo (-). The cold snow decay is given as

$$\alpha_t = \alpha_{t-1} - \frac{\delta t}{a_1} \tag{5.2}$$

where a_1 is the cold snow albedo decay parameter (s). During snowfall, the albedo is refreshed as

$$\alpha_t = \alpha_{t-1} + (\alpha_{max} - \alpha_{t-1}) \frac{S_f}{SWE_{refresh}} \tag{5.3}$$

where α_{max} is the maximum new snow albedo (-), S_f is the snowfall amount (mm), and $SWE_{refresh}$ is the amount of snowfall (mm) that fully refreshes the albedo to α_{max}.

5.4.3 Parameter sensitivity

A sensitivity analysis was performed on parameters associated with key processes parameterizations that have been identified as important for fully coupled energy balance snowmodels (Essery et al., 2013; Schlögl et al., 2016; Lafaysse et al., 2017). This was done to quantify the relative sensitivity of the two energy balance models. These parameterizations impact the surface snowcover energetics via shortwave radiation reflection/absorption (albedo) and turbulent fluxes (surface roughness). The sensitivity analysis was done using the Variogram Analysis of Response Surfaces (VARS) (Razavi and Gupta, 2016) software, using the Nash-Sutcliffe (Nash and Sutcliffe, 1970) of SWE as the objective function. VARS is a general sensitivity analysis framework that uses variogram analysis to provide a characterization of sensitivity (Razavi and Gupta, 2016).

As described above, both energy balance models (Snowpack and Snobal) were configured to use the same albedo decay routine. However, the EBSM and EBSM1 models do not have the same user-configurable albedo parameters or a user-configurable roughness length parameter. Therefore, this parameter sensitivity analysis considers only the two energy balance models (Snobal and Snowpack). There is a large range of reported values for z_0, and values outside of the traditional range have been reported in forest clearings (Conway et al., 2018). For this study, z_0 was varied following ranges from Conway and Cullen (2013) and Schlögl et al. (2016). The parameter uncertainty range is summarized in Table 5.2.

Table 5.2: Ranges for the parameters for albedo (α) and snowcover roughness lengths in the parameter uncertainty study.

Parameter	Description	Range/values
$SWE_{refresh}$	Minimum amount of snowfall to fully refresh albedo	1 mm/hour, 5 mm/hour, 10 mm/hour

Parameter	Description	Range/values
$\alpha_{\min}$	Minimum old snow albedo	0.3, 0.4, 0.5, 0.6
$\alpha_{\max}$	Maximum fresh snow albedo	0.8, 0.85, 0.9, 0.95
α_{a_1}	Cold snow ($< 0^{o}$C) albedo decay	10^7 s, 5.08×10^7 s
α_{a_2}	Melting snow ($= 0^{o}$C) albedo decay	1.2×10^5 s, 9.2×10^5 s
z_0	Aerodynamic roughness length	0.013 m, 0.001 m, 0.0001 m

5.4.4 Input data perturbations

Constant offsets (perturbations) to input meteorological data were used to determine the sensitivity of the snowpack models to input forcing data uncertainty. The forcing variables were chosen to reflect those that have profound impacts on the surface energy balance of the snowpack. The ranges of these perturbations follow the recommendations of Raleigh et al. (2015a) for the normal distribution bias (NB) scenario: incoming solar shortwave radiation, air temperature, incoming longwave radiation, and wind speed. The forcing perturbations are summarized in Table 5.3. For each variable, the ensemble of runs comprised 50 perturbations. Relative humidity (RH) was held constant when temperature was perturbed, making vapour pressure implicitly covariant with temperature. Raleigh et al. (2015a) found and simulations run for the Upper Clearing site (not shown) confirmed, that RH and hence vapour pressure perturbations had an insignificant impact themselves on model outputs and so the impact of varying vapour pressure and RH are not considered further. The precipitation phase for all models was allowed to vary with the air temperature perturbations. In all cases, the perturbed solar radiation, wind speed, and incoming longwave radiation were constrained to be non-negative and non-zero. Although a multi-variate analysis that considered multiple perturbations simultaneously would provide insight into covariant responses in the models, this sensitivity analysis used only the univariate responses and temporally constant perturbations so that the model behaviours could be more readily diagnosed.

Table 5.3: Forcing perturbation details, following Raleigh et al. (2015a) Normal Bias (NB) scenario.

Forcing	Distribution	Range	Units
Air temperature	Normal	[-3.0, 3.0]	^{o}C
Windspeed	Normal	[-3.0, 3.0]	$m \cdot s^{-1}$
Incoming shortwave radiation	Normal	[-100, 100]	$W \cdot m^{-2}$
Incoming longwave radiation	Normal	[-25, 25]	$W \cdot m^{-2}$

5.4.5 Sensitivity measure

To quantify the sensitivity of each model to input perturbations, the coefficient of variation (CV) of the ensemble is used. Consider an ensemble of model outputs, e.g., SWE, with each ensemble member representing the impact of a single forcing perturbation. From this, the CV is calculated for the ensemble at each model timestep. Thus, each timestep has an associated metric (the CV) that is a measure of the spread of model outputs, and therefore model sensitivity, at a given point in time. For a given timestep, if the ensemble spread is low, there is low sensitivity, and if there is a large spread, then the model is more sensitive. The CV values from each timestep can be temporally aggregated to represent a cumulative distribution of CV values for some time period, e.g., monthly. This distribution describes the variability of CV, and any changes in cumulative sensitivity with time. This approach is illustrated in Figure 5.2. Each gray line is a single realization of the ensemble under a specific perturbation for an arbitrary output. The red dots are the model output values, at some time t, used to calculate the CV at that timestep.

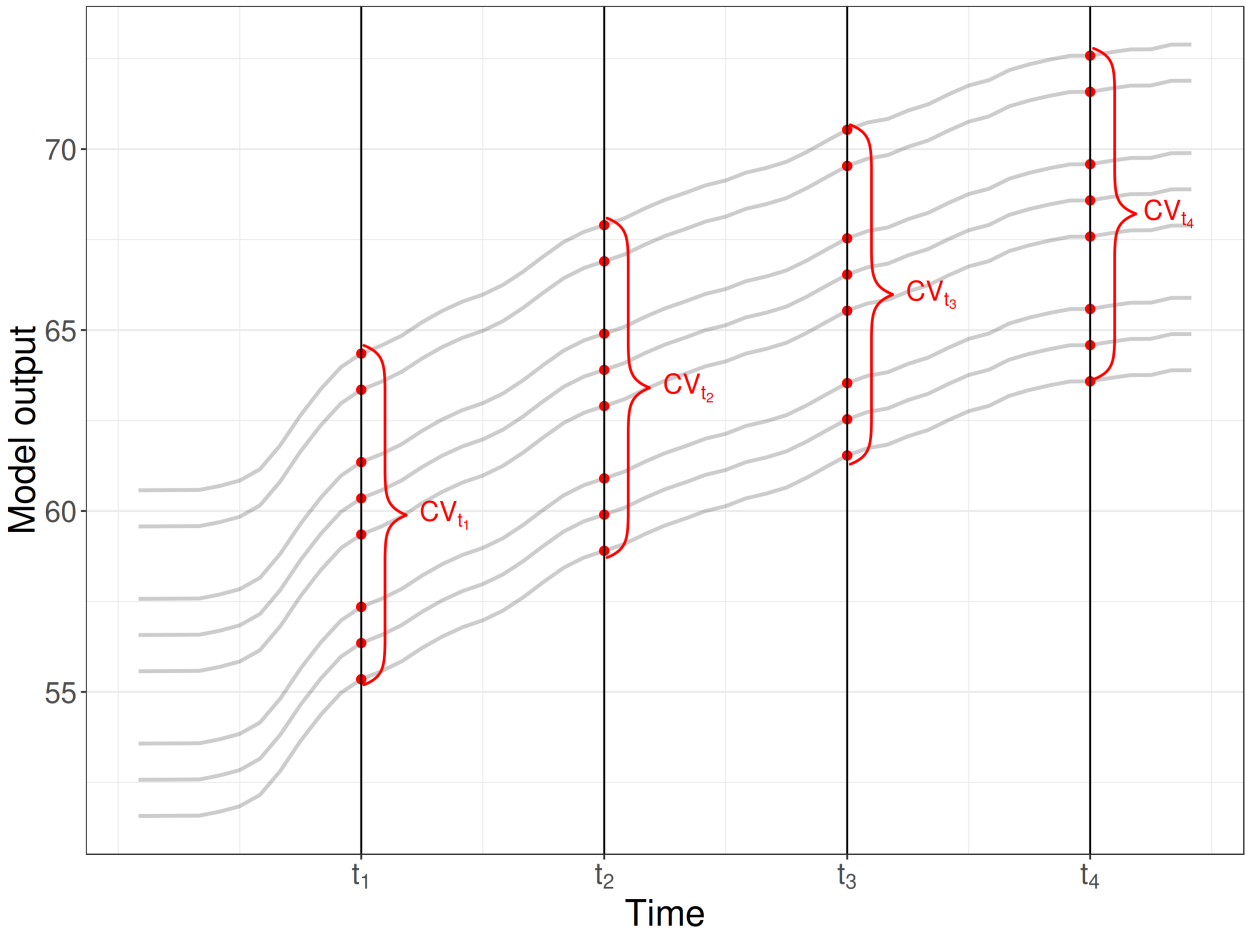

Figure 5.2: The coefficient of variation, CV, is used as a measure of ensemble spread for each timestep.

5.4.6 Terrain shadowing

A snowpack energy budget model may be a robust system due to: 1) covariant energy balance components (Horne and Kavvas, 1997); 2) internal snowpack energy that provides a 'memory' to the system (Jennings et al., 2018); and 3) coupling of the mass and energy balance (Male and Gray, 1975; Gray and Landine, 1988). For instance, alpine snowpacks are often shadowed by the surrounding terrain in mid-winter, reducing shortwave irradiance (Olyphant, 1986b; Chueca and Julián, 2004; Marsh et al., 2012). However, this does not necessarily manifest itself as later or slower melt (Marsh et al., 2012). Shaded snowpacks initially experience a decrease in internal energy that results in decreased longwave radiation exitance, and weakened or reversed turbulent fluxes and ground heat fluxes that can cause an energy gain that can partially compensate for the lower solar irradiance (Pomeroy et al., 2003; Ohara and Kavvas, 2006; DeBeer and Pomeroy, 2010; Jennings et al., 2018). The inverse is true when shaded snowpacks are exposed to the sun. Combined, these couplings may provide a mechanism to dampen a periodic input variability.

To investigate any potential compensatory response in snowpack energetics, the example described above of a partially shaded snowpack was simulated. The results of the four snowpack models driven by shortwave irradiance estimation without terrain shadowing and thus excessive shortwave irradiance was compared to results drive by irradiance that included shadowing. Not including terrain shadows is a common simplification made in modelling mountain terrain.

A virtual location (point approach) was taken. The minimally shadowed Upper Clearing meteorological record was used and the incoming irradiance was calculated following Marsh et al. (2012) with and without using the terrain shadowing of the heavily shadowed Deep Valley site, shown in Figure 5.1.

5.5 Results

5.5.1 Model v. observation

The baseline modelled SWE (mm) for the ten-year study period is shown in Figure 5.3 for all four models. Snow course observations of depth and density used to calculated SWE following Pomeroy et al. (1995) are shown as black dots.

Across all years, simulated SWE from all four models compared generally quite well to observations. The root mean squared error (RMSE) and Mean Bias (MB) are shown in Table 5.4 and Table 5.5 respectively. The mean RMSE and MB values for each model across all years are shown in Table 5.6 and Table 5.7 respectively. From this, Snowpack had the lowest RMSE (31.1 mm), with Snobal and EBSM effectively tied (38.1 mm

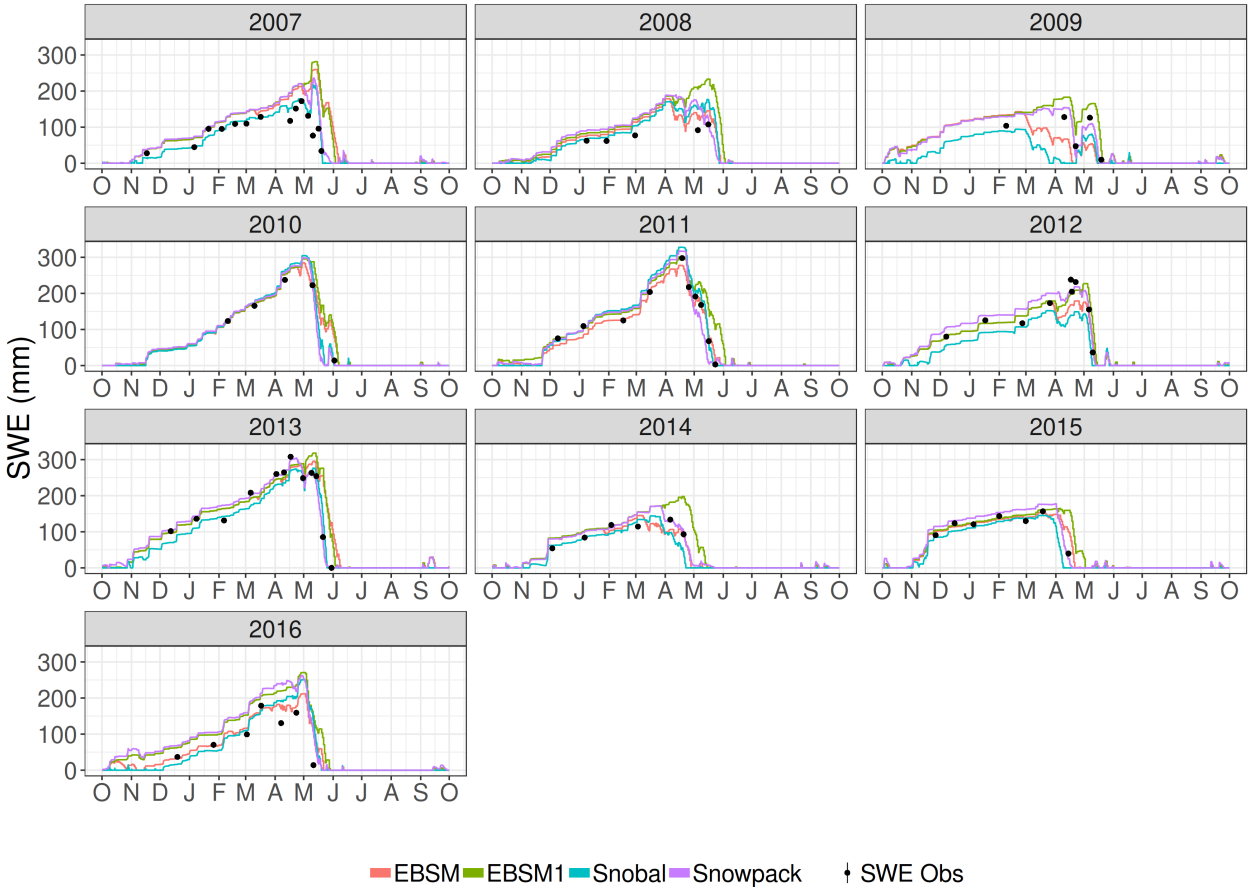

Figure 5.3: Comparison between the four models at Upper Clearing. Snow course observations are in black. The two less complex snow models, EBSM and EBSM1 are shown in red and green respectively, Snobal, the intermediate complexity model, is shown in teal, and the most complex model Snowpack is shown in purple.

and 38.8 mm). EBSM1 was the poorest of all models (57.2 mm). Snobal had the smallest magnitude bias (-3.1 mm), followed by EBSM (11.4 mm), Snowpack (17.3 mm), and EBSM1 (39.6 mm).

Table 5.4: Root Mean Squared Error (RMSE) for each snowpack model.

Year	Snobal RMSE (mm)	Snowpack RMSE (mm)	EBSM RMSE (mm)	EBSM1 RMSE (mm)
2007	40.7	57.1	79.7	88.2
2008	42.4	42.3	29.3	79.8
2009	65.1	22.8	49.7	36.9
2010	20.5	11.4	30.1	46.8
2011	24.2	32.5	14.2	47.2
2012	57.2	22	34.5	34.4
2013	27.2	15.7	63.8	67.2
2014	28.8	21.1	22.2	51.9
2015	19.2	19.5	24.2	46.2
2016	55.5	66.4	40.4	73.7

Table 5.5: Mean Bias (MB) for each of the snowpack models.

Year	Snobal MB (mm)	Snowpack MB (mm)	EBSM MB (mm)	EBSM1 MB (mm)
2007	18.2	45.9	59.3	65.9
2008	33.6	38.1	27.5	65.8
2009	-49.5	-1.1	-32.5	35.3
2010	10.8	3.6	19	32.5
2011	15.1	-8.9	-5.5	32.8
2012	-49.1	7.6	-14.3	8.2
2013	-9.6	-0.3	25.6	32
2014	-13.6	13.8	6	39.6
2015	-13.5	13.7	8.8	20.9
2016	27	60.3	22.1	62.7

Table 5.6: Mean of RMSE values for each model.

Snobal RMSE (mm)	Snowpack RMSE (mm)	EBSM RMSE (mm)	EBSM1 RMSE (mm)
38.1	31.1	38.8	57.2

Table 5.7: Mean of MB values for each model.

Snobal MB (mm)	Snowpack MB (mm)	EBSM MB (mm)	EBSM1 MB (mm)
-3.1	17.3	11.6	39.6

In drier, colder winters, e.g., 2007, 2008, EBSM and EBSM1 models accumulated too much SWE. In warmer years, e.g., 2009 and 2014, EBSM performed better than EBSM1. Compared to Snowpack and Snobal, the EBSM models produced a longer ablation period. Snobal struggled in warm years that had early accumulation, e.g., 2009, 2012, 2016 by producing too low of an accumulation, resulting in a consistent under-estimation of peak SWE. The most egregious was 2009, with a consistent underestimation and early mid-winter melt. Snowpack produced the most consistent results, in best agreement with the observations. However, it was not without fault. The 2007 and 2016 years had a constant over-estimation of SWE.

5.5.2 Parameter sensitivity

The VARS sensitivity analysis for the Snobal and Snowpack snow models is shown in Figure 5.4. For all parameters except the roughness length (z_0), Snobal was more sensitive than Snowpack. The fresh snow albedo (α_{max}) was found to be the most sensitive parameter for the two models, followed by the minimum albedo (α_{min}). The melting snow albedo decay constant (α_2) was more sensitive than the cold snow albedo decay constant (α_1). Snowpack was substantially more sensitive than Snobal to the roughness length.

5.5.3 Forcing perturbation sensitivity

The model response to all forcing perturbations is shown in Figure 5.5. This shows the coefficient of variation (CV) for the ensemble of simulated SWE, for each model, across all input perturbations. The centre line of the boxplot is the median, the bottom and top of the boxplot are the first (25%) and third (75%) quartiles respectively. The thin lines are ± 1.5 times the Inner Quartile Range. This shows that the spread of all the ensembles, and thus the model sensitivity to a variety of input perturbations to forcing data, increased as

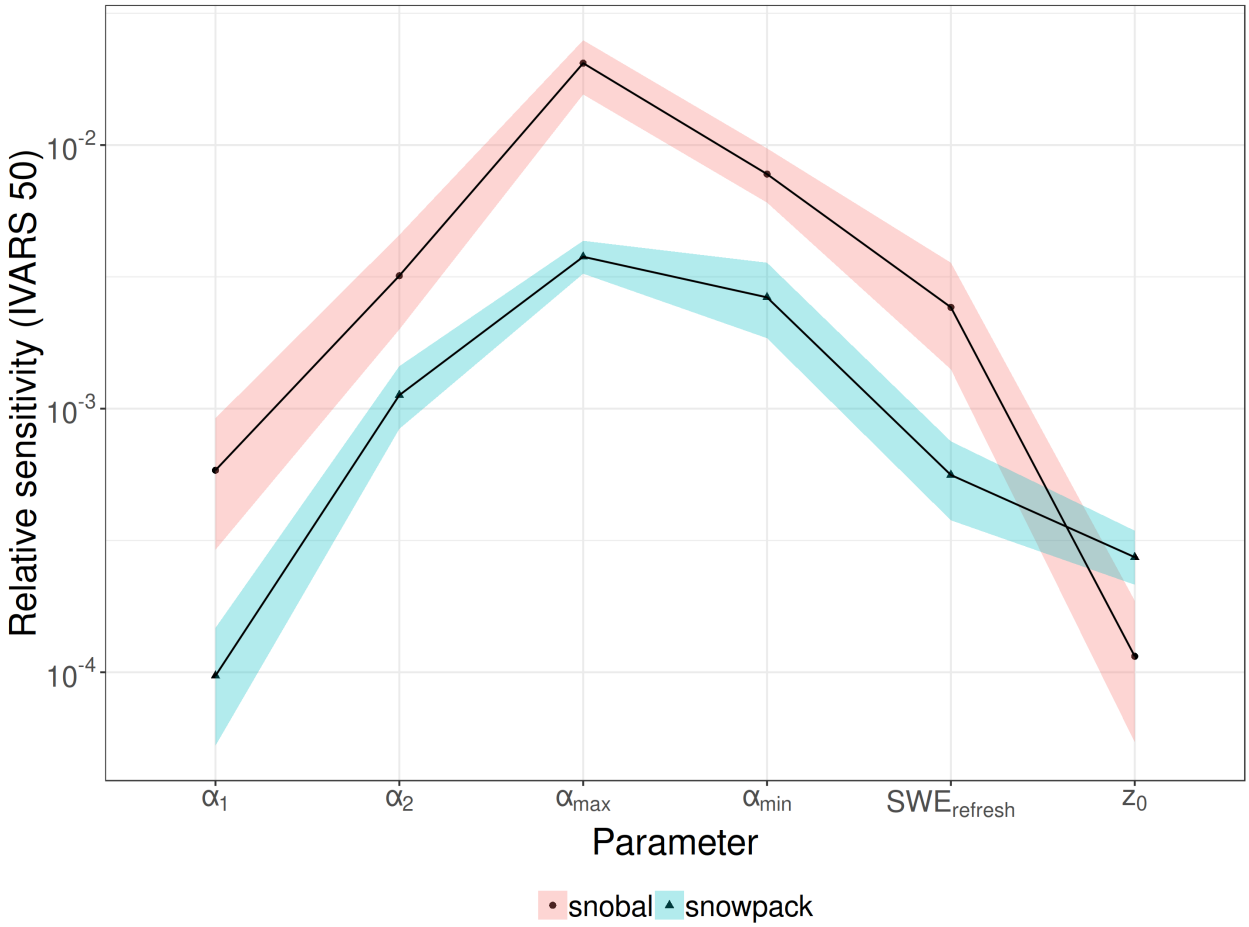

Figure 5.4: A VARS sensitivity analysis for the Snobal and Snowpack snowmodels. Tested parameters include albedo parameters and the snow roughness length. From left to right: cold snow (< 0°C) albedo decay, melting snow ($= 0$°C) albedo decay, maximum fresh snow albedo, minimum amount of snowfall to fully refresh albedo, and aerodynamic roughness length.

the models become more complex including: increased coupling between mass and energy terms, increased number of parameters, discretization of snow layers, and greater physical complexity (e.g., model physics). Although the mean CV value for the EBSM1 model was approximately the same as EBSM, EBSM1 had substantially lower overall CV spread than the EBSM model. This corresponded to an overall lower sensitivity than EBSM. Snobal, and then Snowpack were the most sensitive; they had a larger median as well as greater spread in CV values.

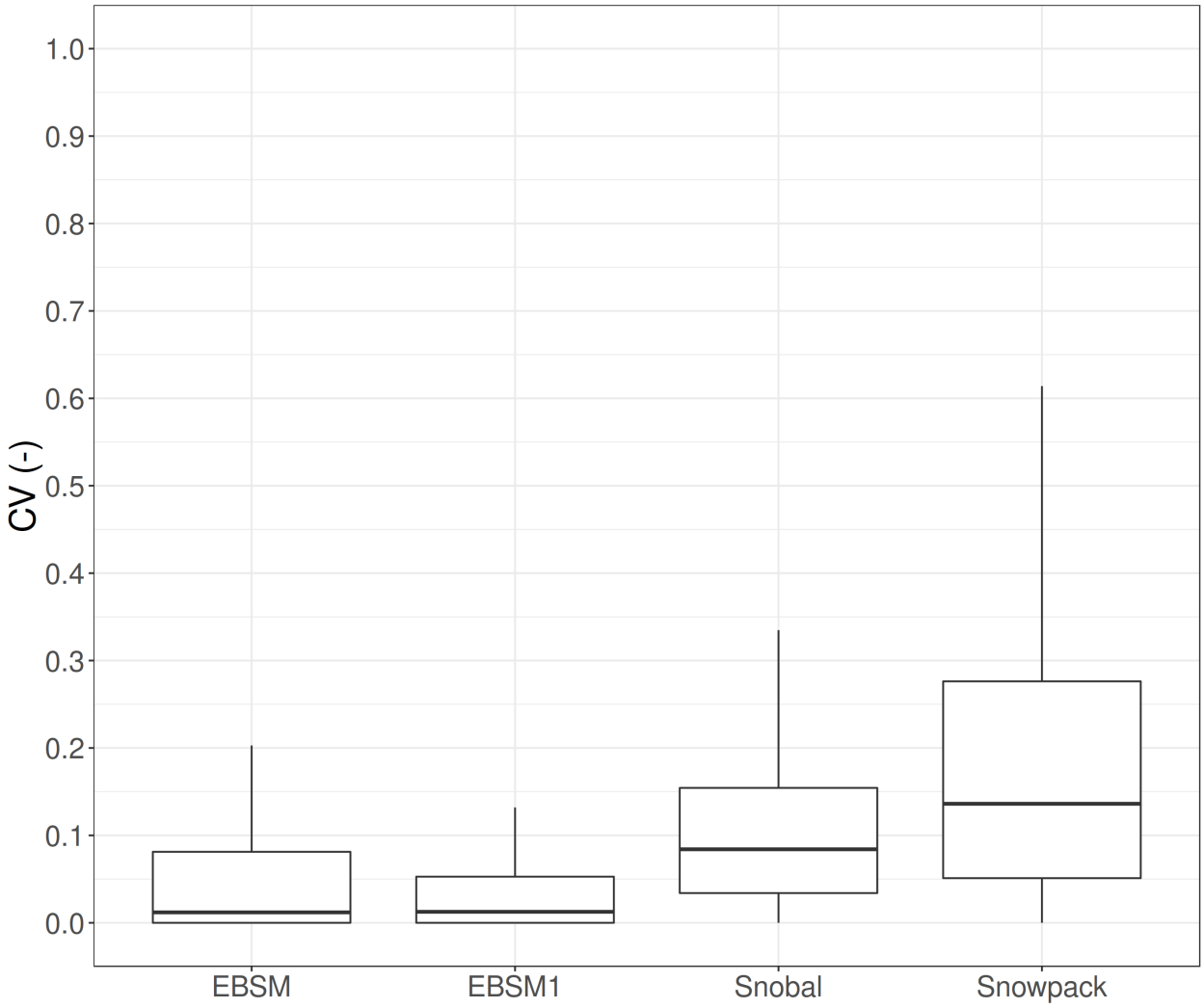

Figure 5.5: The coefficient of variation (CV) for each for the four models (increasing complexity left to right), for all forcing perturbations. As the models become more complex the mean CV value increases indicating increased overall sensitivity. The centre line of the boxplot is the median, the bottom and top of the box plot are the first (25%) and third (75%) quartiles respectively. The thin lines are ± 1.5 times the Inner Quartile Range.

The CV for each model and each input perturbation combination is summarized as boxplots in Figure 5.6. This diagnoses the overall model sensitivity to meteorological perturbations in: longwave irradiance (red),

shortwave irradiance (green), air temperature (teal), and wind speed (purple).

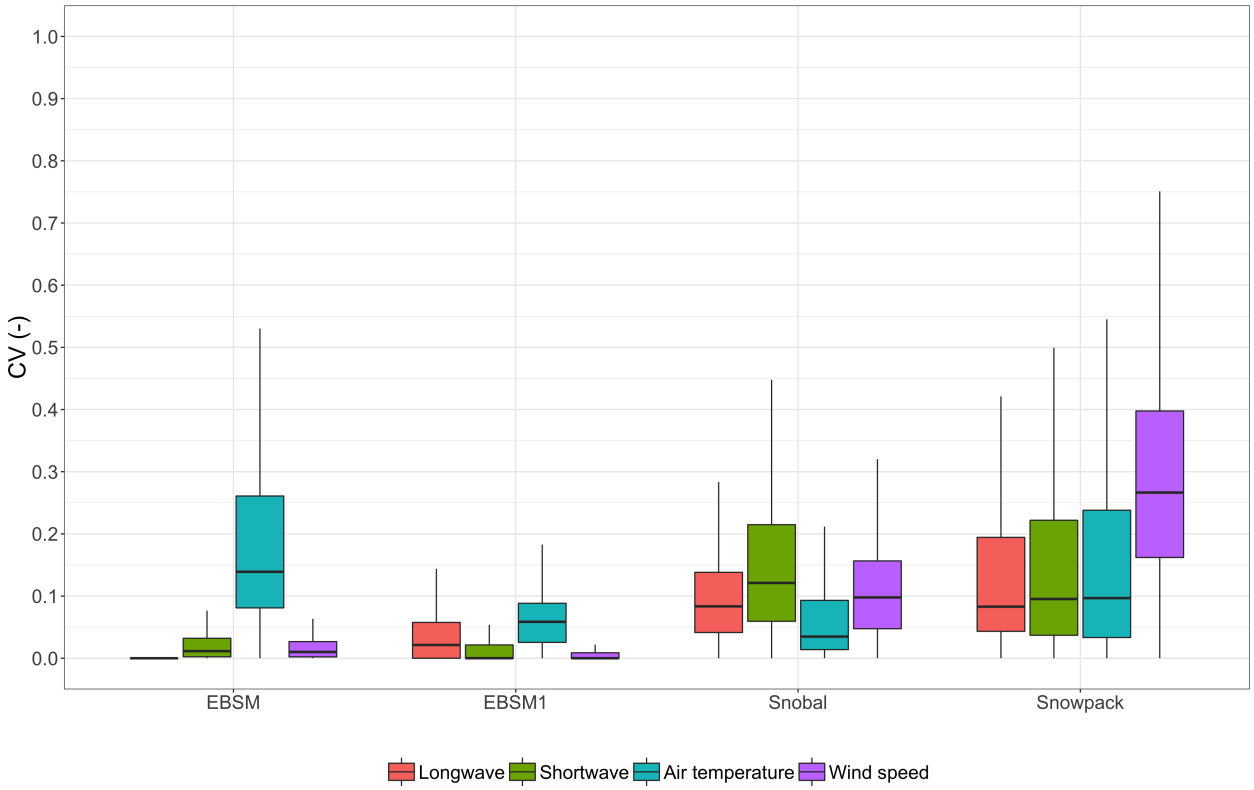

Figure 5.6: The coefficient of variation (CV) for each for the four models (increasing complexity left to right), separated by forcing perturbation. As the models become more complex the mean CV value increases indicating increased overall sensitivity. The centre line of the boxplot is the median, the bottom and top of the box plot are the first (25%) and third (75%) quartiles respectively. The thin lines are ± 1.5 times the Inner Quartile Range.

As model complexity increased (left to right), the models became increasingly sensitive to more forcing variables. EBSM had the largest sensitivity to air temperature, with a median value greater than any other model, and a variability essentially the same as that of Snowpack. EBSM was slightly sensitive to shortwave irradiance and windspeed. Longwave irradiance is not used by EBSM, and thus it had no sensitivity to it. Air temperature remained the dominant sensitivity for EBSM1. Overall sensitivity to air temperature was lower for EBSM1 than EBSM, however the EBSM1 median CV was larger than that of Snobal, with a similar range. Snobal was most sensitive to shortwave irradiance, followed closely by windspeed and longwave irradiance. The air temperature perturbation was the least sensitive input perturbation for Snobal. Snobal had a smaller sensitivity range than Snowpack. Snowpack was most sensitive to windspeed, greater than any of the other three models. Moderate and almost equal sensitivity was found to shortwave irradiance, air temperature, and longwave irradiance.

Overall, EBSM's sensitivity was almost entirely due to air temperature perturbations. EBSM1 had a lower overall spread in model ensemble but was sensitive to more forcing perturbations than EBSM. However, it was

less sensitive than EBSM to air temperature. Snobal was as sensitive as Snowpack for longwave irradiance, but overall less sensitive in all other forcings than Snowpack. Snowpack was the most sensitive of all four models across all input perturbations, and generally had a greater spread in the CV distributions. It was almost equally sensitive for longwave and shortwave irradiance, and air temperature.

5.5.4 Temporal sensitivity

The temporal variability (change in time) of the model sensitivity to the input perturbations is shown grouped on a per-month basis in Figure 5.7 and shown on a per day basis in Figure 5.8. The CVs of the SWE ensembles for all hydrological years were aggregated daily and shown as hex-binned density plots, with a 2-week rolling median shown in black. The models are presented top-to-bottom in increasingly model complexity. Because EBSM does not use longwave irradiance, this plot (top-left in Figure 5.8) is left blank.

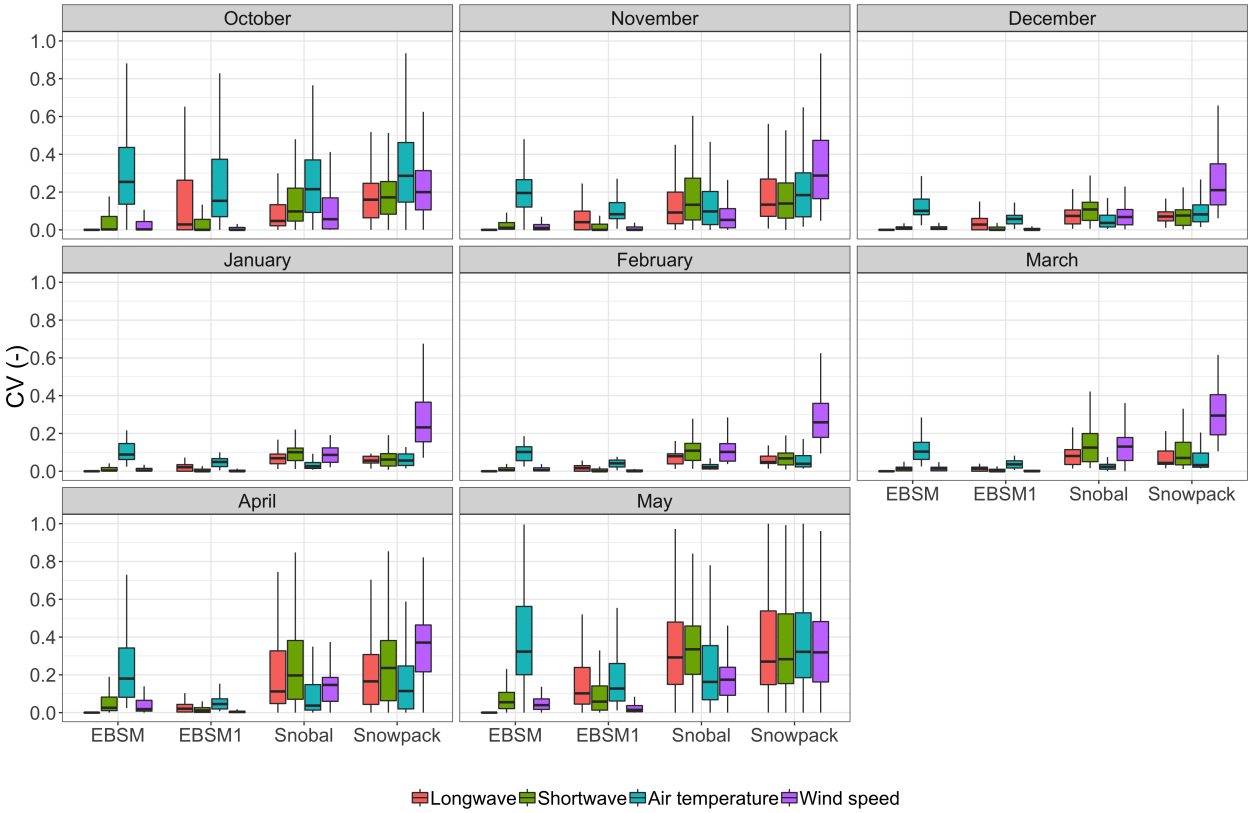

Figure 5.7: The coefficient of variation (CV) of SWE for each for the four models (increasing complexity left to right), separated by forcing perturbation.

Although snowfall occurs in October of most years, the first autumn snowpacks are generally shallow and ablate quickly. It is not until late October and November that snowpacks remain on the ground. There was a strong seasonal variability in sensitivity for perturbations to longwave and shortwave irradiance, and air temperature perturbations. The median CV value and total spread showed an asymmetrical response in

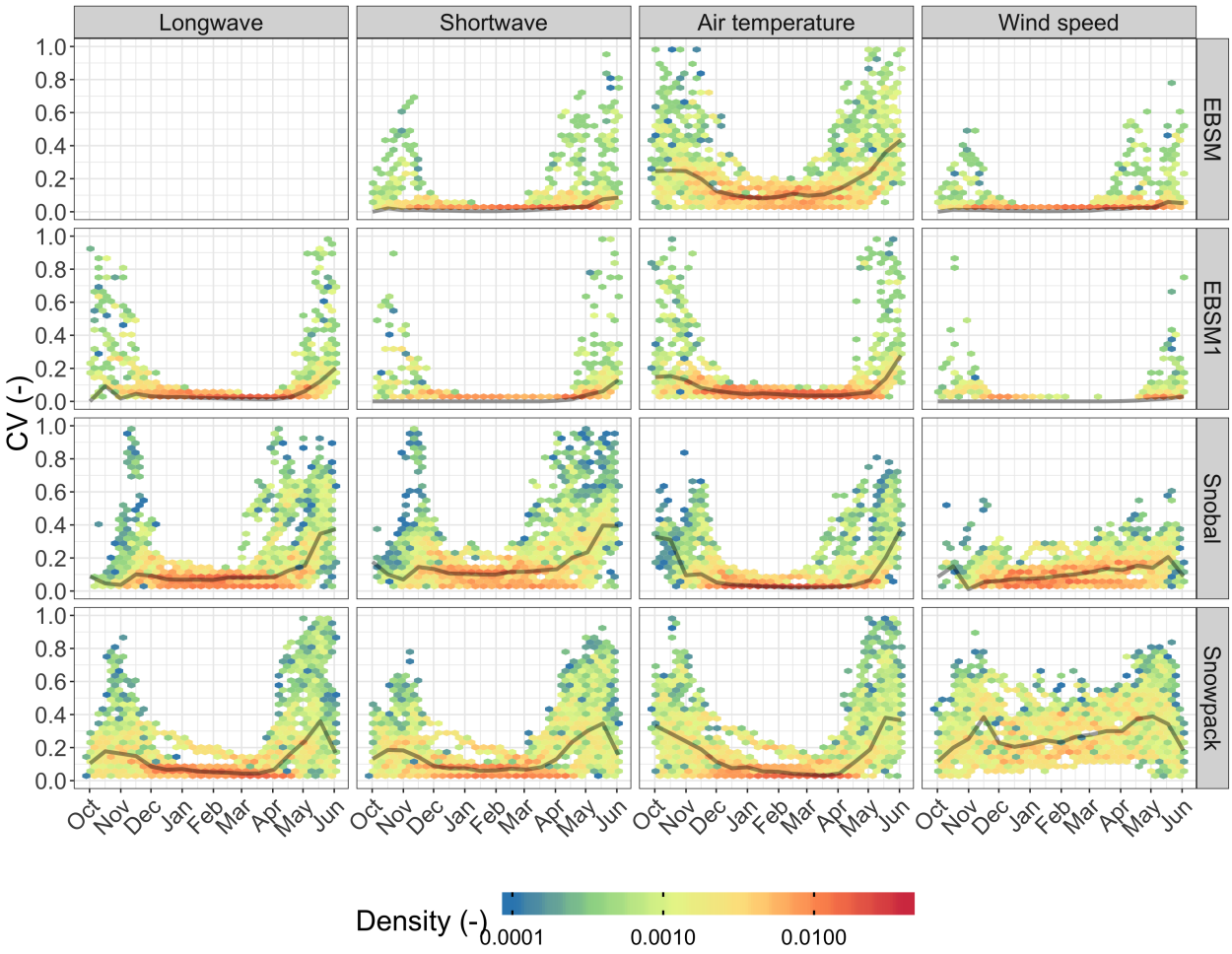

Figure 5.8: The coefficient of variation (CV) of SWE for each for the four models (increasing complexity top to bottom), separated by forcing perturbation. The CV values for all the years are grouped by day of year, and plotted as binned density values with a 2-week rolling median plotted in black. Model response showed greatest sensitivity to the forcing variables in the fall and the spring, with the spring ablation having the greatest sensitivity. Mid-winter sensitivity is quite low, however Snowpack showed a consistent sensitivity to windspeed. EBSM had a greater median sensitivity to air temperature than any other model.

the sensitivity to these forcing perturbations, with the ablation period having greater sensitivity than the accumulation period.

During the accumulation period, the models were most sensitive to the air temperature perturbation. Snowpack had the greatest sensitivity to air temperature in October, and it took longer for this sensitivity to decrease compared to the other models. The simplest model, EBSM, had a greater spread of CV values under the air temperature perturbation than any other model and had a almost as high a median CV as Snowpack for this period. EBSM1 had the lowest sensitivity for this period. Snobal was somewhat less sensitive than Snowpack in October and November.

As the winter progressed through November and December, EBSM and EBSM1 quickly became insensitive to the shortwave irradiance and wind speed perturbations. However, EBSM had the greatest mid-winter sensitivity to air temperature. Mid-winter sensitivity for EBSM1, Snobal, and Snowpack was generally quite low due to cold snowpacks and limited available energy. The EBSM model appeared to lack this dampened response. Snowpack had a substantial mid-winter sensitivity to windspeed that the other models did not have. As the winter progressed from December through February, the spread of the ensemble remained generally low and constant for all models, indicating low mid-winter sensitivity.

Peak SWE generally formed in late April and early May. Increased ensemble variability began in March for all models except EBSM1. In April EBSM had a greater ensemble spread and median value for air temperature perturbations than did Snobal and Snowpack. In May, EBSM matched Snowpack's air temperature sensitivity. Snowpack was equally sensitive across all meteorological variables during this period. Snowpack had substantial sensitivity to wind speed throughout the ablation period. All models had considerable sensitivity to shortwave irradiance with Snobal more sensitive than the other models.

5.5.5 Energy balance response

The sensitivity of the energy balance components of Snobal and Snowpack are shown in Figure 5.9 and Figure 5.10 for Snobal and Snowpack, respectively. The input forcing perturbation variable is shown as horizontal labels for longwave and shortwave irradiance, air temperature, and wind speed perturbations. The energy balance components are shown as vertical plot facets for: the rate of internal snowpack energy change, latent heat flux, ground heat flux, sensible heat flux, and longwave emission. The black line represents a 2-week rolling median.

Throughout the winter period, most of the energy balance components in Snowpack and Snobal had relatively unchanging and small sensitivities due to small incident energy fluxes; this follows from Figure 5.8. The sensitivity to shortwave irradiance and air temperature perturbations was predominately due to adding more energy to the snowpack and changes in albedo state.

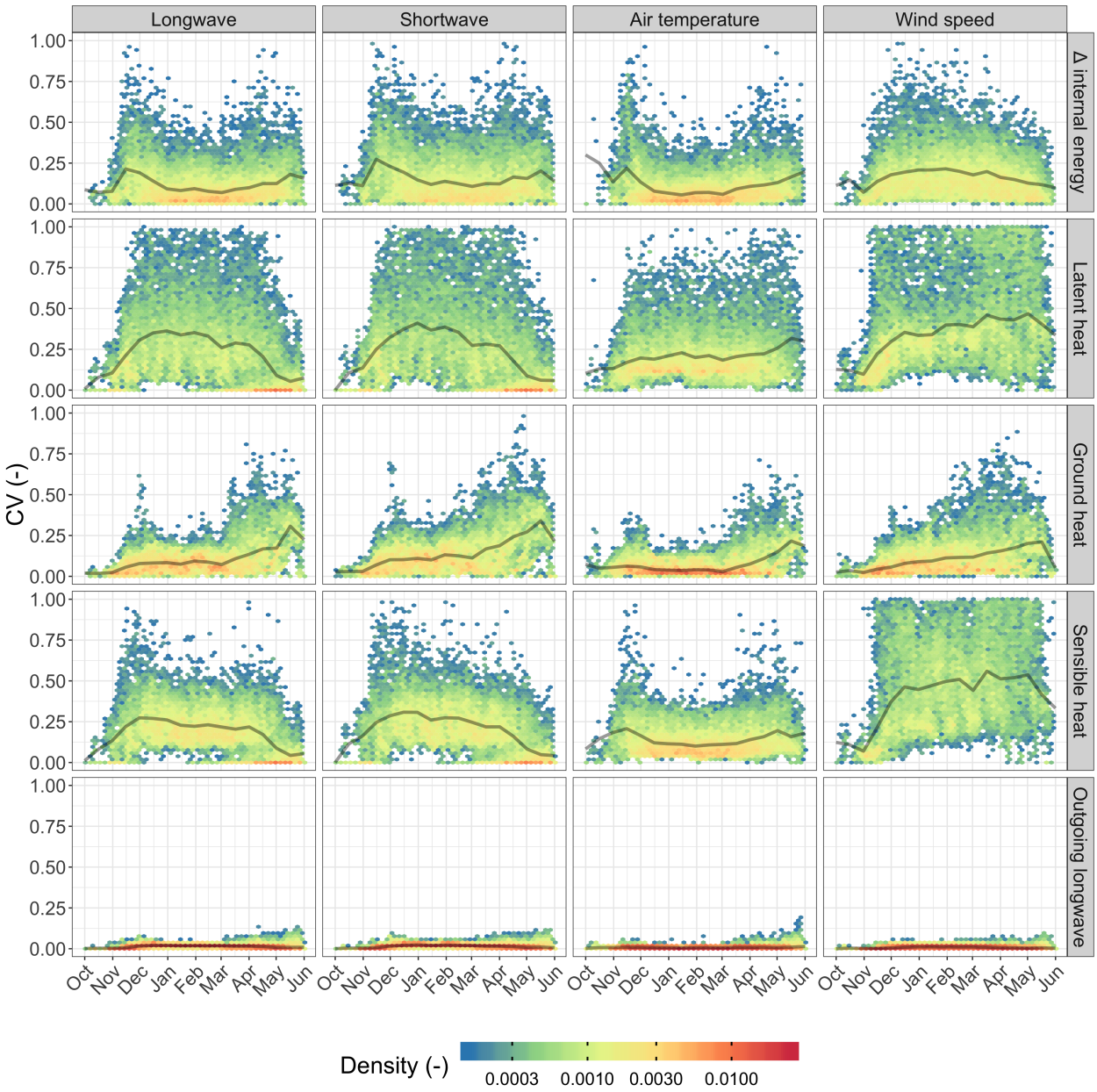

Figure 5.9: Temporal sensitivity for the energy balance components of Snobal under the various forcing perturbations.

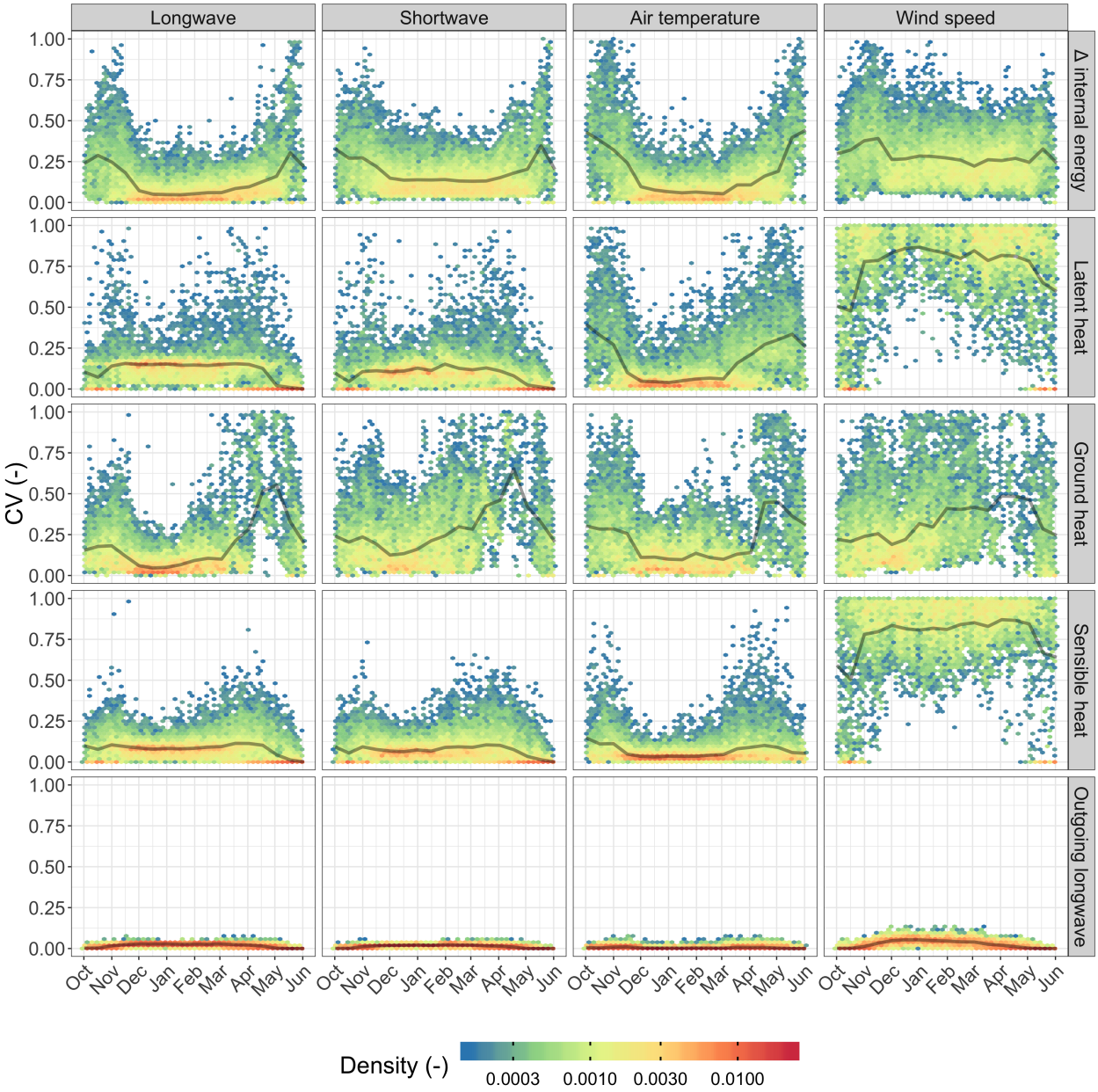

Figure 5.10: Temporal sensitivity for the energy balance components of Snowpack under the various forcing perturbations.

Despite the ground heat flux magnitude being small, there was substantial variability in this flux. This was most pronounced in the ablation and accumulation periods, predominately with shallow snowcovers. There was limited mid-winter sensitivity. The near constant CVs suggest most of the mid-winter variability is due to variability in early winter SWE. Due to Snowpack's large sensitivity to mid-winter windspeeds, it was found that Snowpack had increased sensitivity in mid-winter latent and sensible heat fluxes. In all cases, longwave emissions had limited sensitivity compared to the turbulent fluxes.

During the spring, more variability in the CV values, as well as more non-zero median CV values were found. This corresponded to increased temporal variability and overall sensitivity in the fluxes. Snowpack had a large variability in the ground heat flux across all perturbations, although the median CV value was close to 0. This variability was a result of the shallow snow covers in the later ablation period. Snowpack showed a slight increase in variability versus Snobal in the rate of change in internal energy. The perturbations to wind during the spring had a larger impact on Snowpack than Snobal. As a result, there was substantial sensitivity and temporal variability in the sensitivity in Snowpack's turbulent fluxes.

5.5.6 Terrain shadowing

The virtual point that compared surrounding terrain shadowing influences to an un-shadowed case is shown in Figure 5.11. The unshadowed baseline case is shown in red, and the shadowed case shown in teal. Water years are shown along the top, for each model (vertical facets, increasing complexity from top to bottom). As the complexity of the internal energetics schemes increased in models, there was greater sensitivity in SWE calculations to perturbations in shortwave irradiance. EBSM SWE was almost completely insensitive to this perturbation. EBSM1 showed some sensitivity in SWE near its peak and during subsequent ablation. Snobal and Snowpack were similar in sensitivity to shortwave irradiance, showing a large response in SWE during accumulation and ablation.

In general, the greatest difference between the two scenarios was the magnitude of peak SWE and the rate of melt during spring ablation. This follows from the observed temporal sensitivity to forcing perturbations. However, there are many years with limited differences between the two cases. In order to test the hypothesis that there may be a compensation in the energy balance terms that is compensating for the increased shortwave irradiance in the no-shadow case (herein 'baseline'), the energy balance terms were compared for both scenarios using the Snobal and Snowpack models.

Summarized in Table 5.8 are the mean energy balance fluxes, averaged over the April, May, June period of all years, considering only cases when SWE was present; fluxes were converted to Joules prior to this averaging. Shortwave iraddiance was increased by 42.5 $W \cdot m^{-2}$ for Snobal and 44.8 $W \cdot m^{-2}$ for Snowpack in the non-shadowed scenario versus the shadowed scenario. The difference between shortwave irradiance

for the models is due to differing albedo feedbacks; e.g., different periods when using cold or warm snow decay algorithms. The total energy balance (not include incoming irradiance) for the no-shadow scenario for Snobal and Snowpack was 52.6 $W \cdot m^{-2}$ and 42.8 $W \cdot m^{-2}$ respectively. For the shadow scenario it was 53.0 $W \cdot m^{-2}$ and 41.6 $W \cdot m^{-2}$ for Snobal and Snowpack respectively. That is, the total energy balance between both scenarios was similar.

Table 5.8: Energy balance terms for Snowpack and Snobal under the baseline (no shadow) scenario, and the shadowed case. Energy balance fluxes are: latent heat (E), change in internal energy (dQ), ground heat (G), sensible heat (H), emitted longwave (ilwr_out), shortwave irradiance (iswr), net shortwave (iswr_net), longwave irradiance (ilwr_in).

Variable	Model	Baseline ($W \cdot m^{-2}$)	Shadow ($W \cdot m^{-2}$)	Diff. ($W \cdot m^{-2}$)
E	snobal	-4.4	-2.04	-2.36
dQ	snobal	20.8	20	0.823
G	snobal	12	13.2	-1.19
H	snobal	3.91	6.01	-2.1
ilwr_out	snobal	-301	-299	-1.95
iswr	snobal	193	151	42.5
iswr_net	snobal	54.7	44.1	10.5
ilwr_in	snobal	267	271	-4.24
E	snowpack	-3.26	-2.32	-0.939
dQ	snowpack	20.2	19.7	0.478
G	snowpack	-14.1	-8.38	-5.67
H	snowpack	6.69	7.05	-0.361
ilwr_out	snowpack	-293	-293	-0.818
iswr	snowpack	201	156	44.8
iswr_net	snowpack	60.1	48.2	11.9
ilwr_in	snowpack	267	270	-3.41

To investigate this similarity, the energy balance components can be summed, ignoring shortwave irradiance. The total energy balance difference between the baseline and shadowed scenarios was -11.0 $W \cdot m^{-2}$ and -10.7 $W \cdot m^{-2}$ for Snobal and Snowpack respectively. This showed that despite the increased energy to snowpack (due to ignoring shadows), other energy balance terms compensated, decreasing the total energy of the snowpack. Specifically, there is increased loss to latent heat (E), minimal changes in internal energy rate of change, slightly decreased ground heat flux contributions, and increased long wave loss in the no-shadow scenario. By virtue of having a snowpack present later in the season, the shadow scenario had small adevected

energy from precipitation. As a percentage of the total shortwave irradiance, this compensation in the energy balance was 25.9% and 23.9% for Snobal and Snowpack respectively. Thus, despite the increased energy to the snowpack as a result of ignoring shadows, there was increased energy lost from the snowpack and the additional energy did not go entirely to melt.

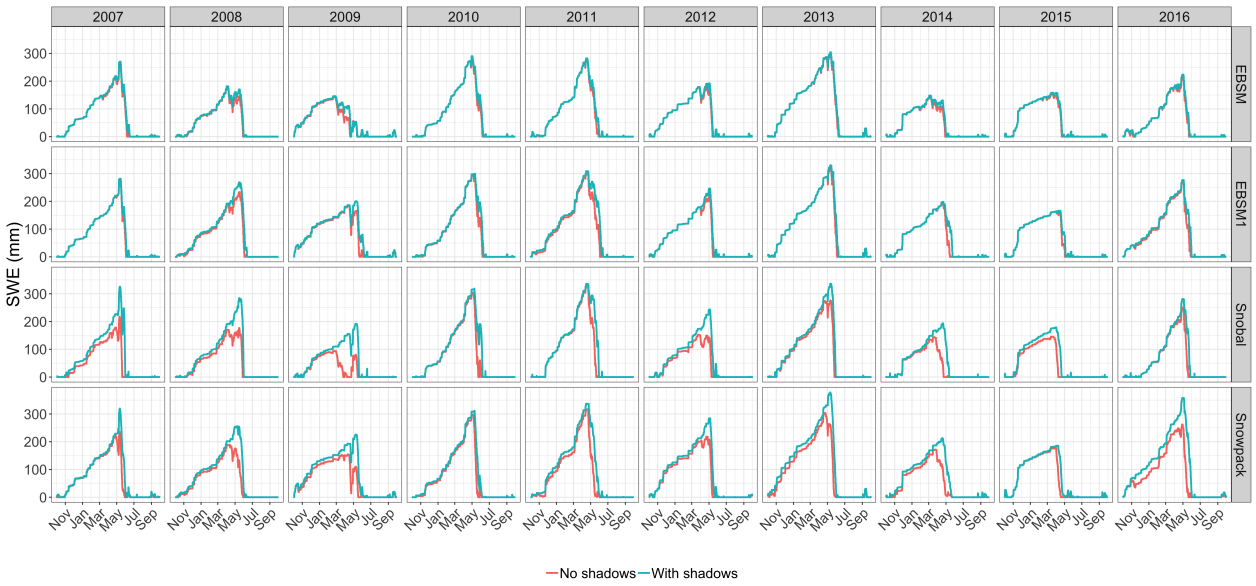

Figure 5.11: Impact of an incoming shortwave radiation perturbation in the form of applying shadowing.

5.6 Discussion

5.6.1 Model v. observations

The four models showed varying levels of skill in prediction over the ten simulation years. The EBSM (single layer) model performed well, especially given the original derivation for shallow prairie snowcovers. Model results improved as explicit mass and energy balance coupling was included with the exception of EBSM1 – it performed less well than EBSM. The overall lower performance of EBSM and EBSM1 was due to applying a single-layer shallow prairie snowcover formulation to deep mountainous snowcovers. The EBSM formulations were missing important physical process in this region including the explicit sublimation of the snowpack, substantial cold content storage, and ground heat flux. EBSM models internal snowpack energetics using the previous nights low temperature; however, this is not appropriate for deep mountain snowpacks that cannot cool as quickly as a shallow snowpack. Although sublimation was added to the EBSM1 variant, it did not improve predictive capacity.

During the cold winters (2010, 2013, 2016), all models tended to perform well. However, EBSM and EBSM1 produced slower ablation rates. During years with early winter melt and lower accumulation (e.g., 2009), the EBSM and EBSM1 models struggled with over accumulation. The Snobal simulation for 2009 is exceptionally poor. For this year, Snobal appears to have had trouble building the snowpack. Early precipitation events are ablated, whereas the other models began to accumulate a snowcover in early winter. This is likely due to Snobal directly ablating very shallow early season snowcovers for numerical stability due to sharp temperature gradients. EBSM also produces poor results, and this suggests that warmer mid-winter events are more difficult to correctly simulate than consistently cold winters. For this year however, EBSM1 and Snowpack are the most consistent.

The overall finding that, on average, EBSM can produce similar results for this site as Snobal is in line with previously observed results in SnowMIP. Despite the more physically-correct surface temperature layer and explicit longwave radiation abalance and inclusion of sublimation in EBSM1, this model was the worst performing. For a straightforward forest clearing such as Upper Clearing, the more complex model only produced a 7 mm SWE RMSE reduction compared to the simplest models. It also demonstrated that extra model complexity does not guarantee improved results.

5.6.2 Model sensitivity

5.6.2.1 Parameter sensitivity

The parameter sensitivity (Figure 5.4) showed that both Snowpack and Snobal were most sensitive to the maximum albedo, followed by the minimum albedo. Although clean fresh snow such as found in the Canadian Rockies generally has a high albedo, fresh snow in many parts of the world can be quickly contaminated reducing the albedo, and increasing absorbed shortwave radiation (Conway et al., 1996; Skiles et al., 2018). The ablating warm snow decay parameter was found to be more sensitive than the cold snow albedo.

An important finding was that Snobal, the 2-layer medium complexity model was found to be more sensitive to the tested parameters than Snowpack, the high complexity multi-layer model. As albedo directly impacts shortwave absorption, the greater Snobal sensitivity is likely due to the relatively thick, single upper layer warming and causing feedbacks with the turbulent transfer and cold content. The thinner upper layers of Snowpack would not affect overall cold content so directly. The snow roughness length had an opposite response, where Snowpack was more sensitive than Snobal. This is due to the different MO stability corrections used in each model. In a sensitivity test of Alpine3D that uses Snowpack, Schlögl et al. (2016) found that Snowpack was quite sensitive to the boundary layer scheme used. These results showed that models of varying complexity respond in very different ways to key energy balance impacting parameters. For this specific albedo routine, snowmodel complexity was not a good predictor of sensitivity. In future work, it would be instructive to examine the temporal sensitivity of the models to these parameters. Given the substantial temporal sensitivity to the forcing perturbations, it is possible that temporal variability exists for the parameters.

5.6.2.2 Forcing data sensitivity

The EBSM, EBSM1, Snobal, and Snowpack models cover a large spectrum of model complexity. Although increased sensitivity to input forcing perturbations increased as model complexity increased, these results succinctly demonstrate how much more input forcing sensitivity is present in a more complex snowmodel than a simple model. Despite Snobal and Snowpack using similar methods for various energy balance parameterizations, e.g., the surface turbulent fluxes, there is a substantially increased overall sensitivity in Snowpack versus Snobal, likely due to the increased number of and decreased thickness of snowpack layers in Snowpack compared to Snobal.

By examining this overall sensitivity with univariate forcing perturbations, the reasons for this range of sensitivities are apparent. As the EBSM-derived models were originally developed for shallow snow covers with a parameterized internal energy content based on the previous night's minimum air temperature, incorrect

estimation of snowpack active layer depth, snow skin temperature, and internal heat conduction could not occur, as in Snobal and Snowpack. Thus EBSM, by virtue of being heavily dependent on air temperature to derive incoming fluxes, resulted in the largest sensitivity to the air temperature. This is a model formulation resulting in a damped response. In EBSM1, the inclusion of snow surface temperature (Pomeroy et al., 2016a) to estimate outgoing longwave radiation and the use of observed longwave irradiance instead of empirical estimates from net solar radiation decreased overall sensitivity. The inclusion of the snow surface temperature (and thus potentially increased longwave loss) may have compensated for errors in internal snowpack temperature – however this was difficult to diagnose as currently implemented. The difference between Snobal and Snowpack's sensitivity suggests that Snowpack is consistently sensitive to a range of input variables, whereas Snobal is most sensitive to shortwave irradiance and wind speed. Although some sensitivity of air temperature is as a result of nudging the precipitation phase, each model was provided identical precipitation phase, and thus would be exposed to a consistent change in precipitation phase. Schlögl et al. (2016) found a large uncertainty associated with the boundary layer formulations in Snowpack. The substantial sensitivity to the wind perturbations herein is likely the same sensitivity. Both Snowpack and Snobal show large variability in the ground heat flux. However, this flux remained quite small over the winter. An analysis (not shown) of shallow and deep snowpacks over the winter and spring periods showed that some of the variability is due to different average snowpack temperatures due to differences in when the snowpack started to accumulated, resulting in an offset of ground heat flux magnitudes. Further, the majority of the variability was found in the spring during periods of shallow snowpacks.

An important result was that the simplest model (EBSM) was more sensitive to air temperature than the moderate complexity model Snobal and slightly more than Snowpack in early ablation and as sensitive during mid-ablation. Although air temperature is an important factor in ablation and models are typically sensitive to it, radiative fluxes dominate most snowpack energy balances (Olyphant, 1986b; Conway et al., 1996). EBSM was sensitive to air temperature because of the impact of air temperature in initiating albedo decay in spring. These results showed that during ablation, the less complex model was producing as much uncertainty than the more physics-based methods. As a result, the temporal variability in the models' sensitivity, and thus uncertainty, is an important consideration when doing 'what-if' forecast scenarios. Considering season-averaged sensitivities may not be appropriate to correctly gauge overall model sensitivity. In doing so, it may bias the analysis by including long periods of insensitivity, during periods that are of limited consequence. This demonstrated that parsimonious models are not necessarily less uncertain during periods of critical importance to snowcovers. With increased mid-winter melt and slower melt rates predicted in some future climate conditions (Musselman et al., 2018), models that are overly sensitive to a single input forcing may not be instructive for diagnosing these future conditions.

5.6.3 Compensation

The virtual point experiment attempted to provide a straightforward examination of how the complex feedbacks in the coupled energy and mass balance react to what is effectively an input energy perturbation due to model simplification — ignoring terrain shadows in a mountain basin. This scenario was useful as it does not impact precipitation phase (as air temperature might), and it has an easily quantifiable input flux.

The substantial heterogeneity in incoming shortwave radiation is a predominate driver of snowcover heterogeneity and melt initiation in many catchments. Previous work (Marsh et al., 2012) investigated basin-wide impacts of terrain shadowing and this showed that the spatial variability in shadowing is important for snowpack melt energetics. However, in areas that cycle through shadows, this study showed that the impact was more dampened than expected from the solar radiation differences alone.

The results here show robust behaviour amongst all four models. However, it is asserted that two types of robustness are exhibited here: an insensitivity due to model structure, and a compensatory robustness. The first type is exhibited by EBSM and EBSM1. They were insensitive to the shortwave irradiance perturbation. However, this is a model formulation insensitivity due to deriving the surface fluxes and albedo decay predominately from air temperature. The insensitivity of EBSM and EBSM1 suggests a problematic behaviour when applied to mountain locations by being insensitive to terrain shadows. That is, their insensitivity does not accurately reflect the processes that have been observed in complex terrain. While this insensitivity can reduce uncertainty in an ideal site such as Upper Clearing or level terrain such as the Canadian Prairies where EBSM was derived, it results in an incorrect behaviour when applied in mountains.

Snobal and Snowpack exhibit increased sensitivity to incoming shortwave radiation than EBSM and EBSM1. Two scenarios, one with mountain terrain shadows considered and one without were compared for the impact on the surface energy balance. Despite increased shortwave irradiance in the non-shadowed case, all other energy loss terms increased.This compensated for the increase in shortwave irradiance. Errors that caused processes to change energy flow into the snowpack were compensated for by changes in processes governing energy flow out of the snowpack. This compensation was not related to the number of model layers The energy balance is thus producing a robust, compensatory behaviour due to coupling between the fluxes. Both Snobal and Snowpack had very similar compensatory responses. Model complexity difference between these two models did not appear to dramatically influence the compensatory response. It is likely that the fixed multi-layer, intermediate complexity model represents the minimum amount of complexity required to simulate snowmelt robustly, and that this is due to its internal process interactions.

5.6.4 Limitations

Snowpack liquid water content (LWC) parameterizations and the subsequent flow of water through snowcovers are a significant source of uncertainty (Wever et al., 2014, 2015; Leroux and Pomeroy, 2017). This liquid water can substantially impact the energy balance of the layer exposed to the atmosphere by influencing the time required to refreeze at night, influencing turbulent energy exchange, impacting albedo, and changing the latent heat partitioning between sublimation and evaporation (Wever et al., 2014). Preferential flow paths may form within the snowpack (Marsh and Woo, 1984; Leroux and Pomeroy, 2017). The infiltration of melt water may also have profound impacts on the internal energetics of the snowpack as the liquid water refreezes causing a release of latent heat (Marsh and Woo, 1984). Further, the refreezing may create ice-lenses or preferential flow paths within the snowpack (Marsh and Woo, 1984; Leroux and Pomeroy, 2017), further influencing how melt-water infiltrates, and thus how energy is advected through the snowpack. Therefore, to properly examine the impact of these parameterizations of LWC would require also diagnosing how the liquid water flows through the snowpack. Such a test was out of the scope of this work, and remains an important topic for future research.

5.7 Conclusion

Four snowmelt models of varying complexity (single layer, multi-later intermediate complexity, and detailed multi-layer) were used to simulate SWE in a mountain forest clearing in the Canadian Rockies. Overall, all models performed well at this site, with improved performance found during the cold mid-winter periods. The Snowpack model performed the best, followed by Snobal, EBSM, and EBSM1. The improved snow surface layer temperature calculation, longwave radiation balance, and sublimation parameterizations in EBSM1 did not improve its simulations over the simpler EBSM.

A parameter sensitivity analysis for the albedo parameterization and snow roughness length was done using VARS. The fresh snow maximum albedo was found to be the most sensitive parameter. Snobal was more sensitive to the albedo parameters than Snowpack. However, Snowpack was more sensitive than Snobal to the roughness length.

The sensitivity of simulated SWE for all four models was examined for perturbations to air temperature, shortwave and longwave irradiance, and wind speed. Overall model sensitivity increased with increasing model complexity from EBSM to EBSM1 to Snobal and to Snowpack. The models were most sensitive to air temperature perturbations. With increasing model complexity, the sensitivity to all forcings became more balanced.

There was a strong seasonal variability in the overall model sensitivity to forcing perturbations; the most

sensitive period was during spring ablation and the lowest sensitivity period was mid-winter. Snowpack was found to be sensitive to mid-winter wind speed perturbations whereas other models were not. During the ablation period, all models were similarly as sensitive to air temperature perturbations.

There may be compensatory effects in the surface energy balance such that meteorological forcing data errors may be dampened. To investigate this, two model realizations were run for a virtual station. This virtual station either had shadowing impacts from surrounding terrain or was exposed to solar radiation resulting in increased incoming shortwave irradiance. This setup mimicked a situation wherein the process of mountain shading is ignored, a common situation in hydrological modelling. The snowpack energy balance response to this increase in energy was investigated. The response in energy fluxes of latent and sensible heat, ground heat, and outgoing longwave radiation as a percentage of increased shortwave irradiance was 25.9% and 23.9% for Snobal and Snowpack respectively. Errors that caused processes to change heat flow into the snowpack were compensated for by changes in processes governing heat flow out of the snowpack and this compensation was not related to the number of model layers. Such compensatory responses are an important aspect of coupled models. Considering how such robustness may be present in a model formulation is important for decisions on warranted model complexity. It is argued that the EBSM and EBSM1 type of model cannot ever express system robustness outside of its original intended application and is rather an example of model insensitivity due to "clever" design. Both Snobal and Snowpack produce the same amount of compensatory response because they incorporate the same set of energy and mass exchange processes.

Increasing the physical realism via inclusion of a fully coupled energy and mass balance produced improved SWE simulations, increased overall model sensitivity, and demonstrated compensatory responses in the energy balance to input errors. The strong temporal variability in the model sensitivity suggests that season-averaged sensitivity analysis may not provide sufficient insight into model sensitivity. Correctly capturing model robustness due to physical realism is of interest for general application of models to unknown conditions, such as future climates and ungauged basins and to applications where there may be errors or uncertainties in the driving variables. It may also be used to guide process representation choices. The coupling of the energy and mass balance components is not new; however, many snowmelt models continue to avoid their explicit inclusion or coupling under the guise of parsimony and the false attraction of empirical, calibrated temperature index methods. The simpler models did not necessarily have lower uncertainty during key periods, such as the ablation period. Given air temperature perturbations are a significant source of uncertainty under future climates, using parsimonious models that are highly sensitive to this input may not provide the predictive capacity and reduced uncertainty that is required for meaningful predictions.

6 A finite volume blowing snow model for use with variable resolution meshes

6.1 Manuscript status

A version of this chapter has been accepted as a manuscript to Water Resources Research.

Marsh, C. B., Pomeroy, J. W., Spiteri, R. J., and Wheater, H. S. (2019), A finite volume blowing snow model for use with variable resolution meshes, Water Resources Research

Author contributions are as follows:

C. Marsh: Initial idea, mathematical derivation, coding, analysis, manuscript preparation.

J. Pomeroy: Original parameterization development, idea refinement, analysis refinement, manuscript revision.

R. Spiteri: Mathematical derivation, manuscript revision.

H. Wheater: Idea refinement, manuscript revision.

6.2 Abstract

Blowing snow is ubiquitous in cold, windswept environments and redistributes snow such that snow on the ground can vary from ephemeral, even in winter, to deep multi-seasonal snowpacks. In some regions, blowing snow sublimation losses can ablate a notable fraction of the seasonal snowfall. It is advantageous to predict alpine snow regimes at the spatial scale of snowdrifts (1 m to 100 m) because of the role of snow redistribution in governing the duration and volume of snowmelt. However, blowing snow processes are often neglected due to computational costs. Here, a 3-dimensional blowing snow model is presented that is spatially discretized using a variable resolution unstructured mesh. This represents the heterogeneity of the surface explicitly yet, for the case study reported, gained a 62% reduction in computational elements versus a fixed-resolution mesh and resulted in a 44% reduction in total runtime. The model was evaluated for a sub-arctic mountain

basin using transects of measured snow water equivalent (SWE) in a tundra valley subject to substantial blowing snow redistribution. Including blowing snow processes in the snow model improved the prediction of SWE by capturing inner-annual snowdrift formation, more than halved the total mean bias error, and increased the coefficient of variation of SWE from 0.04 to 0.36, closely matching the observed CV (0.41). A sensitivity analysis showed that snowdrift locations and immediate up-wind sources of blowing snow are the most sensitive areas of the landscape to wind speed variations.

6.3 Introduction

6.3.1 Blowing snow redistribution is ubiquitous in cold, windswept environments such...

Blowing snow redistribution is ubiquitous in cold, windswept environments such as alpine and arctic tundra, grass and croplands, and glaciers and results in spatial patterns of snowpack ablation or deposition, leaving highly heterogeneous snowcovers (Pomeroy et al., 1997; Marsh, 1999; Sturm et al., 2001; Fang and Pomeroy, 2009; MacDonald et al., 2010; Mott et al., 2010; Winstral et al., 2013; Freudiger et al., 2017; Wayand et al., 2018). Spatially and temporally variable wind speeds arise due to complex topographic and vegetation interactions with meso- and micro-scale winds and are key drivers of blowing snow redistribution. Wind accelerates over hills and ridge crests (Jackson and Hunt, 1975; Mason and Sykes, 1979; Walmsley et al., 1984; Wood, 2000), resulting in enhanced snowpack erosion (Essery et al., 1999). Subsequent deceleration over lee slopes, in topographic depressions, and behind tall vegetation or snow fences (Tabler et al., 1990; Pomeroy et al., 1995) can result in large snowdrift deposits. Spatially variable precipitation fields can further increase this heterogeneity (Lehning et al., 2008). As a result of high rates of ventilation of blowing snow particles, substantial mass loss occurs due to sublimation in undersaturated atmospheres (Dyunin, 1954; Schmidt, 1972, 1982; Pomeroy et al., 1993; Bowling et al., 2004; Vionnet et al., 2014; Mott et al., 2018). The resulting heterogeneity in pre-melt snowcovers is an important factor for the timing and magnitude of spring runoff (Marsh and Pomeroy, 1996; Pomeroy et al., 1997; Luce et al., 1998; Woo and Thorne, 2006; Dornes et al., 2008b; Fang et al., 2013). In alpine regions, blowing snow drifts form cornices (Mott et al., 2010) and influence avalanche formation (Bernhardt et al., 2012) that can further impact basin hydrology (Scally, 1992). Large snowdrift formations on lee slopes can provide important ecosystem services, e.g., polar bear den locations (Blix and Lentfer, 1979; Liston et al., 2016). These drifts often persist into summer (Wayand et al., 2018), when they contribute to rain-on-snow events (Pomeroy et al., 2016b) and can provide late season runoff for downstream users (Viviroli et al., 2007; Nazemi et al., 2013) and agricultural water supplies (Pomeroy and Male, 1986).

The inclusion in hydrological models of blowing snow transport, via saltation near the ground, suspension

diffusing to hundreds of meters above the snow surface, and in-transit sublimation of blowing snow, is critical for simulating the spatial variability and volume of snow accumulation (Pomeroy et al., 1993, 2007; Luce et al., 1998; Dornes et al., 2008b; Fang and Pomeroy, 2009; Fang et al., 2013; Zwaaftink et al., 2013; Freudiger et al., 2017; Mott et al., 2018). The International Network for Alpine Research Catchment Hydrology (INARCH) (Pomeroy et al., 2015), a Global Energy and Water Exchanges (GWEX) project of the World Climate Research Programme, has identified snow-drift resolving scales (1 m to 100 m) as a key component to predicting alpine catchment hydrology (Pomeroy and Bernhardt, 2017). INARCH has resolved that models that do not explicitly include blowing snow processes at sub-100 m scales or parameterize their impacts on snow, cannot adequately represent alpine snow dynamics and hydrological responses.

Despite their importance, blowing snow processes are not often represented in distributed hydrological models (Winstral et al., 2013). Many models compensate for this by relying on calibration of conceptual parameters or adjustments of precipitation to represent the impact of blowing snow on hydrological predictions. Most land surface schemes represent the impacts of blowing snow using a snow water equivalent (SWE) variability parameter that controls the snowcover depletion curve (Pomeroy et al., 1998a). However, how to set this parameter given its inter-annual variability is uncertain, and sublimation losses are not addressed by this approach. Those land surface schemes that do conceptualize redistribution include it as a sub-grid, inter-tile process (Davison et al., 2016).

The omission of blowing snow processes is a fundamental misrepresentation of alpine snow hydrology and increases model uncertainty; reasons cited for this model inadequacy include computational costs (Winstral et al., 2013), meteorological data requirements, and increased model complexity (Luce et al., 1998). When included, applications are often limited to small research areas (Fang et al., 2013), although large area predictions are possible (Pomeroy et al., 2013). Regardless of scale, the need for alpine hydrological model parameter calibration from streamflow can be reduced through full inclusion of alpine snow redistribution processes such as blowing snow (Pomeroy et al., 2013). Cold-regions hydrological model performance is improved by including spatial heterogeneity — e.g., slope, aspect, and vegetation — and representing the full range of hydrological processes operating in these regions, e.g., Bartelt and Lehning (2002); Bowling et al. (2004); Etchevers et al. (2004); Raderschall et al. (2008); Dornes et al. (2008a); Essery et al. (2009); Essery et al. (2013); Fiddes and Gruber (2014); Painter et al. (2016a); Mosier et al. (2016); Musselman et al. (2015a). This suggests that an efficient approach for the explicit inclusion of spatially distributed blowing snow processes would be beneficial in advancing cold regions hydrology.

Point-scale blowing snow transport models are challenging to apply in fully distributed hydrological models due to landscape heterogeneity and complex wind fields, although there has been success at large spatial scales in macro-scale models without spatial coupling, e.g., Bowling et al. (2004) and Yang et al. (2010). Semi-distributed models and terrain parameter-based methods, e.g., Winstral et al. (2013), are either constrained by only capturing the snowcover heterogeneity via *a priori* knowledge of drift locations, e.g., MacDonald et

al. (2009), or require calibration from detailed distributed SWE observations (Schön et al., 2018). Terrain-parameter based models are incapable of calculating blowing snow sublimation losses, which can vary from 1% to 30% of snowfall in alpine catchments (Musselman et al., 2015a; Mott et al., 2018).Wind direction variability over large areas ($>$ a few km) of complex terrain precludes the use of simplifying assumptions about uniform wind direction as was done in some distributed blowing snow models, e.g., Distributed Blowing Snow Model (DBSM; Essery et al., 1999; Fang and Pomeroy, 2009). Use of advection-diffusion equations (scalar-transport), e.g., Alpine3D (Lehning et al., 2006), or spatially distributed formulations, e.g., DBSM and SnowTran3D (Liston and Sturm, 1998), tend to increase computational demand, parametrization requirements, and model complexity as a result of the use of a fixed-resolution spatial discretization. More complex models consider non-steady turbulence, e.g., the point-scale model PIEKTUK (Déry and Yau, 1999). When distributed, these models couple blowing snow transport and sublimation using three-dimensional wind fields computed from atmospheric models, e.g., SURFEX in Meso-NH/Crocus (Vionnet et al., 2014, 2017), Alpine3D (Lehning et al., 2006), and SnowDrift3D (Schneiderbauer and Prokop, 2011), substantially increasing the computational costs.

Aksamit and Pomeroy (2017) note that most models of blowing snow transport have been conceptualized for steady-state conditions based on time-averaged field or wind tunnel observations of snow particle flux and dispersion (Schmidt, 1986; Pomeroy, 1989; Lehning et al., 2006). Thresholds for the initiation or cessation of transport have been based on air temperature, occurrence of melt or rain, and snowpack age (Li and Pomeroy, 1997b, 1997a) as well as surface grain type (Guyomarc'h and Mérindol, 1998). Detailed outdoor field campaigns (Aksamit and Pomeroy, 2016, 2017, 2018) and wind tunnel research (see summary in Paterna et al. (2017)) have investigated the mechanisms that erode and entrain surface snowpack into blowing snow. Two-phase flow is governed at short ($<$ 1 s) time intervals by particle responses to turbulent gusts and sweep-ejection mechanisms rather than scaling with shear stress (Aksamit and Pomeroy, 2016, 2018). This increase in understanding has not yet led to new turbulence-based blowing snow transport models. For the longer time intervals (15 min to 1 hour) employed by hydrological models, mean shear-stress scaling blowing snow models are used and have been adapted to non-fully developed flow conditions by empirically estimating the length scales necessary for establishment of near-surface two-phase flow via saltation (Pomeroy and Gray, 1990; Comola and Lehning, 2017) and explicitly calculating the upward diffusion of suspended blowing snow using plume dispersion equations (Pomeroy and Male, 1992). These methods have been coupled to complex terrain wind flow estimation procedures and used in distributed models, e.g., DBSM, SnowTran3D, Alpine3D, and the Distributed Snow Model (Musselman et al., 2015a).

Efficient calculation of spatially distributed blowing snow fluxes is needed to estimate wind redistribution and sublimation of snow at high resolution over large areas. Using a variable-resolution unstructured triangular mesh (unstructured mesh) to represent and discretize terrain and vegetation cover is one approach that can efficiently accomplish this. An unstructured mesh allows for representing important heterogeneities in the

surface but can reduce computation elements between 50% to 99% compared to a structured grid (raster) representation (Ivanov et al., 2004b; Marsh et al., 2018). The reduction in computation elements can often significantly reduce computation times while at the same time produce more accurate simulations (Ascher et al., 1995). Furthermore, despite the reduction in computational elements, unstructured meshes can preserve heterogeneity in topography and vegetation (Marsh et al., 2018). There is subjectivity in mesh configuration because the mesh acts as an approximation to the underlying source rasters; however, using numerical guarantees of the approximating accuracy in the meshing tool can alleviate much of this.

This work combines the computational benefits of a variable resolution terrain discretization with a distributed blowing snow model based on rigorous field observations of blowing snow (Pomeroy, 1989; Pomeroy et al., 1993; Pomeroy and Li, 2000). A finite volume discretization (FVM) is used and does not require the assumptions of uniform wind direction; it is therefore applicable to areas with complex wind flow. DBSM used a lookup table approach for relative wind speed, derived from a Mason and Sykes-based 3-dimensional wind flow model MS3DJH/3R (Walmsley et al., 1986). This is extended here to include changes to wind direction and to allow for applicability to an unstructured mesh. The variable resolution blowing snow model is used to simulate snow accumulation patterns in a sub-arctic catchment and is compared with five years of observed snow depth and density transects across a large alpine valley that often contained a snowdrift. An uncertainty analysis uses a 50-member ensemble of perturbed windspeeds. This paper investigates the following questions: 1) can a variable resolution blowing snow model predict the spatial and temporal variability in SWE and the volume of snow drifts in an alpine catchment?; 2) does a variable resolution discretization produce similar results to a fixed-resolution discretization?; and 3) what is the spatial sensitivity of the blowing snow model to wind speed calculation? Application of variable resolution meshes represents a novel and efficient distributed representation of blowing snow processes, suitable for multi-scale extents.

6.4 Model Development

6.4.1 Overview

A 2D schematic of the conceptual model for blowing snow transport via saltation and suspension layers is shown in Figure 6.1. The saltation layer acts to provide a lower boundary condition for diffusion into the suspension layer (Pomeroy and Gray, 1990; Pomeroy and Male, 1992). Diffusion from the saltation layer to the suspension layer is driven by turbulent fluctuations in the instantaneous vertical wind speed exceeding the terminal fall velocities of blowing snow particles (Pomeroy and Male, 1992). Sublimation during transport is modelled as a sink term based on turbulent transfer of sensible and latent heat to the blowing snow particles, which are assumed to cool to the ice-bulb temperature (Pomeroy, 1989; Pomeroy et al., 1993). The non-steady effects of upwind fetch are represented by a downwind increase with fetch to a fully developed saturation

level in the saltation concentrations. This is used to calculate suspended concentrations and the increasing height of the suspended snow layer with fetch.

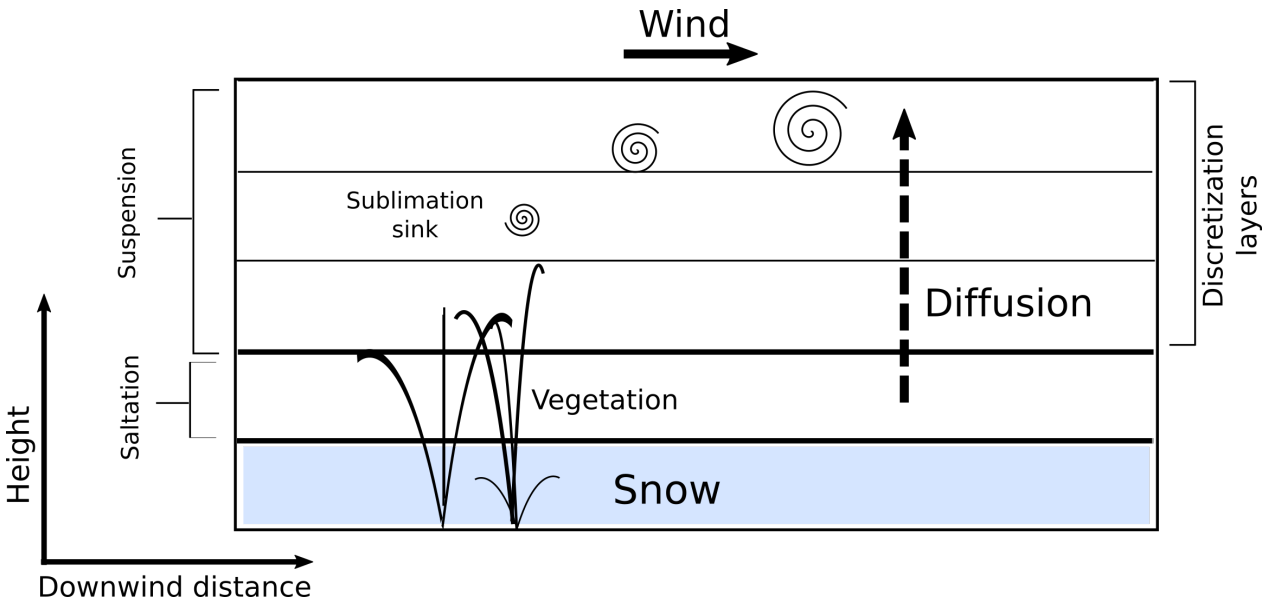

Figure 6.1: A 2-D schematic of the conceptual model of blowing snow transport. A bottom saltation layer is present over a snowpack, with diffusion into the suspension layers. Sublimation is modelled as a sink term. The suspension layer is discretized with a user defined number of layers.

The steady-state saltation flux parameterizations (Pomeroy and Gray, 1990) are used to calculate the saltation layer mass concentration based on an observed relationship between saltation trajectory height and shear stress. Although this saltation model does not explicitly calculate particle trajectories as do, e.g., Doorschot and Lehning (2002) and Clifton and Lehning (2008), it remains in reasonable agreement with these more complex methods and requires fewer parameters and less computational overhead. Its use here does not preclude use of a different parameterization. Saltation, turbulent suspension (Pomeroy and Male, 1992), sublimation (Pomeroy et al., 1993), threshold shear stress for saltation (Li and Pomeroy, 1997a), shear stress partitioning by vegetation and snow, and a probabilistic upscaling (Pomeroy and Li, 2000) parameterizations comprise the blowing snow model. These were found to be consistent with outdoor observations of blowing snow particle flux made using a snow particle detector (Brown et al., 1989; Pomeroy, 1989), changes in blowing snow chemistry due to sublimation (Pomeroy et al., 1991), profile measurements of wind speed, temperature, and humidity in the lowest 3 m of the boundary layer, and snow mass balance measurements (Pomeroy et al., 1993; Pomeroy and Li, 2000; Fang and Pomeroy, 2009; MacDonald et al., 2010; Musselman et al., 2015a). The sublimation parameterization of Pomeroy et al. (1993) was found by Pomeroy and Essery (1999) to be consistent with eddy correlation measurements of latent heat flux. There is a strong motivation to use field observation-based parameterizations versus those from wind tunnels because the latter do not have sufficient fetch and have turbulence features that do not represent natural, outdoor conditions (Aksamit and Pomeroy, 2018).

The advection-diffusion equation implicit in the blowing snow model was discretized in space via the finite volume method on a high-quality, spatially variable mesh generated via the *mesher* code (Marsh et al., 2018). The mesh has well-graded triangles from small to large areas, and all internal angles are greater than 21 degrees. This ensures that there are no sharp transitions between triangles that could cause numerical instabilities. Due to the use of the FVM, neither simplifying assumptions about wind direction nor domain rotations into the wind direction are needed. This allows use where the wind flow is divergent and over large extents. Erosion and deposition are computed as the spatial and temporal divergence of the suspension and saltation fluxes, that is, their rate of change over space and over model time steps.

6.4.2 Numerical background

6.4.2.1 Transport equation

Suspended blowing snow transport was modelled via the steady-state scalar advection-diffusion equation,

$$\nabla \cdot (K \nabla c) - \vec{u} \cdot \nabla c + S = 0 \tag{6.1}$$

where K is the diffusion coefficient ($\mathrm{m}^2 \cdot \mathrm{s}^{-1}$), c is the transported scalar, in this case the mass concentration of blowing snow ($\mathrm{kg} \cdot \mathrm{m}^{-3}$), $\vec{u}$ is the wind vector ($\mathrm{m} \cdot \mathrm{s}^{-1}$), and S is a source or sink term. The wind vector is assumed to have zero divergence; therefore, Equation 6.1 may be written as

$$\nabla \cdot (K \nabla c) - \nabla \cdot (c\vec{u}) + S = 0. \tag{6.2}$$

6.4.2.2 Numerical discretization

Equation 6.2 can be discretized in space using 3-D prisms. To do so, the 2-D triangular mesh is extruded vertically to form a prism, as shown in Figure 6.2. These prisms are stacked vertically to form multiple discretization layers. A prism in a given layer lies exactly above one below; that is, there is no offset or rotation of triangles with height. This planar extrusion of the triangles into prisms causes prisms to align even over areas of high curvature. Using the divergence theorem, Equation 6.2 may be re-written as

$$\int_{\partial V_i} (K_i \nabla c_i) \cdot \hat{n} \ \mathrm{dA} - \int_{\partial V_i} c_i \vec{u}_i \cdot \hat{n} \ dA + \int_{V_i} S_i \mathrm{dV} = 0, \tag{6.3}$$

where V_i is the volume of 3D prism i, ∂V_i is the boundary surface area of the volume V_i, and $\hat{n}$ is an outward pointing unit normal to the volume V_i. Equation 6.3 is applied for each prism i in the mesh and may be rewritten as

$$\sum_{j=1}^{5} A_{i,j} \left(K \nabla c\right) \cdot \hat{n}_{i,j} - \sum_{j=1}^{5} A_{i,j} c\vec{u} \cdot \hat{n}_{i,j} + SV_i = 0, \tag{6.4}$$

for $i \in \{1, 2, ..., number\ of\ triangles\}$ and for each face j of the prism with area $A_{i,j}$. The remaining term, $(K \nabla c) \cdot \hat{n}_{i,\ j}$, is approximated by the directional derivative in the direction $\hat{n}_{i,j}$. Let x_i be the centre of the prism i, and $x_i + n_{i,\ j}$ be the centre of neighbour j of face i in the direction $\hat{n}_{i,\ j}$. Then Equation 6.4 may be written as

$$\sum_{j=1}^{5} A_{i,j} \mathrm{K}\ \frac{c\left(x_i + n_{i,j}\right) - c\left(x_i\right)}{\left\|\left(x_i + n_{i,j}\right) - x_i\right\|_2} - \sum_{j=1}^{5} A_{i,j} c\vec{u} \cdot \hat{n}_{i,j} + SV_i = 0. \tag{6.5}$$

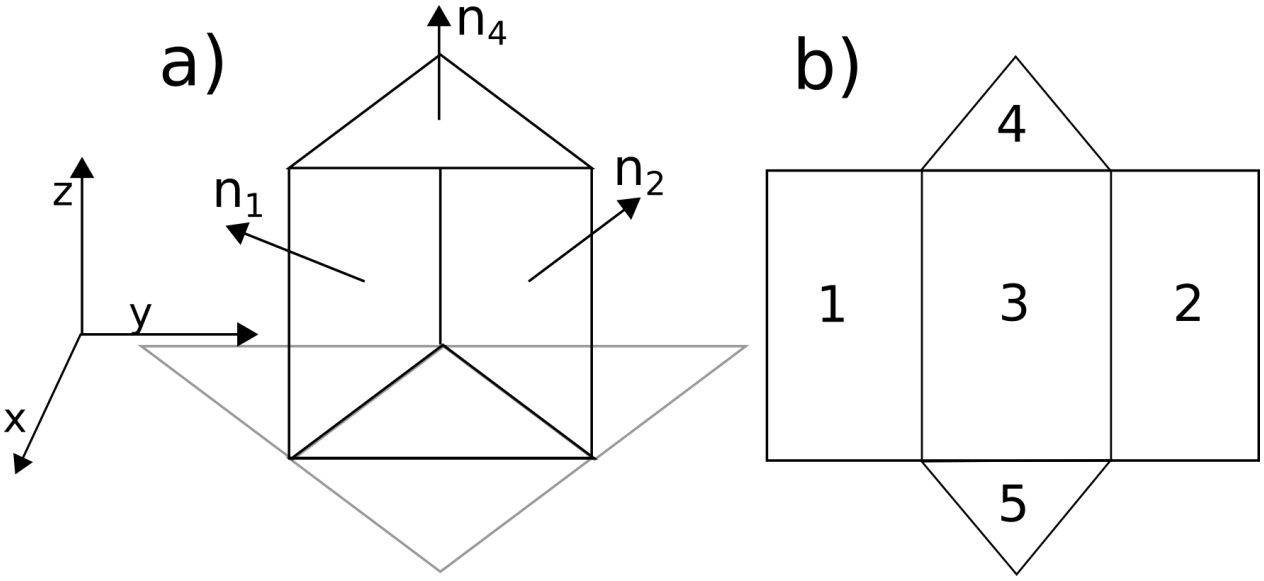

Figure 6.2: a) Diagram of 3D prism with face labels. Three outward-pointing face normals ($\hat{n}$) are shown as examples. Face normal 4 is from the top prism face. A surrounding mesh in shown in grey. B) Diagram of a flattened prism, showing the face labelling. Same orientation as in a). Face 4 is always assumed to be pointing up, and face 5 is always assumed to be pointing down.

Blowing snow transport is dominated by advection. For numerical stability, a first-order up-winding donor scheme is used to approximate the flux across the prism face in the advection term. For each face of each prism, if $\vec{u} \cdot \hat{n}_{i,\ j} > 0$ (vectors point in same direction), then c is approximated with c_i. Alternatively, if $\vec{u} \cdot \hat{n}_{i,\ j} < 0$ (vectors point in different directions), then the c value (c_j) of the 'upwind' neighbour j is used. The inclusion of $\vec{u} \cdot \hat{n}_{i,j}$ captures the variable contribution to down wind prisms. Prisms that have no neighbour follow one of two cases: 1) if the prism is missing an upwind neighbour, then a ghost cell approach

is used, and it is assumed that this upwind cell has the same characteristics as prism i; 2) if the missing prism is downwind, then mass can be removed from the domain. Further, if the prism is in the top layer, then mass can be removed vertically (i.e., $c\left(x_i + n_{i,\ j}\right) = 0$).

6.4.2.3 Suspension flux

The particle terminal fall velocity, ω ($\mathrm{m \cdot s^{-1}}$), was calculated using Carrier's drag law following Pomeroy and Male (1986)

$$\omega = 1.1 \times 10^7 r^{1.8}, \tag{6.6}$$

where the mean particle size, r (m), is given as $r = 4.6 \times 10^{-5} c_z^{-0.258}$ (Pomeroy and Male, 1992) based on measurements by Schmidt (1986) in Wyoming and Budd (1966) in Antarctica and confirmed by field observations in Saskatchewan. The boundary condition for the bottom of the suspension layer is given as

$$c\left(x_i + n_{i,j}\right) = c_{\mathrm{salt}}, \tag{6.7}$$

where c_{salt} is the blowing snow mass concentration ($\mathrm{kg \cdot m^{-3}}$) of the saltation layer. The divergence of suspended flow results in deposition or erosion of snow from the surface without impacting the saltation layer horizontal fluxes.

The eddy diffusion coefficient, K_z ($\mathrm{m^2 \cdot s^{-1}}$), for snow particles is assumed proportional to that for momentum (Pomeroy and Male, 1992). Following Rouault et al. (1991) and as used in Déry and Yau (1999) and Michlmayr et al. (2008), this is given as

$$K_z = \beta u^* l\left(z\right), \tag{6.8}$$

where u^* is the friction velocity ($\mathrm{m \cdot s^{-1}}$) and $l(z)$ is the mixing length given as

$$\frac{1}{l} = \frac{1}{\kappa\left(z + z_0\right)} + \frac{1}{l_{\max}}, \tag{6.9}$$

and κ is the von Kármán constant (0.4), z is the height above the surface (m), z_0 is the roughness length (m), and $l_{\max}$ is a constant generally set to 40 m (Déry and Yau, 1999). The constant of proportionality β has received much debate (Xiao et al., 2000) and generally is taken to range from 0.5 to 1. Herein, β is taken as unity following model inter-comparisons, e.g., Xiao et al. (2000) and the field observations of Pomeroy and Male (1992).

6.4.2.4 Sublimation flux

In Equation 6.5, the term S represents a height dependent sublimation sink, S_z ($\mathrm{kg \cdot s^{-1}}$), given as

$$S_z = c_{\mathrm{subl}_z} c_z, \tag{6.10}$$

where c_{subl_z} is a sublimation coefficient ($\mathrm{s^{-1}}$) derived by Pomeroy et al. (1993) and c_z is the blowing snow mass concentration in the prism at height z. For efficiency, sublimation is calculated for a single (assumed) ice sphere having mean mass $\overline{m}$ (kg) at height z

$$c_{\mathrm{subl}_z} = \frac{1}{\overline{m}\ (z)} \frac{\mathrm{dm}\,(z)}{\mathrm{dt}}. \tag{6.11}$$

The formulation for the rate of change of particle mass used herein is the linearized formulation given by (Schmidt, 1972, 1991) based on the investigations of Thorpe and Mason (1966). This formulation was chosen over the newer formulation by Pomeroy and Li (2000) so as to avoid the more computationally expensive iterative solution. Thus:

$$\frac{\mathrm{dm}}{\mathrm{dt}}(z) = \frac{2\ \ r(z)\,\sigma - \frac{Q_r}{\lambda_t T N u(z)} \left(\frac{L_s M}{\mathrm{RT}} - 1\right)}{\frac{L_s}{\lambda_t T N u(z)} \left(\frac{L_s M}{\mathrm{RT}} - 1\right) + \frac{1}{D \rho_s \mathrm{Sh}}}, \tag{6.12}$$

where z is the height within the suspension layer, $r(z)$ (m) is the radius of the particle of mean mass at height z, D is the diffusivity of water vapour in the air ($\mathrm{m^2 \cdot s^{-1}}$), L_s is the latent heat of sublimation ($\mathrm{J \cdot kg^{-1}}$), Q_r is the radiative energy absorbed by the particle, σ is the under-saturation of water vapour with respect to ice, Nu is the Nusselt number, R is the universal gas constant (8313 $\mathrm{J \cdot mol^{-1} \cdot K^{-1}}$), T is the ambient air temperature (K), ρ_s is the saturation density of water vapour at T, Sh is the Sherwood number, and M is the molecular weight of water (18.01 $\mathrm{kg \cdot kmol^{-1}}$). The vertical profile of under-saturation vapour density is given as a function of that specified at a reference as (Pomeroy and Li, 2000):

$$\sigma = (RH - 1)\,(1.019 + 0.27 \ln(z)), \tag{6.13}$$

where RH (-) is relative humidity with respect to ice. This formulation increases humidity near the surface as would be expected for the water vapour derived from blowing snow sublimation near the surface. However, the sublimation formulation does not include an explicit thermodynamic feedback that reduces under saturation as suggested by Zwaaftink et al. (2013). Pomeroy and Li (2000) and Musselman et al. (2015a) have shown that humidity often decreases during blowing snow due to entrainment of warmer, drier air during

the strong, very turbulent winds that are characteristic of these events. The thermal conductivity of air, λ_t ($\mathrm{J \cdot m^{-1} \cdot s^{-1} \cdot K^{-1}}$), is given by (List, 1971) as

$$\lambda_t = 0.000063T + 0.00673, \tag{6.14}$$

where T is air temperature (K). The latent heat of sublimation is $L_s = 2.83 \times 10^6$ $\mathrm{J \cdot kg^{-1}}$ (Foken, 2018), and the water vapour diffusivity in air is given by (Thorpe and Mason, 1966)

$$D = 2.07 \times 10^5 \left(\frac{T}{273.15} \right)^{1.75}, \tag{6.15}$$

where T is air temperature (K).

6.4.2.5 Saltation flux

The mean mass concentration of snow particles in the saltation layer, c_{salt} ($\mathrm{kg \cdot m^{-3}}$), is given by (Pomeroy and Gray, 1990; Pomeroy and Male, 1992)

$$c_{\mathrm{salt}} = \frac{\rho_{\mathrm{air}}}{3.29 u^*} \left(1 - \frac{{u_n^*}^2}{{u^*}^2} - \frac{{u_t^*}^2}{{u^*}^2} \right), \tag{6.16}$$

where ρ_{air} is the atmospheric density ($\mathrm{kg \cdot m^{-3}}$) and u_t^* ($\mathrm{m \cdot s^{-1}}$) is the friction velocity at the cessation of transport (Li and Pomeroy, 1997b)

$$u_t^* = 0.35 + \frac{T}{150} + \frac{T^2}{8200}, \tag{6.17}$$

where T is the air temperature (ºC) at 2 m height. The shear stress partitioning in Equation 6.16 is via the inclusion of u_n^*, the friction velocity of non-erodible elements (e.g., vegetation). This can be estimated using Raupach et al. (1993):

$$\frac{{u_n^*}^2}{{u^*}^2} = \frac{(m\beta\lambda)}{(1 + m\beta\lambda)}, \tag{6.18}$$

where β is the ratio of the roughness element to surface drag, λ is the roughness element density (-), and m relates the area averaged surface shear stress to the largest shear stress acting at any point on the surface (Raupach et al., 1993). The roughness element density is given by

$$\lambda = \varphi \left(h_v - s_{\text{depth}} \right), \tag{6.19}$$

where h_v (m) is vegetation height and s_{depth} (m) is the snow depth (Pomeroy and Li, 2000). Pomeroy et al. (1993) specified

$$\varphi = N \; d_v, \tag{6.20}$$

where N is the vegetation number density (number $\cdot$ m^{-2}) and d_v is the vegetation stalk diameter (m). For a subarctic mountain tundra catchment, MacDonald et al. (2009) found $m = 0.16$ and $\beta = 202$, $N = 1$, $d_v = 0.8$, and for Arctic tundra, Pomeroy and Li (2000) found $N = 30$, $d_v = 0.8$. Due to the deviation of wind profiles from lognormal, as well as the inclusion of exposed vegetation, the surface roughness z_0 (m) is given as

$$z_0 = \frac{c_2 c_3 {u^*}^2}{2g} + c_4 \lambda, \tag{6.21}$$

where $c_2 = 1.6$, $c_3 = 0.07519$, and $c_4 = 0.5$ (Pomeroy and Li, 2000).

Because Equation 6.16 is a steady-state formulation, applying it where flow is developing is potentially problematic. The impact of fetch was considered by Pomeroy and Male (1986) who developed a hyperbolic fit to observed horizontal profiles of snow transport near the ground in Japan (Takeuchi, 1980). This modified saltation concentration, c_f (kg $\cdot$ m^{-3}), is given as

$$c_f = c_{\text{salt}} \frac{\tanh\left(\frac{4L}{f} - 2\right)}{2} + 0.5, \tag{6.22}$$

where L is the fetch (m), f is the equilibrium distance (300 m). This is then reflected in the suspension layer (Pomeroy, 1991). Upwind fetch was calculated as described in Lapen and Martz (1993) with the *fetchr* algorithm. This was implemented directly on the unstructured mesh.

6.4.2.6 Total transport

The total suspension flux, Q_{susp} (kg $\cdot$ m^{-1} $\cdot$ s^{-1}), is calculated via the integration over all prism layers

$$Q_{\text{susp}} = \int_{h_s}^{z_b} \| \vec{u}_z \| \; c_z \; dz, \tag{6.23}$$

where z_b is the height of the boundary layer (m) and h_s is the saltation layer height (m) given as (Pomeroy and Male, 1992)

$$h_s = 0.8436 {u^*}^{1.27}. \tag{6.24}$$

The saltation flux, Q_{salt} ($\text{kg} \cdot \text{m}^{-1} \cdot \text{s}^{-1}$), is given as

$$Q_{\text{salt}} = \int_0^{h_s} c \cdot u_t^* \cdot c_{\text{salt}} \, dz, \tag{6.25}$$

where $c \cdot u_*^t$ is the wind velocity in the saltation layer (Pomeroy and Gray, 1990). The saltation velocity proportionality constant, c, was found equal to 2.8 in experimental observations (Pomeroy and Gray, 1990).

6.4.2.7 Erosion and deposition

To compute erosion and deposition rates, the rate of change of the snowpack mass, $\frac{\text{d}}{\text{dt}}$ ($\text{kg} \cdot \text{m}^{-2} \cdot \text{s}^{-1}$), is given as

$$\frac{\text{d}}{\text{dt}} = -\nabla \cdot \left(\left(Q_{\text{susp}} + Q_{\text{salt}} \right) \hat{u} \right) + \varepsilon \nabla^2 \frac{d\xi}{\text{dt}}, \tag{6.26}$$

where $\hat{u}$ is a unit vector in the direction of $\vec{u}$; this transforms the scalars quantities Q_{susp} and Q_{salt} into vectors in the direction of the wind.

Multi-dimensional transport equations may have spurious oscillations in the solution (Kuzmin, 2010). The $\varepsilon \nabla^2 \frac{d\xi}{\text{dt}}$ term is a Laplacian smoothing (Kuzmin, 2010) term, without which oscillations between erosion and deposition may appear in the $\frac{\text{d}}{\text{dt}}$ values. The leading coefficient ε is given as

$$\varepsilon = \frac{\alpha^2}{\pi^2}, \tag{6.27}$$

where α (m) is the largest distance over which oscillations are allowed. The value of α should be a few times the average triangle length scale. Equation 6.26 is applied for the 2D case only and has a FVM discretization of

$$\frac{\text{d}}{\text{dt}} V_i = -\sum_{j=1}^{3} E_j Q_t \; \hat{u} \cdot \hat{n} + \varepsilon \sum_{j=1}^{3} E_j \frac{\frac{\text{d}}{\text{dt}}(x_i + n_{i,j}) - \frac{\text{d}}{\text{dt}}}{\left\| (x_i + n_{i,j}) - x_i \right\|_2}, \tag{6.28}$$

where $\frac{\frac{\mathrm{d}}{\mathrm{dt}}(x_i+n_{i,j})-\frac{\mathrm{d}}{\mathrm{dt}}}{\|(x_i+n_{i,j})-x_i\|_2}$ is the directional derivative as described earlier. The flux at the triangle edge, Q_t, is approximated as

$$Q_t = \frac{\left(Q_{\text{susp}} + Q_{\text{salt}}\right)_i + \left(Q_{\text{susp}} + Q_{\text{salt}}\right)_{i,j}}{2}, \tag{6.29}$$

where $\left(Q_{\text{susp}} + Q_{\text{salt}}\right)_{i,j}$ is the flux in direction $x_i + n_{i,j}$.

Equations 6.5, 6.28 were solved separately as two sparse systems of linear equations using the ViennaCL library (Rupp et al., 2016). ViennaCL can exploit shared memory parallelism or hardware accelerators (e.g., GPU). The parallel ChowPatel ILU pre-conditioner was used (3 sweeps; 2 Jacobi iterations) with the GMRES iterative solver (10^{-8} tolerance, maximum of 500 iterations, maximum Krylov space dimension of 30). A single Forward Euler step is taken for the time integration in Equation 6.26.

6.5 Methodology

6.5.1 Study Site

6.5.1.1 Granger Basin

Wolf Creek Research Basin (WCRB) is a cold, snow-dominated basin located in the sub-arctic mountains of southern Yukon, Canada, 15 km from Whitehorse (Figure 6.3)(Janowicz, 1999). It is on the northern edge of the Coast Mountains in a zone of discontinuous permafrost (Pomeroy et al., 1998c). Janowicz (1999) noted that the regional climate is cold continental and that WCRB has three main landcovers: 22% boreal forest consisting of spruce, pine, and aspen woodlands, 58% sub-alpine taiga consisting of shrub tundra and sparse spruce, and 20% alpine tundra consisting of short grasses and sparse shrubs at lower elevations and exposed mineral soils with sparse vegetation at the highest elevation. The mean annual temperature of WCRB is approximately -3 °C with a mean annual precipitation between 300 mm to 400 mm with 40% falling as snow (Janowicz, 1999). The upper elevations of WCRB have substantial and frequent blowing snow redistribution events (Pomeroy et al., 1998c; MacDonald et al., 2009).

Granger Basin (GB) is a small, 8 km^2 (McCartney et al., 2006) sub-basin of WCRB. A subset of GB, about 2 x 2 km in area and shown in red outline in Figure 6.3 was used in this study. Elevation contour lines are shown for 10 m and 25 m intervals. The GB landcover is predominantly exposed mineral soils, grasses, and lichens at high elevations, short birch shrubs (0.3 m to 1.5 m) and grasses at intermediate elevations, and tall willow shrubs (1.5 m) in wet valley bottoms (MacDonald et al., 2009; Ménard et al., 2014b). Tall and short shrubs dominate the north face of the valley with tall shrubs in the valley bottom. Short shrubs and grasses

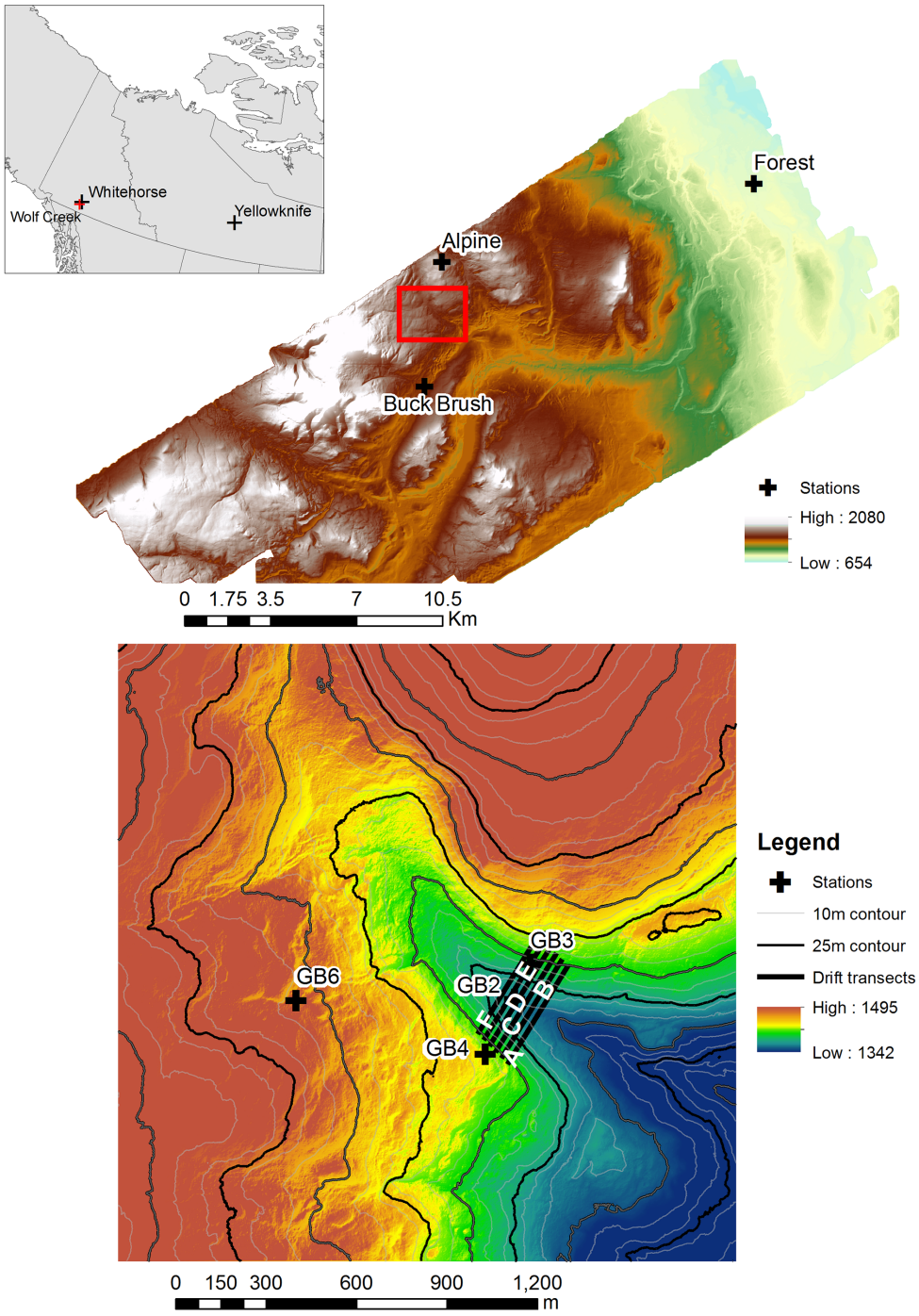

Figure 6.3: The Wolf Creek research basin (top colour figure) is located southwest of the city of Whitehorse, YK, Canada (top inset). The meteorological stations used for this study are shown as black crosses. The extent sub-section of the Granger Creek sub-basin is shown in the red square and enlarged in the bottom colour figure. The snow transects (A-F) used are shown as dark lines that cross the valley. Nearby stations to the Granger Basin subset are shown. Elevation is in metres.

are present on the south facing slope, and short grasses and sparse short shrubs on plateaux to the upwind. The sub-set area landcover is described in detail by Ménard et al. (2014b), who previously modelled blowing snow and shrub interactions on snow accumulation and melt.

6.5.2 Observations

6.5.2.1 Meteorological

The meteorological stations used for this study are shown in Figure 6.3, and their operation and instruments are described in Table 6.1. The stations were controlled by Campbell Scientific 23X dataloggers and powered by storage batteries charged by solar panels with monthly site visits over the winter and frequent visits during spring melt. Meteorological observations were recorded every 10 s and were averaged over 30-minute periods for all sites. Precipitation data were collected by a stand-pipe gauge and MSC (Meteorological Service of Canada) Nipher-shielded snowfall gauges. These data were interpolated, cleaned, and corrected on a daily basis by Rasouli et al. (2014), with the wind under-catch corrections of Nipher-shielded gauges made to snowfall measurements following Goodison et al. (1998). Precipitation phase was determined via the psychometric method of Harder and Pomeroy (2013).

Table 6.1: List of sites in the Wolf Creek basin that were used. The years in operation are listed in the last column. Coordinates are given in UTM Zone 8 metres.

Name	Code	Northing	Easting	Elevation (m)	Years
Valley	GB2	6712350.845	489795.117	1411	2000-2008
South Slope	GB3	6712467.725	489845.377	1451	2000-2008
North Slope	GB4	6712169.026	489696.727	1490	2000-2008
Granger Basin 6	GB6	6712347.671	489069.620	1455	2003
BuckBrush	BB	6709522.453	489176.961	1305	2000-2008
Alpine	Alp	6714603.353	489877.381	1559	2000-2008
Forest	For	6717790.285	502583.402	744	2000-2008

Missing data can occur due to station power failures during the cold, dark sub-arctic winters. Shown in Figure 6.4 is the percentage of missing data for wind speed and direction as a percentage of all time-steps in the period between Oct 01 and May 01 of each winter season. Some of these data gaps spanned all stations and resulted in periods that required use of the nearby Whitehorse airport data, e.g., in 2007 (Ménard et al., 2014b). The 30-minute meteorological data had missing time-steps infilled from surrounding stations when possible. To do so, a multi-variable linear regression between the missing station and other stations

with a measurement at that time-step was used to impute the measurement at the missing time-step. This procedure was only used for winter (October through April) to ensure that regressions were not biased by the summer climate. The data (not shown) for GB agreed with the results of MacDonald et al. (2009) for WCRB that predominant blowing snow event winds were from the S-SW and W-NW.

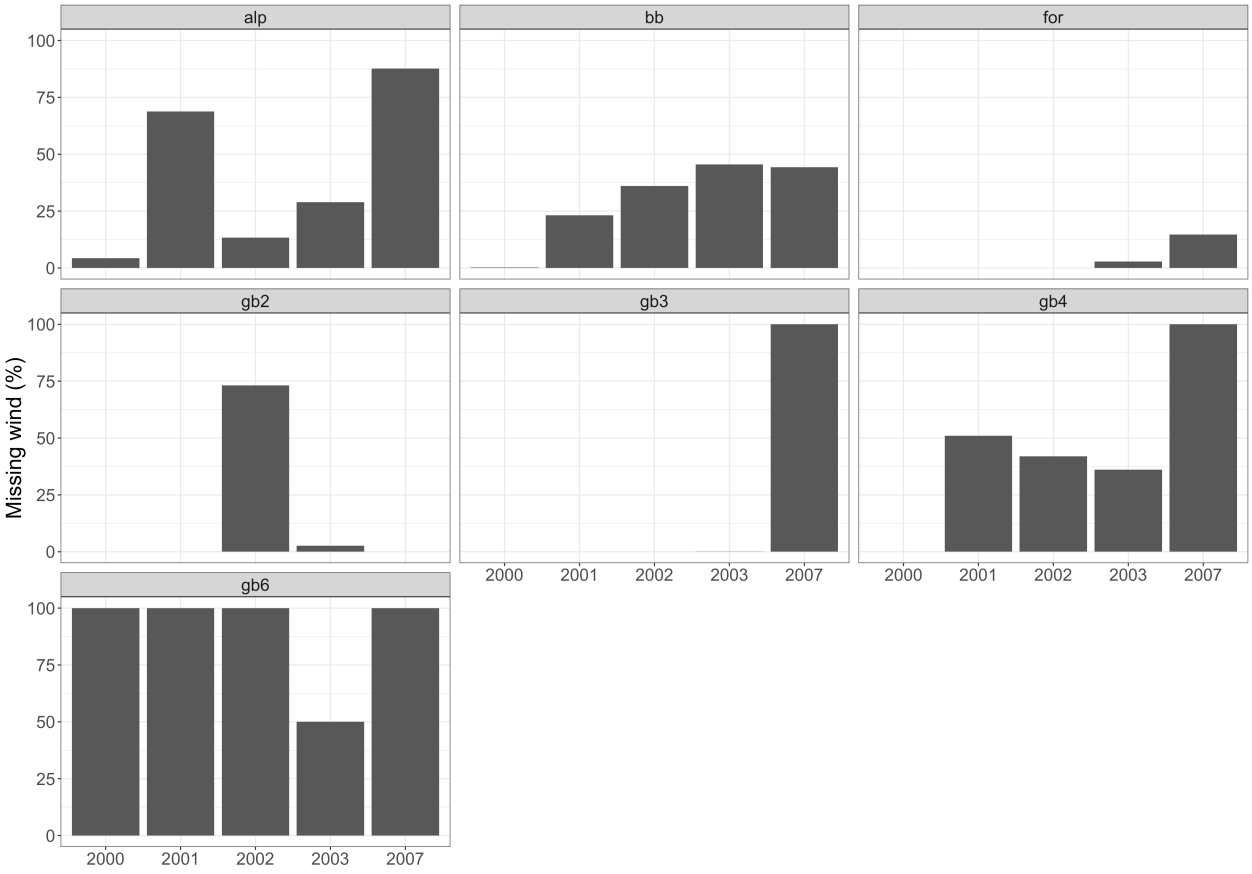

Figure 6.4: The percentage of total time steps between Oct 1 and May 1 that are missing wind data – magnitude or direction. Years with 100% missing data are years the station was not in service.

6.5.2.2 Snow transects

Intensive field campaigns sampled snow depth and density along north-south valley transects (named A-F; $\approx$ 400 m long) in GB (Figure 6.3) for the water years 2000, 2001, 2002, 2003, 2007 (Janowicz et al., 2002; Pomeroy et al., 2003, 2004; McCartney et al., 2006; Dornes et al., 2008a; MacDonald et al., 2009; Ménard et al., 2014b). These transects traverse a large drift ("Granger drift") that forms on the north-facing slope. Depth was sampled every metre, and density was sampled every five to ten metres (depending on year) using Mt. Rose (for deep snow) and ESC-30 (for shallow snow) samplers. End of winter peak SWE sampling was done between April 14 and April 24, depending on the year. As the variability in snow depth tends to be greater than that of density (Dickinson and Whiteley, 1972; Pomeroy et al., 1995; Elder et al., 1998),

representative density measurements were used to estimate transect SWE from a greater number of snow depth observations. The covariance between depth and density was accounted for following Pomeroy et al. (1995).

Using point data to validate a spatial model is difficult due to a conflict of scales (the incommensurability problem, Beven (1989)). Snow survey transects aim to cover a representative area and provide an areal average that should be approximately at the same spatial scale as the model. However, when individual transect points are compared with a numerical model result, it results in comparing point-scale heterogeneity to an areally averaged model element. This discrepancy is exacerbated with an unstructured mesh because of the variable size, shape, and area of elements. Transect sampling uncertainty was estimated following the bootstrapping method proposed by Harder et al. (2018) based on Steppuhn and Dyck (1974). The 95% confidence interval (CI) for SWE is given as

$$\mathrm{CI}_{\mathrm{SWE}} = \sqrt{h_s^2 \mathrm{CI}_{\rho_{\mathrm{snow}}}^2 + \rho_{\mathrm{snow}}^2 \mathrm{CI}_{h_s}^2}, \tag{6.30}$$

where ρ_{snow} is the snow density and h_s is snow depth. This method used 10 000 iterations to estimate the 95% CI. The transect start (0-suffix) and end (1-suffix) locations are given in Table 6.2.

Table 6.2: Snow survey transect locations. Coordinates are given in UTM zone 8N (WGS84) metres.

Transect	x0	x1	y0	y1
A	489770	489972	6.71214e+06	6.71246e+06
B	489750	489952	6.71216e+06	6.71248e+06
C	489730	489932	6.71218e+06	6.7125e+06
D	489710	489912	6.7122e+06	6.71252e+06
E	489690	489892	6.71222e+06	6.71254e+06
F	489681	489900	6.71218e+06	6.71253e+06

6.5.3 Model

6.5.3.1 Mesh generation

A LiDAR derived bare earth DEM and vegetation height at 1 m^2 resolution (Chasmer et al., 2008) was used as input for an unstructured, variable resolution triangular mesh, shown in Figure 6.5. The unstructured mesh was generated using the *mesher* code (Marsh et al., 2018), shown in Figure 6.6. The triangle edges are shown as grey lines on top of the DEM. Triangles were created with a maximum triangle area of 300 m^2, a minimum area of 10 m^2, a vertical error of less than 0.75 m as measured by the root mean squared error (RMSE), and

a RMSE of no more than 0.25 m for vegetation height. In order to ensure that the variable resolution mesh was correctly producing drift locations and to quantify the error associated with this approximation method, a fixed-resolution triangular mesh was created. This mesh had a constant triangle area of 3 m^2 (not shown). The variable resolution mesh has 37,645 triangles, and the fixed-resolution mesh has 99,936 triangles. The vegetation height and wind speed rasters were applied to the triangular mesh by averaging the raster cells that correspond to each triangle and assigning this average to the triangle. No other constraints were used in the generation of the mesh.

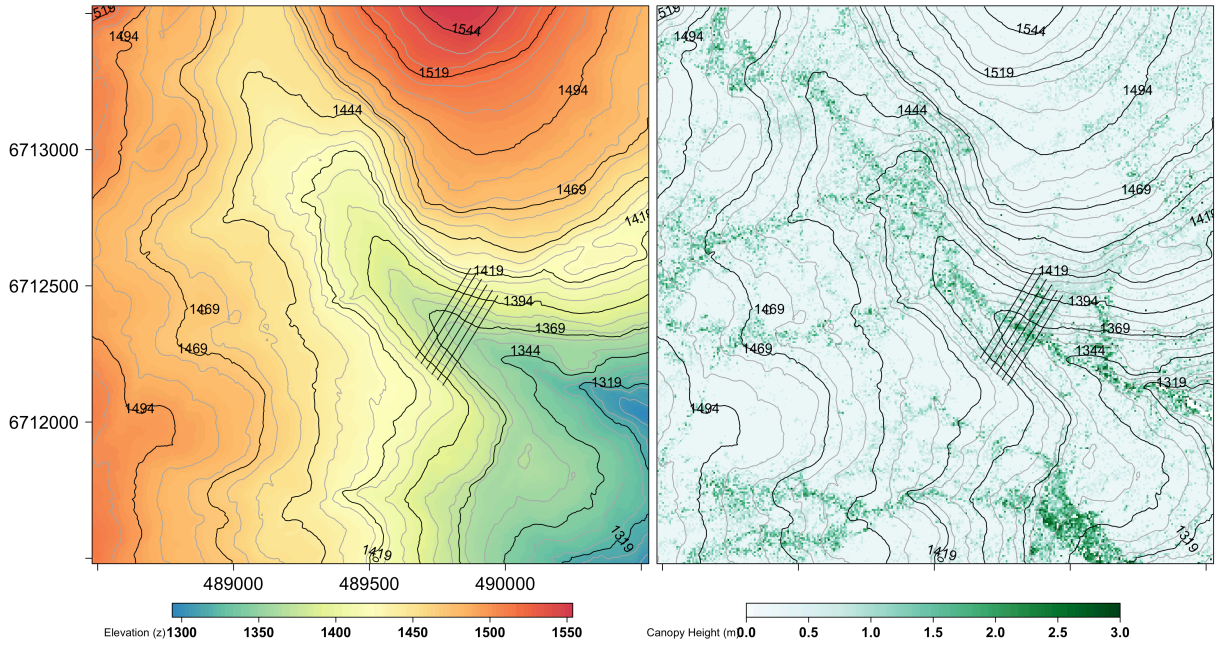

Figure 6.5: LiDAR derived elevation (left) and vegetation height (right) for the Granger basin sub-set. Transects are shown as lines crossing the valley, A-F going up-valley.

6.5.3.2 Snowpack model

A physically based snowpack energetics and mass balance model, Snobal (Marks et al., 1999), was used for snowcover simulation. It approximates the snowpack using two layers where the surface fixed-thickness active layer (taken as 0.1 m) is used to estimate surface temperature for outgoing longwave radiation and atmosphere-snow temperature gradients for the turbulent heat flux. Snobal features coupled energy and mass balance, internal energy, and liquid water storage calculations. Turbulent fluxes are explicitly calculated using a bulk transfer approach that includes a Monin-Obukhov stability correction based on Brutsaert (1982; Marks et al., 1992, 2008). The ground heat flux assumes heat flow to a single soil layer of known temperature and thermal conductivity. The model does not consider sub-canopy energetics, snowcover depletion, or the horizontal advection of energy as was done in the model employed in the same region by Ménard et al. (2014b). Snow-surface shortwave radiation albedo was estimated an exponential, time-dependent decay with an asymptotic

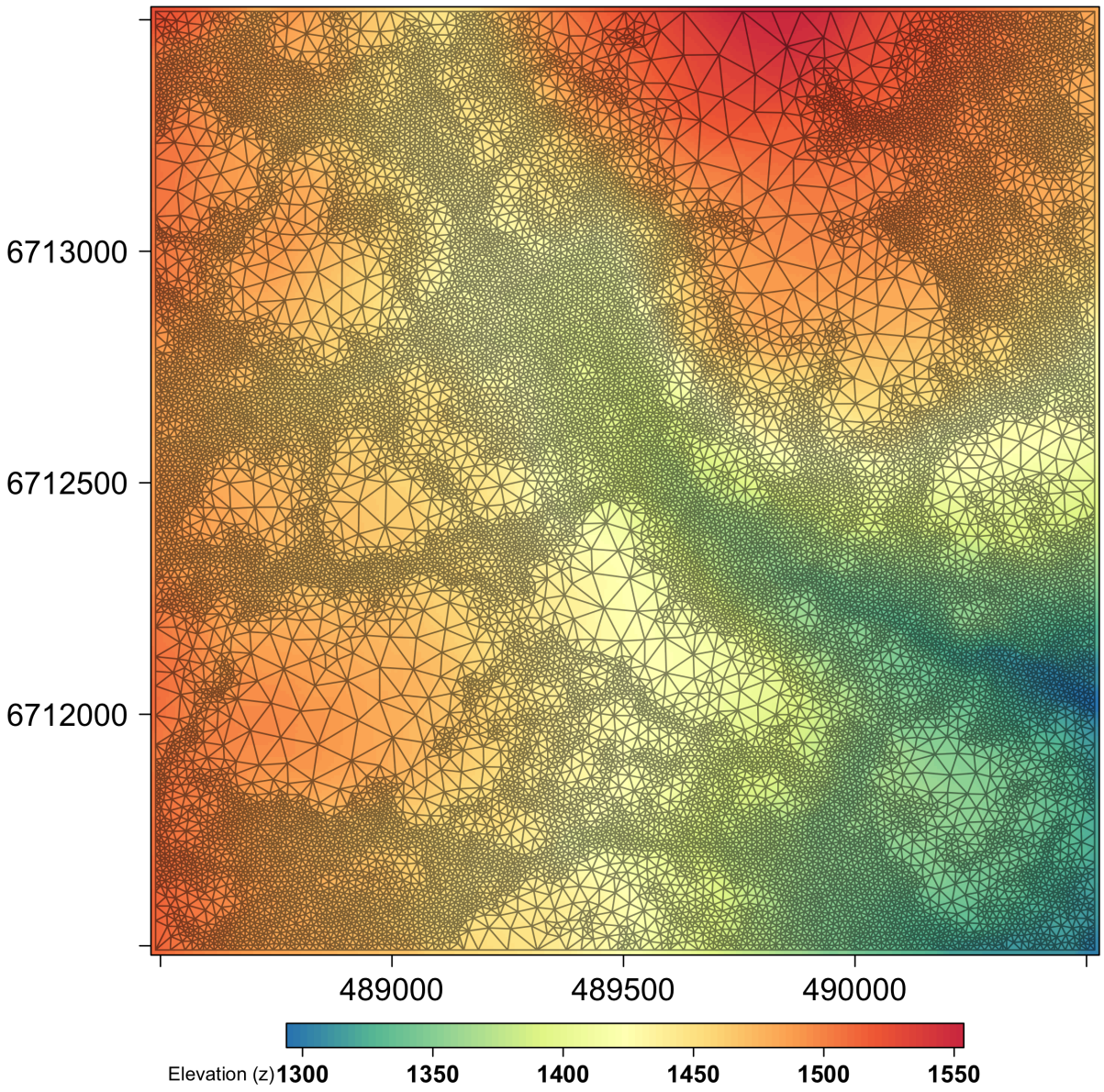

Figure 6.6: Unstructured mesh for the Granger basin sub-set shown as light-gray triangles, overlain on the elevation raster. Triangles were created with a maximum triangle area of 300 m^2, a minimum area of 10 m^2, a vertical error of less than 0.75 m as measured by the root mean squared error (RMSE), and an RMSE of 0.25 m to the vegetation height.

minimum parameterization Verseghy (1991), detailed in Essery and Etchevers (2004), and used in this area by Ménard et al. (2014a). Snobal was driven using observed or interpolated snowfall, rainfall, incoming solar radiation, incoming longwave radiation, wind speed, air temperature, ground temperature, and relative humidity at a 30-minute time interval. A variant of Snobal has been applied successfully in arctic and sub-arctic regions previously within the Cold Regions Hydrological Model (CRHM) platform (Pomeroy et al., 2007), e.g., Dornes et al. (2008b), MacDonald et al. (2009), Rasouli et al. (2014), López-Moreno et al. (2016), Krogh et al. (2017).

6.5.3.3 Meterological distribution

The infilled meteorological data were spatially interpolated to the triangle centres using the thin-plate spline with tension. Topographic gradients for air temperature, precipitation, and relative humidity used linear lapse rate adjustments; lapse rates were calculated from the surrounding stations. Incoming shortwave solar radiation was corrected for slope and aspect. Local terrain shadowing and the impact on shortwave radiation were calculated using the algorithm of Marsh et al. (2012). Longwave radiation for each triangle was estimated from measured transmittance and interpolated air temperature and relative humidity following Sicart et al. (2006) and the sky-view factor calculated using the algorithm of Dozier and Frew (1990).

6.5.3.4 Wind fields

Due to the non-suitability of terrain-curvature wind models, e.g., Liston and Elder (2006), for blowing snow (Musselman et al., 2015a), the use of a more detailed approach is required. Here, the windflow over the terrain was modelled using WindNinja (Forthofer et al., 2014a, 2014b). WindNinja is a mass and momentum conserving diagnostic wind model that simulates mechanical effects of terrain on windflow (Wagenbrenner et al., 2016). It has been applied to downscale numerical weather prediction models over complex terrain (Wagenbrenner et al., 2016) and is able to produce windfield maps at a variety of scales and spatial extents. In addition, WindNinja is under active development and is a modern code that allows for future extensibility. WindNinja was run as a pre-processing step on the 1 m x 1 m LiDAR derived bare-earth DEM (Chasmer et al., 2008; Hopkinson and Chasmer, 2009) using a spatially constant, bare-earth roughness length ($z_0 = 0.01$ m). This approach neglects the feedbacks associated with shrub bending, burying, and erection over the course of winter and spring (Ménard et al., 2014b) and filling up the topography with snow.

Using the WindNinja model, normalized wind speeds for zonal u and v components as well as wind magnitude ($w = \sqrt{u^2 + v^2}$), were calculated for eight wind directions (N, N-E, E, ..., N-W). These were normalized against the domain mean value. The normalized windspeed maps, for each direction, for the w component are shown in Figure 6.7. These normalized wind speed rasters were applied to the triangles in the unstructured mesh

using the *mesher* code (Marsh et al., 2018). Thus for each of the eight directions, each triangle has a normalized wind speed factor for zonal u, zonal v, and w components.

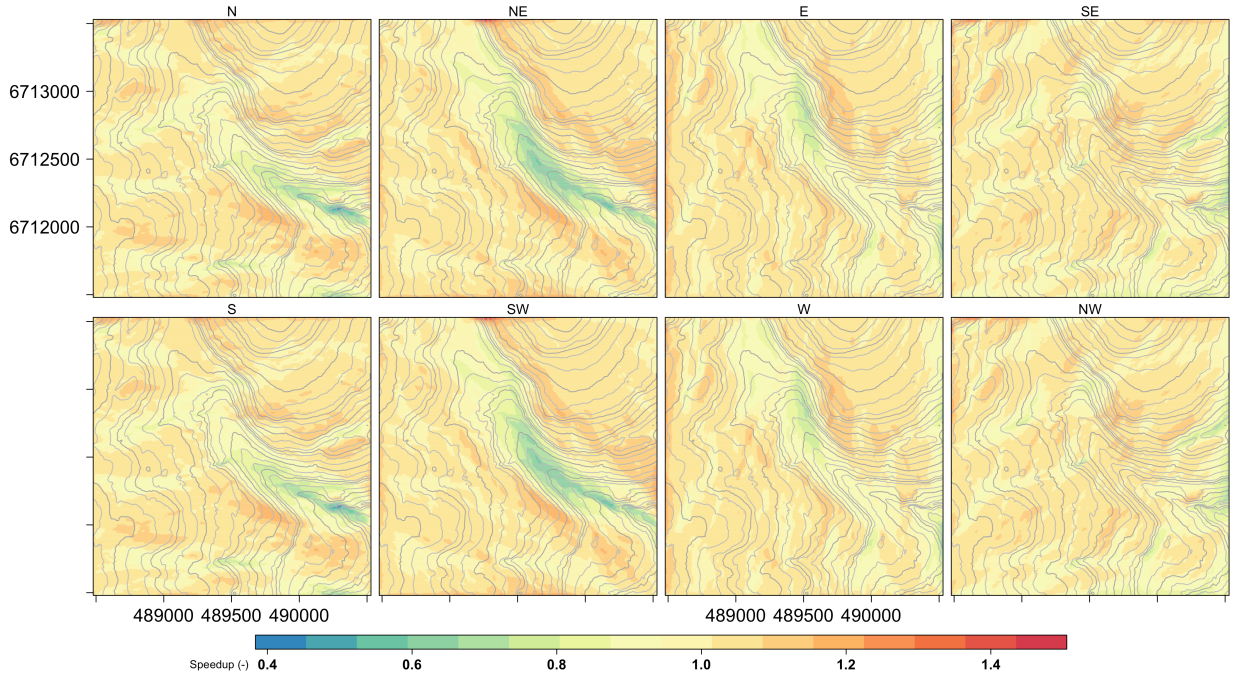

Figure 6.7: Normalized windspeed due to terrain influences. The speedup was calculated for 8 directions and used as a lookup table in the model.

For each time-step of the blowing snow model, the observed wind speed and wind direction from each meteorological station were converted to zonal u and v components. The observed zonal wind components were then spatially interpolated to the triangle centres using the thin plate spline with tension interpolant (Chang, 2008); this ensures no spurious overshoots in the interpolated values. For each triangle, the wind direction was reconstructed from the interpolated zonal u and v components and the appropriate per-triangle normalized wind speed map was selected. The interpolated zonal u and v components were modified via the normalized wind speed map, thus incorporating terrain influences. Finally, the newly computed zonal wind components were converted to a wind speed and direction for use with the blowing snow model. Wind speeds were then modified to include vegetation interactions using the vegetation heights from the LiDAR dataset (via Equation 6.21).

6.5.3.5 Other details

The blowing snow model was run for the October 01 water years 2000, 2001, 2002, 2003, and 2007 corresponding to years where suitable transects of SWE and depth were available. The simulation period began

on October 01 and was run until May 01. The model time step was 30 minutes. The blowing snow model discretized a 5 m boundary layer with 10 numerical discretization layers; this depth is representative of fully developed flow in this region (Pomeroy and Li, 2000). Model results were compared to observations using the root mean squared error (RMSE), mean bias (MB), and coefficient of variation (CV). All simulated end-of-winter snowcovers were rasterized to a 1 m x 1 m raster for computation of error metrics.

6.5.4 Wind field uncertainty

6.5.4.1 There are uncertainties in the distributed wind field stemming from inaccuracies...

There are uncertainties in the distributed wind field stemming from inaccuracies in the wind fields, vegetation interactions, and *in situ* observational errors, e.g., Raleigh et al. (2015a). These uncertainties are likely dominated by wind speed uncertainty because the topography is relatively simple (for a mountain basin) and there is an observed predominant wind direction throughout the winter (MacDonald et al., 2009). To diagnose the impact of these wind speed uncertainties on the spatial pattern of blowing snow, a linear perturbation approach was used. This quantified the uncertainty associated with the wind fields using 50 realizations of a perturbed wind field. The perturbation magnitude followed the range proposed in Raleigh et al. (2015a): a ± 3.0 m $\cdot$ s^{-1} perturbation was drawn from a truncated normal distribution and was applied as a temporally constant bias to the observed wind speed. To diagnose the sensitivity to wind direction, a $\pm 45.0^{\circ}$ perturbation was applied to the wind direction following the same procedure as the perturbation to windspeed. These perturbations in wind speed and direction were added to the observed wind velocities at each meteorological station before interpolation.

Each of these realizations resulted in the calculation of a new, spatially distributed snowcover as a result of the perturbed windfield. The end of winter SWE, from each realization, was rasterized to a 1 m x 1 m raster. For each grid cell i of the raster, the cell CV was computed via

$$CV_i = \frac{\sigma_i}{\mu_i}, \tag{6.31}$$

where σ_i and μ_i are standard deviation and mean, respectively, across all ensemble runs for cell i. The larger the variability between the ensemble members at a cell, the larger the CV. This is therefore a quantification of the spatial sensitivity of the blowing snow model to the wind field.

6.6 Results

6.6.1 Distributed SWE

Shown in Figure 6.8 is the simulated spatial distribution of SWE (mm) for the five water years for the GB subset area. Elevation contours are shown in light grey every 10 m. The output from the variable resolution unstructured mesh is shown. The variable resolution mesh resulted in a reduction in computational elements of 62% versus the fixed resolution mesh and a 44% reduction in total runtime.

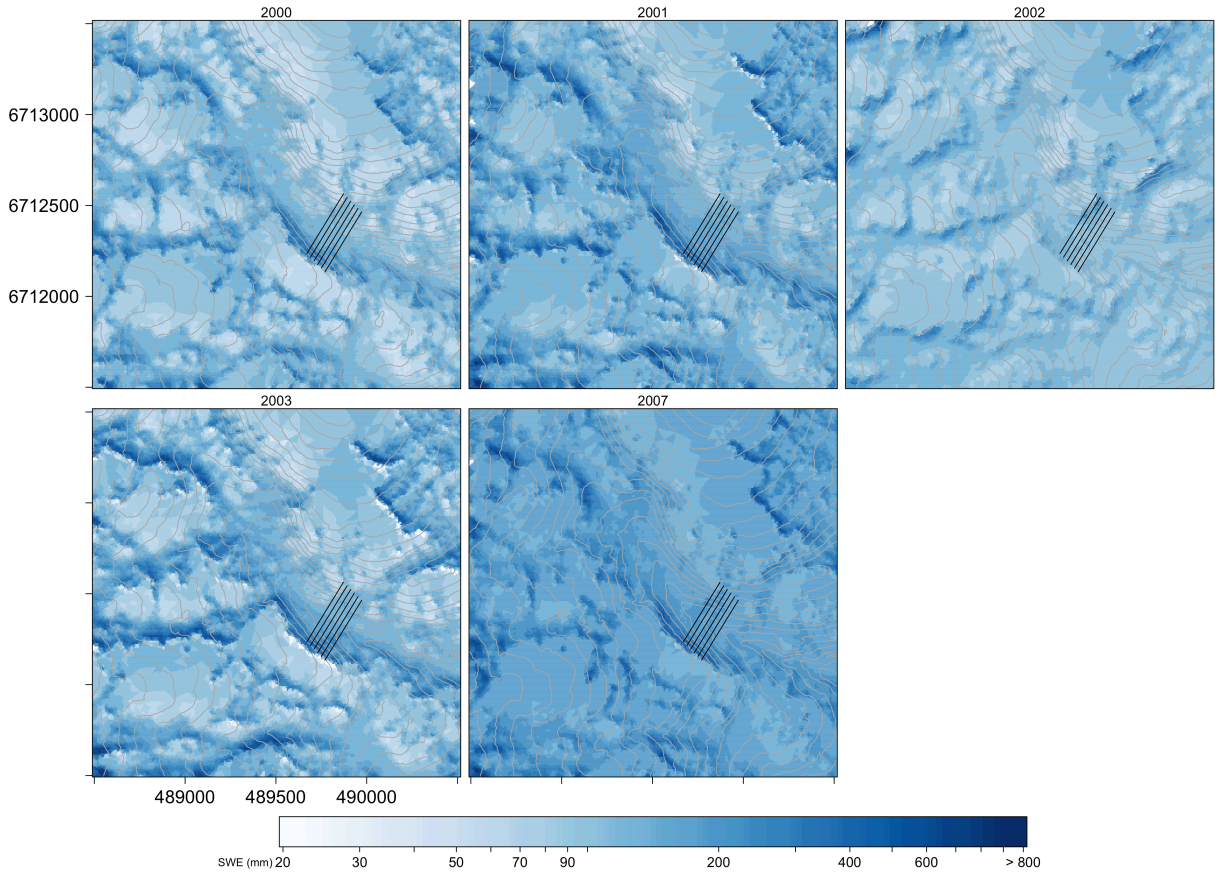

Figure 6.8: Spatial distribution of SWE for the end of winter snow cover (April 14) for the five water years for the variable resolution unstructured mesh. The large Granger drift is located in approximately the middle of the domain.

Substantial spatial and inter-annual SWE heterogeneity was found. As expected, drifts were the greatest deposition areas, with substantial upwind erosion resulting in shallow upwind snow covers. The large Granger drift is visible along the ridge-line in the lower two-thirds of each panel, as are other large drift features. In years 2000, 2001, and 2003, the Granger drift was the most pronounced. This variability in drift was due to fewer wind events from the S-W direction in other years, a requirement for the formation of the drift.

The inter-annual variability of this drift is an important feature of the hydrology of this region (Dornes et al., 2008a) and has been noted for the Canadian Prairies as well (Pomeroy et al., 1995). This interannual variability in snow redistribution adds considerable uncertainty to fixed empirical sub-grid estimates of SWE variability that are employed in many land surface hydrological models.

Both the variable resolution mesh and the constant resolution mesh provided similar heterogeneity in simulated SWE. CV values, for all years for both meshes, are shown in Table 6.3. The constant resolution mesh (not shown) had increased erosion and drift due to a more detailed vegetation height representation. Other differences were due to small-scale topographic features being smoothed out in the variable resolution mesh. The left-most drift in the domain, located at $x = 48900, y = 6712250$, was more sharply represented in the constant resolution mesh and thus accumulated more snow. The mean CV for all years for the variable resolution mesh was 0.46, slightly lower than the 0.56 for the constant resolution mesh. The increased CV for the constant resolution mesh is as a result of the increased topographic variability and the subsequent filling of small topographic depressions.

Table 6.3: Coefficient of variation (CV) for the variable resolution mesh and the constant resolution mesh for the end of winter (April 14) snow cover for each water year.

Year	CV var. mesh	CV const. mesh
2000	0.48	0.54
2001	0.52	0.68
2002	0.36	0.45
2003	0.6	0.68
2007	0.35	0.45

6.6.2 Transects

Simulated SWE (mm) across the six transects for the five water years is shown in Figure 6.9 in blue. Blowing snow calculations were disabled for comparison, and this result is shown in green. Shown in red are the results from the constant resolution mesh. Observations are shown as dots with the observation uncertainty bounds shown in gray.

Substantial inter-annual variability was found in observed SWE and CV for all transects. This is most notable for the Granger drift, located on south (far left) side of all transects. This drift varied in SWE from under 100 mm in some years (2002) to over 600 mm (2001). The CV along the transects varied from 0.24 to 0.54. In 2001, there is a notable increase in SWE along the north face (right hand side) of the transects. The high uncertainty for the observed SWE values in transect F for 2001 was due to the limited number of density

samples available. The water years 2002 and 2007 had the smallest Granger drift due to fewer S-SW wind events.

The observed inter-annual and spatial variability in SWE was generally well represented by the blowing snow model using the variable resolution mesh. Generally, the Granger drift (far left side of transect) was well represented in both magnitude of SWE and shape. Transect A in 2000 was the most poorly simulated transect due to the magnitude and location of the drift being missed. In other years, the drift tended to be correctly simulated or slightly over estimated (2007). The simulation results for 2007 may have been negatively impacted due to the substantial use of airport data required to infill the missing data. The low drifts of transect A in 2002 were well simulated; however, the short but deep drift on transect F was under-estimated. Across all transects and years, the most consistent simulation error was an under-representation of the mid-valley SWE, where tall vegetation dominates the landscape along the creek. As this area undergoes minimal snow redistribution, this may indicate an underestimation of seasonal snowfall in the observations.

The constant resolution mesh tends to have similar drift formation as the variable resolution mesh. However, in some years (2001, 2003), the drift is over-estimated by approximately 150 mm . This increase in transport is likely as a result of increased transport from the source plateaux regions, where more small triangles in the constant resolution mesh have greater opportunities for transport initiation. This increase in transport into the drift also manifests as increased transport into the valley. As a result, the mid-valley SWE is better represented by the constant resolution mesh.

Summarized in Table 6.4 are the RMSE and CV values for SWE versus the observations for each entire transect. For all years, and all transects, no blowing snow produced a homogeneous snow cover with a small variability due to spatial differences in over-winter snowpack energetics (CV < 0.1). These simulations showed none of the observed inter-annual variability. Landscape-averaged values of RMSE and CV across all years and transects are shown in Table 6.5. The mean RMSE and MB of SWE were 86 mm and -20 mm, respectively. On average, the model SWE CV closely matched observed CV, 0.36 versus 0.41, respectively. The constant resolution mesh had an RMSE of 120 mm, an MB of -1.3 mm, and a CV of 0.37. Without blowing snow, the RMSE and MB were 98 mm and -49 mm, respectively, with a CV of 0.04. Overall, use of the variable resolution mesh tends to produce better drift prediction than the constant resolution mesh, but it under predicts mid-valley transport.

Table 6.4: The RMSE values for simulated SWE versus observations are given along with the CV values for simulated SWE using the variable resolution mesh and observed SWE.

Year	Transect	RMSE (mm)	MB (mm)	CV (-)	Obs CV (-)
2000	A	120	-86	0.27	0.46
2000	B	61	-43	0.35	0.24
2000	C	88	-63	0.41	0.38
2000	D	100	-85	0.49	0.31
2000	E	81	-36	0.43	0.38
2000	F	42	-8.1	0.47	0.55
2001	A	95	59	0.37	0.54
2001	B	96	-38	0.41	0.48
2001	C	85	43	0.41	0.4
2001	D	120	-78	0.44	0.32
2001	E	93	-33	0.43	0.4
2001	F	170	-130	0.43	0.38
2002	A	63	-12	0.058	0.55
2002	F	100	-64	0.26	0.5
2003	A	56	19	0.3	0.39
2003	B	61	27	0.43	0.39
2003	C	72	-4.2	0.42	0.3
2003	F	75	2.9	0.47	0.36
2007	A	91	82	0.27	0.46
2007	C	62	6.4	0.26	0.32
2007	F	77	17	0.28	0.5

Table 6.5: The mean RMSE and CV values for simulated SWE using the variable resolution and constant resolution mesh. Observed CV, across all years and all transects are given.

Simulation type	RMSE (mm)	MB (mm)	CV (-)	Obs CV (-)
Const. Res. PBSM3D	120	-1.3	0.37	0.5
No blowing snow	110	-45	0.036	0.5
With PBSM3D	99	-20	0.31	0.5

6.6.3 Sublimation

The model was run with and without blowing snow sublimation, and this difference (sublimation-no sublimation) in the end of winter SWE is shown in Figure 6.10. The largest differences were found in the sink locations where substantially more snow was deposited when there was no sublimation. With no blowing snow sublimation, large areas of up-wind blowing snow source (e.g., the plateaux) transported substantially more snow into the drift sinks. With sublimation, this mass was lost to the atmosphere resulting in lower drift sizes. As a result, better simulation results are found when including the blowing snow sublimation process. Shown in Table 6.6 is the domain-averaged sublimation loss as a percentage of total winter time precipitation. The inter-annual variability in total precipitation and blowing snow events resulted in a 6% to 14% loss to sublimation. This demonstrates the importance of including sublimation processes for not only simulating total mass but also for including the feedbacks that lead to spatial heterogeneity in the snowcovers.

Table 6.6: Simulation domain mean simulated sublimation loss as a percentage of total winter precipitation.

Year	% precip as sublimation
2000	12
2001	14
2002	6
2003	11
2007	10

6.6.4 Wind uncertainty

Due to the substantial heterogeneity in wind field and to feedbacks between snow cover, SWE, and blowing snow, there was heterogeneity in the sensitivity of the blowing snow model. Shown in Figure 6.11 and Figure 6.12 is the coefficient of variation of SWE, for each grid cell, across the entire 50-member ensemble for the April 15 snowcover of each year for windspeed and wind direction perturbations respectively. The 2007 year is not shown for clarity due to low sensitivity. Low CV values were associated with limited variability in the ensemble (i.e., the wind field perturbation did not result in much change), and high CV values were associated with large variability in the ensemble, i.e., the wind field perturbation dramatically changed the SWE. Therefore, this figure is interpreted as a sensitivity index showing regions of limited and large variability as a result of the wind field perturbation.

There was substantial variability in the sensitivity between years, in both degree of sensitivity and spatial

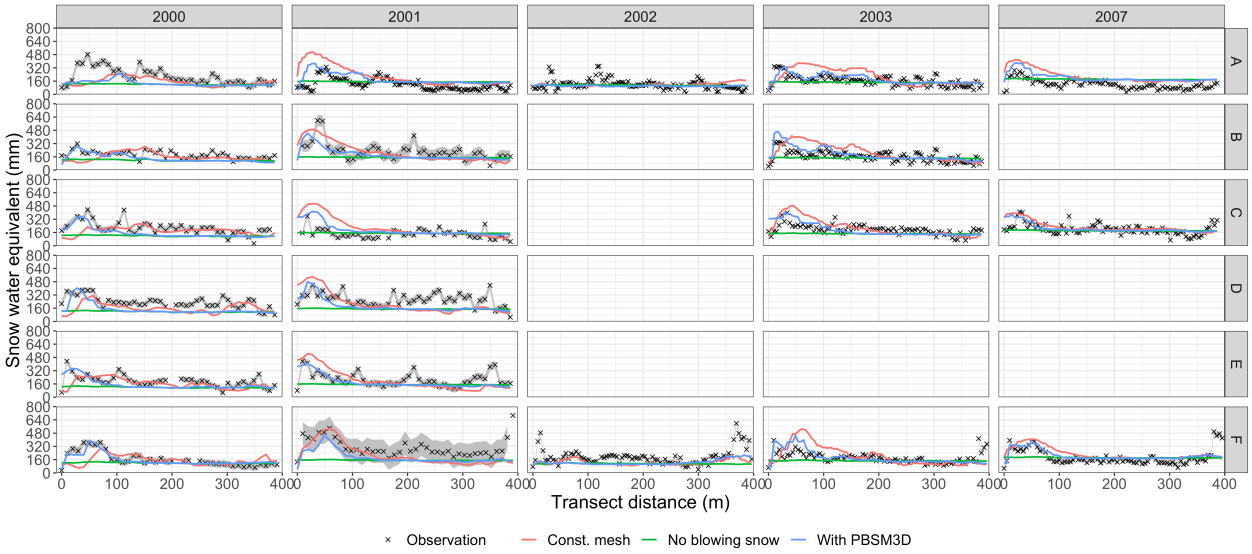

Figure 6.9: Simulated snow water equivalent for end of winter (April 14) across the six transects for the five water years is shown in blue. Observations are shown as dots, and an uncertainty bound shown in gray. No blowing snow is shown in green and a constant resolution mesh in red. Only transects with observations are shown.

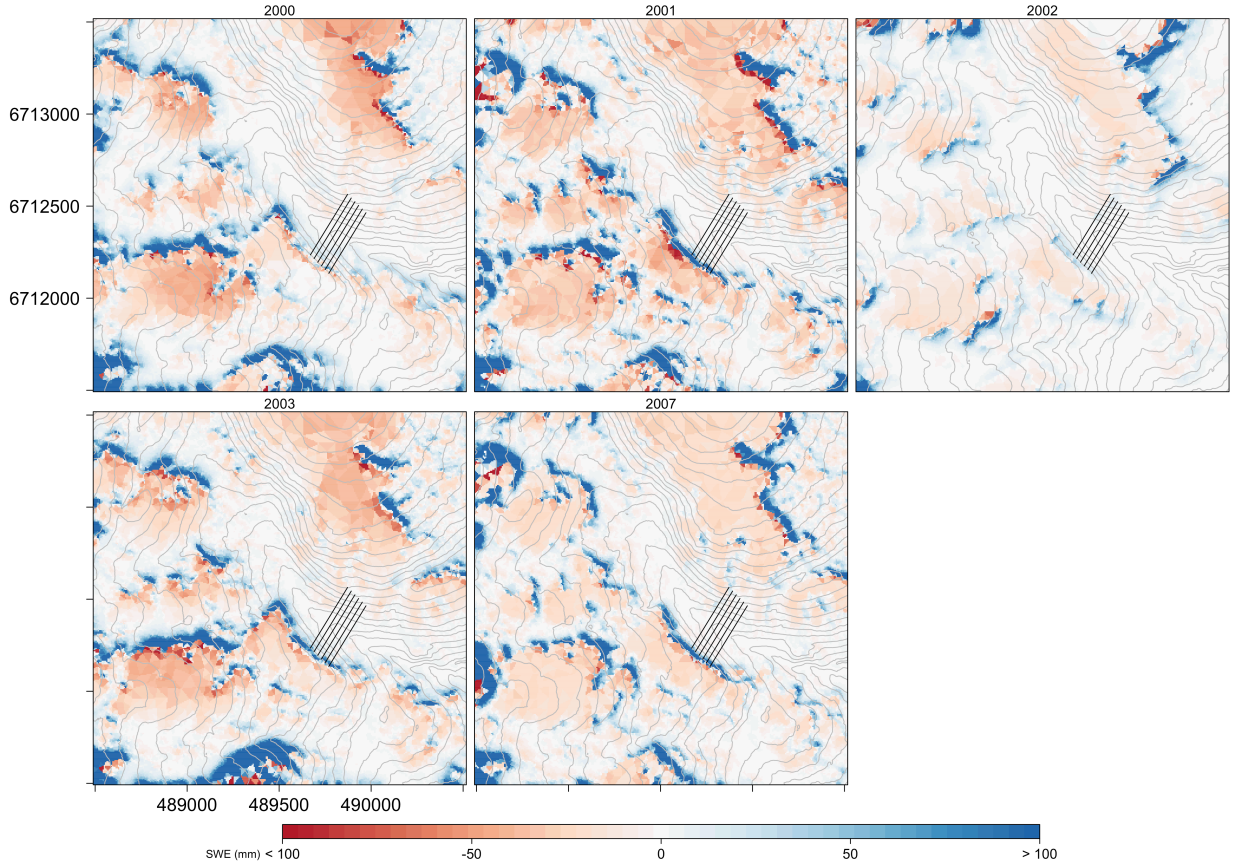

Figure 6.10: Difference in end of winter SWE (taken as April 14 for all years) with and without blowing snow sublimation.

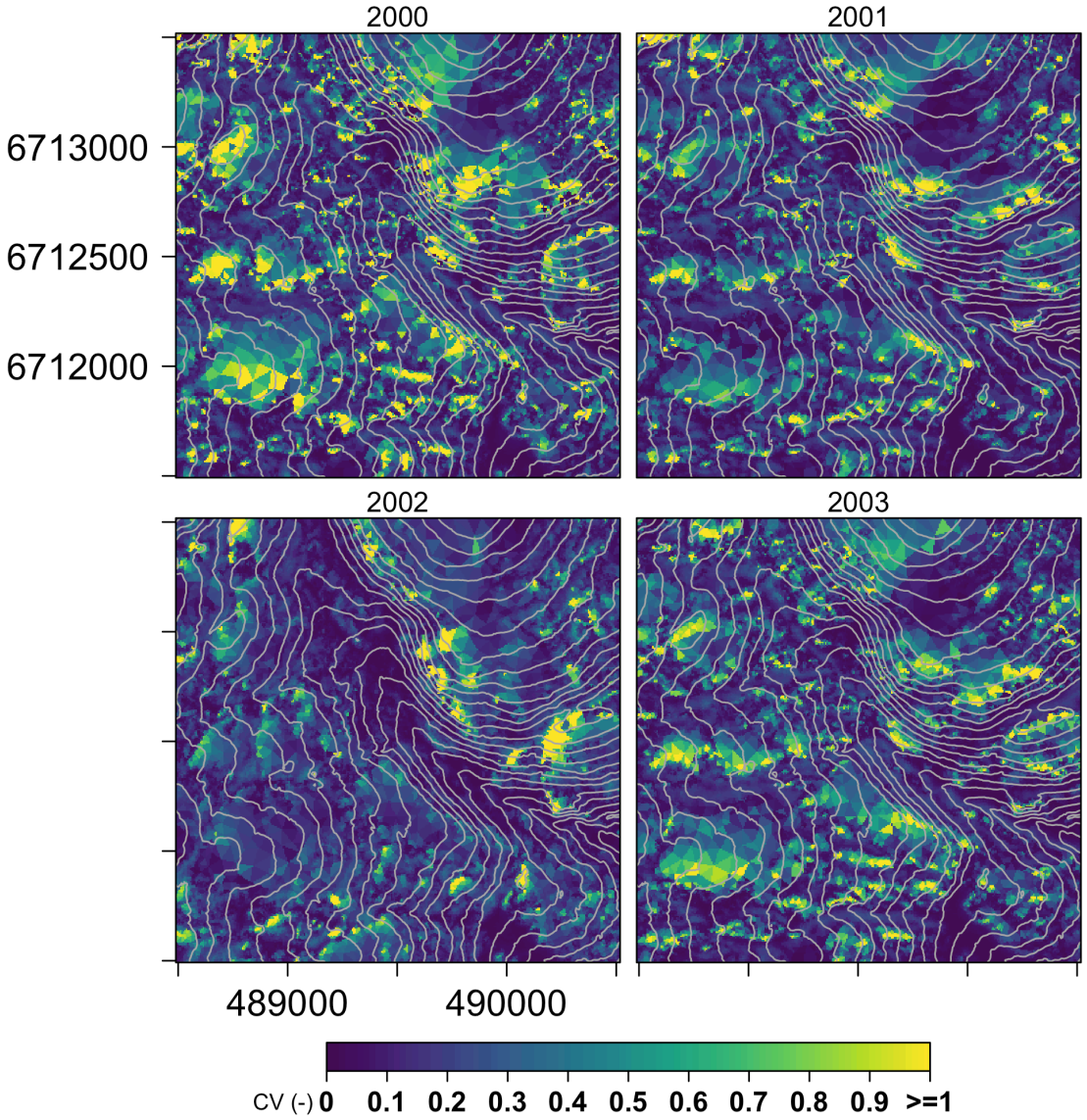

Figure 6.11: A 50-member ensemble was run with perturbations to the wind magnitude. The unstructured mesh representing end of winter SWE (April 14), for each member, was rasterized to a 1 m x 1 m raster. The coefficient of variation was computed for the SWE across the ensemble at each grid cell. The larger the variability at a cell, the larger the CV. Therefore this can be interpreted as a map showing the spatial sensitivity of the model to windspeed.

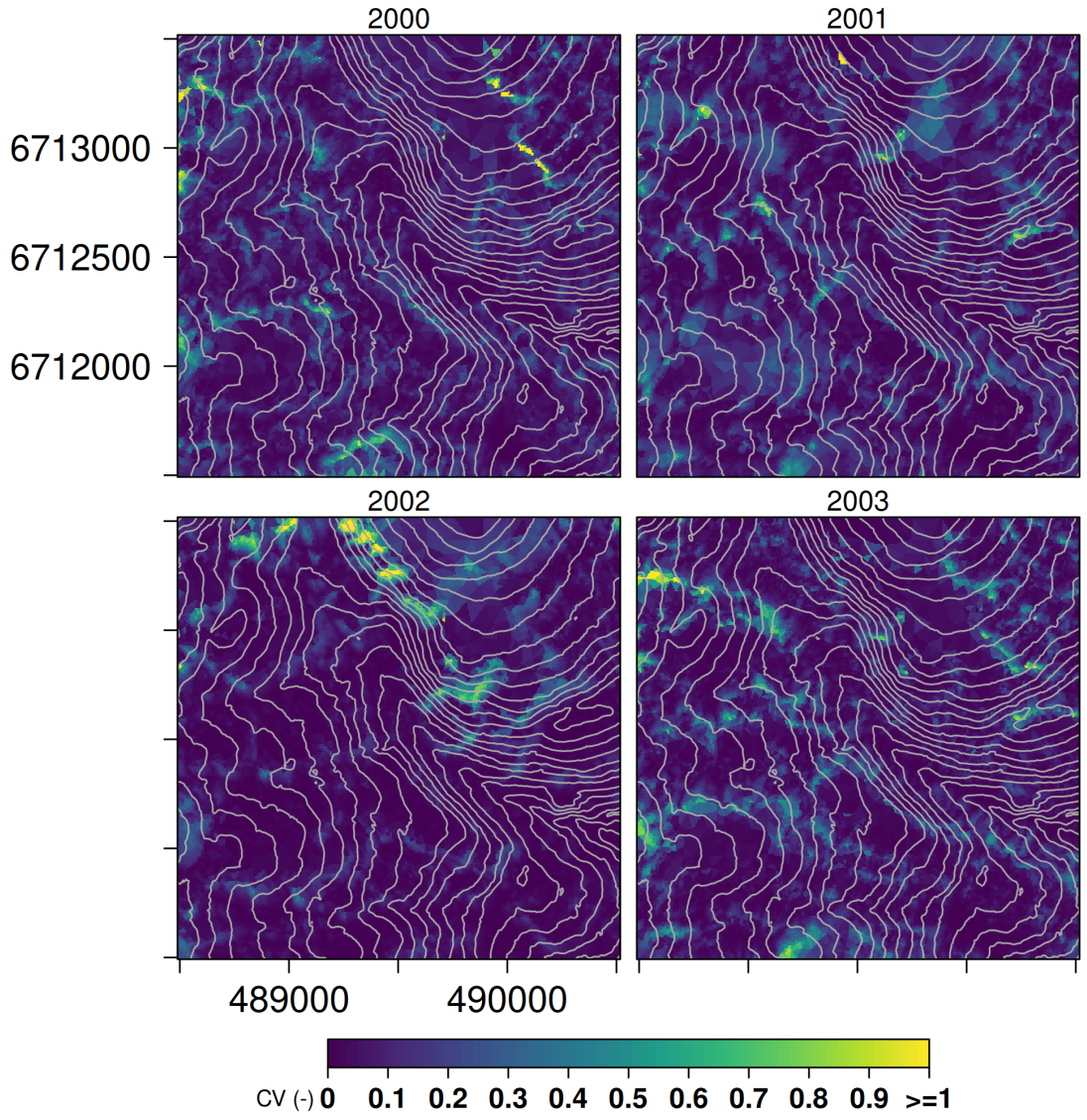

Figure 6.12: A 50-member ensemble was run with perturbations to the wind direction. The unstructured mesh representing end of winter SWE (April 14), for each member, was rasterized to a 1 m x 1 m raster. The coefficient of variation was computed for the SWE across the ensemble at each grid cell. The larger the variability at a cell, the larger the CV. Therefore this can be interpreted as a map showing the spatial sensitivity of the model to wind direction.

distribution of sensitivity to wind speed. The years that produce the large Granger drift (2000, 2001, 2003) had the greatest areas of increased sensitivity. In all years, the areas with high CV were spatially correlated with drift locations and the immediate upwind scour zones. The further upwind sources for the drifts were generally the least sensitive. This suggests that the drifts are integrating all the blowing snow sensitivity from the upwind areas. That is, even though limited sensitivity was found in the majority of the up-wind sources for the drift, e.g., plateaux, all the small sensitivities are compounded and expressed as large uncertainty in the drifts.

The wind direction sensitivity was less spatially variable than wind speed. The areas with greatest sensitivity are the drift (deposition) locations — the upper plateaux tend to be source areas of snow regardless. In the 2000, 2001, and 2003 years, the Granger Creek valley wall had substantial variability in drift locations. In 2002, the drift locations at the north-end of the domain were the greatest regions of sensitivity. Overall, the sensitivity was confined to the drift locations changing location due to differences in the gradient in the wind field, and the upper plateaux remained consistent mass sources.

6.7 Discussion

6.7.1 Synthesis

As increased attention is focused on hyper-resolution (< 1 km) atmospheric modelling (Wood et al., 2011), ensuring that hydrological models adopt snowdrift-resolving scales (Pomeroy and Bernhardt, 2017) is now possible and of substantial importance for cold-regions simulations. Due to the importance of representing landscape heterogeneity on cold regions snow-coverd area and runoff calculations, e.g., Dornes et al. (2008b) and Dornes et al. (2008a), explicit inclusion of blowing snow and related sublimation losses should be considered a priority. Common assumptions that drifts are the same relative size and in the same location every year and that the CV is the same every year are not supported by field data observations. Simulating this inter-annual variability is an important capability and is critical to improving snow simulations in the alpine.

The model presented herein shows a way towards inclusion of this process in large-extent hydrological models. As described in Marsh et al. (2018), the unstructured meshing algorithm can ensure inclusion of substantial topographic and vegetation heterogeneity while significantly reducing the total number of computational elements. A 62% reduction in computational elements was found when using the variable resolution mesh versus the fixed resolution mesh. Although this did not result in a directly proportional reduction in computational time, there were still substantial computation savings of 44%. This decrease in simulation time is important when applying distributed models to large extents and is a substantial decrease in required computational

resources versus fixed-resolution models.

A coarser discretization can be expected to average out variability, and this was observed in the missing small-scale topographic variability in the upper plateaux. However, all the major topographic features were represented by the variable resolution mesh. The similarities in SWE heterogeneity (measured by the CV) between the fixed and variable resolution meshes suggests that the variable resolution mesh is capturing essentially as much heterogeneity as the fixed resolution. The larger triangle elements in the variable resolution discretization were predominately in the source-area plateaux. As a result, the constant resolution mesh had comparatively more triangles in the source plateaux areas. This resulted in more triangles that could potentially transport snow down-wind. Therefore, in some years, there was increased transport into the drift area versus the variable resolution mesh. This increased transport is likely as a result of uncertainties, e.g., in the LiDAR derived vegetation heights, impacting threshold saltation initiation. As a result, the variable resolution mesh tends to produce more accurate results, likely as a result of reducing some of this uncertainty via aggregation of the landscape. These results suggest that the use of a spatially variable resolution mesh is appropriate for this domain.

It has been well established by many field and modelling experiments that blowing snow is a required process to consider in order to accurately simulate end of winter snow cover heterogeneity in wind-blown environments, e.g., Pomeroy et al. (1993);Pomeroy et al. (1993) and Luce et al. (1998). The results presented here further substantiate this. As measured by the CV, including blowing snow redistribution processes in the model dramatically increases the spatial heterogeneity of snow mass. Indeed, the non-blowing snow simulations produced very low CV values (CV$\approx$ 0.04), well below observed values anywhere in the world (Pomeroy et al., 1998a). The simulated CV values on a per-transect basins agree with the observed CV as well as existing literature values for this domain, e.g., Pomeroy et al. (1998a). Inclusion of blowing snow sublimation resulted in a domain-averaged 6% to 14% loss of snow mass as a percentage of total snowfall. Reported sublimation losses are highly variable between studies, as summarized by Mott et al. (2018). The simulated sublimation losses herein are somewhat lower than what Pomeroy and Li (2000) reported (22%), lower than MacDonald et al. (2009) (19%-81%) (same basin but different domain), and similar in the range reported by Liston and Sturm (1998) (9% to 22%) for other Arctic sites. As a result, this caused feedbacks in the threshold processes that govern blowing snow initiation. This resulted in less SWE in the upwind plateaux source regions and decreased drift sizes due to less snow being transported in. Without blowing snow, there is little reason to expect that snow mass heterogeneity would be accurately captured, and this is observed in these results.

A key component to successfully modelling blowing snow is generating an appropriately accurate wind field (Raderschall et al., 2008; Mott et al., 2010; Musselman et al., 2015a; Vionnet et al., 2017). Evaluating point-scale wind speeds alone is insufficient. Musselman et al. (2015a) demonstrated that terrain curvature methods are insufficiently detailed to produce the emergent spatial behaviour via the accumulation of non-linear processes of blowing snow despite simulating reasonable wind speeds. The accuracy of a wind field for

blowing snow simulation depends heavily on the input wind speed and direction data as well as the impacts of topography and vegetation. Input wind data may be either interpolated weather station observations, such as those found in research basins, or the output of numerical weather prediction models. Due to the harsh conditions of remote arctic research basins, obtaining time-series data without any faults or quality issues can be difficult. The results herein showed that interpolated wind fields from nearby but not in-basin observations (such as the airport data) were insufficient to capture all the blowing snow dynamics. The inclusion of these airport data may have contributed to the weaker results when included. The inclusion of vegetation interactions on the wind field is a major source of uncertainty, and properly capturing the wind flow through protruding vegetation would require even greater detail in the wind model and is an open research question. Previous work in this basin by Ménard et al. (2014b) showed modest improvements in snowpack ablation simulation by considering the dynamics of shrub bending, where (some) shrubs are bent over and buried by winter snowcovers. Coupling these dynamics with a wind flow model greatly increases uncertainty and computational costs. Such an inclusion in a model requires further work to ensure such a coupling would not further increase uncertainty with no improvements. Lastly, the steady-state assumptions in the wind field are known to be incorrect for at least the small scale processes that govern blowing snow (Aksamit and Pomeroy, 2016, 2018). However, for moderate-complexity models to be applied to large extents in order to improve snow cover heterogeneity estimates for hydrological models, these uncertainties in the wind field are likely outweighed by the improved simulations of SWE heterogeneity. Future work should consider the benefit to including increased detail of vegetation-snowcover feedbacks such as shrub bending and re-computing the wind flow speedup using the snowcover surface.

Previous distributed blowing snow modelling has either focused on distributed models that have used empirical models with substantial errors in the wind field (Liston and Sturm, 1998; Musselman et al., 2015a), assumptions regarding wind that limits applicability to large extents due to complex wind flows, e.g., Essery et al. (1999), or coupling with atmospheric models, e.g., Lehning et al. (2008), Vionnet et al. (2014). The look-up table method used here extends the approach of Essery et al. (1999) by incorporating per-element wind flow direction and applying those directions on a per-element basis without any mean-direction assumptions. This approach is functional with sparse or dense point-scale meteorological observations or atmospheric model outputs, is not tied to any particular numerical weather model, and is therefore suitable for a wide range of applications around the world. This method can be extended to large areas without requiring the use of a complex wind flow model run each time step. This model therefore is a pathway for the inclusion of critical cold-regions processes without massive computational overhead.

The ensemble run of various wind field perturbations is a novel way of examining the spatial sensitivity of a distributed blowing snow model. The results showed that there is substantial spatial variability in sensitivity, and that this sensitivity varies on a per-year basis. Presumably, there also is mid-winter variability in this sensitivity. Considering these spatial sensitivities is important when adopting snowdrift-resolving scales in

hydrological models due to being able to diagnose areas that drive large scale hydrological responses to the cryosphere. This approach allows for inter-comparisons of blowing snow transport and sublimation to different wind field models, as per Musselman et al. (2015a). The ensemble results showed that the wind speed perturbations had the greatest impact on the results compared to the wind direction. The snowdrifts and immediate up-wind blowing snow source areas are the most sensitive areas of the catchment and that the further upwind plateaux are less sensitive. That is, the drifts are acting to integrate all the upwind uncertainties as suggested by Tabler (1974) and shown in the Canadian Prairies by Fang and Pomeroy (2009). Perturbations to wind direction resulted in changes in drift location; however, the plateaux remained mass sources, regardless of wind direction. Thus, small changes in upwind features, e.g., snow model density estimation for snow depth (and subsequently vegetation burial), are likely to have substantial downwind impacts due to wind variability. This suggests that these drift locations are likely some of the most difficult areas to simulate on the landscape.

This result has implications for hydrological simulations in areas undergoing wide-spread vegetation changes, such as the increased shrub cover of the tundra (Sturm et al., 2001). As upland tundra changes to a shrub-dominated land cover, the upwind source areas for blowing snow will hold more snow and so less will be available for downwind transport and sublimation (Anon, 2004; Ménard et al., 2014b). This would then result in less mass transported into the large drifts. The drift contribution in maintaining summer streamflow during warm dry periods will then have important implications for the region's hydrology as shown by Rasouli et al. (2018) in Wolf Creek and by Krogh and Pomeroy (2018a) near Inuvik, NWT. The likely result is less drift formation, , unless winter snowfall increases as is suggested by recent climate modelling in the area (Rasouli et al., 2019). Therefore, this suggests that not only are drift locations difficult to model but they may also be increasingly sensitive areas under climate change induced landscape changes such as shrub expansion that are concomitant with temperature and precipitation increases.

6.7.2 Uncertainties

There are substantial uncertainties associated with using distributed models in remote cold regions:

1. Uncertainties associated with meteorological forcing are substantial, even in well-instrumented research basins (Raleigh et al., 2015a). Gauge under-catch associated with solid-phase precipitation is an on-going challenge in cold regions. Operating a research basin in the sub-arctic is incredibly challenging. Despite many meteorological research stations in the area, some periods had data gaps that necessitated interpolating wind velocity from the Meteorological Service of Canada Whitehorse Airport station (MacDonald et al., 2009; Ménard et al., 2014b). In water year 2000, there was no meteorological data infilling required, whilst in other years there was substantial infilling required. This may explain the weaker results in those years. It is possible that uncertainty in infilling resulted in unrealistic wind

fields. Uncertainties in interpolation mean that the model cannot rely entirely on observations remote from the area for interest for prediction. This suggests that either collocated stations or high-resolution atmospheric model output is important for applying these types of models.

2. For computational complexity reasons and due to uncertainties in how to apply horizontal advection over a variable mesh model, the models used here ignored known processes such as shrub-bending under winter snowloads and shrub-erection during spring snowmelt, radiation and snowmelt energetics under and near shrub canopies, and the advection of sensible energy from shrubs and bare ground patches to snow patches during melt (Pomeroy et al., 2006; Bewley et al., 2007; Ménard et al., 2014b, 2014a). The purpose of the modelling here was to isolate and show the impact of blowing snow processes, but a more complete snowcover model would include all of those impacts and that of latent heat advection (Harder et al., 2017; Mott et al., 2017; Schlögl et al., 2018).
3. The wind flow model uses a bare-earth representation year-round that neglects the feedbacks associated with shrub bending, burying, and erection over the course of winter and spring, filling up the topography with snow, and does not include flow separation. However, there is no evidence of flow separation in this environment – plumes of snow have never been observed to form on the ridge tops in the modelling domain subset of the GB.
4. A potentially important process that was not considered here is preferential deposition (Mott et al., 2014; Vionnet et al., 2017; Wang and Huang, 2017; Gerber et al., 2019). Preferential deposition results in decreased snow deposition on the windward slopes and increased deposition on the leeward slopes, strongly shaping final snow deposition patterns (Mott et al., 2018). It is an important process in regions of sharp mountain topography where snowfall occurs during strong winds. However, this process has not been studied in this region and the degree to which, if any, it impacts snow accumulation this relatively mild mountain topography is uncertain. Despite being a mountainous region, the topography in Granger Basin is less complex than those for where preferential depositions is generally reported as important. Therefore, it is unknown how important preferential deposition is for this region.
5. Using transects of point data to validate a spatial model is difficult due to a conflict of scales. Snow survey transects aim to cover a representative area and provide an areal average that should be approximately at the same spatial scale as the model. However, for validation of a distributed model against transects like those used here, it is not a perfect match. This scale mismatch can give enormous weight to a single observation point. It also means that comparison with a numerical model results in comparing point-scale, sub-grid heterogeneity to an areal averaged model element. This skewed weighting is exacerbated with an unstructured mesh because of the variable size, shape, and area of elements. Use of various remote-sensing data, such as terrestrial laser scanning (TLS) (Prokop, 2008; Grünewald et al., 2010), photogrammetry via unmanned aerial vehicles (UAV) (Harder et al., 2016), and aerial LiDAR (Hopkinson et al., 2011b; Deems et al., 2013; Painter et al., 2016b) can provide snow-on/snow-off spatial datasets that provide an estimate of snow depth. Such spatially distributed

data could partially mitigate the above mentioned scale conflicts. However, *in situ* density observations must still be done to quantify SWE. Unfortunately, no repeat multi-year UAV, TLS, or aerial data sets exist for this region. Due to the importance of quantifying whether the model can reproduce observed inter-annual variability in SWE, the transect observations were the best available data. Future work will utilize these spatially distributed data as they become available for this region.

6.8 Conclusions

A 3-D advection-diffusion blowing snow transport and sublimation model using a finite volume method discretization on a variable resolution unstructured mesh was presented. The use of the unstructured mesh provided a 62% reduction in computational elements versus a fixed-resolution mesh and a 44% decrease in computation time. Transects of a large drift formation in a sub-arctic valley were used to gauge the accuracy of the model. The model generally captures the drift dynamics; over all transects, an RMSE and MB of 86 mm and -20 mm, respectively, were found. Falsifying the model by removing the blowing snow processes increased the SWE RMSE to 98 mm for SWE and more than doubled the MB to -49 mm. Further, the removal of blowing snow resulted in a CV of ≈ 0.04, well below the observed CV (0.41). Inclusion of blowing snow resulted in transect and basin-wide CVs that agreed well with observed values and previously published results (0.36 versus 0.41). The SWE from the variable resolution mesh was similar to the computationally expensive fixed resolution mesh, including the CV. The inclusion of this blowing snow model dramatically increased the spatial heterogeneity of SWE and highlights the critical importance of including this process in cold-regions hydrological models.

The windflow model used here extends previous work by incorporating a lookup table approach that uses per-element wind directions. The blowing snow model presented here demonstrates a computationally efficient method to include blowing snow over large areas without requiring the use of a complex wind flow model run each time step. Poorer predictions of SWE occurred in years with increased infilling from the nearby airport weather station. This suggests that this method should be applied using either collocated weather stations such as are found in research basins or high-resolution atmospheric model outputs. Future research will need to examine how predictive efficiency relies on atmospheric model resolution.

An ensemble of model runs with various perturbations to the wind field were used to establish a spatial sensitivity measure. This showed that SWE is most sensitive in the snowdrifts and the immediate up-wind source areas and that the SWE further upwind on the high plateaux are less sensitive to wind perturbations. Therefore, the snowdrifts appear to be integrating all the up-wind uncertainties in blowing snow processes, as proposed by Tabler (1974). As a result, the drift locations are the most difficult areas of the landscape to simulate as small errors across the landscape are accumulated. However, these areas are critical sources for

summer runoff generation, and so their correct simulation is extremely important in alpine catchments.

The importance of blowing snow processes on shaping the seasonal snowcover and their resulting impact on spring snowmelt volume and timing are well documented throughout the cold regions literature. Despite its importance, this critical process is often neglected in hydrological models, especially in large-extent models because of challenges from discretizing the landscape, interpolating wind fields, and associated computational costs. The new 3-D blowing snow model presented here utilizes a variable resolution discretization to dramatically reduce the total number of computational elements and produces heterogeneous snowcovers without the need for calibration. This presents a way forward for including blowing snow processes at snowdrift-resolving scales in large-extent hydrological models.

7 Conclusions and Synthesis

7.1 Conclusions

The research presented in thesis addressed key deficiencies in cold regions modelling capacity. A working definition of emergence was introduced for use in cold regions hydrology, and it was argued that the explicit representation of heterogeneity and sufficiently realistic models are required to produce these behaviours. Model validation should include not only a basin-integrated results but should also consider the correct simulation of sub-basin features and process cascades.

From the gaps established in the literature review, the following research questions arise and were addressed in this thesis:

1. What are the technical and software design decisions of a hydrological model that can enable the investigation of the impact of model structure, process representation and coupling, and spatial discretization on process cascades and emergence?
2. Can variable resolution, unstructured triangular meshes represent surface heterogeneity, including topography and vegetation, for use in a distributed model?
3. How does the coupling of mass and energy balance in snowpack models impact: a) model sensitivity to uncertainty in parameters and forcing data?; and b) possible compensatory behaviours, and might these behaviours be important?
4. Can blowing snow redistribution equations be up-scaled to variable resolution unstructured meshes to capture the spatial heterogeneity of snow covers at multiple scales?

A new modelling framework, the Canadian Hydrological Model (CHM), was presented in Chapter 3 and addressed research question one. It was identified that existing modern cold regions hydrological models were either flexible in structure but were not spatially distributed or were spatially distributed but were limited in structure. Further, the distributed models used fixed resolution grids that dramatically increased computational costs. A primary design goal of CHM was to address these short-comings by ensuring flexibility in model structure that allowed for inter-comparison of existing process representations and was flexible in spatial and temporal scale. Key design goals to address the identified limitations of existing models included: the ability to capture spatial heterogeneity in an efficient manner; to include multiple process representations;

to be able to change, remove, and decouple hydrological process algorithms; reduced computational overhead to facilitate uncertainty analysis and reduce uncertainty; the ability to scale to multiple spatial extents and scales; and to utilize a variety of forcing fields (boundary and initial conditions).

A novel multi-objective unstructured mesh generation software was developed in Chapter 4 to address research question two. The software described, *mesher*, is an unstructured triangular mesh generator. This approach represents the landscape using a set of non-overlapping, variably sized triangles that provided a multi-scale, variable resolution surface representation. Importantly, this method allowed for explicitly capturing the spatial heterogeneity important that is required for emergent behaviours and cold regions processes but also reduced the total number of computational elements. Specifically, *mesher* allowed mesh generation to consider an arbitrary number of hydrologically important features while maintaining a variable spatial resolution. For example, this allowed for ensuring vegetation cover heterogeneity was correctly represented by the mesh. In addition, using an RMSE error metric provided a better distribution of triangle sizes and errors compared to the maximum difference metric used in existing tools. Including additional constraints resulted in an improved representation of spatial heterogeneity than that of a classic topography-only approach. The variable spatial representation resulted in a 50% to 90% reduction in computational elements versus a uniform mesh. This novel approach is therefore a way towards inclusion of explicit surface heterogeneity in hydrological models at a fraction of the computation cost associated with the historically used fixed-resolution raster approaches.

Chapter 5 addressed research question three that hypothesized that processes interactions may occur within a single process representation. Specifically, it was suggested that there may be compensatory effects in the snowpack surface energy balance such that errors, e.g., input forcing errors, may be dampened or compensated for. Four snowmelt models of varying complexity and energy and mass balance coupling were used to simulate SWE in an alpine forest clearing in the Canadian Rocky Mountains. The inclusion of a fully coupled energy and mass budget improved SWE simulations, but this improvement was not related to the number of model layers. A compensatory response was found in the fully coupled models' energy and mass balance that reduced their sensitivity to errors in solar irradiance. Errors that caused processes to change heat flow into the snowpack were compensated for by changes in processes governing heat flow out of the snowpack and this compensation was not related to the number of model layers. The weakly coupled models produced less accurate simulations and were more sensitive to errors in forcing meteorology (air temperature) and albedo during some times of the year. The results suggest that the inclusion of a fully coupled mass and energy budget improves prediction of snow accumulation and ablation, but there was little advantage by introducing a finite-element multi-layered snowpack scheme. This helps to established warranted model complexity decisions for non-avalanche hazard forecasting applications in mountainous basins. That is, fully coupled mass and energy balance models should be exclusively used in these regions due to improved predictive capacity as well as capturing important system dynamics.

The CHM framework and a variable resolution unstructured mesh were used to address research question four

in Chapter 6. A 3-D advection-diffusion blowing snow transport and sublimation model using a finite volume method discretization via a variable resolution unstructured mesh was developed. The use of the unstructured mesh provided a 62% reduction in computational elements than a fixed-resolution mesh. Without the inclusion of blowing snow, unrealistic homogenous snow covers were simulated which would lead to incorrect melt rates and runoff contributions. The use of a variable resolution mesh with the FVM discretization did not result in worse predictions that previous work in this region, e.g., Ménard et al. (2014b). Therefore this approach provides a more generalizable and a more computationally efficient discretization than previous methods. A novel approach was used via an ensemble of model runs with various perturbations to the wind field to establish a spatial sensitivity measure to errors in wind fields. This showed that simulated SWE was most sensitive in the snowdrifts and the immediate up-wind source areas and that the SWE further upwind on the high plateaux were less sensitive to wind perturbations. Therefore, the snowdrifts appeared to be integrating all the up-wind uncertainties in blowing snow processes, as proposed by Tabler (1974). As a result, the drift locations were the most difficult areas of the landscape to simulate because small errors across the landscape were accumulated. However, these areas are critical sources for summer runoff generation, and so their correct simulation is extremely important in alpine catchments. This spatial sensitivity and feedback are likely further examples of emergent processes, and the correct simulation of these snowdrift locations are key aspects of this basin's hydrology.

In summary, this thesis contributes to cold regions hydrology by: 1) providing a new model framework that builds on the success of previous approaches used in hydrology and cold regions and provides a flexible model structure to investigate process representations at a variety of scales; 2) provides a new landscape representation that ensures heterogeneity is preserved but dramatically reduces data and computational burdens; 3) provides model complexity guidelines for snowpack representations in mountain basis by using both model output performance and the ability to produce compensatory behaviours; and 4) introduces an efficient blowing snow model and allows for including this critical process more efficiently in hydrological models.

7.2 Synthesis

There is an increasing burden placed on hydrological models to provide accurate and timely forecasts of water resources. This is especially true for the cold mountainous regions of the world where snowpacks provide important spring and summer freshwater flows for downstream users and ecosystems. Under anthropogenic climate change, the behaviour of these systems is changing including more mid-winter ablation (Musselman et al., 2017) and rain on snow events (Pomeroy et al., 2016b). In order to provide societies with pertinent predictions, the modelling approaches used must continue to advance.

Three broad themes emerged from this research.

First, research questions one and two highlighted the significant incentive to use and improve explicitly distributed models to capture the temporally variable snowcover heterogeneity present in mountainous regions. As identified by INARCH, it is important these models to be at hyper-resolution ($<$ 1 km) and snow-drift resolving scales (~1 m to 100 m). Capturing the spatial heterogeneity of snowcovers is critical for accurate melt simulation and runoff prediction. However, to provide forecasts for downstream users, this requires expanding to large spatial extents and moving beyond individual basin experiments. Preliminary and experimental work has applied CHM and the mesh generator to the entirety of the Yukon territory in order to downscale GEM output, shown in Figure 7.1. This demonstrates that the model framework and mesh generator scale to the spatial extents required for next-generation model outputs. This provides a direction forward for large-extent application of distributed, snow-drift resolving models.

Stemming from research question three, the second theme is that the use of weakly coupled mass and energy balance snowpack models in mountainous cold regions were insufficient for accurate snowcover predictions. Despite having fewer parameters and thus lower initial uncertainty, they were more sensitive than the fully coupled energy and mass budget models to meteorological errors during melt. These results further support that 'sufficient' realism for mountain domains requires multi-layer, coupled energy and mass balance snowpack models. Under uncertain future climates, vegetation changes, and aerosol depositions, capturing the emergent process of compensation in the energy balance is likely to produce less uncertain predictions. As increased mid-winter ablation events and rain-on-snow events become more common due to climate change (Rasouli et al., 2015), highly calibrated empirical models will likely be insufficient to provide the predictive capacity required for societal needs. Although there is still much debate on the ideal conceptualization of a snowpack model (Armstrong and Brun, 2008) and difficulties remain in fully validating energy balance approaches (Conway et al., 2018), there is likely limited benefit to using parsimonious approaches for the sake of parsimoniousness. Historically, limited observed meteorological data complicated application of energy budget models and supported use of simple temperature-index methods. However, bias-corrected use of numerical weather prediction and reanalysis data is a viable option in data-sparse regions (Krogh et al., 2015), and their use should be examined further. Correctly simulating compensatory behaviours in the model may also provide a basin-line minimum model realism threshold. Investigating warranted model complexity should also consider that, as large extents are simulated, utilizing the same snowpack model everywhere may be inappropriate. Therefore, by using the flexible structure of CHM, different snowpack models may be used in different regions as appropriate. Thus, utilizing warranted complexity studies to define these multi-model strategies should be a long term goal. Overall, there is substantial motivation for the improvement and use of coupled mass and energy balance snowpack models to provide realistic snowpack predictions.

Finally, the third theme from research question four is that the inclusion of lateral blowing snow transport, a major contributor to observed snowcover heterogeneity, is a computational burden for hydrological models.

The introduction of a novel multi-scale mesh generator and model framework present a way towards including this critical process. It was found that non-linear feedbacks and accumulations of simulated blowing processes matched the observed spatial heterogeneity, and critically these patterns were variable year-to-year. Yet, the simulations were at a fraction of the cost of fixed-resolution approaches. This year-to-year variability implies that constant snow cover depletion approaches will not correctly reproduce the observed heterogeneity of snow covers and, by extension, will fail to predict accurate runoff. The blowing snow model presented here removes some of the limitations of existing approaches by decreasing the computational costs and, importantly, removing the assumptions about a single wind direction. Further, these generalizations did not result in worse predictive capacity than previous approaches, e.g., Ménard et al. (2014b). This generalization will allow for application to much larger extents, such as the Yukon territory, the Rocky Mountains or, eventually, the Canadina Western Cordillera, to better predict the spatial heterogeneity of SWE. However, there likely remain computational challenges for application to domains such extents that will require improved high performance computing optimizations. Despite these challenges, there is no reason to expect snowmelt simulations to be correct without this process, and thus decreasing the computational burden is a key advance. The CHM framework allows for easily integrating next-generation remote sensed products, inclusion of numerical weather prediction outputs over large extents, and snowdrift-resolving scales where required – it is the foundation upon which next-generation, large-extent hydrology can be done in complex terrain.

There is long term value in considering complex systems through a weak emergence lens as it provides a framework to identify process interactions and linkages in order to diagnose system-wide behaviours. The identification of these behaviours in both observations and simulation results can provide evidence that the simulation is right for (some of) the right reasons. However, the explicit identification of a behaviour as emergent has some degree of subjectivity. Future work should consider reposing the identification of emergence as identifying the accumulation of non-linear processes interactions. Although this was done for winter-time processes in this thesis, the complexity is greatly increased when considering linked winter and summer processes. Identifying these accumulated interactions should be done in a falsifiable manner where removing a process linkage from a simulation degrades the prediction. Further, the process removal should have clear mechanistic knock-on effects that explain the behaviours. Such an approach is described more fully in Chapter 8. This could lead to having a library of simulated emergent candidates and observations of such behaviours. The creation of such a library should be a long term goal. By doing so, process models that aim to simulate basin responses can draw upon these datasets to aid in validation of existing models as well as to aid in the design of future models. With climate change dramatically impacting the hydrological cycle, increased priority will likely be placed on hydrological models to provide inter-disciplinary predictions that will require accurate simulation of such sub-basin processes. Demonstrating clear skill in simulating a library of these novel basin behaviours may provide evidence that the predictions are of high quality and can be trusted for use by other disciplines.

Although this thesis primarily addressed snowpacks and their heterogeneity which are important sources of runoff, ultimately spring runoff and summer precipitation must be routed to provide hydrological predictions. When using an triangular mesh, there is precedent to use the triangle edges for routing. However, the examples in the literature did not use the same type of variable resolution mesh as generated by *mesher* but there is likely little reason these methods cannot be applied. More critically however, is how Prairie basins, a key economic area of Canada, are represented with unstructured meshes. Explicitly capturing every wetland may be computationally intractable even for a multi-resolution meshes such as those used herein. Large triangles with a sub-grid HRU approach or similar may provide a best-of-both-worlds solution for these complicated landscapes. Such an approach would therefore require running different process representations on different parts of the domain thus allowing for spatially explicit process interactions where possible, but falling back to coarser, semi-distributed approaches where more appropriate. In addition, the inclusion of hydrodynamic models may require use of a multiple-grid approach that links a triangular mesh with an underlying structured mesh. Structured meshes are more common in this application in order to capture flood events than exceed river banks. If a multi-grid approach is not appropriate, then conversion for use with an unstructured mesh may require runtime refinement of the mesh to accurately capture these events if the mesh is too coarse. Thus, there remains substantial work to be done on how to merge these various model conceptualizations and link with the above mentioned routing. However there is significant value in doing so as it allows a variety of modelling approaches to be applied where appropriate.

Despite the extraordinary quantities of remote sensed data currently available, the quantification of sub-surface processes remains data poor. Although there is certainly hope in next-generation data acquisition platforms, the limitations impact current predictive capacity. As a result sub-grid, aggregation approaches, such as those described above, must continue to be used. Because of the flexibility of a model such as CHM in both the process representation and the spatial representation, the spatial discretization can be optimized to include data availability. Incorporating sub-grid variability into a triangular mesh is an important next step, but this remains an open research question.

The inclusion of blowing snow processes in large-extent hydrological simulations is an important step towards accurate predictions of snowpack heterogeneity, which is important for runoff generation. A major deficiency for the inclusion of blowing snow at these extents are the large uncertainties regarding the wind fields. The look-up table approach outlined in Chapter 6 is likely applicable to very large extents. However, there remains significant uncertainty if larger-scale features in mountains, such as lee-side recirculation and flow separation can be correctly parameterized with this method. Although daunting, windflow and the subsequent impact on mass transport in many regions is critical and continued effort should be placed upon this long term challenge.

In summary, these results show that there is increasing incentive to move away from empirical snowpack models in mountainous terrain due to limited predictive capacity and increased uncertainty versus energy budget

methods under climate change. There is a need to capture snow-drift resolving scales in next-generation hydrological models, and the variable resolution unstructured meshes provide a mechanism to do so with reduced computational burdens. By exploiting this mesh, a substantial computational decrease was found when implementing lateral blowing snow transport opening up the possibility of applying this method to much larger extents. Diagnosing model success by capturing temporal and spatial heterogeneity of snow covers is possible by utilizing modern computational tools and high-performance systems, and evaluating the performance against observations and emergent behaviours. Future work should focus on identifying emergent behaviours in a rigorously quantifiable manner to help diagnose models, and the representation of sub-grid processes in conjunction with an unstructured mesh is a key activity for future research.

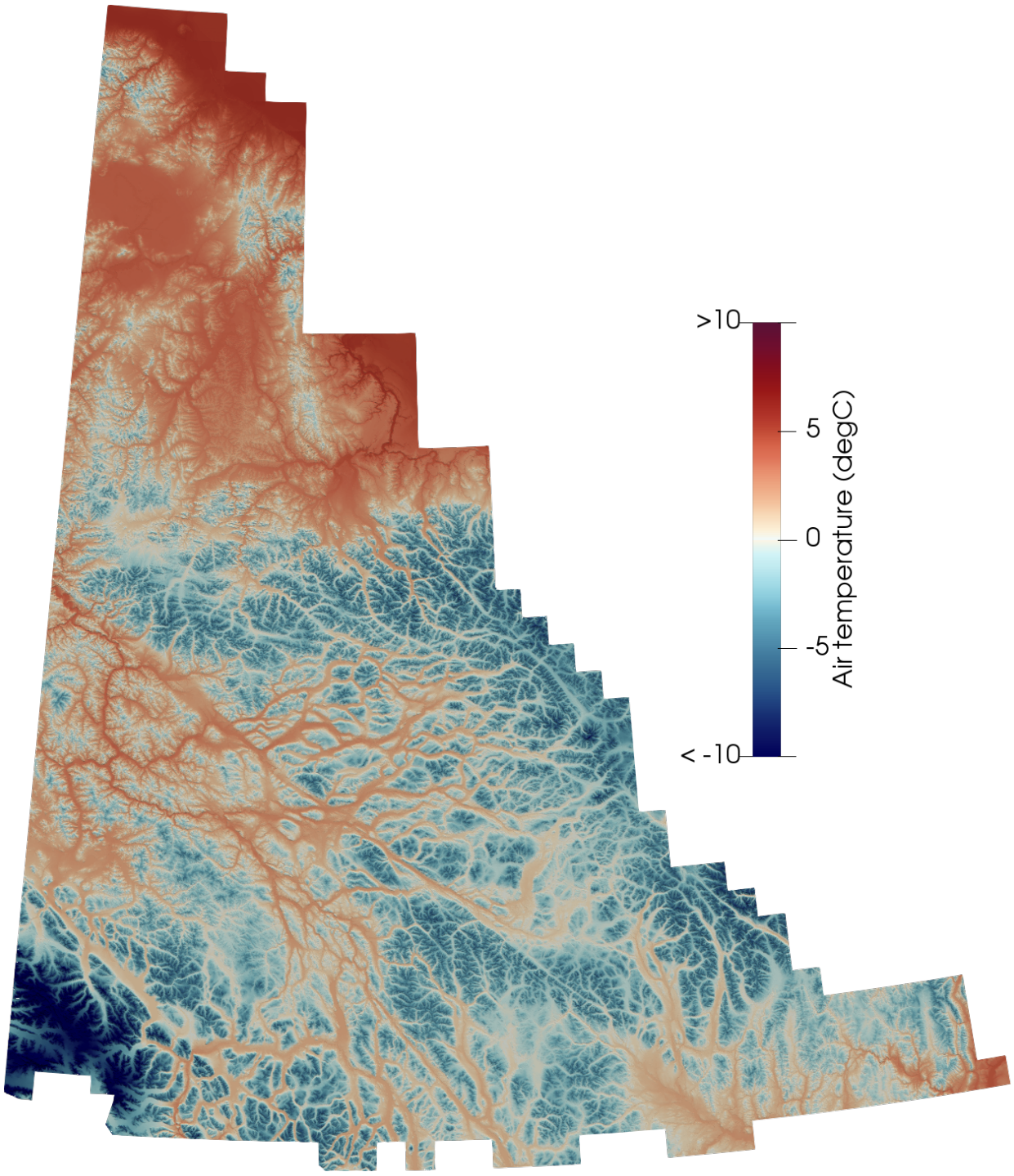

Figure 7.1: CHM downscaling GEM temperature output for the entirety of the Yukon Territory.

8 Future work

Despite substantial progress in surface cold regions modelling and process representation, there is still significant work to be done to understand and quantify how these processes interact to produce emergent hydrological behaviours. For example, successful prediction of a single process may not result in correct prediction of subsequent processes that rely upon it, such as shown by Musselman et al. (2015a) where adequate wind field predictions did not translate into correct blowing snow transport. Critically, there needs to be more research regarding how emergent processes are numerically quantified in model output in order to be able to use these behaviours to more broadly evaluate model output. This section therefore details a possible approach to link winter emergent processes with their impact on hydrological processes.

The broad theme of this future work should frame simulated emergent behaviours in a falsifiable context, through process-cascades that allow for falsifying individual process contributions. It is suggested that examining the loss of hydrological prediction with increasing model simplification (i.e., likely decreasing realism) would be a possible way forward. Importantly it should diagnose the loss of prediction in hydrological processes by considering the loss of emergent phenomena (i.e., process feedbacks).

It is hypothesized that one example of an emergent behaviour is manifested as a covariance between SWE, frozen soil infiltration, and soil moisture. Because snowpack evolution is a result of the cascading winter-time processes, it is hypothesized that a 'sufficiently' complex and realistic model is required to simulate these spring runoff patterns and therefore soil moisture contributions. These cascading processes are hypothesized to be as follows: 1) snowcover heterogeneity due to blowing snow transport deposition and erosion; 2) the transport deposition results in large drift formations; 3) this snowcover heterogeneity results in spatially and temporally variable spring ablation; 4) the heterogeneity in the melt flux results in spatio-temporal variability in frozen-soil infiltration and influences the resulting soil moisture. Specifically, this research should address the following questions: 1) can reducing the high-dimensional model output via empirical orthogonal functions (EOF) (Lorenz, 1956) meaningfully quantify emergent behaviours? 2) Does falsifying key processes provide insight into key controls on these emergent beavhiours?; 3) Can spatially distributed EOF measures, along with spatially and temporally variable sensitivity metrics be used to quantify how, where, and when portions of the landscape 'switch on' and 'switch off'?

Such an approach is hypothesized to show how interacting mid-winter processes must be included in a model to produce the emergence of observed spatial patterns in spring frozen soil infiltration and subsequent soil

moisture. It will likely demonstrate that this behaviour cannot be modelled without the inclusion of a full cascade of processes, appropriately linked, and using an efficient, but explicitly spatially distributed model. Specifically, it is hypothesized that: 1) failure to properly consider process interactions will be detrimental to hydrological simulations; 2) process realism must be 'sufficient' in order to capture emergence, and using only aggregate metrics will not facilitate determining warranted model complexity; and 3) terrain heterogeneity must be explicitly represented. It is expected that this analysis will show that accurate basin wide melt processes (ablation, infiltration, and runoff) require a minimum level of process complexity, realism, and representation. Incorrect wind fields will likely have a significant cascading impact on frozen soil infiltration and runoff as a result of incorrect end of winter snow cover spatial heterogeneity. A spatial sensitivity analysis would show how sensitivity to important parameters are spatially and temporally variable and quantify how different parts of the landscape 'switch on' and 'off'. The aim of this future research is not to be just a sensitivity study; rather, the objective is to discuss complexity, realism, and emergence in the context of cascading processes and their algorithmic representation as needed for hydrological prediction. Such a study will provide further insight into cold-regions emergence and complex systems and provide numerical measures of the behaviours in order to guide future research.

References

Ahrens, J., B. Geveci, and C. Law (2005), Paraview: An End-user Tool For Large Data Visualization, in *Visualization handbook*, Elsevier. [online] Available from: http://www.worldcat.org/title/visualization-handbook/oclc/1047806062

Aksamit, N. O., and J. W. Pomeroy (2016), Near-surface Snow Particle Dynamics From Particle Tracking Velocimetry And Turbulence Measurements During Alpine Blowing snow storms, *The Cryosphere*, *10*, 3043–3062, doi:10.5194/tc-10-3043-2016.

Aksamit, N. O., and J. W. Pomeroy (2017), The Effect Of Coherent Structures In The Atmospheric Surface Layer On Blowing-snow Transport, *Boundary-Layer Meteorology*, *167*, 211–233, doi:10.1007/s10546-017-0318-2.

Aksamit, N. O., and J. W. Pomeroy (2018), Scale Interactions In Turbulence For Mountain Blowing Snow, *Journal of Hydrometeorology*, *19*, 305–320, doi:10.1175/jhm-d-17-0179.1.

Anderton, S. P., S. M. White, and B. Alvera (2004), Evaluation Of Spatial Variability In Snow Water Equivalent For A High Mountain Catchment, *Hydrological Processes*, *18*, 435 453, doi:10.1002/hyp.1319.

Anon (2004), Vegetation And Topographic Control Of Wind-blown Snow Distributions In Distributed And Aggregated Simulations For An Arctic Tundra Basin, *5*, 735 744.

Armstrong, R., and E. Brun (2008), *Snow And Climate: Physical Processes, Surface Energy Exchange And Modeling*, Cambridge, UK.

Armstrong, R. N., J. W. Pomeroy, and L. W. Martz (2008), Evaluation Of Three Evaporation Estimation Methods In A Canadian Prairie Landscape, *Hydrological Processes*, *22*, 2801 2815.

Ascher, U. M., R. M. M. Mattheij, and R. D. Russell (1995), *Numerical Solution Of Boundary Value Problems For Ordinary Differential Equations*, Society for Industrial; Applied Mathematics.

Avanzi, F., C. D. Michele, S. Morin, C. M. Carmagnola, and Y. Lejeune (2016), Model Complexity And Data Requirements In Snow Hydrology : Seeking A Balance In Practical Applications, doi:10.1002/hyp.10782.

Aziz-Alaoui, M. A. (2006), Complex Emergent Properties And Chaos (de) Synchronization, in *Emergent*

properties in natural and artificial dynamical systems: Understanding complex systems, edited by C. B. M A Aziz-Alaoui, p. 129 147, Springer Berlin Heidelberg.

Bahremand, A. (2015), Hess Opinions: Advocating Process Modeling And De-emphasizing Parameter Estimation, *Hydrology and Earth System Sciences Discussions*, *12*, 12377 12393, doi:10.5194/hessd-12-12377-2015.

Barnes, R. (2017), Parallel Non-divergent Flow Accumulation For Trillion Cell Digital Elevation Models On Desktops Or Clusters, *Environmental Modelling & Software*, *92*, 202 212, doi:10.1016/j.envsoft.2017.02.022.

Bartelt, P., and M. Lehning (2002), A Physical Snowpack Model For The Swiss Avalanche Warning Part I: Numerical Model, *Cold Regions Science and Technology*, *35*, 123 145, doi:10.1016/s0165-232x(02)00074-5.

Bavay, M., and T. Egger (2014), Meteoio 2.4.2: A Preprocessing Library For Meteorological Data, *Geoscientific Model Development*, *7*, 3135 3151, doi:10.5194/gmd-7-3135-2014.

Bárdossy, A., and S. K. Singh (2008), Robust Estimation Of Hydrological Model Parameters, *Hydrology and Earth System Sciences*, *12*, 1273 1283, doi:10.5194/hess-12-1273-2008.

Bedau, M. A. (2011), Weak Emergence And Computer Simulation, in *Models, simulations, and representations*, edited by C. I. P Humphreys, p. 91 114, Routledge, New York.

Bentley, J. L. (1975), Multidimensional Binary Search Trees Used For Associative Searching, *arXiv.org*, *18*, 509 517, doi:10.1145/361002.361007.

Berger, M. J., and P. Colella (1989), Local Adaptive Mesh Refinement For Shock Hydrodynamics, *Journal of Computational Physics*, *82*, 64 84, doi:10.1016/0021-9991(89)90035-1.

Bernhardt, M., and K. Schulz (2010), Snowslide: A Simple Routine For Calculating Gravitational Snow Transport, *Geophysical Research Letters*, *37*, n/a–n/a, doi:10.1029/2010gl043086.

Bernhardt, M., K. Schulz, G. E. Liston, and G. Zängl (2012), The Influence Of Lateral Snow Redistribution Processes On Snow Melt And Sublimation In Alpine Regions, *Water Resources Research*, *424-425*, 196–206, doi:10.1016/j.jhydrol.2012.01.001.

Beven, K. (1989), Changing Ideas In Hydrology — The Case Of Physically-based Models, *Journal of Hydrology*, *105*, 157–172, doi:10.1016/0022-1694(89)90101-7.

Beven, K. (1993), Prophecy, Reality And Uncertainty In Distributed Hydrological Modelling, *Advances in Water Resources*, *16*, 41–51, doi:10.1016/0309-1708(93)90028-e.

Beven, K. (2006a), A Manifesto For The Equifinality Thesis, *Water Resources Research*, *320*, 18 36, doi:10.1016/j.jhydrol.2005.07.007.

Beven, K. (2006b), Searching For The Holy Grail Of Scientific Hydrology: Qt=(s, R, Δt)a As Closure, *Hydrology and Earth System Sciences*, *10*, 609 618, doi:10.5194/hess-10-609-2006.

Beven, K., and A. Binley (1992), The Future Of Distributed Models: Model Calibration And Uncertainty Prediction, *Hydrological Processes*, *6*, 279 298.

Beven, K., and P. Germann (2013), Macropores And Water Flow In Soils Revisited, *Water Resources Research*, *49*, 3071 3092, doi:10.1002/wrcr.20156.

Beven, K., and I. Westerberg (2011), On Red Herrings And Real Herrings: Disinformation And Information In Hydrological Inference, *Hydrological Processes*, *25*, 1676 1680, doi:10.1002/hyp.7963.

Beven, K., and E. F. Wood (1983), Catchment Geomorphology And The Dynamics Of Runoff Contributing Areas, *Journal of Hydrology*, *65*, 139 158.

Beven, K., and P. Young (2013), A Guide To Good Practice In Modelling Semantics For Authors And Referees, *Water Resources Research*.

Beven, K. J. (1996), A Discussion Of Distributed Hydrological Modelling, in *Distributed hydrological modelling*, pp. 255–278, Springer, Netherlands.

Bewley, D., J. W. Pomeroy, and R. L. H. Essery (2007), Solar Radiation Transfer Through A Subarctic Shrub Canopy, *Arctic, Antarctic, and Alpine Research*, *46*, 365–374, doi:10.1657/1523-0430(06-023)[bewley]2.0.co;2.

Bilskie, M. V., and S. C. Hagen (2013), Topographic Accuracy Assessment Of Bare Earth Lidar-derived Unstructured Meshes, *Advances in Water Resources*, *52*, 165–177, doi:10.1016/j.advwatres.2012.09.003.

Bilskie, M. V., D. Coggin, S. C. Hagen, and S. C. Medeiros (2015), Terrain-driven Unstructured Mesh Development Through Semi-automatic Vertical Feature Extraction, *Advances in Water Resources*, *86*, 102–118, doi:10.1016/j.advwatres.2015.09.020.

Binley, A., J. Elgy, and K. Beven (1989), A Physically Based Model Of Heterogeneous Hillslopes: 1. Runoff Production, *Water Resources Research*, *25*, 1219–1226, doi:10.1029/wr025i006p01219.

Bliudze, S., and D. Krob (2009), Modelling Of Complex Systems: Systems As Dataflow Machines, *Fundamenta Informaticae*, *91*, 251 274, doi:10.3233/fi-2009-0043.

Blix, A. S., and J. W. Lentfer (1979), Modes Of Thermal Protection In Polar Bear Cubs–at Birth And On Emergence From The Den, *American Journal of Physiology-Regulatory, Integrative and Comparative Physiology*, *236*, R67 R74, doi:10.1152/ajpregu.1979.236.1.r67.

Blöschl, G., and M. Sivapalan (1995), Scale Issues In Hydrological Modelling: A Review, *Hydrological Processes*, *9*, 251 290, doi:10.1002/hyp.3360090305.

Bowling, L. C., J. W. Pomeroy, and D. P. Lettenmaier (2004), Parameterization Of Blowing-snow Sublimation In A Macroscale Hydrology Model, *Journal of Hydrometeorology*, *5*, 745–762, doi:10.1175/1525-7541(2004)005<0745:pobsia>2.0.co;2.

Boyd, J., and S. Banzhaf (2007), What Are Ecosystem Services? The Need For Standardized Environmental Accounting Units, *Ecological Economics*, *63*, 616 626, doi:10.1016/j.ecolecon.2007.01.002.

Brigode, P., L. Oudin, and C. Perrin (2013), Hydrological Model Parameter Instability: A Source Of Additional Uncertainty In Estimating The Hydrological Impacts Of Climate Change?, *Water Resources Research*, *476*, 410 425, doi:10.1016/j.jhydrol.2012.11.012.

Bring, A., I. Fedorova, Y. Dibike, L. Hinzman, J. Mård, S. H. Mernild, T. Prowse, O. Semenova, S. L. Stuefer, and M. Woo (2016), Arctic Terrestrial Hydrology: A Synthesis Of Processes, Regional Effects, And Research Challenges, *Journal of Geophysical Research: Biogeosciences*, *121*, 621–649, doi:10.1002/2015jg003131.

Brown, P. N., G. D. Byrne, and A. C. Hindmarsh (1989), Vode: A Variable-coefficient Ode Solver, *SIAM J. Sci. Stat. Comput.*, *10*, 1038 1051, doi:http://dx.doi.org/10.1137/0910062.

Brown, R. D., and R. O. Braaten (1998), Spatial And Temporal Variability Of Canadian Monthly Snow Depths, 1946–1995, *Atmosphere-Ocean*, *36*, 37–54, doi:10.1080/07055900.1998.9649605.

Brutsaert, W. (1982), Evaporation Into The Atmosphere, Theory, History And Applications, 197–208, doi:10.1007/978-94-017-1497-6_9.

Budd, W. F. (1966), The Drifting Of Nonuniform Snow Particles, *Studies in Antarctic meterology*, 59–70, doi:10.1029/ar009p0059.

Burridge, D. M., and A. J. Gadd (1975), *The Meteorological Office Opererational 10-level Numerical Weather Prediction Model*.

Bühler, Y., M. S. Adams, R. Bösch, and A. Stoffel (2016), Mapping Snow Depth In Alpine Terrain With Unmanned Aerial Systems (uass): Potential And Limitations, *The Cryosphere*, *10*, 1075 1088, doi:10.5194/tc-10-1075-2016.

Carey, S. K., and M. Woo (2001), Spatial Variability Of Hillslope Water Balance, Wolf Creek Basin, Subarctic Yukon, *Hydrological Processes*, *15*, 3113–3132, doi:10.1002/hyp.319.

Carey, S. K., and M.-k. Woo (1998), Snowmelt Hydrology Of Two Subarctic Slopes, Southern Yukon, Canadapaper Presented At The 11th Northern Res. Basins Symposium/workshop (prudhoe Bay To Fairbanks, Alaska, Usa – Aug. 18-22,1997), *Hydrology Research*, *29*, 331 346, doi:10.2166/nh.1998.0022.

Carey, S. K., and M. K. Woo (2000), The Role Of Soil Pipes As A Slope Runoff Mechanism, Subarctic Yukon,

Canada, *Water Resources Research*, *233*, 206 222, doi:10.1016/s0022-1694(00)00234-1.

Carey, S. K. et al. (2010), Inter-comparison Of Hydro-climatic Regimes Across Northern Catchments: Synchronicity, Resistance And Resilience, *Hydrological Processes*, *24*, 3591–3602, doi:10.1002/hyp.7880.

Carlson, J. M., and J. Doyle (2002), Complexity And Robustness, *Proceedings of the National Academy of Sciences*, *99*, 2538 2545, doi:10.1073/pnas.012582499.

Caviedes-Voullième, D., P. García-Navarro, and J. Murillo (2012), Influence Of Mesh Structure On 2d Full Shallow Water Equations And Scs Curve Number Simulation Of Rainfall/runoff Events, *Journal of Hydrology*, *448*, 39–59, doi:10.1016/j.jhydrol.2012.04.006.

Chang, F., and C. J. Chen (2003), A Component-labeling Algorithm Using Contour Tracing Technique, *Proceedings of the International Conference on Document Analysis and Recognition, ICDAR*, *2003-Janua*, 741 745, doi:10.1109/icdar.2003.1227760.

Chang, K.-t. (2008), *Introduction To Geographic Information Systems*, 4th ed.

Chasmer, L., C. Hopkinson, P. Treitz, H. Mccaughey, A. Barr, and A. Black (2008), A Lidar-based Hierarchical Approach For Assessing Modis Fpar, *Remote Sensing of Environment*, *112*, 4344–4357, doi:10.1016/j.rse.2008.08.003.

Chen, M., and J. Cihlar (1996), Retrieving Leaf Area Index Of Boreal Conifer Forests Using Landsat Tm Images, *Remote Sensing of Environment*, *55*, 153 162.

Cherkauer, K. a, L. C. Bowling, and D. P. Lettenmaier (2003), Variable Infiltration Capacity Cold Land Process Model Updates, *Global and Planetary Change*, *38*, 151 159, doi:10.1016/s0921-8181(03)00025-0.

Chueca, J., and A. Julián (2004), Relationship Between Solar Radiation And The Development And Morphology Of Small Cirque Glaciers (maladeta Mountain Massif, Central Pyrenees, Spain), *Geografiska Annaler: Series A, Physical Geography*, *86*, 81 89, doi:10.1111/j.0435-3676.2004.00215.x.

Clark, M. P., A. G. Slater, D. E. Rupp, R. A. Woods, J. A. Vrugt, H. V. Gupta, T. Wagener, and L. E. Hay (2008), Framework For Understanding Structural Errors (fuse): A Modular Framework To Diagnose Differences Between Hydrological Models, *Water Resources Research*, *44*, n/a–n/a, doi:10.1029/2007wr006735.

Clark, M. P., D. Kavetski, and F. Fenicia (2011a), Pursuing The Method Of Multiple Working Hypotheses For Hydrological Modeling, *Water Resources Research*, *47*, doi:10.1029/2010wr009827.

Clark, M. P., J. Hendrikx, A. G. Slater, D. Kavetski, B. Anderson, N. J. Cullen, T. Kerr, E. Ö. Hreinsson, and R. A. Woods (2011b), Representing Spatial Variability Of Snow Water Equivalent In Hydrologic And Land-surface Models: A Review, *Water Resources Research*, *47*, n/a–n/a, doi:10.1029/2011wr010745.

Clark, M. P. et al. (2015), A Unified Approach For Process-based Hydrologic Modeling: 1. Modeling Concept, *Water Resources Research*, *51*, 2498–2514, doi:10.1002/2015wr017198.

Clark, M. P., M. F. P. Bierkens, L. Samaniego, R. A. Woods, R. Uijlenhoet, K. E. Bennett, V. R. N. Pauwels, X. Cai, A. W. Wood, and C. D. Peters-Lidard (2017), The Evolution Of Process-based Hydrologic Models: Historical Challenges And The Collective Quest For Physical Realism, *Hydrology and Earth System Sciences*, *21*, 3427–3440, doi:10.5194/hess-21-3427-2017.

Clifton, A., and M. Lehning (2008), Improvement And Validation Of A Snow Saltation Model Using Wind Tunnel Measurements, *Earth Surface Processes and Landforms*, *33*, 2156–2173, doi:10.1002/esp.1673.

Comola, F., and M. Lehning (2017), Energy- And Momentum-conserving Model Of Splash Entrainment In Sand And Snow Saltation, *Geophysical Research Letters*, *44*, 1601–1609, doi:10.1002/2016gl071822.

Conover, W. J. (1971), *Practical Nonparametric Statistics*, New York.

Conway, H., A. Gades, and C. F. Raymond (1996), Albedo Of Dirty Snow During Conditions Of Melt, *Water Resources Research*, *32*, 1713–1718, doi:10.1029/96wr00712.

Conway, J. P., and N. J. Cullen (2013), Constraining Turbulent Heat Flux Parameterization Over A Temperate Maritime Glacier In New Zealand, *Annals of Glaciology*, *54*, 41 51, doi:10.3189/2013aog63a604.

Conway, J. P., J. W. Pomeroy, W. D. Helgason, and N. J. Kinar (2018), Challenges In Modelling Turbulent Heat Fluxes To Snowpacks In Forest Clearings. Challenges In Modelling Turbulent Heat Fluxes To Snowpacks In Forest Clearings., *Journal of Hydrometeorology*, doi:10.1175/jhm-d-18-0050.1.

Corripio, J. G. (2004), Snow Surface Albedo Estimation Using Terrestrial Photography, *International Journal of Remote Sensing*, *25*, 5705 5729, doi:10.1080/01431160410001709002.

Côté, J., S. Gravel, A. Méthot, A. Patoine, M. Roch, and A. Staniforth (1998), The Operational Cmc–mrb Global Environmental Multiscale (gem) Model. Part I: Design Considerations And Formulation, *Monthly Weather Review*, *126*, 1373–1395, doi:10.1175/1520-0493(1998)126<1373:tocmge>2.0.co;2.

Crick, F. (1994), *The Astonishing Hypothesis: The Scientific Search For The Soul*, New York.

Cullen, R. M., and S. J. Marshall (2011), Mesoscale Temperature Patterns In The Rocky Mountains And Foothills Region Of Southern Alberta, *Atmosphere-Ocean*, *49*, 189–205, doi:10.1080/07055900.2011.592130.

Dall'Amico, M., S. Endrizzi, S. Gruber, and R. Rigon (2011), A Robust And Energy-conserving Model Of Freezing Variably-saturated Soil, *The Cryosphere*, *5*, 469 484, doi:10.5194/tc-5-469-2011.

Darley, V. (1994), Emergent Phenomena And Complexity, edited by P. M. R A Brooks, p. 411 416, Cambridge, MA.

Das, T., A. Bárdossy, E. Zehe, and Y. He (2008), Comparison Of Conceptual Model Performance Using Different Representations Of Spatial Variability, *Water Resources Research*, *356*, 106 118, doi:10.1016/j.jhydrol.2008.04.008.

Davies, T. D., P. Brimblecombe, M. Tranter, S. Tsiouris, C. E. Vincent, P. Abrahams, and I. L. Blackwood (1987), Seasonal Snowcovers: Physics, Chemistry, Hydrology, in *Seasonal snowcovers: Physics, chemistry, hydrology*, edited by W. J. O.-T. H G Jones, pp. 337–392, D. Reidel Publishing Company, Dordrecht, Holland.

Davison, B., A. Pietroniro, V. Fortin, R. Leconte, M. Mamo, and M. K. Yau (2016), What Is Missing From The Prescription Of Hydrology For Land Surface Schemes?, *Journal of Hydrometeorology*, *17*, 2013–2039, doi:10.1175/jhm-d-13-055.1.

Debeer, C., and J. Pomeroy (2016), *Report On The Ccrn Theme B Cold Regions Hydrological Model (crhm) Expert Workshop*.

Debeer, C. M., H. S. Wheater, W. L. Quinton, S. K. Carey, R. E. Stewart, M. D. MacKay, and P. Marsh (2015), The Changing Cold Regions Network: Observation, Diagnosis And Prediction Of Environmental Change In The Saskatchewan And Mackenzie River Basins, Canada, *Science China Earth Sciences*, *58*, 46–60, doi:10.1007/s11430-014-5001-6.

DeBeer, C. M., and J. W. Pomeroy (2009), Modelling Snow Melt And Snowcover Depletion In A Small Alpine Cirque, Canadian Rocky Mountains, *Hydrological Processes*, *23*, 2584–2599, doi:10.1002/hyp.7346.

DeBeer, C. M., and J. W. Pomeroy (2010), Simulation Of The Snowmelt Runoff Contributing Area In A Small Alpine Basin, *Hydrology and Earth System Sciences*, *14*, 1205 1219, doi:10.5194/hess-14-1205-2010.

DeBeer, C. M., and J. W. Pomeroy (2017), Influence Of Snowpack And Melt Energy Heterogeneity On Snow Cover Depletion And Snowmelt Runoff Simulation In A Cold Mountain Environment, *Journal of Hydrology*, *553*, 199–213, doi:10.1016/j.jhydrol.2017.07.051.

Decharme, B., E. Brun, A. Boone, C. Delire, P. L. Moigne, and S. Morin (2016), Impacts Of Snow And Organic Soils Parameterization On Northern Eurasian Soil Temperature Profiles Simulated By The Isba Land Surface Model, *Cryosphere*, *10*, 853 877, doi:10.5194/tc-10-853-2016.

Dee, D. P. et al. (2011), The Era-interim Reanalysis: Configuration And Performance Of The Data Assimilation System, *Quarterly Journal of the Royal Meteorological Society*, *137*, 553 597, doi:10.1002/qj.828.

Deems, J. S., T. H. Painter, and D. C. Finnegan (2013), Lidar Measurement Of Snow Depth: A Review, *Journal of Glaciology*, *59*, 467–479(13), doi:10.3189/2013jog12j154.

Déry, S. J., and M. K. Yau (1999), A Bulk Blowing Snow Model, *Boundary-Layer Meteorology*, *93*, 237–251, doi:10.1023/a:1002065615856.

Diaconescu, E. P., R. Laprise, and A. Zadra (2012), Singular Vector Decomposition Of The Internal Variability Of The Canadian Regional Climate Model, *Climate Dynamics*, *38*, 1093–1113, doi:10.1007/s00382-011-1179-x.

Dickinson, W. T., and H. R. Whiteley (1972), A Sampling Scheme For Shallow Snowpacks, *Hydrological Sciences Bulletin*, *17*, 247–258, doi:10.1080/02626667209493832.

Dingman, S. L. (2002), *Physical Hydrology*, Second., Long Grove, IL, USA.

Dodson, R., and D. Marks (1997), Daily Air Temperature Interpolated At High Spatial Resolution Over A Large Mountainous Region, *Climate Research*, *8*, 1 20, doi:10.3354/cr008001.

Doorschot, J. J. J., and M. Lehning (2002), Equilibrium Saltation: Mass Fluxes, Aerodynamic Entrainment, And Dependence On Grain Properties, *Boundary-Layer Meteorology*, *104*, 111–130, doi:10.1023/a:1015516420286.

Dornes, P., J. W. Pomeroy, A. Pietroniro, and D. L. Verseghy (2008a), Effects Of Spatial Aggregation Of Initial Conditions And Forcing Data On Modeling Snowmelt Using A Land Surface Scheme, *Journal of Hydrometeorology*, *9*, 789–803, doi:10.1175/2007jhm958.1.

Dornes, P. F., J. W. Pomeroy, a Pietroniro, and S. K. Careyc (2006), The Use Of Inductive And Deductive Reasoning To Model Snowmelt Runoff From Northern Mountain Catchments,

Dornes, P. F., J. W. Pomeroy, A. Pietroniro, S. K. Carey, and W. L. Quinton (2008b), Influence Of Landscape Aggregation In Modelling Snow-cover Ablation And Snowmelt Runoff In A Sub-arctic Mountainous Environment, *Hydrological Sciences Journal*, *53*, 725–740, doi:10.1623/hysj.53.4.725.

Douville, H., J. Royer, and J. Mahfouf (1995), A New Snow Parameterization For The Meteo-france Climate Model, *Climate Dynamics*, *35*, 21 35, doi:10.1007/bf00208760.

Dozier, J., and J. Frew (1990), Rapid Calculation Of Terrain Parameters For Radiation Modeling From Digital Elevation Data, *IEEE Transactions on Geoscience and Remote Sensing*, *28*, 963–969, doi:10.1109/36.58986.

Dozier, J., J. Bruno, and P. Downey (1981), Faster Solution To The Horizon Problem, *Computers & Geosciences*, *7*, 145 151.

Duarte, C. M., T. M. Lenton, P. Wadhams, and P. Wassmann (2012), Abrupt Climate Change In The Arctic, *Nature Climate Change*, *2*, 60 62, doi:10.1038/nclimate1386.

Dunne, T., and R. D. Black (1970), Partial Area Contributions To Storm Runoff In A Small New England Watershed, *Water Resources Research*, *6*, 1296–1311, doi:10.1029/wr006i005p01296.

Dyunin, A. K. (1954), Solid Flux Of Snow-bearing Air Flow, *Trudy Transportno-Energeticheskogo Instituta*, (1102), 71–88.

E, O. T. (2006), *A Guide To Numpy*.

Eder, G., M. Sivapalan, and H. P. Nachtnebel (2003), Modelling Water Balances In An Alpine Catchment Through Exploitation Of Emergent Properties Over Changing Time Scales, *Hydrological Processes*, *17*, 2125–2149, doi:10.1002/hyp.1325.

Elder, K., J. Dozier, and J. Michaelsen (1991), Snow Accumulation And Distribution In An Alpine Watershed, *Water Resources Research*, *27*, 1541 1552.

Elder, K., W. Rosenthal, and R. E. Davis (1998), Estimating The Spatial Distribution Of Snow Water Equivalence In A Montane Watershed, *Hydrological Processes*, *12*, 1793–1808, doi:10.1002/(sici)1099-1085(199808/09)12:10/11<1793::aid-hyp695>3.3.co;2-b.

Ellis, C., J. W. Pomeroy, T. Brown, and J. MacDonald (2010), Simulation Of Snow Accumulation And Melt In Needleleaf Forest Environments, *Hydrology and Earth System Sciences*, *14*, 925 940, doi:10.5194/hess-14-925-2010.

El-Shimy, N., C. Valeo, and A. Habib (2005), *Digital Terrain Modeling: Aquisition, Manipulation, And Applications*, Norwood, MA.

Endrizzi, S., M. Dall'Amico, S. Gruber, and R. Rigon (2011), *Geotop Users Manual*.

Endrizzi, S., S. Gruber, M. D. Amico, and R. Rigon (2013), Geotop 2.0: Simulating The Combined Energy And Water Balance At And Below The Land Surface Accounting For Soil Freezing , Snow Cover And Terrain Effects, *Geoscientific Model Development*.

Endrizzi, S., S. Gruber, M. Dall'Amico, and R. Rigon (2014), Geotop 2.0: Simulating The Combined Energy And Water Balance At And Below The Land Surface Accounting For Soil Freezing, Snow Cover And Terrain Effects, *Geoscientific Model Development*, *7*, 2831 2857, doi:10.5194/gmd-7-2831-2014.

Entekhabi, D. et al. (2010), The Soil Moisture Active Passive (smap) Mission, *Proceedings of the IEEE*, *98*, 704–716, doi:10.1109/jproc.2010.2043918.

Essery, R. (2015), A Factorial Snowpack Model (fsm 1.0), *Geoscientific Model Development*, *8*, 3867 3876, doi:10.5194/gmd-8-3867-2015.

Essery, R., and P. Etchevers (2004), Parameter Sensitivity In Simulations Of Snowmelt, *Journal of Geophysical Research: Atmospheres (1984–2012)*, *109*, 1–15, doi:10.1029/2004jd005036.

Essery, R., L. Li, and J. Pomeroy (1999), A Distributed Model Of Blowing Snow Over Complex

Terrain, *Hydrological Processes*, *13*, 2423–2438, doi:10.1002/(sici)1099-1085(199910)13:14/15<2423::aid-hyp853>3.0.co;2-u.

Essery, R., N. Rutter, J. Pomeroy, R. Baxter, D. Gustafsson, A. Barr, P. Bartlett, E. Elder, and M. Stahli (2009), Snowmip2: An Evaluation Of Forest Snow Process Simulations, *Bulletin of the American Meteorological Society*, *90*, 1120–1135, doi:10.1175/2009bams2629.1.

Essery, R., S. Morin, Y. Lejeune, and C. B. Ménard (2013), A Comparison Of 1701 Snow Models Using Observations From An Alpine Site, *Advances in Water Resources*, *55*, 131–148, doi:10.1016/j.advwatres.2012.07.013.

Etchevers, P. et al. (2004), Validation Of The Energy Budget Of An Alpine Snowpack Simulated By Several Snow Models (snowmip Project), *Annals of Glaciology*, *38*, 150–158, doi:10.3189/172756404781814825.

Evans, C., T. D. Davies, and P. S. Murdoch (1999), Component Flow Processes At Four Streams In The Catskill Mountains, New York, Analysed Using Episodic Concentration/discharge Relationships, *Hydrological Processes*, *575*, 563 575.

Fang, X., and J. W. Pomeroy (2009), Modelling Blowing Snow Redistribution To Prairie Wetlands, edited by B. B. James Buttle, *Hydrological Processes*, *23*, 2557–2569, doi:10.1002/hyp.7348.

Fang, X., J. W. Pomeroy, C. R. Ellis, M. K. MacDonald, C. M. DeBeer, and T. Brown (2013), Multi-variable Evaluation Of Hydrological Model Predictions For A Headwater Basin In The Canadian Rocky Mountains, *Hydrology and Earth System Sciences*, *17*, 1635–1659, doi:10.5194/hess-17-1635-2013.

Fang, X., J. W. Pomeroy, C. M. DeBeer, P. Harder, and E. Siemens (2019), Hydrometeorological Data From Marmot Creek Research Basin, Canadian Rockies, *Earth System Science Data*, *11*, 455–471, doi:10.5194/essd-11-455-2019.

Fatichi, S. et al. (2016), An Overview Of Current Applications, Challenges, And Future Trends In Distributed Process-based Models In Hydrology, *Journal of Hydrology*, *537*, 45 60.

Fenicia, F., D. Kavetski, and H. H. G. Savenije (2011), Elements Of A Flexible Approach For Conceptual Hydrological Modeling: 1. Motivation And Theoretical Development, *Water Resources Research*, *47*, n/a–n/a, doi:10.1029/2010wr010174.

Fiddes, J., and S. Gruber (2014), Toposcale V.1.0: Downscaling Gridded Climate Data In Complex Terrain, *Geoscientific Model Development*, *7*, 387 405, doi:10.5194/gmd-7-387-2014.

Flerchinger, G. N., and K. E. Saxton (1989a), Simultaneous Heat And Water Model Of A Freezing Snow-residue-soil System Ii. Field Verification, *Trans. ASAE*, *32*, 573 578.

Flerchinger, G. N., and K. E. Saxton (1989b), Simultaneous Heat And Water Model Of A Freezing Snow-

residue-soil System I. Theory And Development, *Trans. ASAE*, *32*, 565 567.

Flügel, W. A. (1995), Hydrological Response Units (hrus) To Preserve Basin Heterogeneity In Hydrological Modelling Using Prms/mms-case Study In The Brol Basin, Germany, IAHS, Boulder, CO.

Foken, T. (2008), The Energy Balance Closure Problem: An Overview, *Ecological Applications*, *18*, 1351 1367, doi:10.1890/06-0922.1.

Foken, T. (2018), *Micrometeorology*, Second.

Forthofer, J. M., B. W. Butler, C. W. McHugh, M. A. Finney, L. S. Bradshaw, R. D. Stratton, K. S. Shannon, and N. S. Wagenbrenner (2014a), A Comparison Of Three Approaches For Simulating Fine-scale Surface Winds In Support Of Wildland Fire Management. Part Ii. An Exploratory Study Of The Effect Of Simulated Winds On Fire Growth Simulations, *International Journal of Wildland Fire*, *23*, 982–994, doi:10.1071/wf12090.

Forthofer, J. M., B. W. Butler, and N. S. Wagenbrenner (2014b), A Comparison Of Three Approaches For Simulating Fine-scale Surface Winds In Support Of Wildland Fire Management. Part I. Model Formulation And Comparison Against Measurements, *International Journal of Wildland Fire*, *23*, 969–981, doi:10.1071/wf12089.

Fortin, V., G. Roy, N. Donaldson, and A. Mahidjiba (2015), Assimilation Of Radar Quantitative Precipitation Estimations In The Canadian Precipitation Analysis (capa), *Journal of Hydrology*, *531*, 296–307, doi:10.1016/j.jhydrol.2015.08.003.

Freeze, R. A. (1974), Streamflow Generation, *Reviews of Geophysics*, *12*, 627–647, doi:10.1029/rg012i004p00627.

Freeze, R. A., and R. L. Harlan (1969), Blueprint For A Physically-based, Digitally-simulated Hydrologic Response Model, *Journal of Hydrology*, *9*, 237 258, doi:10.1016/0022-1694(69)90020-1.

Freudiger, D., I. Kohn, J. Seibert, K. Stahl, and M. Weiler (2017), Snow Redistribution For The Hydrological Modeling Of Alpine Catchments, *Wiley Interdisciplinary Reviews: Water*, *4*, e1232, doi:10.1002/wat2.1232.

Fu, P., and P. M. Rich (1999), Design And Implementation Of The Solar Analyst: An Arcview Extension For Modeling Solar Radiation At Landscape Scales, p. 1 33, San Diego, USA.

Garnier, B. J., and A. Ohmura (1968), A Method Of Calculating The Direct Shortwave Radiation Income Of Slopes, *Journal of Applied Meteorology*, *7*, 796 800, doi:10.1175/1520-0450(1968)007<0796:amoctd>2.0.co;2.

Gelfan, A. N., J. W. Pomeroy, and L. S. Kuchment (2004), Modeling Forest Cover Influences On Snow Accumulation, Sublimation, And Melt, *Journal of Hydrometeorology*, *5*, 785–803, doi:10.1175/1525-7541(2004)005<0785:mfcios>2.0.co;2.

Gerber, F., M. Lehning, S. W. Hoch, and R. Mott (2017), A Close-ridge Small-scale Atmospheric Flow Field And Its Influence On Snow Accumulation, *Journal of Geophysical Research: Atmospheres*, *122*, 7737–7754, doi:10.1002/2016jd026258.

Gerber, F., R. Mott, and M. Lehning (2019), The Importance Of Near-surface Winter Precipitation Processes In Complex Alpine Terrain The Importance Of Near-surface Winter Precipitation Processes In Complex Alpine Terrain, *Journal of Hydrometeorology*, doi:10.1175/jhm-d-18-0055.1.

Golden, B., M. Aiguier, and D. Krob (2012), Modeling Of Complex Systems Ii: A Minimalist And Unified Semantics For Heterogeneous Integrated Systems, *Applied Mathematics and Computation*, *218*, 8039 8055, doi:10.1016/j.amc.2012.01.048.

Golding, D. L. (1970), Research Results From Marmot Creek Experimental Watershed, Alberta, Canada, p. 397 404, Wellington, New Zealand.

Goldstein, J. (1999), Emergence As A Construct: History And Issues, *Emergence*, *1*, 49–72.

Goodison, B. E., P. Y. Louie, and D. Yang (1998), *Wmo Solid Solid Precipitiation Measurement Intercomparison*, World Meteorological Organization, Geneva, Switzerland.

Gray, D. M., and P. G. Landine (1987), Albedo Model For Shallow Prairie Snow Covers, *Canadian Journal of Earth Sciences*, *24*, 1760–1768, doi:10.1139/e87-168.

Gray, D. M., and P. G. Landine (1988), An Energy-budget Snowmelt Model For The Canadian Prairies, *Canadian Journal of Earth Sciences*, *25*, 1292 1303, doi:10.1139/e88-124.

Gray, D. M., and D. H. Male (1981), *Handbook Of Snow: Principles, Processes, Management, And Use*, Toronto, Canada.

Gray, D. M., B. Toth, L. Zhao, J. W. Pomeroy, and R. J. Granger (2001), Estimating Areal Snowmelt Infiltration Into Frozen Soils, *Hydrological Processes*, *15*, 3095–3111, doi:10.1002/hyp.320.

Grayson, R., and G. Blöschl (2000), *Spatial Patterns In Catchment Hydrology: Observations And Modelling*, edited by G. B. Rodger Grayson.

Grayson, R. B., I. D. Moore, and T. A. McMahon (1992), Physically Based Hydrologic Modeling: 2. Is The Concept Realistic?, *Water Resources Research*, *28*, 2659–2666, doi:10.1029/92wr01259.

Groisman, P. Y., and T. D. Davies (2001), Snow Cover And The Climate System, in *Snow ecology: An interdisciplinary examination of snow-covered ecosystems*, edited by D. A. W. H G Jones J W Pomeroy, p. 1 44, Cambridge University Press, Cambridge, UK.

Grünewald, T., M. Schirmer, R. Mott, and M. Lehning (2010), Spatial And Temporal Variability Of Snow

Depth And Ablation Rates In A Small Mountain Catchment, *The Cryosphere*, *4*, 215–225, doi:10.5194/tc-4-215-2010.

Guerrero, J., I. K. Westerberg, S. Halldin, L. Lundin, and C. Xu (2013), Exploring The Hydrological Robustness Of Model-parameter Values With Alpha Shapes, *Water Resources Research*, *49*, 6700–6715, doi:10.1002/wrcr.20533.

Guyomarc'h, G., and L. Mérindol (1998), Validation Of An Application For Forecasting Blowing Snow, *Annals of Glaciology*, *26*, 138–143, doi:10.3189/1998aog26-1-138-143.

Hagen, S. C., J. J. Westerink, and R. L. Kolar (2000), One-dimensional Finite Element Grids Based On A Localized Truncation Error Analysis, *International Journal for Numerical Methods in Fluids*, *32*, 241–262, doi:10.1002/(sici)1097-0363(20000130)32:2<241::aid-fld947>3.0.co;2-\#.

Hagen, S. C., J. J. Westerink, R. L. Kolar, and O. Horstmann (2001), Two-dimensional, Unstructured Mesh Generation For Tidal Models, *International Journal for Numerical Methods in Fluids*, *35*, 669–686, doi:10.1002/1097-0363(20010330)35:6<669::aid-fld108>3.0.co;2-\#.

Hagen, S. C., O. Horstmann, and R. J. Bennett (2002), An Unstructured Mesh Generation Algorithm For Shallow Water Modeling, *International Journal of Computational Fluid Dynamics*, *16*, 83–91, doi:10.1080/10618560290017176.

Haghnegahdar, A., S. Razavi, F. Yassin, and H. Wheater (2017), Multicriteria Sensitivity Analysis As A Diagnostic Tool For Understanding Model Behaviour And Characterizing Model Uncertainty, *Hydrological Processes*, *31*, 4462–4476, doi:10.1002/hyp.11358.

Hansson, K., J. von S. imu u nek, M. Mizoguchi, L.-C. Lundin, and M. T. V. Genuchten (2004), Water Flow And Heat Transport In Frozen Soil, *Vadose Zone Journal*, *3*, 693 704.

Harder, P., and J. Pomeroy (2013), Estimating Precipitation Phase Using A Psychrometric Energy Balance Method, *Hydrological Processes*, *27*, 1901–1914, doi:10.1002/hyp.9799.

Harder, P., J. W. Pomeroy, and C. J. Westbrook (2015), Hydrological Resilience Of A Canadian Rockies Headwaters Basin Subject To Changing Climate, Extreme Weather, And Forest Management, *Hydrological Processes*, *29*, 3905–3924, doi:10.1002/hyp.10596.

Harder, P., M. Schirmer, J. Pomeroy, and W. Helgason (2016), Accuracy Of Snow Depth Estimation In Mountain And Prairie Environments By An Unmanned Aerial Vehicle, *The Cryosphere*, *10*, 2559–2571, doi:10.5194/tc-10-2559-2016.

Harder, P., J. W. Pomeroy, and W. Helgason (2017), Local-scale Advection Of Sensible And Latent Heat During Snowmelt, *Geophysical Research Letters*, *44*, 9769–9777, doi:10.1002/2017gl074394.

Harder, P., W. D. Helgason, and J. W. Pomeroy (2018), Modeling The Snowpack Energy Balance During Melt Under Exposed Crop Stubble, *Journal of Hydrometeorology*, *19*, 1191–1214, doi:10.1175/jhm-d-18-0039.1.

Harder, P., J. W. Pomeroy, and W. D. Helgason (2019a), A Simple Model For Local-scale Sensible And Latent Heat Advection Contributions To Snowmelt, *Hydrology and Earth System Sciences*, *23*, 1–17, doi:10.5194/hess-23-1-2019.

Harder, P., J. W. Pomeroy, and W. D. Helgason (2019b), Implications Of Stubble Management On Snow Hydrology And Meltwater Partitioning, *Canadian Water Resources Journal / Revue canadienne des ressources hydriques*, 1–12, doi:10.1080/07011784.2019.1575774.

Hedstrom, N. R., and J. W. Pomeroy (1998), Measurements And Modelling Of Snow Interception In The Boreal Forest, *Hydrological Processes*, *12*, 1611 1625, doi:10.1002/(sici)1099-1085(199808/09)12:10/11<1611::aid-hyp684>3.0.co;2-4.

Hewitt, K. (2011), Glacier Change, Concentration, And Elevation Effects In The Karakoram Himalaya, Upper Indus Basin, *Mountain Research and Development*, *34*, 188 200, doi:10.1659/mrd-journal-d-11-00020.1.

Hiller, R., M. J. Zeeman, and W. Eugster (2008), Eddy-covariance Flux Measurements In The Complex Terrain Of An Alpine Valley In Switzerland, *Boundary-Layer Meteorology*, *127*, 449 467, doi:10.1007/s10546-008-9267-0.

Hock, R. (2003), Temperature Index Melt Modelling In Mountain Areas, *Water Resources Research*, *282*, 104 115, doi:10.1016/s0022-1694(03)00257-9.

Hoffmann, J. (2005), The Future Of Satellite Remote Sensing In Hydrogeology, *Hydrogeology Journal*, *13*, 247 250, doi:10.1007/s10040-004-0409-2.

Hood, J. L. (2013), Quantifying Snowmelt Inputs In An Alpine Watershed For The Purpose Of Investigating The Role Of Groundwater Storage, PhD thesis.

Hopkinson, C., and L. Chasmer (2009), Testing Lidar Models Of Fractional Cover Across Multiple Forest Ecozones, *Remote Sensing of Environment*, *113*, 275–288, doi:10.1016/j.rse.2008.09.012.

Hopkinson, C., N. Crasto, P. Marsh, D. Forbes, and L. Lesack (2011a), Investigating The Spatial Distribution Of Water Levels In The Mackenzie Delta Using Airborne Lidar, *Hydrological Processes*, *25*, 2995–3011, doi:10.1002/hyp.8167.

Hopkinson, C., J. Pomeroy, C. Debeer, C. Ellis, and A. Anderson (2011b), Relationships Between Snowpack Depth And Primary Lidar Point Cloud Derivatives In A Mountainous Environment, Proceedings of a symposium held at Jackson Hole, Wyoming, USA, September 2010. IAHS.

Horne, F. E., and M. L. Kavvas (1997), Physics Of The Spatially Averaged Snowmelt Process, *Journal of Hydrology*, *191*, 179 207, doi:10.1016/s0022-1694(96)03063-6.

Hrachowitz, M., and M. P. Clark (2017), Hess Opinions: The Complementary Merits Of Competing Modelling Philosophies In Hydrology, *Hydrology and Earth System Sciences*, *21*, 3953 3973, doi:10.5194/hess-21-3953-2017.

Hubbard, S. S. et al. (2013), Quantifying And Relating Land-surface And Subsurface Variability In Permafrost Environments Using Lidar And Surface Geophysical Datasets, *Hydrogeology Journal*, *21*, 149 169, doi:10.1007/s10040-012-0939-y.

Hughes, D. A. (2010), Hydrological Models: Mathematics Or Science?, *Hydrological Processes*, *24*, 2199–2201, doi:10.1002/hyp.7805.

Husain, S. Z., N. Alavi, S. Bélair, M. Carrera, S. Zhang, V. Fortin, M. Abrahamowicz, and N. Gauthier (2016), The Multibudget Soil, Vegetation, And Snow (svs) Scheme For Land Surface Parameterization: Offline Warm Season Evaluation, *Journal of Hydrometeorology*, *17*, 2293 2313, doi:10.1175/jhm-d-15-0228.1.

Imre, A. R., and J. Novotný (2016), Fractals And The Korcak-law: A History And A Correction, *The European Physical Journal H*, *41*, 69–91, doi:10.1140/epjh/e2016-60039-8.

Iqbal, M. (1980), Prediction Of Hourly Diffuse Solar Radiation From Measured Hourly Global Radiation On A Horizontal Surface, *Solar Energy*, *24*, 491–503, doi:10.1016/0038-092x(80)90317-5.

Ivanov, V., E. Vivoni, R. Bras, and D. Entekhabi (2004a), Preserving High-resolution Surface And Rainfall Data In Operational-scale Basin Hydrology: A Fully-distributed Physically-based Approach, *Water Resources Research*, *298*, 80 111, doi:10.1016/j.jhydrol.2004.03.041.

Ivanov, V. Y., E. R. Vivoni, R. L. Bras, and D. Entekhabi (2004b), Catchment Hydrologic Response With A Fully Distributed Triangulated Irregular Network Model, *Water Resources Research*, *40*, 1–23, doi:10.1029/2004wr003218.

Jackson, P. S., and J. C. R. Hunt (1975), Turbulent Wind Flow Over A Low Hill, *Quarterly Journal of the Royal Meteorological Society*, *101*, 929–955, doi:10.1002/qj.49710143015.

Janowicz, J. R. (1999), Wolf Creek Research Basin-overview, edited by R. J. G. J. W. Pomeroy, pp. 121–130, Saskatoon.

Janowicz, R., D. M. Gray, and J. W. Pomeroy (2002), Characterisation Of Snowmelt Infiltration Scaling Parameters Within A Mountainous Subarctic Watershed, pp. 67–81, Proceedings of the 59th Eastern Snow Conference, Stowe, Vermont.

Jen, E. (2003), Stable Or Robust? What's The Difference?, *Complexity*, *8*, 12–18, doi:10.1002/cplx.10077.

Jennings, K. S., T. G. F. Kittel, and N. P. Molotch (2018), Observations And Simulations Of The Seasonal Evolution Of Snowpack Cold Content And Its Relation To Snowmelt And The Snowpack Energy Budget, *The Cryosphere*, *12*, 1595–1614, doi:10.5194/tc-12-1595-2018.

John, V. (2000), A Numerical Study Of A Posteriori Error Estimators For Convection–diffusion Equations, *Computer Methods in Applied Mechanics and Engineering*, *190*, 757–781, doi:10.1016/s0045-7825(99)00440-5.

Jones, E., T. Oliphant, and P. Peterson (2018), *Scipy: Open Source Scientific Tools For Python*.

Jordan, R. (1991), *A One-dimensional Temperature Model For A Snow Cover. Tehcnical Documentation For Sntherm.89*.

Kavvas, M. L. (1999), On The Coarse-graining Of Hydrologic Processes With Increasing Scales, *Water Resources Research*, *217*, 191 202, doi:10.1016/s0022-1694(98)00252-2.

Kirchner, J. W. (2006), Getting The Right Answers For The Right Reasons: Linking Measurements, Analyses, And Models To Advance The Science Of Hydrology, *Water Resources Research*, *42*, doi:10.1029/2005wr004362.

Kite, G. W., and A. Pietroniro (1996), Remote Sensing Applications In Hydrological Modelling, *Hydrological Sciences Journal/Journal des Sciences Hydrologiques*, *41*, 563 591, doi:10.1080/02626669609491526.

Klemeš, V. (1983), Conceptualization And Scale In Hydrology, *Journal of Hydrology*, *65*, 1 23, doi:10.1016/0022-1694(83)90208-1.

Klemeš, V. (1986), Operational Testing Of Hydrological Simulation Models, *Hydrological Sciences Journal*, *31*, 13–24, doi:10.1080/02626668609491024.

Krogh, S. A., and J. W. Pomeroy (2018a), Impact Of Future Climate And Vegetation On The Hydrology Of An Arctic Headwater Basin At The Tundra-taiga Transition Impact Of Future Climate And Vegetation On The Hydrology Of An Arctic Headwater Basin At The Tundra-taiga Transition, *Journal of Hydrometeorology*, doi:10.1175/jhm-d-18-0187.1.

Krogh, S. A., and J. W. Pomeroy (2018b), Recent Changes To The Hydrological Cycle Of An Arctic Basin At The Tundra–taiga Transition, *Hydrology and Earth System Sciences*, *22*, 3993–4014, doi:10.5194/hess-22-3993-2018.

Krogh, S. A., J. W. Pomeroy, and J. McPhee (2015), Physically Based Mountain Hydrological Modeling Using Reanalysis Data In Patagonia, *Journal of Hydrometeorology*, *16*, 172–193, doi:10.1175/jhm-d-13-0178.1.

Krogh, S. A., J. W. Pomeroy, and P. Marsh (2017), Diagnosis Of The Hydrology Of A Small Arctic Basin

At The Tundra-taiga Transition Using A Physically Based Hydrological Model, *Water Resources Research*, *550*, 685–703, doi:10.1016/j.jhydrol.2017.05.042.

Kuchment, L., and A. Gelfan (2004), Physicomathematical Model Of Snow Accumulation And Melt In A Forest, *Russian Meteorology and Hydrology*, 57—65.

Kumar, M., G. Bhatt, and C. J. C. J. Duffy (2009a), An Efficient Domain Decomposition Framework For Accurate Representation Of Geodata In Distributed Hydrologic Models, *International Journal of Geographical Information Science*, *23*, 1569 1596, doi:10.1080/13658810802344143.

Kumar, M., C. J. Duffy, and K. M. Salvage (2009b), A Second-order Accurate, Finite Volume–based, Integrated Hydrologic Modeling (fihm) Framework For Simulation Of Surface And Subsurface Flow, *Vadose Zone Journal*, *8*, 873, doi:10.2136/vzj2009.0014.

Kumar, M., D. Marks, J. Dozier, M. Reba, and A. Winstral (2013), Evaluation Of Distributed Hydrologic Impacts Of Temperature-index And Energy-based Snow Models, *Advances in Water Resources*, *56*, 77 89, doi:10.1016/j.advwatres.2013.03.006.

Kunkel, K. E. (1989), Simple Procedures For Extrapolation Of Humidity Variables In The Mountainous Western United States, *Journal of Climate*, *2*, 656 669.

Kuzmin, D. (2010), *A Guide To Numerical Methods For Transport Equations*, University Erlangen-Nuremberg.

Lafaysse, M., B. Cluzet, M. Dumont, Y. Lejeune, V. Vionnet, and S. Morin (2017), A Multiphysical Ensemble System Of Numerical Snow Modelling, *Cryosphere*, *11*, 1173 1198, doi:10.5194/tc-11-1173-2017.

Lapen, D. R., and L. W. Martz (1993), The Measurement Of Two Simple Topographic Indices Of Wind Sheltering-exposure From Raster Digital Elevation Models, *Computers & Geosciences*, *19*, 769–779, doi:10.1016/0098-3004(93)90049-b.

Latifovic, R., and D. Pouliot (2007), Analysis Of Climate Change Impacts On Lake Ice Phenology In Canada Using The Historical Satellite Data Record, *Remote Sensing of Environment*, *106*, 492 507, doi:10.1016/j.rse.2006.09.015.

Lawrence, D. M. et al. (2011), Parameterization Improvements And Functional And Structural Advances In Version 4 Of The Community Land Model, *Journal of Advances in Modeling Earth Systems*, *3*, doi:10.1029/2011ms000045.

Leavesley, G. H., S. L. Markstrom, P. J. Restrepo, and R. J. Viger (2002), A Modular Approach To Addressing Model Design, Scale, And Parameter Estimation Issues In Distributed Hydrological Modelling, *Hydrological Processes*, *16*, 173–187, doi:10.1002/hyp.344.

Lee, J. (1991), Comparison Of Existing Methods For Building Triangular Irregular Network, Models Of Terrain From Grid Digital Elevation Models, *International journal of geographical information systems*, *5*, 267–285, doi:10.1080/02693799108927855.

Lehmann, P., C. Hinz, G. McGrath, H. J. T.-v. Meerveld, and J. J. McDonnell (2007), Rainfall Threshold For Hillslope Outflow: An Emergent Property Of Flow Pathway Connectivity, *Hydrology and Earth System Sciences*, *11*, 1047–1063, doi:10.5194/hess-11-1047-2007.

Lehning, M., P. Bartelt, B. Brown, C. Fierz, and P. Satyawali (2002), A Physical Snowpack Model For The Swiss Avalanche Warning Part Ii. Snow Microstructure, *Cold Regions Science and Technology*, *35*, 147–167, doi:10.1016/s0165-232x(02)00073-3.

Lehning, M., I. Völksch, D. Gustafsson, T. A. Nguyen, M. Stähli, and M. Zappa (2006), Alpine3d: A Detailed Model Of Mountain Surface Processes And Its Application To Snow Hydrology, *Hydrological Processes*, *20*, 2111–2128, doi:10.1002/hyp.6204.

Lehning, M., H. Löwe, M. Ryser, and N. Raderschall (2008), Inhomogeneous Precipitation Distribution And Snow Transport In Steep Terrain, *Water Resources Research*, *44*, doi:10.1029/2007wr006545.

Leroux, N. R., and J. W. Pomeroy (2017), Modelling capillary hysteresis effects on preferential flow through melting and cold layered snowpacks, *Advances in Water Resources*, *107*, 250 264, doi:10.1016/j.advwatres.2017.06.024.

Li, L., and J. W. Pomeroy (1997a), Estimates Of Threshold Wind Speeds For Snow Transport Using Meteorological Data, *Journal of Applied Meteorology*, *36*, 205–213, doi:10.1175/1520-0450(1997)036<0205:eotwsf>2.0.co;2.

Li, L., and J. W. Pomeroy (1997b), Probability Of Occurrence Of Blowing Snow, *Journal of Geophysical Research: Atmospheres*, *102*, 21955–21964, doi:10.1029/97jd01522.

Lissack, M. R. (1999), Complexity: The Science, Its Vocabulary, And Its Relation To Organizations, *Emergence*, *1*, 110–126, doi:10.1207/s15327000em0101_7.

List, R. J. (1971), *Smithsonian Meteorological Tables*, Washington, DC.

Liston, G. E., and K. Elder (2006), A Meteorological Distribution System For High-resolution Terrestrial Modeling (micromet), *Journal of Hydrometeorology*, *7*, 217–234, doi:10.1175/jhm486.1.

Liston, G. E., and M. Sturm (1998), A Snow-transport Model For Complex Terrain, *Journal of Glaciology*, *44*, 498–516, doi:10.3189/s0022143000002021.

Liston, G. E., C. J. Perham, R. T. Shideler, and A. N. Cheuvront (2016), Modeling Snowdrift Habitat For Polar Bear Dens, *Ecological Modelling*, *320*, 114–134, doi:10.1016/j.ecolmodel.2015.09.010.

Lorenz, E. N. (1956), *Empirical Orthogonal Functions And Statistical Weather Prediction*, M.I.T., Cambridge, MA.

López-Moreno, J. I., J. Boike, A. Sanchez-Lorenzo, and J. W. Pomeroy (2016), Impact Of Climate Warming On Snow Processes In Ny-ålesund, A Polar Maritime Site At Svalbard, *Global and Planetary Change*, *146*, 10–21, doi:10.1016/j.gloplacha.2016.09.006.

López-Moreno, J. I. et al. (2017), Different Sensitivities Of Snowpacks To Warming In Mediterranean Climate Mountain Areas, *Environmental Research Letters*, *12*, 074006, doi:10.1088/1748-9326/aa70cb.

Luce, C. H., D. G. Tarboton, and K. R. Cooley (1998), The Influence Of The Spatial Distribution Of Snow On Basin-averaged Snowmelt, *Hydrological Processes*, *12*, 1671–1683, doi:10.1002/(sici)1099-1085(199808/09)12:10/11<1671::aid-hyp688>3.0.co;2-n.

Lundberg, A., P. Ala-Aho, O. Eklo, B. Klöve, J. Kværner, and C. Stumpp (2016), Snow And Frost: Implications For Spatiotemporal Infiltration Patterns – A Review, *Hydrological Processes*, *30*, 1230–1250, doi:10.1002/hyp.10703.

MacDonald, M. K., J. W. Pomeroy, and A. Pietroniro (2009), Parameterizing Redistribution And Sublimation Of Blowing Snow For Hydrological Models: Tests In A Mountainous Subarctic Catchment, *Hydrological Processes*, *23*, 2570–2583, doi:10.1002/hyp.7356.

MacDonald, M. K., J. W. Pomeroy, and a Pietroniro (2010), On The Importance Of Sublimation To An Alpine Snow Mass Balance In The Canadian Rocky Mountains, *Hydrology and Earth System Sciences*, *14*, 1401–1415, doi:10.5194/hess-14-1401-2010.

Mahfouf, J., B. Brasnett, and S. Gagnon (2007), A Canadian Precipitation Analysis (capa) Project: Description And Preliminary Results, *ATMOSPHERE-OCEAN*, *45*, 1–17, doi:10.3137/ao.v450101.

Male, D. H., and D. M. Gray (1975), Problems In Developing A Physically Based Snowmelt Model, *Canadian Journal of Civil Engineering*, *2*, 474–488, doi:10.1139/l75-044.

Marks, D., J. Dozier, and R. E. Davis (1992), Climate And Energy Exchange At The Snow Surface In The Alpine Region Of The Sierra Nevada: 1. Meteorological Measurements And Monitoring, *Water Resources Research*, *28*, 3029–3042, doi:10.1029/92wr01482.

Marks, D., J. Kimball, D. Tingey, and T. Link (1998), The Sensitivity Of Snowmelt Processes To Climate Conditions And Forest Cover During Rain-on-snow: A Case Study Of The 1996 Pacific Northwest Flood, *Hydrological Processes*, *12*, 1569 1587, doi:10.1002/(sici)1099-1085(199808/09)12:10/11<1569::aid-hyp682>3.0.co;2-l.

Marks, D., J. Domingo, D. Susong, T. Link, and D. Garen (1999), A Spatially Distributed Energy

Balance Snowmelt Model For Application In Mountain Basins, *Hydrological Processes*, *13*, 1935–1959, doi:10.1002/(sici)1099-1085(199909)13:12/13<1935::aid-hyp868>3.0.co;2-c.

Marks, D., A. Winstral, G. Flerchinger, M. Reba, J. Pomeroy, T. Link, and K. Elder (2008), Comparing Simulated And Measured Sensible And Latent Heat Fluxes Over Snow Under A Pine Canopy To Improve An Energy Balance Snowmelt Model, *Journal of Hydrometeorology*, *9*, 1506–1522, doi:10.1175/2008jhm874.1.

Marks, D., A. Winstral, M. Reba, J. Pomeroy, and M. Kumar (2013), An Evaluation Of Methods For Determining During-storm Precipitation Phase And The Rain/snow Transition Elevation At The Surface In A Mountain Basin, *Advances in Water Resources*, *55*, 98 110, doi:10.1016/j.advwatres.2012.11.012.

Marsh, C. B., J. W. Pomeroy, and R. J. Spiteri (2011), Implication Of Mountain Shading And Topographic Scaling On Energy For Snowmelt, Banff, Alberta, Canada.

Marsh, C. B., J. W. Pomeroy, and R. J. Spiteri (2012), Implications Of Mountain Shading On Calculating Energy For Snowmelt Using Unstructured Triangular Meshes, *Hydrological Processes*, *26*, 1767–1778, doi:10.1002/hyp.9329.

Marsh, C. B., R. J. Spiteri, J. W. Pomeroy, and H. S. Wheater (2018), Multi-objective Unstructured Triangular Mesh Generation For Use In Hydrological And Land Surface Models, *Computers & Geosciences*, *119*, 49–67, doi:10.1016/j.cageo.2018.06.009.

Marsh, C. B., J. W. Pomeroy, and H. S. Wheater (2019), The Canadian Hydrological Model (chm): A Multi-scale, Multi-extent, Variable-complexity Hydrological Model – Design And Overview, *Geoscientific Model Development Discussions*, 1–44, doi:10.5194/gmd-2019-109.

Marsh, P. (1999), Snowcover Formation And Melt: Recent Advances And Future Prospects, *Hydrological Processes*, *13*, 2117–2134, doi:10.1002/(sici)1099-1085(199910)13:14/15<2117::aid-hyp869>3.0.co;2-9.

Marsh, P., and J. W. Pomeroy (1996), Meltwater Fluxes At An Arctic Forest-tundra Site, *Hydrological Processes*, *10*, 1383–1400, doi:10.1002/(sici)1099-1085(199610)10:10<1383::aid-hyp468>3.0.co;2-w.

Marsh, P., and M.-k. Woo (1984), Wetting Front Advance And Freezing Of Meltwater Within A Snow Cover: 1. Observations In The Canadian Arctic, *Water Resources Research*, *20*, 1853 1864, doi:10.1029/wr020i012p01853.

Marty, C., R. Philipona, C. Fröhlich, and A. Ohmura (2002), Altitude Dependence Of Surface Radiation Fluxes And Cloud Forcing In The Alps: Results From The Alpine Surface Radiation Budget Network, *Theoretical and Applied Climatology*, *72*, 137–155, doi:10.1007/s007040200019.

Mason, P., and R. Sykes (1979), Flow Over An Isolated Hill Of Moderate Slope, *Quarterly Journal of the Royal Meteorological Society*, *105*, 383–395, doi:10.1002/qj.49710544405.

Maxwell, R. M., and S. J. Kollet (2008), Interdependence Of Groundwater Dynamics And Land-energy Feedbacks Under Climate Change, *Nature Geoscience*, *1*, 665 669, doi:10.1038/ngeo315.

McCartney, S. E., S. K. Carey, and J. W. Pomeroy (2006), Intra-basin Variability Of Snowmelt Water Balance Calculations In A Subarctic Catchment, *Hydrological Processes*, *20*, 1001–1016, doi:10.1002/hyp.6125.

McCauley, C. a, D. M. White, M. R. Lilly, and D. M. Nyman (2002), A Comparison Of Hydraulic Conductivities, Permeabilities And Infiltration Rates In Frozen And Unfrozen Soils, *Cold Regions Science and Technology*, *34*, 117 125, doi:10.1016/s0165-232x(01)00064-7.

McClymont, A. F., J. W. Roy, M. Hayashi, L. R. Bentley, H. Maurer, and G. Langston (2011), Investigating Groundwater Flow Paths Within Proglacial Moraine Using Multiple Geophysical Methods, *Water Resources Research*, *399*, 57 69, doi:10.1016/j.jhydrol.2010.12.036.

McDonnell, J. J. et al. (2007), Moving Beyond Heterogeneity And Process Complexity: A New Vision For Watershed Hydrology, *Water Resources Research*, *43*, n/a–n/a, doi:10.1029/2006wr005467.

McGarigal, K., and B. J. Marks (1994), Fragstats: Spatial Pattern Analysis Program For Quantifying Landscapesstructure, *General Technical Report PNW-GTR-351. U.S. Department of Agriculture, Forest Service, Pacific Northwest Research Station. Portland, OR*, *97331*, 134.

Melsen, L. A., A. J. Teuling, P. J. J. F. Torfs, R. Uijlenhoet, N. Mizukami, and M. P. Clark (2016), Hess Opinions: The Need For Process-based Evaluation Of Large-domain Hyper-resolution Models, *Hydrology and Earth System Sciences*, *20*, 1069–1079, doi:10.5194/hess-20-1069-2016.

Mendoza, P. A., M. P. Clark, M. Barlage, B. Rajagopalan, L. Samaniego, G. Abramowitz, and H. Gupta (2015), Are We Unnecessarily Constraining The Agility Of Complex Process-based Models?, *Water Resources Research*, *51*, 716–728, doi:10.1002/2014wr015820.

Mens, M. J. P., F. Klijn, K. M. de Bruijn, and E. van Beek (2011), The Meaning Of System Robustness For Flood Risk Management, *Environmental Science & Policy*, *14*, 1121 1131, doi:10.1016/j.envsci.2011.08.003.

Mesinger, F. et al. (2006), North American Regional Reanalysis, *Bulletin of the American Meteorological Society*, *87*, 343–360, doi:10.1175/bams-87-3-343.

Ménard, C. B., R. Essery, J. Pomeroy, P. Marsh, and D. B. Clark (2014a), A Shrub Bending Model To Calculate The Albedo Of Shrub-tundra, *Hydrological Processes*, *28*, 341–351, doi:10.1002/hyp.9582.

Ménard, C. B., R. Essery, and J. Pomeroy (2014b), Modelled Sensitivity Of The Snow Regime To Topography, Shrub Fraction And Shrub Height, *Hydrology and Earth System Sciences*, *18*, 2375–2392, doi:10.5194/hess-18-2375-2014.

Michlmayr, G., M. Lehning, G. Koboltschnig, H. Holzmann, M. Zappa, R. Mott, and W. Schöner (2008), Application Of The Alpine 3d Model For Glacier Mass Balance And Glacier Runoff Studies At Goldbergkees, Austria, *Hydrological Processes*, *22*, 3941–3949, doi:10.1002/hyp.7102.

Milly, P. C. D., J. Betancourt, M. Falkenmark, R. M. Hirsch, Z. Kundzewicz, D. P. Lettenmaier, and R. J. Stouffer (2008), Stationarity Is Dead: Whither Water Management?, *2Science*, *319*, 573 574.

Mohanty, B. P. (2013), Soil Hydraulic Property Estimation Using Remote Sensing: A Review, *Vadose Zone Journal*, *12*, 0, doi:10.2136/vzj2013.06.0100.

Monin, A. S., and A. M. Obukhov (1954), Basic Laws Of Turbulent Mixing In The Surface Layer Of The Atmosphere, *Contrib. Geophys. Inst. Acad. Sci. USSR*, *24*, 163 187.

Montero, G., J. M. Escobar, E. Rodriguez, R. Montenegro, and E. R. i guez (2009), Solar Radiation And Shadow Modelling With Adaptive Triangular Meshes, *Solar Energy*, *83*, 998 1012, doi:10.1016/j.solener.2009.01.004.

Mosier, T. M., D. F. Hill, and K. V. Sharp (2016), How Much Cryosphere Model Complexity Is Just Right? Exploration Using The Conceptual Cryrosphere Hydrology Framework, *The Cryosphere Discussions*, 1–33, doi:10.5194/tc-2016-17.

Mote, P. W., A. F. Hamlet, M. P. Clark, and D. P. Lettenmaier (2005), Declining Mountain Snowpack In Western North America*, *Bulletin of the American Meteorological Society*, *86*, 39 49, doi:10.1175/bams-86-1-39.

Mott, R., F. Faure, M. Lehning, H. L WE, B. Hynek, G. Michlmayer, A. Prokop, and W. Sch ner (2008), Simulation Of Seasonal Snow-cover Distribution For Glacierized Sites On Sonnblick, Austria, With The Alpine3d Model, *Annals of Glaciology*, *49*, 155–160, doi:10.3189/172756408787814924.

Mott, R., M. Schirmer, M. Bavay, T. Grünewald, and M. Lehning (2010), Understanding Snow-transport Processes Shaping The Mountain Snow-cover, *The Cryosphere*, *4*, 545–559, doi:10.5194/tc-4-545-2010.

Mott, R., C. Gromke, T. Grünewald, and M. Lehning (2013), Relative Importance Of Advective Heat Transport And Boundary Layer Decoupling In The Melt Dynamics Of A Patchy Snow Cover, *Advances in Water Resources*, *55*, 88–97, doi:10.1016/j.advwatres.2012.03.001.

Mott, R., D. Scipión, M. Schneebeli, N. Dawes, A. Berne, and M. Lehning (2014), Orographic Effects On Snow Deposition Patterns In Mountainous Terrain, *Journal of Geophysical Research: Atmospheres*, *119*, 1419–1439, doi:10.1002/2013jd019880.

Mott, R., S. Schlögl, L. Dirks, and M. Lehning (2017), Impact Of Extreme Land-surface Heterogeneity On Micrometeorology Over Spring Snow-cover, *Journal of Hydrometeorology*, doi:10.1175/jhm-d-17-0074.1.

Mott, R., V. Vionnet, and T. Grünewald (2018), The Seasonal Snow Cover Dynamics: Review On Wind-driven Coupling Processes, *Frontiers in Earth Science*, *6*, 197, doi:10.3389/feart.2018.00197.

Munro, D. S., and G. J. Young (1982), An Operational Net Shortwave Radiation Model For Glacier Basins, *Water Resources Research*, *18*, 220–230, doi:10.1029/wr018i002p00220.

Musselman, K. N., J. W. Pomeroy, R. L. H. Essery, and N. Leroux (2015a), Impact Of Windflow Calculations On Simulations Of Alpine Snow Accumulation, Redistribution And Ablation, *Hydrological Processes*, *29*, 3983–3999, doi:10.1002/hyp.10595.

Musselman, K. N., J. W. Pomeroy, and T. E. Link (2015b), Variability In Shortwave Irradiance Caused By Forest Gaps: Measurements, Modelling, And Implications For Snow Energetics, *Agricultural and Forest Meteorology*, *207*, 69 82, doi:10.1016/j.agrformet.2015.03.014.

Musselman, K. N., M. P. Clark, C. Liu, K. Ikeda, and R. Rasmussen (2017), Slower Snowmelt In A Warmer World, *Nature Climate Change*, *7*, 214 219, doi:10.1038/nclimate3225.

Musselman, K. N., F. Lehner, K. Ikeda, M. P. Clark, A. F. Prein, C. Liu, M. Barlage, and R. Rasmussen (2018), Projected Increases And Shifts In Rain-on-snow Flood Risk Over Western North America, *Nature Climate Change*, *239*, 59, doi:10.1038/s41558-018-0236-4.

Nash, J. E., and J. V. Sutcliffe (1970), River Flow Forecasting Through Conceptual Models Part I — A Discussion Of Principles, *Journal of Hydrology*, *10*, 282 290, doi:10.1016/0022-1694(70)90255-6.

Nazemi, A., H. S. Wheater, K. P. Chun, and A. Elshorbagy (2013), A Stochastic Reconstruction Framework For Analysis Of Water Resource System Vulnerability To Climate-induced Changes In River Flow Regime, *Water Resources Research*, *49*, 291–305, doi:10.1029/2012wr012755.

O'Callaghan, J. F., and D. M. Mark (1984), The Extraction Of Drainage Networks From Digital Elevation Data, *Computer Vision, Graphics, and Image Processing*, *28*, 323–344, doi:10.1016/s0734-189x(84)80011-0.

Ohara, N., and M. L. Kavvas (2006), Field Observations And Numerical Model Experiments For The Snowmelt Process At A Field Site, *Advances in Water Resources*, *29*, 194 211, doi:10.1016/j.advwatres.2005.03.016.

Olyphant, G. A. (1986a), Longwave Radiation In Mountainous Areas And Its Influence On The Energy Balance Of Alpine Snowfields, *Water Resources Research*, *22*, 62–66, doi:10.1029/wr022i001p00062.

Olyphant, G. A. (1986b), The Components Of Incoming Radiation Within A Mid-latitude Alpine Watershed During The Snowmelt Season, *Arctic and Alpine Research*, *18*, 163 169, doi:10.2307/1551125.

Or, D., P. Lehmann, and S. Assouline (2015), Natural Length Scales Define The Range Of Applicability Of The Richards Equation For Capillary Flows, *Water Resources Research*, *51*, 7130–7144,

doi:10.1002/2015wr017034.

Painter, S. L., E. T. Coon, A. L. Atchley, M. Berndt, R. Garimella, J. D. Moulton, D. Svyatskiy, and C. J. Wilson (2016a), Integrated Surface/subsurface Permafrost Thermal Hydrology: Model Formulation And Proof-of-concept Simulations, *Water Resources Research*, *52*, 6062–6077, doi:10.1002/2015wr018427.

Painter, T. H. et al. (2016b), The Airborne Snow Observatory: Fusion Of Scanning Lidar, Imaging Spectrometer, And Physically-based Modeling For Mapping Snow Water Equivalent And Snow Albedo, *Remote Sensing of Environment*, *184*, 139–152, doi:10.1016/j.rse.2016.06.018.

Paniconi, C., and M. Putti (2015), Physically Based Modeling In Catchment Hydrology At 50: Survey And Outlook, *Water Resources Research*, *51*, 7090–7129, doi:10.1002/2015wr017780.

Parrish, D. M., and S. C. Hagen (2007), 2d Unstructured Mesh Generation For Oceanic And Coastal Tidal Models From A Localized Truncation Error Analysis With Complex Derivatives, *International Journal of Computational Fluid Dynamics*, *21*, 277–296, doi:10.1080/10618560701582500.

Paterna, E., P. Crivelli, and M. Lehning (2017), Wind Tunnel Observations Of Weak And Strong Snow Saltation Dynamics, *Journal of Geophysical Research: Earth Surface*, *122*, 1589–1604, doi:10.1002/2016jf004111.

Perrin, C., C. Michel, and V. Andréassian (2001), Does A Large Number Of Parameters Enhance Model Performance? Comparative Assessment Of Common Catchment Model Structures On 429 Catchments, *Journal of Hydrology*, *242*, 275 301, doi:10.1016/s0022-1694(00)00393-0.

Pietroniro, a et al. (2007), Development Of The Mesh Modelling System For Hydrological Ensemble Forecasting Of The Laurentian Great Lakes At The Regional Scale, *Hydrology and Earth System Sciences*, *11*, 1279 1294, doi:10.5194/hess-11-1279-2007.

Plüss, C., and A. Ohmura (1997), Longwave Radiation On Snow-covered Mountainous Surfaces, *Journal of Applied Meteorology*, *36*, 818 824, doi:10.1175/1520-0450-36.6.818.

Pomeroy, J., and M. Bernhardt (2017), *Project Report For The 2017 Gewex Ghp Meeting*, Kathmandu, Nepal.

Pomeroy, J., R. Essery, and B. Toth (2004), Implications Of Spatial Distributions Of Snow Mass And Melt Rate For Snow-cover Depletion: Observations In A Subarctic Mountain Catchment, *Annals of Glaciology*, *38*, 195–201, doi:10.3189/172756404781814744.

Pomeroy, J., X. Fang, and C. Ellis (2012), Sensitivity Of Snowmelt Hydrology In Marmot Creek, Alberta, To Forest Cover Disturbance, *Hydrological Processes*, *26*, 1891 1904, doi:10.1002/hyp.9248.

Pomeroy, J. W. (1989), A Process-based Model Of Snow Drifting, *Annals of Glaciology*, *13*, 237–240, doi:10.3189/s0260305500007965.

Pomeroy, J. W. (1991), Transport And Sublimation Of Snow In Wind-scoured Alpine Terrain, in *Snow, hydrology and forests in high alpine areas*, p. 131 140, IAHS Press.

Pomeroy, J. W., and R. L. H. Essery (1999), Turbulent Fluxes During Blowing Snow: Field Tests Of Model Sublimation Predictions, *Hydrological Processes*, *13*, 2963–2975, doi:10.1002/(sici)1099-1085(19991230)13:18<2963::aid-hyp11>3.0.co;2-9.

Pomeroy, J. W., and D. M. Gray (1990), Saltation Of Snow, *Water Resources Research*, *26*, 1583–1594, doi:10.1029/wr026i007p01583.

Pomeroy, J. W., and L. Li (2000), Prairie And Arctic Areal Snow Cover Mass Balance Using A Blowing Snow Model, *Journal of Geophysical Research: Atmospheres*, *105*, 26619–26634, doi:10.1029/2000jd900149.

Pomeroy, J. W., and D. H. Male (1986), Physical Modelling Of Blowing Snow For Agricultural Production, edited by Steppuhn, pp. 1–24, Proceedings, Snow Management for Agriculture Symposium, Lincoln, NB.

Pomeroy, J. W., and D. H. Male (1992), Steady-state Suspension Of Snow, *Journal of Hydrology*, *136*, 275–301, doi:10.1016/0022-1694(92)90015-n.

Pomeroy, J. W., T. D. Davies, and M. Tranter (1991), Seasonal Snowpacks, Processes Of Compositional Change, in *Seasonal snowpacks: Processes of compositional change*, edited by T D Davies M Tranter, pp. 71–113, NATO ASI Series G 28, Springer-Verlag, Berlin.

Pomeroy, J. W., D. M. Gray, and P. G. Landine (1993), The Prairie Blowing Snow Model: Characteristics, Validation, Operation, *Journal of Hydrology*, *144*, 165–192, doi:10.1016/0022-1694(93)90171-5.

Pomeroy, J. W., P. Marsh, H. G. Jones, and T. D. Davies (1995), Spatial Distribution Of Snow Chemical Load At The Tundra-taiga Transition, in *Biogeochemistry of seasonally snow-covered catchments*, p. 191 206, IAHS Publ. No. 228.

Pomeroy, J. W., P. Marsh, and D. M. Gray (1997), Application Of A Distributed Blowing Snow Model To The Arctic, *Hydrological Processes*, *11*, 1451–1464, doi:10.1002/(sici)1099-1085(199709)11:11<1451::aid-hyp449>3.0.co;2-q.

Pomeroy, J. W., D. M. Gray, K. R. Shook, B. Toth, R. L. H. Essery, A. Pietroniro, and N. Hedstrom (1998a), An Evaluation Of Snow Accumulation And Ablation Processes For Land Surface Modelling, *Hydrological Processes*, *12*, 2339–2367, doi:10.1002/(sici)1099-1085(199812)12:15<2339::aid-hyp800>3.3.co;2-c.

Pomeroy, J. W., J. Parviainen, N. Hedstrom, and D. M. Gray (1998b), Coupled Modelling Of Forest Snow Interception And Sublimation, *Hydrological Processes*, *12*, 2317–2337, doi:10.1002/(sici)1099-1085(199812)12:15<2317::aid-hyp799>3.0.co;2-x.

Pomeroy, J. W., N. Hedstrom, and J. Parviainen (1998c), The Snow Mass Balance Of Wolf Creek , Yukon: Effects Of Snow Sublimation And Redistribution, pp. 15–30, Saskatoon.

Pomeroy, J. W., B. Toth, R. J. Granger, N. R. Hedstrom, and R. L. H. Essery (2003), Variation In Surface Energetics During Snowmelt In A Subarctic Mountain Catchment, *Journal of Hydrometeorology*, *4*, 702–719, doi:10.1175/1525-7541(2003)004<0702:viseds>2.0.co;2.

Pomeroy, J. W., D. S. Bewley, R. L. H. Essery, N. R. Hedstrom, T. Link, R. J. Granger, J. E. Sicart, C. R. Ellis, and J. R. Janowicz (2006), Shrub Tundra Snowmelt, *Hydrological Processes*, *20*, 923–941, doi:10.1002/hyp.6124.

Pomeroy, J. W., D. M. Gray, T. Brown, N. R. Hedstrom, W. L. Quinton, R. J. Granger, and S. K. Carey (2007), The Cold Regions Hydrological Model: A Platform For Basing Process Representation And Model Structure On Physical Evidence, *Hydrological Processes*, *21*, 2650–2667, doi:10.1002/hyp.6787.

Pomeroy, J. W., A. Rowlands, J. Hardy, T. Link, D. Marks, R. Essery, J. E. Sicart, and C. Ellis (2008), Spatial Variability Of Shortwave Irradiance For Snowmelt In Forests, *Journal of Hydrometeorology*, *9*, 1482.

Pomeroy, J. W., X. Fang, K. Shook, and P. H. Whitfield (2013), Predicting In Ungauged Basins Using Physical Principles Obtained Using The Deductive, Inductive, And Abdyctive Reasoning Approach, in *Putting prediction in ungauged basins into practice*, edited by J W Pomeroy P H Whitfield, pp. 41–62, Canadian Water Resources Association.

Pomeroy, J. W., M. Bernhardt, and D. Marks (2015), Water Resources: Research Network To Track Alpine Water, *Nature (Correspondance)*, *521*, 32, doi:10.1038/521032c.

Pomeroy, J. W., R. L. H. Essery, and W. D. Helgason (2016a), Aerodynamic And Radiative Controls On The Snow Surface Temperature, *Journal of Hydrometeorology*, *17*, 2175 2189, doi:10.1175/jhm-d-15-0226.1.

Pomeroy, J. W., X. Fang, and D. G. Marks (2016b), The Cold Rain-on-snow Event Of June 2013 In The Canadian Rockies — Characteristics And Diagnosis, *Hydrological Processes*, *30*, 2899–2914, doi:10.1002/hyp.10905.

Prokop, A. (2008), Assessing The Applicability Of Terrestrial Laser Scanning For Spatial Snow Depth Measurements, *Cold Regions Science and Technology*, *54*, 155–163, doi:10.1016/j.coldregions.2008.07.002.

Qu, Y. (2004), An Integrated Hydrologic Model For Multi-process Simulation Using Semi-discrete Finite Volume Approach, PhD thesis, 143 pp.

Qu, Y., and C. J. Duffy (2007), A Semidiscrete Finite Volume Formulation For Multiprocess Watershed Simulation, *Water Resources Research*, *43*, n/a–n/a, doi:10.1029/2006wr005752.

Raderschall, N., M. Lehning, and C. Schär (2008), Fine-scale Modeling Of The Boundary Layer Wind Field

Over Steep Topography, *Water Resources Research*, *44*, 1–18, doi:10.1029/2007wr006544.

Raleigh, M. S., J. D. Lundquist, and M. P. Clark (2015a), Exploring The Impact Of Forcing Error Characteristics On Physically Based Snow Simulations Within A Global Sensitivity Analysis Framework, *Hydrology and Earth System Sciences*, *19*, 3153–3179, doi:10.5194/hess-19-3153-2015.

Raleigh, M. S., B. Livneh, K. Lapo, and J. D. Lundquist (2015b), How Does Availability Of Meteorological Forcing Data Impact Physically-based Snowpack Simulations?, *Journal of Hydrometeorology*, 150904104740009, doi:10.1175/jhm-d-14-0235.1.

Rasouli, K., J. W. Pomeroy, J. R. Janowicz, S. K. Carey, and T. J. Williams (2014), Hydrological Sensitivity Of A Northern Mountain Basin To Climate Change, *Hydrological Processes*, doi:10.1002/hyp.10244.

Rasouli, K., J. W. Pomeroy, and D. G. Marks (2015), Snowpack Sensitivity To Perturbed Climate In A Cool Mid-latitude Mountain Catchment, *Hydrological Processes*, *29*, 3925–3940, doi:10.1002/hyp.10587.

Rasouli, K., J. W. Pomeroy, J. R. Janowicz, T. J. Williams, and S. K. Carey (2018), A Long-term Hydrometeorological Dataset (1993–2014) Of A Northern Mountain Basin: Wolf Creek Research Basin, Yukon Territory, Canada, *Earth System Science Data Discussions*, 1–22, doi:10.5194/essd-2018-118.

Rasouli, K., J. W. Pomeroy, and P. H. Whitfield (2019), Hydrological Responses Of Headwater Basins To Monthly Perturbed Climate In The North American Cordillera, *Journal of Hydrometeorology*, *20*, 863–882, doi:10.1175/jhm-d-18-0166.1.

Raupach, M. R., D. A. Gillette, and J. F. Leys (1993), The Effect Of Roughness Elements On Wind Erosion Threshold, *Journal of Geophysical Research: Atmospheres*, *98*, 3023–3029, doi:10.1029/92jd01922.

Razavi, S., and H. V. Gupta (2016), A New Framework For Comprehensive, Robust, And Efficient Global Sensitivity Analysis: 1. Theory, *Water Resources Research*, *52*, 423–439, doi:10.1002/2015wr017558.

Rew, R., and G. Davis (1990), Netcdf: An Interface For Scientific Data Access, *IEEE Computer Graphics and Applications*, *10*, 76 82, doi:10.1109/38.56302.

Rice, K. C., and G. M. Hornberger (1998), Comparison Of Hydrochemical Tracers To Estimate Source Contributions To Peak Flow In A Small, Forested, Headwater Catchment, *Water Resources Research*, *34*, 1755 1766, doi:10.1029/98wr00917.

Rigon, R., G. Bertoldi, and T. M. Over (2006), Geotop: A Distributed Hydrological Model With Coupled Water And Energy Budgets, *Journal of Hydrometeorology*, *7*, 371 388, doi:10.1175/jhm497.1.

Rineau, L. (2016), 2d Conforming Triangulations And Meshes, in *Cgal user and reference manual*, CGAL Editorial Board.

Roesch, A., M. Wild, H. Gilgen, and A. Ohmura (2001), A New Snow Cover Fraction Parametrization For The Echam4 Gcm, *Climate Dynamics*, *17*.

Rothwell, R., G. Hillman, and J. W. Pomeroy (2016), Marmot Creek Experimental Watershed Study, *Forestry Chronicle*, *92*, 32 36, doi:10.5558/tfc2016-010.

Rouault, M. P., P. G. Mestayer, and R. Schiestel (1991), A Model Of Evaporating Spray Droplet Dispersion, *Journal of Geophysical Research: Oceans*, *96*, 7181–7200, doi:10.1029/90jc02569.

Rouse, W. R., C. J. Oswald, J. Binyamin, C. Spence, W. M. Schertzer, P. D. Blanken, N. Bussières, and C. R. Duguay (2005), The Role Of Northern Lakes In A Regional Energy Balance, *Journal of Hydrometeorology*, *6*, 291 305, doi:10.1175/jhm421.1.

Roy, D. P. et al. (2014), Landsat-8: Science And Product Vision For Terrestrial Global Change Research, *Remote Sensing of Environment*, *145*, 154 172, doi:10.1016/j.rse.2014.02.001.

Rupp, K., P. Tillet, F. Rudolf, J. Weinbub, A. Morhammer, T. Grasser, A. Jüngel, and S. Selberherr (2016), Viennacl—linear Algebra Library For Multi- And Many-core Architectures, *SIAM J. Matrix Anal. Appl.*, *38*, 412 439, doi:10.1137/090750688.

Ruppert, J. (1995), A Delaunay Refinement Algorithm For Quality 2-dimensional Mesh Generation, *Journal of Algorithms*, *18*, 548–585, doi:10.1006/jagm.1995.1021.

Ryerson, C. C. (1984), Mapping Solar Access In High Relief Areas For Regional Energy Planning, *The Professional Geographer*, *36*, 345 352.

Samaniego, L. et al. (2017), Toward Seamless Hydrologic Predictions Across Spatial Scales, *Hydrology and Earth System Sciences*, *21*, 4323 4346, doi:10.5194/hess-21-4323-2017.

Savenije, H. H. G. (2009), Hess Opinions "the Art Of Hydrology", *Hydrology and Earth System Sciences*, *13*, 157 161, doi:10.5194/hess-13-157-2009.

Scally, F. A. de (1992), Influence Of Avalanche Snow Transport On Snowmelt Runoff, *Water Resources Research*, *137*, 73–97, doi:10.1016/0022-1694(92)90049-2.

Schaerer, P. (1988), The Yield Of Avalanche Snow At Rogers Pass, British Columbia, Canada, *Journal of Glaciology*, *34*, 1 6.

Schlögl, S., C. Marty, M. Bavay, and M. Lehning (2016), Sensitivity Of Alpine3d Modeled Snow Cover To Modifications In Dem Resolution, Station Coverage And Meteorological Input Quantities, *Environmental Modelling & Software*, *83*, 387 396, doi:10.1016/j.envsoft.2016.02.017.

Schlögl, S., M. Lehning, C. Fierz, and R. Mott (2018), Representation Of Horizontal Transport Processes In Snowmelt Modeling By Applying A Footprint Approach, *Frontiers in Earth Science*, *6*, 120, doi:10.3389/feart.2018.00120.

Schmidt, R. A. (1972), *Sublimation Of Wind-transported Snow – A Model*, Rocky Mountain Forest; Range Experiment Station. Forest Service, U.S. Department of Agriculture; USDA Forest Service Research Paper RM-90, Fort Collins, Colorado.

Schmidt, R. A. (1982), Properties Of Blowing Snow, *Reviews of Geophysics*, *20*, 39–44, doi:10.1029/rg020i001p00039.

Schmidt, R. A. (1986), Transport Rate Of Drifting Snow And The Mean Wind Speed Profile, *Boundary-Layer Meteorology*, *34*, 213–241, doi:10.1007/bf00122380.

Schmidt, R. A. (1991), Sublimation Of Snow Intercepted By An Artificial Conifer, *Agricultural and Forest Meteorology*, *54*, 1–27, doi:10.1016/0168-1923(91)90038-r.

Schneiderbauer, S., and A. Prokop (2011), The Atmospheric Snow-transport Model: Snowdrift3d, *Journal of Glaciology*, *57*, 526–542, doi:10.3189/002214311796905677.

Schoups, G., N. C. van de Giesen, and H. H. G. Savenije (2008), Model Complexity Control For Hydrologic Prediction, *Water Resources Research*, *44*, n/a n/a, doi:10.1029/2008wr006836.

Schön, P., F. Naaim-Bouvet, V. Vionnet, and A. Prokop (2018), Merging A Terrain-based Parameter With Blowing Snow Fluxes For Assessing Snow Redistribution In Alpine Terrain, *Cold Regions Science and Technology*, doi:10.1016/j.coldregions.2018.08.002.

Schroeder, W., K. Martin, and B. Lorensen (2006), *The Visualization Toolkit*, 4th ed.

Seyfried, M. S., and B. P. Wilcox (1995), Scale And The Nature Of Spatial Variability: Field Examples Having Implications For Hydrologic Modeling, *Water Resources Research*, *31*, 173 184, doi:10.1029/94wr02025.

Shewchuk, J. (1996), Triangle: Engineering A 2d Quality Mesh Generator And Delaunay Triangulator, in *Applied computational geometry towards geometric engineering*, p. 203 222, Springer Berlin / Heidelberg.

Shewchuk, J. R. (2002), Delaunay Refinement Algorithms For Triangular Mesh Generation, *Computational Geometry*, *22*, 21–74, doi:10.1016/s0925-7721(01)00047-5.

Shi, X., P. Marsh, and D. Yang (2015), Warming Spring Air Temperatures, But Delayed Spring Streamflow In An Arctic Headwater Basin, *Environmental Research Letters*, *10*, 064003, doi:10.1088/1748-9326/10/6/064003.

Shook, K., and D. M. Gray (1996), Small-scale Spatial Structure Of Shallow Snowcovers, *Hydrological Processes*, *10*, 1283 1292, doi:10.1002/(sici)1099-1085(199610)10:10<1283::aid-hyp460>3.0.co;2-m.

Shook, K., and D. M. Gray (1997), Snowmelt Resulting From Advection, *Hydrological Processes*, *11*, 1725–1736, doi:10.1002/(sici)1099-1085(19971030)11:13<1725::aid-hyp601>3.0.co;2-p.

Shook, K., D. M. Gray, and J. W. Pomeroy (1993a), Temporal Variation In Snowcover Area During Melt In Prairie And Alpine Environmentspaper Presented At The 9th Northern Res. Basin Symposium/workshop (whitehorse/dawson/inuvik, Canada - August 1992), *Hydrology Research*, *24*, 183–198, doi:10.2166/nh.1993.0021.

Shook, K., J. Pomeroy, and G. van der Kamp (2015), The Transformation Of Frequency Distributions Of Winter Precipitation To Spring Streamflow Probabilities In Cold Regions; Case Studies From The Canadian Prairies, *Journal of Hydrology*, *521*, 395–409, doi:10.1016/j.jhydrol.2014.12.014.

Shook, K. R., D. M. Gray, and J. W. Pomeroy (1993b), Geometry Of Patchy Snowcovers, p. 89 98, Quebec City.

Sicart, J. E., J. W. Pomeroy, R. L. H. Essery, and D. Bewley (2006), Incoming Longwave Radiation To Melting Snow: Observations, Sensitivity And Estimation In Northern Environments, *Hydrological Processes*, *20*, 3697–3708, doi:10.1002/hyp.6383.

Sidle, R. C., S. Noguchi, Y. Tsuboyama, and K. Laursen (2001), A Conceptual Model Of Preferential Flow Systems In Forested Hillslopes: Evidence Of Self-organization, *Hydrological Processes*, *15*, 1675 1692, doi:10.1002/hyp.233.

Sivapalan, M. (2017), From Engineering Hydrology To Earth System Science : Milestones In The Transformation Of Hydrologic Science, *Hydrology and Earth System Sciences Discussions*, 1 47, doi:10.5194/hess-2017-670.

Skiles, S. M., M. Flanner, J. M. Cook, M. Dumont, and T. H. Painter (2018), Radiative Forcing By Light-absorbing Particles In Snow, *Nature Climate Change*, *8*, 964–971, doi:10.1038/s41558-018-0296-5.

Slater, a G., a P. Barrett, M. P. Clark, J. D. Lundquist, and M. S. Raleigh (2013), Uncertainty In Seasonal Snow Reconstruction: Relative Impacts Of Model Forcing And Image Availability, *Advances in Water Resources*, *55*, 165 177, doi:10.1016/j.advwatres.2012.07.006.

Slingsby, A. (2002), An Object-orientated Approach To Hydrological Modeling Using Triangular Irregular Networks, PhD thesis, 36 pp.

Sloan, P. G., and I. D. Moore (1984), Modeling Subsurface Stormflow On Steeply Sloping Forested Watersheds, *Water Resources Research*, *20*, 1815 1822.

Smith, C. D. (2009), The Relationship Between Snowfall Catch Efficiency And Wind Speed For The Geonor T-200b Precipitation Gauge Utilizing Various Wind Shield Configurations., pp. 115–121.

Spence, C. (2010), A Paradigm Shift In Hydrology: Storage Thresholds Across Scales Influence Catchment Runoff Generation, *Geography Compass*, *4*, 819 833, doi:10.1111/j.1749-8198.2010.00341.x.

Spence, C., and S. Mengistu (2016), Deployment Of An Unmanned Aerial System To Assist In Mapping An Intermittent Stream, *Hydrological Processes*, *30*, 493–500, doi:10.1002/hyp.10597.

Stephens, G. L., and C. D. Kummerow (2007), *The Remote Sensing Of Clouds And Precipitation From Space: A Review*.

Steppuhn, H., and G. E. Dyck (1974), Estimating True Basin Snowcover, pp. 314–328, National Academy of Science, Washington, D.C.

Stewart, R., J. W. Pomeroy, and R. Lawford (2008), A Drought Research Initiative For The Canadian Prairies, *CMOS Bulletin SCMO, 36(3), 87-96.*, *36*, 87 96.

Stewart, R. E. (1985), Precipitation Types In Winter Storms, *Pure and Applied Geophysics PAGEOPH*, *123*, 597 609, doi:10.1007/bf00877456.

Sturm, M., J. P. McFadden, G. E. Liston, F. S. Chapin, C. H. Racine, and J. Holmgren (2001), Snow-shrub Interactions In Arctic Tundra: A Hypothesis With Climatic Implications, *Journal of Climate*, *14*, 336–344, doi:10.1175/1520-0442(2001)014<0336:ssiiat>2.0.co;2.

Tabler, R. D. (1974), New Engineering Criteria For Snow Fence Systems, *Transportation Research Record*, 65–78.

Tabler, R. D., J. W. Pomeroy, and B. W. Santana (1990), Drifting Snow, in *Cold regions science and hydraulics*, pp. 95–145, American Society of Civil Engineers.

Takeuchi, M. (1980), Vertical Profile And Horizontal Increase Of Drift-snow Transport, *Journal of Glaciology*, *26*, 481–492, doi:10.3189/s0022143000010996.

Tanaka, T., M. Yasuhara, H. Sakai, and A. Marui (1988), The Hachioji Experimental Basin Study — Storm Runoff Processes And The Mechanism Of Its Generation, *Journal of Hydrology*, *102*, 139–164, doi:10.1016/0022-1694(88)90095-9.

Tangelder, H., and A. Fabri (2018), Dd Spatial Searching, in *Cgal user and reference manual*, CGAL Editorial Board.

Tani, M. (1997), Runoff Generation Processes Estimated From Hydrological Observations On A Steep Forested Hillslope With A Thin Soil Layer, *Water Resources Research*, *200*, 84 109, doi:10.1016/s0022-1694(97)00018-8.

Tapley, B. D., and S. Bettadpur (2004), The Gravity Recovery And Climate Experiment: Mission Overview And Early Results, *Geophysical Research ….*

Tarboton, D. G., C. H. Luce, and U. F. Service (1996), *Utah Energy Balance Snow Accumulation And Melt Model (Ueb).*

Team, G. D. (2016), *Gdal - Geospatial Data Abstraction Library, Version 2.1.1*, Open Source Geospatial Foundation.

Tetzlaff, D., and J. J. McDonnell (2008), Conceptualizing Catchment Processes: Simply Too Complex?, *Hydrological Processes*, *22*, 1727–1730, doi:10.1002/hyp.

Thornton, P. E., S. W. Running, and M. A. White (1997), Generating Surfaces Of Daily Meteorological Variables Over Large Regions Of Complex Terrain, *Water Resources Research*, *190*, 214 251, doi:10.1016/s0022-1694(96)03128-9.

Thorpe, A. D., and B. J. Mason (1966), The Evaporation Of Ice Spheres And Ice Crystals, *British Journal of Applied Physics*, *17*, 541–548, doi:10.1088/0508-3443/17/4/316.

Tiwari, V. M., J. Wahr, and S. Swenson (2009), Dwindling Groundwater Resources In Northern India, From Satellite Gravity Observations, *Geophysical Research Letters*, *36*, L18401, doi:10.1029/2009gl039401.

Todini, E. (1988), Rainfall-runoff Modeling - Past, Present And Future, *Water Resources Research*, *100*, 341 352, doi:10.1016/0022-1694(88)90191-6.

Tournois, J., P. Alliez, and O. Devillers (2010), 2d Centroidal Voronoi Tessellations With Constraints, *Numerical Mathematics: Theory, Methods and Applications*, *3*, 212 222, doi:10.4208/nmtma.2010.32s.6.

Tucker, G. (2001), An Object-oriented Framework For Distributed Hydrologic And Geomorphic Modeling Using Triangulated Irregular Networks, *Computers & Geosciences*, *27*, 959 973, doi:10.1016/s0098-3004(00)00134-5.

Tushinsky, G. K. (1975), The Part Avalanches Play In The Formation And Dynamics Of Mountain Glaciers And Snow Patches In The Territory Of The Ussr, vol. 104, p. 381 389, Moscow.

Uchida, T., K. Kosugi, and T. Mizuyama (1999), Runoff Characteristics Of Pipeflow And Effects Of Pipeflow On Rainfall-runoff Phenomena In A Mountainous Watershed, *Water Resources Research*, *222*, 18 36, doi:10.1016/s0022-1694(99)00090-6.

VanDerWal, J. (2016), *Sdmtools*.

Vaze, J., D. a Post, F. H. S. Chiew, J. M. Perraud, N. R. Viney, and J. Teng (2010), Climate Non-stationarity – Validity Of Calibrated Rainfall–runoff Models For Use In Climate Change Studies, *Water Resources Research*,

394, 447 457, doi:10.1016/j.jhydrol.2010.09.018.

Verfürth, R. (2005), Robust A Posteriori Error Estimates For Stationary Convection-diffusion Equations, *SIAM Journal on Numerical Analysis*, *43*, 1766–1782, doi:10.1137/040604261.

Verseghy, D. L. (1991), Class—a Canadian Land Surface Scheme For Gcms. I. Soil Model, *International Journal of Climatology*, *11*, 111–133, doi:10.1002/joc.3370110202.

Verseghy, D. L., N. A. McFarlane, and M. Lazare (1993), Class—a Canadian Land Surface Scheme For Gcms, Ii. Vegetation Model And Coupled Runs, *International Journal of Climatology*, *13*, 347–370, doi:10.1002/joc.3370130402.

Vionnet, V., E. Brun, S. Morin, A. Boone, S. Faroux, P. L. Moigne, E. Martin, and J. M. Willemet (2012), The Detailed Snowpack Scheme Crocus And Its Implementation In Surfex V7.2, *Geoscientific Model Development*, *5*, 773 791, doi:10.5194/gmd-5-773-2012.

Vionnet, V., E. Martin, V. Masson, G. Guyomarc'H, F. Naaim-Bouvet, A. Prokop, Y. Durand, and C. Lac (2014), Simulation Of Wind-induced Snow Transport And Sublimation In Alpine Terrain Using A Fully Coupled Snowpack/atmosphere Model, *Cryosphere*, *8*, 395–415, doi:10.5194/tc-8-395-2014.

Vionnet, V., E. Martin, V. Masson, C. Lac, F. N. Bouvet, and G. Guyomarc'h (2017), High-resolution Large Eddy Simulation Of Snow Accumulation In Alpine Terrain, *Journal of Geophysical Research: Atmospheres*, *122*, 11, 005–11, 021, doi:10.1002/2017jd026947.

Vishwakarma, B. D., B. Devaraju, and N. Sneeuw (2018), What Is The Spatial Resolution Of Grace Satellite Products For Hydrology?, *Remote Sensing*, *10*, 852, doi:10.3390/rs10060852.

Viviroli, D., H. H. Dürr, B. Messerli, M. Meybeck, and R. Weingartner (2007), Mountains Of The World, Water Towers For Humanity: Typology, Mapping, And Global Significance, *Water Resources Research*, *43*, 1–13, doi:10.1029/2006wr005653.

Viviroli, D. et al. (2011), Climate Change And Mountain Water Resources: Overview And Recommendations For Research, Management And Policy, *Hydrology and Earth System Sciences*, *15*, 471–504, doi:10.5194/hess-15-471-2011.

Vivoni, E. R., V. Y. Ivanov, R. L. Bras, and D. Entekhabi (2004), Generation Of Triangulated Irregular Networks Based On Hydrological Similarity, *Journal of Hydrologic Engineering*, *9*, 288–302, doi:10.1061/(asce)1084-0699(2004)9:4(288).

Vrugt, J. a, C. J. F. ter Braak, M. P. Clark, J. M. Hyman, and B. a Robinson (2008), Treatment Of Input Uncertainty In Hydrologic Modeling: Doing Hydrology Backward With Markov Chain Monte Carlo Simulation, *Water Resources Research*, *44*, 937, doi:10.1029/2007wr006720.

Wagenbrenner, N. S., J. M. Forthofer, B. K. Lamb, K. S. Shannon, and B. W. Butler (2016), Downscaling Surface Wind Predictions From Numerical Weather Prediction Models In Complex Terrain With Windninja, *Atmospheric Chemistry and Physics*, *16*, 5229–5241, doi:10.5194/acp-16-5229-2016.

Wagener, T. (2003), Evaluation Of Catchment Models, *Hydrological Processes*, *17*, 3375–3378, doi:10.1002/hyp.5158.

Wagener, T., and A. Montanari (2011), Convergence Of Approaches Toward Reducing Uncertainty In Predictions In Ungauged Basins, *Water Resources Research*, *47*, W06301, doi:10.1029/2010wr009469.

Wagener, T., M. Sivapalan, P. Troch, and R. Woods (2007), Catchment Classification And Hydrologic Similarity, *Geography Compass*, *1*, 901–931, doi:10.1111/j.1749-8198.2007.00039.x.

Wagner, S., B. Fersch, F. Yuan, Z. Yu, and H. Kunstmann (2016), Fully Coupled Atmospheric-hydrological Modeling At Regional And Long-term Scales: Development, Application, And Analysis Of Wrf-hms, *Water Resources Research*, *52*, 3187–3211, doi:10.1002/2015wr018185.

Walcek, C. J. (1994), Cloud Cover And Its Relationship To Relative Humidity During A Springtime Midlatitude Cyclone, *Monthly Weather Review*, *122*, 1021 1035.

Walmsley, J. L., P. A. Taylor, and J. R. Salmon (1984), Simple Guidelines For Estimating Wind Speed Variations Due To Small Scale Topographic Features, *Climatological bulletin*, *23*, 3–14.

Walmsley, J. L., P. A. Taylor, and T. Keith (1986), A Simple Model Of Neutrally Stratified Boundary-layer Flow Over Complex Terrain With Surface Roughness Modulations (ms3djh/3r), *Boundary-Layer Meteorology*, *36*, 157–186, doi:10.1007/bf00117466.

Walmsley, J. L., P. A. Taylor, and J. R. Salmon (1989), Simple Guidelines For Estimating Wind Speed Variations Due To Small-scale Topographic Features - An Update, *Climatol. Bull*, *23*.

Walvoord, M. A., and B. L. Kurylyk (2016), Hydrologic Impacts Of Thawing Permafrost—a Review, *Vadose Zone Journal*, *15*, doi:10.2136/vzj2016.01.0010.

Wang, Z., and N. Huang (2017), Numerical Simulation Of The Falling Snow Deposition Over Complex Terrain, *Journal of Geophysical Research: Atmospheres*, *122*, 980–1000, doi:10.1002/2016jd025316.

Wayand, N. E., C. B. Marsh, J. M. Shea, and J. W. Pomeroy (2018), Globally Scalable Alpine Snow Metrics, *Remote Sensing of Environment*, *213*, 61–72, doi:10.1016/j.rse.2018.05.012.

Wensong, W., P. A. Taylor, and J. L. Walmsley (2000), Guidelines For Airflow Over Complex Terrain: Model Developments, *Journal of Wind Engineering and Industrial Aerodynamics*, *86*, 169 186, doi:10.1016/s0167-6105(00)00009-x.

Westoby, M. J., J. Brasington, N. F. Glasser, M. J. Hambrey, and J. M. Reynolds (2012), 'structure-from-motion' Photogrammetry: A Low-cost, Effective Tool For Geoscience Applications, *Geomorphology*, *179*, 300 314, doi:10.1016/j.geomorph.2012.08.021.

Wever, N., C. Fierz, C. Mitterer, H. Hirashima, and M. Lehning (2014), Solving Richards Equation For Snow Improves Snowpack Meltwater Runoff Estimations In Detailed Multi-layer Snowpack Model, *The Cryosphere*, *8*, 257–274, doi:10.5194/tc-8-257-2014.

Wever, N., L. Schmid, A. Heilig, O. Eisen, C. Fierz, and M. Lehning (2015), Verification Of The Multi-layer Snowpack Model With Different Water Transport Schemes, *The Cryosphere*, *9*, 2271–2293, doi:10.5194/tc-9-2271-2015.

Wheater, H. S. (2015), Water Security – Science And Management Challenges, *Proceedings of the International Association of Hydrological Sciences*, *366*, 23 30, doi:10.5194/piahs-366-23-2015.

Wheater, H. S., A. J. Jakeman, and K. J. Beven (1993), Progress And Directions In Rainfall-runoff Modelling, in *Modelling change in environmental systems*, p. 101 132.

Winstral, A., K. Elder, and R. E. Davis (2002), Spatial Snow Modeling Of Wind-redistributed Snow Using Terrain-based Parameters, *Journal of Hydrometeorology*, *3*, 524 538, doi:10.1175/1525-7541(2002)003<0524:ssmowr>2.0.co;2.

Winstral, A., D. Marks, and R. Gurney (2013), Simulating Wind-affected Snow Accumulations At Catchment To Basin Scales, *Advances in Water Resources*, *55*, 64–79, doi:10.1016/j.advwatres.2012.08.011.

Woo, M., and R. Thorne (2006), Snowmelt Contribution To Discharge From A Large Mountainous Catchment In Subarctic Canada, *Hydrological Processes*, *20*, 2129–2139, doi:10.1002/hyp.6205.

Woo, M., W. R. Rouse, R. E. Stewart, and J. M. R. Stone (2008), The Mackenzie Gewex Study: A Contribution To Cold Region Atmospheric And Hydrologic Sciences, in *Cold region atmospheric and hydrologic studies volume 1: Atmospheric dynamics*, edited by M.-k. Woo, p. 1 22, Springer-Verlag, Berlin, Germany.

Woo, M.-k., and K. Young (2004), Modeling Arctic Snow Distribution And Melt At The 1 Km Grid Scale., *Nordic Hydrology*, *35*, 295 307.

Wood, E. F. et al. (2011), Hyperresolution Global Land Surface Modeling: Meeting A Grand Challenge For Monitoring Earth's Terrestrial Water, *Water Resources Research*, *47*, doi:10.1029/2010wr010090.

Wood, N. (2000), Wind Flow Over Complex Terrain: A Historical Perspective And The Prospect For Large-eddy Modelling, *Boundary-Layer Meteorology*, *96*, 11–32, doi:10.1023/a:1002017732694.

Wulder, M. A., T. Han, J. C. White, T. Sweda, and H. Tsuzuki (2007a), Integrating Profiling Lidar With

Landsat Data For Regional Boreal Forest Canopy Attribute Estimation And Change Characterization, *Remote Sensing of Environment*, *110*, 123–137, doi:10.1016/j.rse.2007.02.002.

Wulder, M. a, and T. a Nelson (2003), Eosd Land Cover Classification Legend Report Version 2, *Development*, 1 81.

Wulder, M. A., M. Cranny, R. J. Hall, J. Luther, A. Beaudoin, J. C. White, D. G. Goodenough, and J. Dechka (2007b), Satellite Land Cover Mapping Of Canada's Forests: The Eosd Land Cover Project, in *North american land cover summit*, p. 21 30.

Xiao, J., R. Bintanja, S. J. Dery, G. W. Mann, and P. A. Taylor (2000), An Intercomparison Among Four Models Of Blowing Snow, *Boundary-Layer Meteorology*, *97*, 109–135, doi:10.1023/a:1002795531073.

Yang, J., M. K. Yau, X. Fang, and J. W. Pomeroy (2010), A Triple-moment Blowing Snow-atmospheric Model And Its Application In Computing The Seasonal Wintertime Snow Mass Budget, *Hydrology and Earth System Sciences*, *14*, 1063–1079, doi:10.5194/hess-14-1063-2010.

Yeh, P. J. F., S. C. Swenson, J. S. Famiglietti, and M. Rodell (2006), Remote Sensing Of Groundwater Storage Changes In Illinois Using The Gravity Recovery And Climate Experiment (grace), *Water Resources Research*, *42*, doi:10.1029/2006wr005374.

Young, P. C. (2013), Hypothetico-inductive Data-based Mechanistic Modeling Of Hydrological Systems, *Water Resources Research*, *49*, 915 935, doi:10.1002/wrcr.20068.

Zalikhanov, M. C. (1971), Hydrological Role Of Avalanches In The Caucasus, p. 390 394, Moscow.

Zhang, Y., S. K. Carey, and W. L. Quinton (2008), Evaluation Of The Algorithms And Parameterizations For Ground Thawing And Freezing Simulation In Permafrost Regions, *Journal of Geophysical Research*, *113*, D17116, doi:10.1029/2007jd009343.

Zhao, L., and D. M. Gray (1999), Estimating Snowmelt Infiltration Into Frozen Soils, *Hydrological Processes*, *13*, 1827 1842, doi:10.1002/(sici)1099-1085(199909)13:12/13<1827::aid-hyp896>3.0.co;2-d.

Zwaaftink, C. D. G., R. Mott, and M. Lehning (2013), Seasonal Simulation Of Drifting Snow Sublimation In Alpine Terrain, *Water Resources Research*, *49*, 1581–1590, doi:10.1002/wrcr.20137.